2021

TORREFACTION OF MIXED SOLID WASTE

Zhuo Xu
Michigan Technological University, zhuoxu@mtu.edu

TORREFACTION OF MIXED SOLID WASTE

By

Zhuo Xu

A DISSERTATION

Submitted in partial fulfillment of the requirements for the degree of

DOCTOR OF PHILOSOPHY

In Mechanical Engineering – Engineering Mechanics

MICHIGAN TECHNOLOGICAL UNIVERSITY

2021

This dissertation has been approved in partial fulfillment of the requirements for the Degree of DOCTOR OF PHILOSOPHY in Mechanical Engineering – Engineering Mechanics.

Department of Mechanical Engineering – Engineering Mechanics

Dissertation Co-Advisor:	*Dr. Ezra Bar-Ziv*
Dissertation Co-Advisor:	*Dr. Jordan L. Klinger*
Committee Member:	*Dr. George W. Huber*
Committee Member:	*Dr. David R. Shonnard*
Committee Member:	*Dr. Armando G. McDonald*
Department Chair:	*Dr. William W. Predebon*

Table of Contents

List of Figures

List of Tables

Author Contribution Statement

This doctoral dissertation contains 8 chapters, as follows:

Chapter 1 provides the motivation for the research, the literature review that discusses current knowledge of torrefaction and the challenges of using waste as a feedstock, and the thesis objectives.

Chapter 2 to 7 contain the publications and submitted journal during the Ph.D. study.

Chapter 2, 3 and **4** shows the studies regarding torrefied wastes and their properties. It includes:

Chapter 2: Reprinted (adapted) with permission from Z. Xu, S. Zinchik, SS. Kolapkar, E. Bar-Ziv, T. Hansen, D. Conn, AG. McDonald. 2018. Properties of torrefied US Waste blends. Frontiers in Energy Research 6, 65. Copyright 2018 Xu, Zinchik, Kolapkar, Bar-Ziv, Hansen, Conn and McDonald.

Chapter 3: Reprinted (adapted) with permission from S. Zinchik, Z. Xu, SS. Kolapkar, E. Bar-Ziv, AG. McDonald. 2020. Properties of pellets of torrefied US waste blends. Waste Management 104, 130-138. Copyright 2020 Elsevier B.V.

Chapter 4: Reprinted (adapted) with permission from Z. Xu, S. Zinchik, SS. Kolapkar, E. Bar-Ziv, J. Klinger, E. Fillerup, K. Schaller, C. Pilgrim. 2021. In preparation to be submitted to Polymer Degradation and Stability Elsevier B.V.

Chapter 5: Reprinted (adapted) with permission from Z Xu, SS Kolapkar, S Zinchik, E Bar-Ziv, L Ewurum, AG McDonald, J. Klinger, E. Fillerup, K. Schaller, C. Pilgrim. 2021. Bypassing Energy Barriers in Fiber-Polymer Torrefaction. Frontiers in Energy Research 9, 75. Copyright 2021 Xu, Kolapkar, Zinchik, Bar-Ziv, Ewurum, McDonald, Klinger, Fillerup, Schaller and Pilgrim.

Chapter 6 and 7 discusses the dechlorination of wastes by torrefaction, it includes:

Chapter 6: Reprinted (adapted) with permission from Z. Xu, SS. Kolapkar, S. Zinchik, E. Bar-Ziv, AG. McDonald. 2020. Comprehensive kinetic study of thermal degradation of polyvinylchloride (PVC). Polymer Degradation and Stability, 109148. Copyright 2020 Elsevier B.V.

Chapter 7: Reprinted (adapted) with permission from Z. Xu, JW. Albrecht, SS. Kolapkar, S. Zinchik, E. Bar-Ziv. 2020. Chlorine Removal from US Solid Waste Blends through Torrefaction. Applied Sciences 10 (9), 3337. Copyright 2020 Xu, Albrecht, Kolapkar, Zinchik, Bar-Ziv.

Chapter 8 discusses the overall conclusion of the study and future work.

Acknowledgements

I would like to acknowledge the financial support I received from the Mechanical Engineering – Engineering Mechanics department at Michigan Tech, Battelle/INL (Contract #209856) and NSF-PFI, grant number 1827364.

I would like to acknowledge the mentoring of my co-advisors Dr. Ezra Bar-Ziv and Dr. Jordan L. Klinger. Without your patience and help I could not finish this work. I really appreciate the countless help and guidance that you provided, especially the in the chemistry criteria.

I would like to acknowledge Dr. George Huber, Dr. David R. Shonnard, and Dr. Armando G. McDonald for serving on my advisory committee, and for their careful review and support of my work. Your critical comments and discussions always kept my thoughts and research interpretations grounded, realistic, and focused.

I would like to acknowledge the many thoughtful discussions, contributions, and antics of my undergraduate research assistants (Josh Albrecht) and fellow/past graduate students, particularly Dr. Stas Zinchik, Shreyas Kolapkar, Medhavi Kamran and Victor Ierulli.

I would like to acknowledge the staff and students at APSRC for there help during my three-and-half year researches. I have learned a lot from you.

I would also like to acknowledge the support of my father Lixin Xu, my mother Dongli Zhang and other relatives that helped me through these years. I would not be able to keep motivated during the COVID times without your help.

Abstract

The world is witnessing unprecedented accumulation of solid wastes in the environment and landfills with well-documented ecological, environmental, health, and economic consequences. With population growth and rise in living standards, solid wastes generation will increase, making the issue more pressing. In addition, current practices of solid waste disposal are creating an immediate challenge and a long-term disaster-scale problem. The solid wastes comprises two main groups of materials: (i) fiber wastes (paper, food, wood, trimming, 61% of U.S. municipal solid waste) and (ii)uniquely challenging subset of plastic wastes (13%) that become a threat to global sustainability including dangers to marine and terrestrial wildlife. Thermal treatment can turn these high calorific value wastes into fuels that can be used in small-to-large power plants. However, there exist several hurdles: (i) huge heterogeneity of the wastes that would produce ununiform products; (ii) high chlorine content that is corrosive and its emission is strictly controlled; (iii) requires binder for compaction.

This work focused on two main aspects: (i) studying the properties of waste blends after torrefaction at various conditions; (ii) researching the dechlorination of wastes through torrefaction. The work started by studying the effect of torrefaction on different types of wastes and comparing the properties of the product to coal. It was found that the grinding characteristics and size distribution after grinding were similar to coal, with the heat content increased as the mass loss increased. And with the help of extrusion, the product has significantly higher uniformity, durability and water resistance. The results showed that torrefied wastes can be a drop-in-fuel in coal power generation facilities. During the study of torrefaction of wastes, it was observed that there existed synergistic effects between fiber and plastic wastes. In order to understand this interaction, synergy within the fiber wastes and between fiber and plastic wastes were further studied. A multi-consecutive reaction mechanism that focuses on solid products was developed for fiber waste thermal degradation. And further insights between fiber and plastic wastes during torrefaction were also investigated.

The study then focused on the dechlorination of wastes through torrefaction. A multi-consecutive reaction mechanism that focuses on gaseous products were developed for PVC thermal degradation. The kinetic parameters provided unique insight into the thermal degradation mechanism. The model was then validated by applying to different reactor design and sample sizes. The study of chlorine removal through torrefaction from waste with different chlorine levels was also carried out. It was found that despite of different chlorine levels, the torrefaction behaviors the materials were comparable, and their heat contents and chlorine removal efficiencies were also similarly correlated to torrefaction. The chlorine removal efficiency increased as mass loss increased, reaching an asymptotic value of ~80% at ~ 40% mass loss, while the remaining 20% of chlorine can be attributed to inorganic sources. The above studies could greatly help with the process design for treating wastes and turn them into fuels.

1 Introduction

The U.S. Environmental Protection Agency (EPA) has accelerated regulatory pressure on utilities burning pulverized coal by issuing carbon emission guidelines on June 18, 2014. (US-EPA, 2014). The EPA has proposed state by state goals to achieve CO2 emission reductions; 30% from the power sector as compared to CO2 emission levels in 2005 (US-EPA, 2015). The ultimate fate and form of the EPA proposed rule may not be known for some time until the rule-making process is complete but the past history of utility emissions regulation and Supreme Court decisions on EPA rule-making authority indicate a high probability that some form of CO2 regulation will be implemented (White, 2014). Internationally, the U.S. has announced the reduction of greenhouse gas emissions by 26-28% below 2005 levels by 2025 (Nakamura and Mufson, 2014).

Torrefied-biomass is a high-energy fuel that can be used in combustion, gasification, and pyrolysis, and is considered either fully or partially renewable and complies with the above EPA regulations (US-EPA, 2015). Kiel suggested the use of biomass for coal power plants as a renewable fuel (Kiel, 2011). Other potential users are suggested to produce bio-oil (De Rezende Pinho et al., 2017; Wang et al., 2016) and syngas producers (TRI, 2018).

Considerable amount of studies, pilot-scale plants, patents and commercial efforts have been devoted to torrefaction and torrefied materials. The entries "torrefaction" and "torrefied" in the title, shows 790 papers, 19 reviews, and 50 patents, between 1990 and 2017. The 50 patents comprise many technologies for torrefaction, most of which are based on mechanical mixing. This well-documented technology could be utilized to treat feedstocks and produce products with enhanced properties. Currently, solid waste accumulation with a significant amount being landfilled has become a global concern. For example, the amount of fiber and plastic wastes recovered in the U.S. per annum are 50.8 million tons and 33.25 million tons (US-EPA, 2014) respectively. If the torrefaction product is ~15% mass loss, these two waste streams together could, in principle, produce 71.4 million tons of biocoal.

Although torrefaction is well known for technological achievements, the technology has not yet materialized because of the following main reasons:

1. Inhomogeneity during the torrefaction process that yields non-uniform products.
2. The cost of woody biomass, the main feedstock used in torrefaction, is in the range $100-120/ton of feedstock for a ton of torrefied product (Bridgwater, 2018), which is economically prohibitive.
3. Chlorine is a major hazard that must be removed because (1) it is a hazardous pollutant with major health and environmental consequences, and (2) it is highly corrosive in boilers (Baxter et al., 1998). Chlorine has rather severe EPA emission standards; thus, it must be removed prior to being emitted through the stack (US-EPA, 2016).
4. There are inherent safety issues due to the high reactivity of the torrefied material (Arias et al., 2017). Safety issues are well documented (Stelte et al., 2016) and has not been resolved fully yet.

5. Densification is still a major issue, essential for safety, durability, and out-door product storage. The main hindrance is the use of binders that do not provide properties to the densified material to meet these requirements.

The conclusion is that the above-mentioned hindrances originate from the use of high cost feedstock and inappropriate binders. We propose to address these obstacles as follows: (i) the use of wastes as the feedstock, which is being collected and paid for by municipalities and industry can solve the cost problem; the cost of this feedstock in worst case scenario is zero and if joining a waste management company, it can be negative. Much of these wastes comprise high renewable content, which is considered to conform to renewable requirements (US-EPA, 2016). In Table 1.1 there are 12 waste streams that have been tested by MTU for torrefaction and found to yield outstanding material that can replace coal. Results of some of these attempts and favorable economics are described below in detail (Bar-Ziv and Saveliev, 2013; Klinger et al., 2013; 2014; 2015); (ii) the use of plastic waste is an enabler and a key in the torrefaction process, densification, product quality, durability, water resistance, safety, and storage. The features of plastic will be presented in detail in the following sections. Plastic seems to be the best binder that has ever been attempted for densification of torrefied materials (Auprakul et al., 2017; Garrido et al., 2014). (iii) the use of extrusion for densification, as opposed to pelletization (by ring dies or similar) (Adefisan et al., 2017), and various briquetting methods (Drozd et al., 2013). Extrusion can be used due to the plastic material in the blend that lowers significantly the viscosity and reduces significantly the densification energy. It also has an essential role in safety as it densified the blend to its intrinsic density, hence reducing porosity to zero, such that the densified material does not show reactivity at ambient temperature; this point had to be further investigated

Table 1.1. MTU's experience in torrefaction.

Feedstock	**Feedstock**
Energy Crops	13. Wheat
1. Arundo Donax	14. Rice husk
2. Miscanthus	**Wastes**
3. Switch Grass	15. C&D Waste
4. 3 energy crops blend	16. MSW
5. Sorghum	17. Compost
Woody Biomass	18. Scrap tire
6. Forest Residues	19. Polyethylene
7. Pine	20. Polypropylene
8. Hybrid poplar	21. Animal manure
9. Tulip poplar	22. Sewage sludge
10. Pinion Juniper	23. Fiber waste
11. Sawdust	24. Plastic waste
Ag Residues	25. MRF/RDF
12. Corn stover	26. Fiber-plastic blend

The use of wastes (for example, municipal solid wastes – MSW – or industrial manufacturing residuals – fiber and plastic blends) can be the answer to the deployment of this technology as tipping fees are paid for the waste destined for landfill. U.S. wastes possess substantial energy content that can be utilized for energy and power (US-EIA, 2010). Wastes, as a feedstock in torrefaction, has been suggested by Bar-Ziv et al. (Bar-Ziv and Saveliev, 2013; Bar-Ziv et al., 2016) and others, using regular torrefaction (Yuan et al., 2015), wet torrefaction (Mumin et al., 2017), and microwave torrefaction (Iroba et al., 2017; Iroba et al., 2017). However, some difficulties have been recognized while using waste for torrefaction because of difficulties in conveying, pretreatment and potential emissions. Other hurdles were also identified while using waste feedstocks in torrefaction: (i) inconsistency in feedstock, (ii) possibility of high Cl, S, and N content, (iii) binders required for compaction of torrefied biomass (Bar-Ziv and Saveliev, 2013; Bar-Ziv et al., 2016), (iv) high moisture content in MSW and the like, and (v) high contaminant content that leads to emissions issues.

The EPA regulatory actions (US-EPA, 2014; US-EPA, 2015) regarding the use of alternative fuels raise the likelihood that torrefied waste will find a market to replace pulverized coal in energy production. One other recent development affecting the market for torrefied biomass from MSW was a memorandum from the EPA's Office of Air and Radiation addressing the framework for determining the carbon neutrality of biomass (McCabe, 2014).

Table 1.2. U.S. wastes, quantities and heat content.

Waste type	**Qty, in 1000 ton (EPA, 2016)**	**%**	**Heat content (db), MJ/kg**	**Source**
Paper	19,470	18%	14.7	Demirbas, 1999
Plastic	25,100	23%	35.7	Themelis and Mussche, 2014
Rubber and leather	4,150	4%	36.5	Unapumnuk et al., 2006
Textile	10,000	9%	17	Miranda et al., 2007
Wood	11,010	10%	15-16	McKendry, 2002
Food	29,319	27%	15-16	US-EIA, 2010
Yard trimmings	10,790	10%	15-16	McKendry, 2002
Total	109,839	100%		

There is a significant amount of waste in the U.S., which is being disposed of in landfills, which can be used as an energy source. Table 1.2 summarizes the various wastes, totaling ~110 million tons per year, as well as their calorific values. This significant amount, if torrefied, can replace coal and be considered renewable and clean fuel. From an energy perspective, except plastic wastes with very high heat content ~ 36 MJ/kg, the rest have heat values in the range 15-17 MJ/kg. The weighted average heat content in U.S. waste is ~21 MJ/kg, which is comparable to that of Powder River Basin (PRB) coal that has a heat content of 17-19 MJ/kg (Luppens, 2011). This indicates that 1 dry ton of U.S. waste can

replace 1 ton of PRB coal. With current coal consumption of ~650,000 tons/d of coal in the US (with over 50% PRB coal) (US-EIA, 2018), U.S. waste could replace well over 15% of the U.S. coal.

The main objective of this work is studying and evaluating a novel torrefaction-extrusion process that uses biomass and fiber wastes blended with plastic waste, to produce clean, renewable, and affordable and drop-in fuel for bioenergy and biopower. Specifically, the study deals with wastes blends from paper/carton (wood fibers) and plastics. As such, the torrefied fuel should be shown to match the characteristics and properties of coals.

The specific objectives of this Ph.D. thesis are:

1. Study the torrefaction process of fiber and plastic wastes and how the extent of torrefaction affects the product properties, such as grindability, heat content, and removal of undesired materials (chlorine).
2. Study the effect of extent of torrefaction as well as extrusion process parameters on the properties of densified torrefied materials, specifically blends of plastics with fibers and biomass.

1.1 Works Cited

Auprakul, U., Promwungkwa, A., Tippayawong, N., & Chaiklangmuang, S. (2014). Densified fuels from mixed plastic wastes and corn stover. In *Advanced Materials Research* (Vol. 931, pp. 1117-1121). Trans Tech Publications.

Bar-Ziv, E., and Saveliev, R. (2013). Torrefied-Biomass from Municipal Solid Waste for Power Production. ASME-Power2013-98044.

Bar-Ziv, E., Klinger, J., Zinchik, S., and Donepudi, Y. (2016). Torrefied-Biomass from Municipal Solid Waste for Power Production. ASME-PowerEnergy2016-59179.

Bates, R.B., and Ghoniem, A.F. (2013). Biomass torrefaction: Modeling of reaction thermochemistry. Bioresource Technology 134, 331-340.

Baxter, L. L., Miles, T. R., Miles Jr, T. R., Jenkins, B. M., Milne, T., Dayton, D., ... & Oden, L. L. (1998). The behavior of inorganic material in biomass-fired power boilers: field and laboratory experiences. *Fuel processing technology*, *54*(1-3), 47-78.

Bridgwater, A. V. (2018); Techno-economic and uncertainty analysis of Biomass to Liquid (BTL) systems for transport fuel production. *Renewable and Sustainable Energy Reviews*, *88*, 160-175.

Demirbas, A. (1999). Physical properties of briquettes from waste paper and wheat straw mixtures. Energy Conversion & Management 40, 437-445.

Garrido, M. A., Conesa, J. A., & Garcia, M. D. (2017). Characterization and production of fuel briquettes made from biomass and plastic wastes. *Energies*, 10(7), 850.

Iroba, K.L., Baik, O.D., and Tabil, L.G. (2017). Torrefaction of biomass from municipal solid waste fractions I: Temperature profiles, moisture content, energy

consumption, mass yield, and thermochemical properties. Biomass and Bioenergy 106, 8-20. Biomass and Bioenergy 105 (2017a) 320-330.

Kiel, J. (2011). Torrefaction for upgrading biomass into commodity fuel. In Status and ECN Technology Development. EUBIONET III Workshop, Espoo, Finland (Vol. 15).

Luppens, J.A. (2011), A critical review of published coal quality data from the southwestern part of the Powder River Basin, Wyoming: U.S. Geological Survey Open-File Report 2011-1148, 23.

McKendry, P. (2002). Energy production from biomass (part 2): conversion technologies. Bioresource Technology Volume 83, Issue 1, May 2002, 47-54.

Mumin, G.G., Prawisudha, P., Zaini, I.N., Aziz, M., and Pasek, A.D. (2017). Municipal solid waste processing and separation employing wet torrefaction for alternative fuel production and aluminum reclamation. Waste Management 67, 106-120.

Nakamura, D., and Mufson, S. (2014). China, U.S. Agree to Limit Greenhouse Gases. The Washington Post, 12.

Themelis, N.J., and Mussche, C. (2014). 2014 Energy and Economic Value of Municipal Solid Waste (MSW), Including Non-Recycled Plastics (NRP), Currently Landfilled in the Fifty States.

TRI, ThermoChem Recovery International, (2018). "Reforming gasification," 2017. http://tri-inc.net/steam-reforming-gasification/.

US-EIA, U.S. Energy Information Administration, based on U.S. Environmental Protection Agency. (2010) 2010 MSW Facts and Figures Factsheet. Retrieved from https://www.eia.gov/todayinenergy/detail.php?id=8010.

US-EPA, Environmental Protection Agency "Carbon Pollution Emission Guidelines for Existing Stationary Sources: Electric Utility Generating Units." Federal Register. Environmental Protection Agency, 18 June 2014. Web. 30 Nov. 2014.

US-EPA, Environmental Protection Agency, 2015, "Carbon pollution emission guidelines for existing stationary sources: electric utility generation units," EPA-HQ-OAR-2013-0602, 1560 pp., published 08-03-2015.

US-EPA, Environmental Protection Agency, "Assessing Trends in Material Generation, Recycling, Composting, Combustion with Energy Recovery and Landfilling in the United States," Report EPA 530-R-17-01, 91 pp., November 2016.

US-EPA. (2018). Advancing Sustainable Materials Management: 2015 Fact Sheet Assessing Trends in Material Generation, Recycling, Composting, Combustion with Energy Recovery and Landfilling in the United States.

Wang, C., Li, M., and Fang, Y. (2016). Coprocessing of Catalytic-Pyrolysis-Derived Bio-Oil with VGO in a Pilot-Scale FCC Riser. Ind. Eng. Chem. Res. 55, 3525−3534.

2 Properties of Torrefied U.S. Waste Blends

This section is based on the following peer-reviewed paper:

Z. Xu, S. Zinchik, SS. Kolapkar, E. Bar-Ziv, T. Hansen, D. Conn, AG. McDonald. 2018. Properties of torrefied US Waste blends. Frontiers in Energy Research 6, 65. doi.org/10.3389/fenrg.2018.00065

2.1 Abstract

Power generation facilities in the U.S. are looking for a potential renewable fuel that is sustainable, low-cost, complies with environmental regulation standards and is a drop-in fuel in the existing infrastructure. Although torrefied woody biomass, meets most of these requirements, its high cost, due to the use of woody biomass, prevented its commercialization. Industrial waste blends are suitable for torrefaction and are an economically viable solution, this may prolong the life of some of the existing coal power plants and provide a renewable (partially) solid fuel to be used in for power production applications. We focus on the torrefaction dynamics of the paper fiber-plastic waste blend of 60% fiber and 40% plastic and the characterization of its torrefied product as a function of reaction extent (mass loss). Two forms of the blend are used, one is un-densified and the other is in the form of pellets with three times the density of the un-densified material. Torrefaction of these blends was conducted at 300°C in the mass loss range of 0-51%. The torrefied product was characterized by moisture content, grindability, particle size distribution, energy content, molecular functional structure, and chlorine content. It was shown that although torrefaction dynamics of the two forms differs significantly from each other, their properties and composition depend on the mass loss. Fiber content was shown to decrease relative to plastic upon the extent of torrefaction. Further, the torrefied product demonstrates a similar grinding behavior to Powder River Basin (PRB) coal. Upon grinding, the fiber was concentrated in the smaller size fractions, while the plastic was concentrated in the larger size fractions.

2.2 Introduction

The U.S. Environmental Protection Agency (EPA) has accelerated regulatory pressure on utilities burning pulverized coal by issuing carbon emission guidelines on June 18, 2014. (EPA, 2014). The EPA has proposed state by state goals to achieve CO2 emission reductions; 30% from the power sector as compared to CO2 emission levels in 2005 (EPA, 2015). The ultimate fate and form of the EPA proposed rule may not be known for some time until the rule-making process is complete but the past history of utility emissions regulation and Supreme Court decisions on EPA rule-making authority indicate a high probability that some form of CO2 regulation will be implemented (White, 2014). Internationally, the U.S. has announced the reduction of greenhouse gas emissions by 26-28% below 2005 levels by 2025 (Nakamura and Mufson, 2014).

Torrefied biomass is a high-energy fuel that can be used in combustion, gasification, and pyrolysis, and is considered either fully or partially renewable and complies with the above EPA regulations (EPA, 2015). Kiel (Kiel, 2012) suggested the use of biomass for coal

power plants. Potential users of torrefied biomass are suggested for refineries to produce bio-oil (De Rezende Pinho et al., 2017; Wang et al., 2016) and syngas producers (TRI, 2018). A considerable amount of studies, pilot-scale plants, patents and commercial efforts have been devoted to torrefaction and torrefied materials. The entries "torrefaction" and "torrefied" in the title, shows 790 papers, 19 reviews, and 50 patents, between 1990 and 2017. The 50 patents comprise many technologies for torrefaction, most of which are based on mechanical mixing. Although torrefaction technology is well developed, it has not yet moved to the commercial market. The consensus is that the main hindrance to the commercialization of this technology is the use of high-cost woody biomass as a feedstock (Kumar et al., 2017; Radics et al., 2017).

The use of wastes (for example, municipal solid wastes – MSW – or industrial manufacturing residuals – fiber and plastic blends) can be the answer to the deployment of this technology as tipping fees are paid for the waste destined for landfill. U.S. wastes possess substantial energy content that can be utilized for energy and power (US-EIA, 2010). Wastes, as a feedstock in torrefaction, has been suggested by Bar-Ziv et al. (Bar-Ziv and Saveliev, 2013; Bar-Ziv et al., 2016) and others, using regular torrefaction (Yuan et al., 2015), wet torrefaction (Mumin et al., 2017), and microwave torrefaction (Iroba et al., 2017; Iroba et al., 2017). Some difficulties have been recognized while using waste for torrefaction because of difficulties in conveying, pretreatment and potential emissions. Other hurdles were also identified while using waste feedstocks in torrefaction: (i) inconsistency in feedstock, (ii) possibility of high Cl, S, and N content, (iii) binders required for compaction of torrefied biomass (Bar-Ziv and Saveliev, 2013; Bar-Ziv et al., 2016), (iv) high moisture content in MSW and the like, and (v) high contaminant content that leads to emissions issues.

The EPA regulatory actions (EPA, 2014; EPA, 2015) regarding the use of alternative fuels raise the likelihood that torrefied waste will find a market to replace pulverized coal in energy production. One other recent development affecting the market for torrefied biomass from MSW was a memorandum from the EPA's Office of Air and Radiation addressing the framework for determining the carbon neutrality of biomass (McCabe, 2014).

There is a significant amount of waste in the U.S., which is being disposed of in landfills, that can be used as an energy source. Table 2.1 summarizes the various wastes, totaling ~110,000 ton per year, as well as their calorific values. This significant amount, if torrefied, can replace coal and be considered renewable and clean fuel. From an energy perspective, except plastic wastes with very high heat content ~ 36 MJ/kg, the rest have heat values in the range 15-17 MJ/kg. The weighted average heat content in U.S. waste is ~21 MJ/kg, which is comparable to that of Powder River Basin (PRB) coal that has a heat content of ~ 17 to 19 MJ/kg (Luppens, 2011). This indicates that 1 dry ton of U.S. waste can replace 1 ton of PRB coal. With current coal consumption of ~650,000 tons/d of coal in the US (with over 50% PRB coal) (US-EIA, 2018), U.S. waste could replace well over 15% of the U.S. coal.

Table 2.1. U.S. wastes, quantities and heat content. *

Waste type	Quantity, in 1000 ton	%	Heat content (db), MJ/kg	Source
Paper	19,470	18%	14.7	Demirbas, 1999
Plastic	25,100	23%	35.7	Themelis and Mussche, 2014
Rubber and leather	4,150	4%	36.5	Unapumnuk et al., 2006
Textile	10,000	9%	17	Miranda et al., 2007
Wood	11,010	10%	15-16	McKendry, 2002
Food	29,319	27%	15-16	US-EIA, 2010
Yard trimmings	10,790	10%	15-16	McKendry, 2002
Total	109,839	100%	-	-

The present paper deals with torrefaction of certain U.S. wastes, including plastics, which can be converted into drop-in fuels as a replacement of coal in coal power plants. Specifically, the paper deals with wastes blends from the paper/carton (wood fibers) and plastics. As such, the torrefied fuel should be shown to match the characteristics and properties of coals.

2.3 Material and Methods

Convergen Energy (CE) developed a fuel, by sorting and blending feedstocks of fiber and plastic, removing metal and shredding down to 25 mm by 1 mm flakes by which waste blends of fibers (from paper, label matrix residuals, and laminated non-recyclable papers/plastics and the like) and plastics, become uniform, flowable and consistent, with a bulk density in the range 200-300 kg/m^3. CE also developed a pelletization process that produces pellets (12 mm OD and 50 mm long) that are rather uniform with a density of 750-800 kg/m^3 and bulk density of 400-450 kg/m^3. The binder for the CE palletization process was the plastic component in the blend.

2.3.1 Materials

CE characterized their product for over seven years with properties that showed rather consistent products. Table 2.2 shows the average properties of waste blends of 60% fiber with 40% plastics, with standard deviations of its product over a seven-year period. As seen, the properties in Table 2.2 are indicative of reproducible and consistent material. This material was the feedstock in the torrefaction process, both in un-densified and densified forms.

Table 2.2. Properties of CE material averaged over a seven-year period.

Proximate	Values	Ash	Values, %	Other	Values, ppm	Fusion Temp	Value °C
Moisture, %	3.3±0.5	SiO2	33±18	Cl	1162±487	Reducing	
Ash, %	6.0±0.6	A2O3	27±11	F	75±75	Deformation	1,319
Volatiles, %	83.5±2.6	TiO2	7.2±3.4	Hg	0.01±0.01	Softening	1,359
Fixed Carbon, %	7.2±2.0	Fe2O3	0.9±0.9	Sn	2.9±0.9	Hemispherical	1,374
Sulfur, %	0.2±0.1	CaO	21±12	As	1.1±0.9	Fluid	1,396
HHV, MJ/kg	26.1±1.1	MgO	3.0±3.0	Be	0.3±0.8	Oxidizing	
Ultimate	Values, %	K2O	0.6±0.4	Cr	2.2±1.2	Deformation	1,327
Carbon	55.4±1.8	Na2O	1.6±0.7	Co	0.21±0.16	Softening	1,369
Hydrogen	7.9±0.3	MnO2	0.02±0.01	Pb	1.1±1.4	Hemispherical	1,384
Nitrogen	0.3±0.1	BaO	0.2±0.2	Ni	0.81±0.57	Fluid	1,406
Oxygen	27.1±1.6	Others	2.8±1.4	Se	1.5±1.8		

In this study, both the un-densified as well as the densified material (pellets indicated above) were used. Figure 2.1 shows both forms before torrefaction, used in this study: (a) un-densified CE material; and (b) CE pellets.

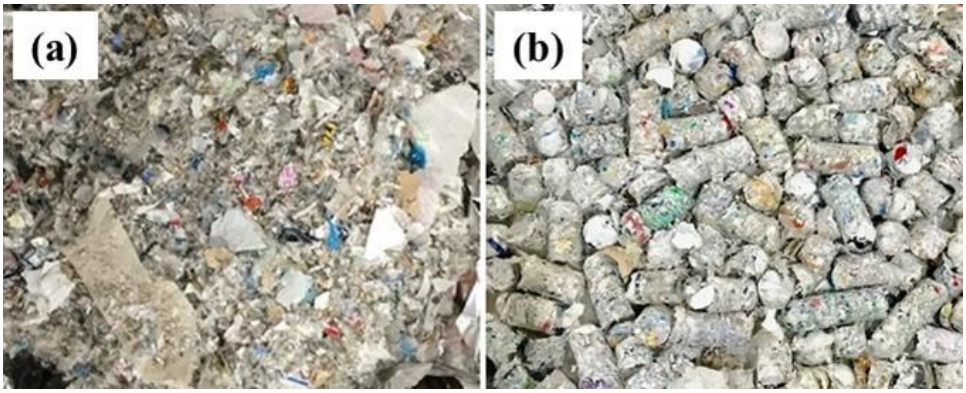

Figure 2.1. (a) Un-densified CE material. (b) Densified (pellets) CE material.

2.3.2 Waste and Product Characterization

The properties depicted in Table 2.2 are part of the routine characterization of CE products, both before and after pelletization. Other characterization methods are as follows. All data presented in this paper were averaged over 3-5 data points.

2.3.2.1 Grinding

Grindability is an important characteristic that has an essential impact on the applicability of torrefied material as a drop-in fuel in coal power plants. Typically, coal power plant use pulverizers of type MPS 89 (Storm, 2009), however, for the grinding tests, blade grinders

(that operate at 24,000 rpm) were used. The grinding results presented in this paper are for comparison purposes. Two blade grinders were used in this study: Model CIT-FW-800 and Model CIT-FW-200. An on-line power meter - Wattsup pro was used for power vs. time measurements. Also, note that CE material was torrefied in both non-densified and densified (pellets) forms and grinding tests were carried out for both materials. Two types of grinding tests were performed as follows:

1. A 100-200 g torrefied sample (either un-densified or pellet form) was placed in the grinder, which was continuously operated for up to 120 s time interval (to avoid damage to the motor); the power was measured continuously during the experiment. If necessary, grinding was repeated in a similar manner for a total of 1800 s.
2. A 100-200 g torrefied sample was placed in the grinder and operated for short time intervals - 15-30 s. After each grinding run (time interval) the pulverized material was sifted to seven sizes, in the range of 150-2,000 µm, after which all size fractions were mixed and were further pulverized for another time interval. This process was repeated until the size fractions reached asymptotic values.

In both methods, the power was measured with and without the sample in the grinder. The power without the sample was subtracted from that with the sample, which provided the net power required to grind the sample. Figure 2.2 shows a typical plot of power vs. time with and without a sample (in this case, 200 g of a torrefied non-densified material at 21.4% mass loss during torrefaction). Note that the startup is accompanied by an overshoot, in both cases.

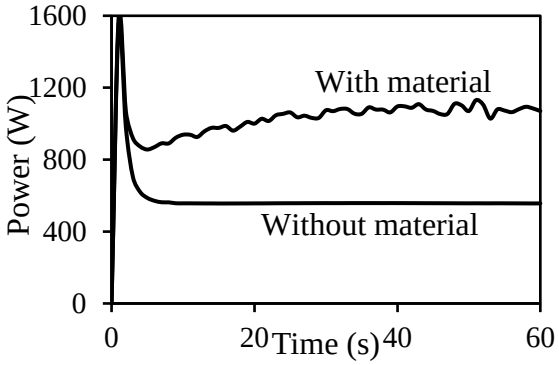

Figure 2.2. Examples of power vs. time traces of the grinder without material and with 200 g torrefied un-densified material.

2.3.2.2 Sifting

Sifting of the pulverized material was carried out in a W.S Tyler, RX-86 model sieve shaker. Seven size fractions were obtained with screen sizes of 75 µm, 150 µm, 180 µm, 250 µm, 425µm, and 850 µm. At each time interval after grinding, all the material inside the grinder was taken out and put into the shaker to sift for an hour. The weights of all the screens before and after the sifting were measured. The difference in these weights provided the sample weight of each size fractions.

2.3.2.3 Heat Content

Heat content was measured by Parr 6100 Compensated Jacket Calorimeter, where 1 g samples were placed inside sampling bowl/tray, and the sample was connected to the electric circuit using fuse string. This setup was put into a bomb and then filled with oxygen. The bomb was then put into a bucket with 2,000 ±0.5 g of distilled water. The process involved the ignition of the sample using an ignition circuit and subsequent measurement of temperature difference after the burning of the measured sample. The heating value was displayed by the calorimeter based on the calibration and temperature difference.

2.3.2.4 Moisture Content

Moisture content was measured using HFT-1000 moisture analyzer. Around 1 g of sample was put into the analyzer. After starting the analysis, the heating coil would heat up and the moisture inside the material would volatilize. The analyzer would show the moisture content by measuring the difference of the weight before and after the experiment. Moisture content was measured before and after torrefaction. The values were rather consistent before torrefaction moisture was in range 2-3% and after torrefaction, 0%.

2.3.2.5 Density Measurements

Density measurement of pellets was done using a scale (model A&D HR-60) with a readability of 0.0001 g. The Archimedes' principle/buoyancy method was used for density measurement. A simple stand with suspended metal wire setup was used to dip the pellet in water. The procedure followed was as below:

1. The pellet was placed on a scale and dry weight, *w*, was noted.
2. A beaker filled with a set level of distilled water was placed on the scale and tared zero.
3. The stand and wire setup were placed next to scale such that some part of wire dipped in the water. The scaled was tared zeroed again.
4. The sample was attached to a wire and the sample was dipped in water. Care was taken that entire sample dipped in well and did not touch the bottom of the beaker. The reading with the suspended sample, *w*s, was noted.
5. The density was obtained from the ratio of suspended sample weight, ws and dry weight w.

2.3.2.6 FTIR

FTIR spectra were obtained on (i) 20 randomly selected pieces of mixed waste and (ii) screened fractions of the torrefied material (in triplicate) using a Nicolet-iS5 FTIR spectrometer, 64 scans, with an attenuated total reflectance accessory (ZnSe crystal, iD5) and data analyzed and averaged with the OMNIC v9.8 software and Aldrich, Hummel, and Nicolet spectral libraries. Carbonyl index (CI), cellulose index (CeI), and hydroxyl index (HI) were calculated as the ratio of the band intensity (absorbance) at 1720 cm^{-1}, 1024 cm^{-1}, and 3342 cm^{-1}, respectively, to the band 2916 cm^{-1} for the -CH_2- groups (Wei et al., 2013).

2.4 Experiments

2.4.1 Torrefaction

Torrefaction experiments were carried out by placing a sample, motionless, at the center of a convection furnace, Lindenberg/Blue type BF51828C-1, with flow of inert gas, either N_2 or CO_2 to avoid oxidation of the material. For un-densified CE material, typically samples of 150 g were placed in a thin aluminum foil at the furnace center, with residence time in the range 1-40 min. For CE pellets, sample size was ~300 g and torrefaction residence time was between 3 to 120 min.

2.4.2 Removal of Soluble Minerals

Soluble minerals in the torrefied material were removed by a method developed by Donepudi (Donepudi, 2017). In the present study, a 7.5 g torrefied sample was placed in a high shear mixer of Charles Ross & Son Company (Model HSM- 100LSK-1) where water was added to the sample in 20:1 ratio by weight and the mixer was rotated at ~7,000 rpm for 5min. A suspension generated was filtered by 11μm porosity paper filter (Whatman 1001-0155 quantitative filter paper circles), followed by another filtration by 1.6μm porosity paper filter (Whatman 1820-047 glass microfiber binder free filter). The two filtration processes produced a transparent solution with no apparent suspend particles or colloids. The aqueous solution was measured for chloride as described above.

2.5 Results

2.5.1 Torrefaction

As mentioned, all current torrefaction experiments were carried out by introducing un-densified material and pellets in a convective furnace at 300 ^{o}C, with the initial temperature of the particle, T_o, at ambient temperature. The material was placed in the furnace center and was kept stationary. In this case, the particle was heated by heat transported from the hot walls at temperature (T_w) to the particle surface by convection; the heat was then transported into the particle by conduction. Numerous torrefaction experiments were carried out for pellets as well as un-densified material. In both cases, the results show clear trends, with a delay in the onset of mass loss followed by an increase in the mass loss with time. The dynamic behavior in the two cases differed significantly from each other; for the un-densified material, the mass loss starts at around 3 min, whereas for the pellets, it starts at around 9 min. Further, for the un-densified material, mass loss increase with time was faster compared to pellets. This behavior was indicative of the heat-transfer-chemical-reaction system. To determine the regime that best fits the description of the system behavior, one should start with the analysis with Biot number (*Bi*) and thermal Thiele modulus (*M*); the former is related to the heating regime of the particle, and the latter relates to the propagation of the torrefaction reaction within the particle. The *Bi* and *M*, which are defined as:

$$Bi = \frac{h}{\lambda/L_c} \tag{2.1}$$

$$M = \frac{R^{\dagger}}{\lambda/(c_p L_c^2)} \tag{2.2}$$

where h is the convective heat transfer coefficient, λ is the particle thermal conductivity, L_c is the particle characteristic length, $R^{\dagger}$ is the torrefaction reaction rate within the particle, c_p is the particle heat capacity, and ρ is particle density.

The parameters required to determine *Bi* and *M* from Eqs. 2.1 and 2.2 are not easy to determine as the material is not well defined and therefore, can only provide an estimate. The value of heat transfer coefficient, *h*, was selected to be 10 (W/m^2-K) and was the closest to the flow conditions prevailing in the furnace (Incropera & DeWitt, 2002). The value for thermal conductivity, λ, varies between 0.15 (W/m-K) for PVC, to 0.38 (W/m-K) for polyethylene (Incropera & DeWitt, 2002; Patterson & Miers, 2010); for biomass and fibers the values range in 0.03-0.29 (W/m-K) (Mason, Darvell, Jones, Williams, 2016). A value of 0.2 (W/m-K) was selected which was an average of the above. Literature data on reaction rates of the material used were even more scattered than thermal conductivity, therefore they were measured by thermogravimetry in the furnace. The rate of mass loss of the CE material from both measurements at 300 ^{o}C was about 0.03%/s, where the material temperature has been equal to the wall temperature (T_w); using the density of each form to obtain a value of 0.2-0.3 (kg/m^3-s) for the un-densified material and 0.1-0.2 (kg/m^3-s) for the pellets. In this study, the density was 1,150 (kg/m^3) for the un-densified material and 850 (kg/m^3) for the pellets. Heat capacity was both taken from the literature (Incropera & DeWitt, 2002) and measured to yield an acceptable value of 1,600 (J/kg-K) (Donepudi, 2017). The characteristic lengths of the two forms were measured (very accurately for the pellets and rather scattered for the un-densified material).

Table 2.3 summarizes all properties required for the determination of *Bi* and *M*, yielding values for (i) *Bi* of ~0.1 for the un-densified material and ~0.35 for the pellets and (ii) *M* of ~0.01 for the un-densified material and ~0.08 for the pellets. The values for *Bi* in the range 0.1-0.35 indicate that the rate of heat transfer by convection from the furnace walls to the particle was lower than the rate of heat transfer into the particle. The values of *M* are in the range 0.01-0.08 which indicate that the reaction rate was significantly slower than the heat transfer into the particle, and the particles equilibrate its temperature faster than the reaction rate. This analysis indicates that the reaction propagation was controlled by the rate of heat transfer from the furnace walls to the particle surface, after which the particle temperature equilibrates instantly.

Table 2.3. Estimated values for the parameters to determine the Bi and M.

Parameter	Value	Source
h, W/m^2-K	10	Incropera and DeWitt, 2002
λ for CE material, W/m-K	0.2	Incropera and DeWitt, 2002
$R^{\dagger}$ for un-densified material, kg/m^3-s	0.3	Measured in current study
$R^{\dagger}$ for pellets, kg/m^3-s	0.2	Measured in current study
ρ for un-densified material, kg/m^3	1150	Measured in current study
ρ for pellets, kg/m^3	850	Measured in current study
c_p, J/kg-K	1600	Incropera and DeWitt, 2002 Donepudi, 2017
L_c thickness for un-densified material, m	0.002	Measured in current study
L_c diameter for pellets, m	0.007	Measured in current study
368Bi for un-densified material	0.1	Current result
Bi for pellets	0.35	Current result
M for un-densified material	0.01	Current result
M for pellets	0.08	Current result

Establishing that the torrefaction reaction rate was controlled by the heat transfer from the walls to the particle surface and that the particle temperature was uniform at all times, means that the reaction propagates with the rate of the ramp-up of the particle temperature. To calculate the particle temperature, the equation of the heat rate, *dQ(t)/dt*, from the walls to the particle surface was needed to be solved, which was equal to

$$\frac{dQ(t)}{dt} = hA[T_w - T_s(t)] \tag{2.3}$$

where Tw and Ts(t)=T(t) are wall and particle surface (or particle) temperatures, respectively. *Q(t)* is the heat required to increase the particle temperature, or

$$Q(t) = mc_p[T(t) - T_o] + mh_r \tag{2.4}$$

where m and c_p are particle mass and specific heat capacity, respectively, T_o is the particle core temperature, which is also equal to the initial temperature of the particle, and h_r is enthalpy of reaction.

It was a challenge to find values for h_r as the torrefied material was not well defined, it comprises fibers (mostly cellulose) and a large variety of plastic materials. Cellulose torrefaction in the 25-300°C temperature range starts as an endothermic reaction and continues as an exothermic reaction (Bates and Ghoniem, 2012). Enthalpies of reaction for plastic in the same temperature range were always positive and vary in the range (12.55-147.86 J/kg) (Zhao, Liu, & Zhang 2017), which is smaller than the value of $c_p(T-T_o)$ (~400 kJ/kg) in Eq. (2.4). Thus, for simplification, this term was ignored. Introducing Eq. (2.4), without h_r, into Eq. (2.3) and integration from T_w to *T(t)* yields

$$\frac{T_w - T(t)}{T_w - T_o} = e^{-\frac{t}{\tau}} \tag{2.5}$$

where τ is a characteristic time, defined as

$$\tau = \frac{mc_p}{hA} \tag{2.6}$$

For the pellets (cylinders), $\tau_{cyl}=d\rho c_p/4h$ (d is cylinder diameter, ρ is particle density) and for the un-densified material (slab) it is $\tau_{slab}=d\rho c_p/2h$ (d is slab thickness). Rearrangement of Eq. (2.5) yields

$$T^*(t) = 1 - (1 - \frac{T_o}{T_w})e^{-\frac{t}{\tau}} \tag{2.7}$$

T^* is defined as

$$T^*(t) = \frac{T(t)}{T_w} \tag{2.8}$$

To model the mass loss, the torrefaction reaction rate was assumed to be represented by a first-order reaction, which a rather common assumption in many torrefaction studies (Lédé, 2010; Funke, 2017), or

$$R^{\dagger} = \rho \frac{d\alpha(t)}{dt} = -\rho k \alpha(t) \tag{2.9}$$

where $\alpha = m/m_o$ is the ratio of mass-to-initial-mass, k is rate coefficient assumed to follow an Arrhenius behavior,

$$\rho k(T) = A^{\dagger} e^{\frac{-T_a}{T(t)}} \tag{2.10}$$

where $A^{\dagger}$ is a pre-exponential factor and T_a is a characteristic temperature equals $T_a = E_a/R$, E_a is activation energy and R is gas constant. Introducing Eq. (2.10) into Eq. (2.9) and integrating yields an expression for the mass loss, $1-\alpha$, equals

$$1 - \alpha = 1 - e^{-\int_0^t k dt} \tag{2.11}$$

The required values for determining τ, Eq. (2.6), for each case are given in Table 2.3. Introducing these values in Eq. (2.6) yields $\tau_{slab}=184$ (s) and $\tau_{cyl}= 475$ (s), the subscript *slab* is for the un-densified material and *cyl* is for the pellets. Using these values, the particle temperatures were calculated and presented in Figure 2.3.

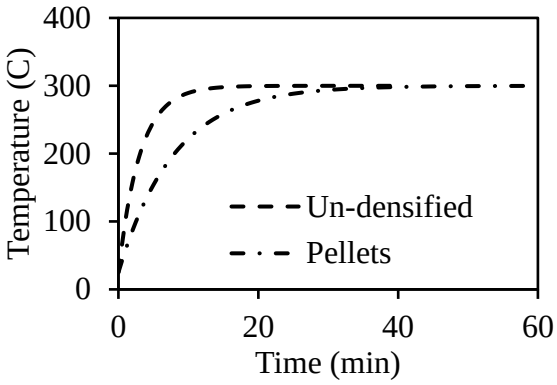

Figure 2.3. Temperature transient for the un-densified material and the pellets, using Eq. (2.7) and characteristic times of 160 (s) for the former and 475 (s) for the later

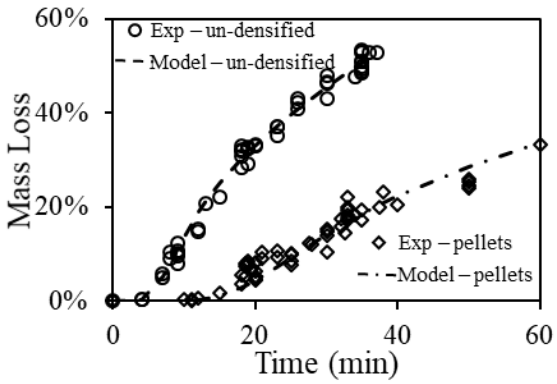

Figure 2.4. Experimental and modeled mass loss transients for the un-densified material and the pellets, using Eq. (2.11), the temperature transients of Figure 3 and fitting for T_a and A†.

As noted, the particle temperature in the un-densified case increases much faster than that of the pellets. Note from Figure 2.3 the temperature of the un-densified material reaches the wall temperature after 10 minutes, whereas for the pellets, it reaches the wall temperature after 30 minutes. The values for $(A^{\dagger}/\rho)$ and T_a were determined by fitting the model results for mass loss of Eq. (2.11), using the temperature transients of Eq. (2.7) (Figure 2.3), to the experimental results. Figure 2.4 shows the measured mass loss vs. time data (scattered results) and the model results using Eq. (2.11). Clearly, the model results yielded an excellent fit to the experimental data. The fitting process yielded for the un-densified material (slab) values of $(A^{\dagger}/\rho)_{slab}=1.23x10^{8}$ and $(T_a)_{slab}=15,200\ (K)$, and for the pellets (slab) values of $(A^{\dagger}/\rho)_{slab}=1.08x10^{8}$ and $(T_a)_{cyl}=15,800\ (K)$. The values of $A^{\dagger}/\rho$ and T_a for both forms of materials are very close to each other which is a strong indication that the model proposed here is representing the actual system behavior rather well.

2.5.2 Grinding Energy

The method of determining the grinding behavior has been explained above, with power that was continuously measured as a function of time during grinding for a given sample

weight. Numerous grinding tests were conducted, in the mass loss range 10-51%, for the two forms of torrefied materials: un-densified and pellets. All net power transient results portrayed distinct behavior that showed two characteristic times: short and much longer. Further, the net grinding power transients for all samples fitted a double exponential rise of the form:

$$P(t) = a_1\left(1 - e^{-\frac{t}{\tau_1}}\right) + a_2\left(1 - e^{-\frac{t}{\tau_2}}\right) \tag{2.12}$$

where τ_1 and τ_2 are the short and long characteristic times, respectively, and a_1 and a_2 are the asymptotic values of the power for the short and long characteristic times, respectively.

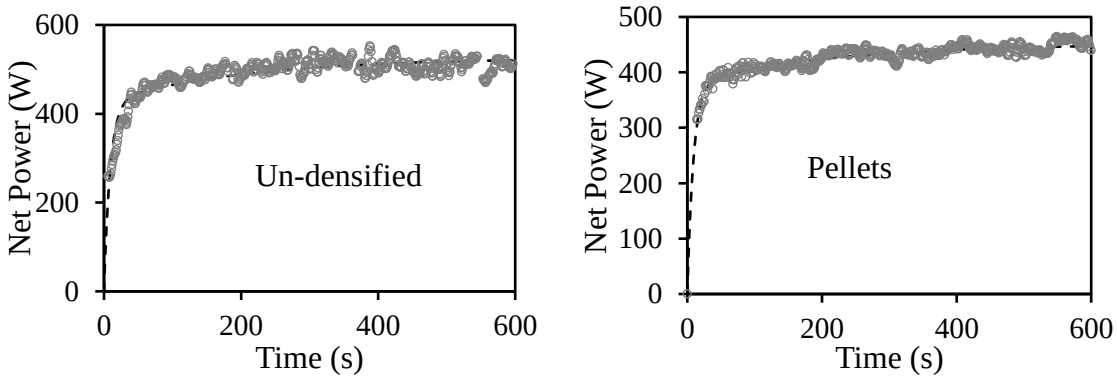

Figure 2.5. Symbols - measured net power vs. time of 200 g samples during grinding of torrefied CE, un-densified material and pellets. Dashed lines, fits of net power to Eq. (2.12) for the short characteristic time, τ_1=9.2s; and characteristic time τ_2=203.0 s.

Figure 2.5 shows typical examples of the measured (symbols) net power vs. time of two 200 g samples during grinding of torrefied CE, un-densified material and pellets and fits (dashed lines) of the net power to Eq. (2.12). In both cases, the short characteristic time was found τ_1=9.2 s and characteristic time τ_2=203 s.

All results for the torrefied samples and pellets in the range 10-51% mass loss were fitted to Eq. (2.12) to yield: for the short characteristic time of τ_1=*9.1±0.5* s, and for a long time, it was τ_2=*203±10* s with the respective asymptotic values of a_1=*378.1* W and a_2=73.0 W that varied within ±5%. To demonstrate the general behavior of torrefied samples**,** Figure 2.6 shows normalized net grinding power (by the asymptotic values) vs. time for the short time range, showing clearly identical behavior for all samples tested. The dashed line in the figure is a unity line that shows the normalized asymptotic value. The fact that the grinding dynamics is characterized by two characteristic times, that significantly differ from each other, indicates clearly that there are two materials. A detailed discussion of these two materials is given in the energy content section below.

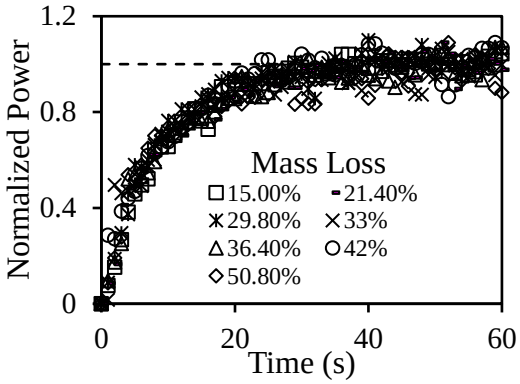

Figure 2.6. Normalized net grinding power vs time for torrefied material at various mass losses; with τ_g=9.1 (s)

As shown below, most of the material was ground and characteristic grinding energy can be determined by integrating the power over a certain time, which we selected as 1 τ_g, 2 τ_g, and 3 τ_g (or, 8.1 s, 16.2 s, 24.3 s). Table 2.4 shows the values of the specific grinding energy for three characteristic grinding times, *1* τ_g, *2* τ_g, *3* τ_g, where τ_g *=8.1* (s) in kJ/kg and is commonly used kWh/ton units. The values determined here are similar to values obtained in other studies at 8.23 kWh/ton (Khalsa, 2016). For comparison, grinding characteristics of PRB were also studied with power vs. time results for a 200 g PRB coal sample shown in Figure 2.7. A fit of these results with characteristic grinding time, τ_g, of 8.1 was done and specific grinding energies were calculated as shown in Table 2.4. The values for the specific grinding energies for the torrefied (un-densified) material are within the experimental uncertainty to those of the PRB coal and smaller than the energy required to grind the torrefied biomass (Wang et al., 2017).

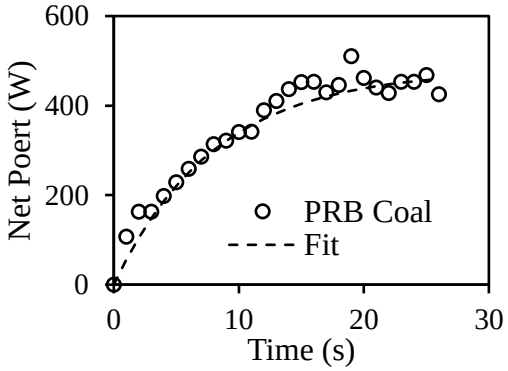

Figure 2.7. Grinding power vs. time for PRB coal with τ_g=9.1 (s).

Table 2.4. Specific grinding energy

	Integration time		
Grinding specific energy	1 τ_g	2 τ_g	3 τ_g
Torrefied un-densified material, kJ/kg	9.3±0.8	25.7±1.5	44.7±2.5
PRB coal, kJ/kg	8.6±0.5	24.3±1.4	42.4±2.4
Torrefied biomass, kJ/kg (kWh/ton)	N/A	N/A	43-54 (12-15)

2.5.3 Sizing Distribution

Many sifting experiments were done as a function of grinding time (or grinding energy), where the samples were sifted in size range 150 µm – 3 mm in 5 size fractions: x<150 µm, 150<x<250 µm, 250<x<425 µm, 425<x<850 µm, x>850 µm (x denotes size). It was observed that after reaching steady-state (i.e., the net grinding power reached an asymptotic value), the size distribution did not change anymore. Therefore, most of the sifting experiments were done after reaching grinding steady state. The initial sample was around 100 grams, and after grinding and sifting, there was ~ 1 gram of sample loss during the transferring procedure, which occurred only once during the process. Therefore, the loss was not more than 1%. Although there is scatter in the results, there are clear trends: the size fraction >850 µm decreased with mass loss and the size fraction <150 µm increased with mass loss and the size fractions in between did not change much with mass loss. Therefore, the behavior in two size fractions: under and above 850 µm was further investigated. Figure 2.8 shows the size fraction as a function of mass loss for the torrefied un-densified material and pellets for these two size fractions. It is interesting to note that for each size fraction, the dependence on mass loss is rather similar (the line is a fit to a straight line). For the size under 850 µm, its fraction starts at 82% for 4.5% mass loss and reaches almost 100% at 51% mass loss, the size fraction above 850 µm balances the smaller size fraction.

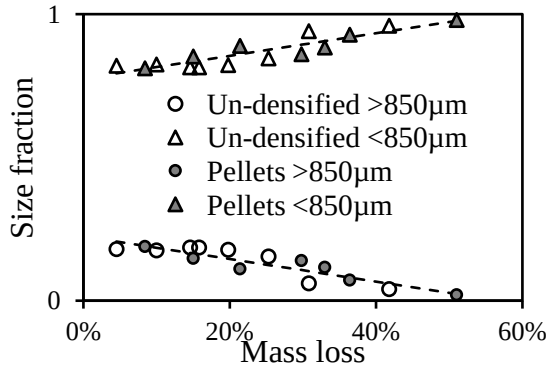

Figure 2.8. Size fraction for the torrefied un-densified material and pellets vs. mass loss for size fractions under and above 850 µm.

Table 2.5 shows fraction<74 µm of pulverized torrefied material at various mass losses. The table indicates that above 8.4% mass loss, after grinding the fraction of <74 µm is >70%, which is consistent with of the typical coal power plant requirements (Helble, Srinivasachar & Boni 1990).

Table 2.5. Fraction <74 µm of torrefied material in various mass losses

Mass loss	Fraction <74 µm
8.4%	67.0%
15.0%	73.9%
21.4%	77.3%
33.0%	77.5%
36.4%	89.2%
51.0%	95.4%

2.5.4 FTIR Spectroscopic Characterization

The CE waste mix plus fiber (20 random pieces selected) was analyzed by FTIR spectroscopy to determine their chemical identity with spectra library matching. The mix was shown to be comprised of three cellulose/paper, three polypropylene (PP), three polyethylene (PE), four polyethylene terephthalate (PET), silicone, three cellulose/silicone mix, two paper/acrylate mix, and one nylon samples. A composite FTIR spectrum is shown in Figure 2.9a and shows the major bands associated with PE, PP, PET, and paper. No characteristic bands at 610 cm^{-1} (C-Cl stretch) and 1425 cm^{-1} (C-H_2 bending) were observed for polyvinylchloride (Krimm, 1963).

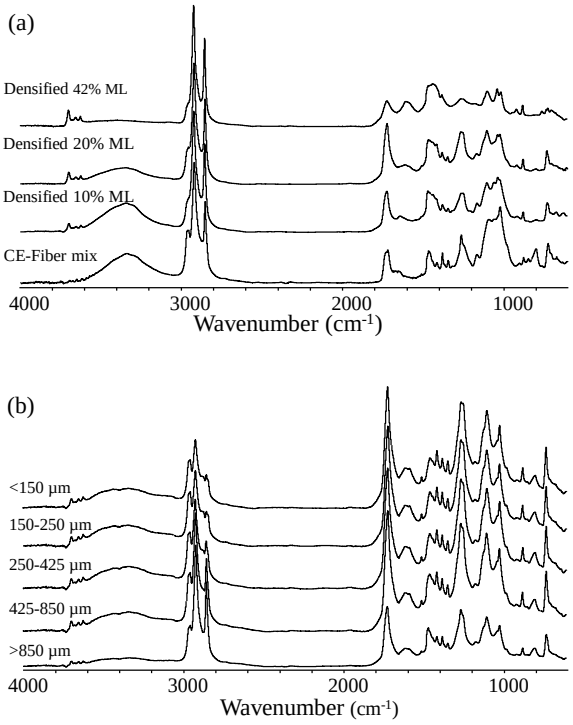

Figure 2.9. FTIR spectra of (a) CE-fiber mix and ground/screened (425-850 µm) torrefied (10, 20 and 42% mass loss) densified material and (b) ground/screened (<150 µm, 150-250 µm, 250-425 µm, 425-850 µm, and >850 µm) un-densified torrefied (30% mass loss) material

The major chemical changes that occurred upon torrefaction on densified and un-densified material and subsequent particle screening (<150 µm, 150<x<250 µm, 250<x<425 µm, 425<x<850 µm, and >850 µm) after grinding were also monitored by FTIR spectroscopy. The spectra for the ground screened 425<x<850 µm fraction for the densified torrefied (10, 20 and 42% mass loss) material as well as the CE-fiber mix are shown in Figure 2.9a. The spectra for the ground screened fractions for the un-densified torrefied (30% mass loss) material are shown in Figure 2.9b. Specific spectral bands can provide information on specific chemical changes that occur during thermal treatment (Balogun, Sotoudehniakarani, McDonald, 2017). All the samples had C-H stretching bands at assigned to methyl (2960 cm^{-1} and 2870 cm^{-1}) and methylene (2916 cm^{-1} and 2850 cm^{-1}) groups mainly associated with PP and PE plastic (Mayo, 2004a). In the ground screened torrefied material, plastic was generally concentrated in the larger sized fractions (425<x<850 µm and >850 µm) (Figure 2.9b). The O-H stretching band 3100-3600 cm^{-1} was present in all samples and progressively decreased in intensity upon the extent of torrefaction due to dehydration reactions (Wang et al. 2014) (Figure 2.9b). A broad carbonyl (C=O) band at 1690-1750 cm^{-1} was observed and assigned to mainly an ester in linkage in PET and acrylate and an amide linkage in nylon (Mayo, 2004b). A small band at 1505 cm^{-1} was assigned to lignin from paper (Faix, 1992). The spectral region between 1000 and 1070 cm^{-1} has been assigned to C–O stretching in wood cellulose and hemicellulose and decreased in intensity with torrefaction mass loss (Pandey, 1999). All samples were shown to have cis- and trans-vinylene bands at 727 cm^{-1} and 974 cm^{-1}, respectively (Miller, 2004).

The relative changes in carbonyl, cellulose and hydroxyl content to methylene groups (plastic) that occurred during torrefaction were examined by calculating CI, CeI and HI, respectively (Figure 2.10). Low values of CI, CeI, and HI means that there was a higher level of polyolefin plastic in the material. The CI generally decreased for all torrefied samples with an increase in particle size (from <150 µm to 425<x<850 µm), except for the >850 µm fraction (Figure 2.10a)

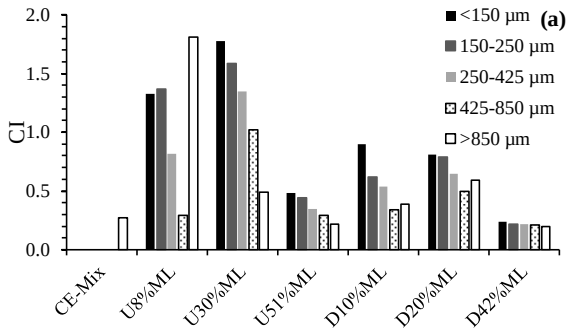

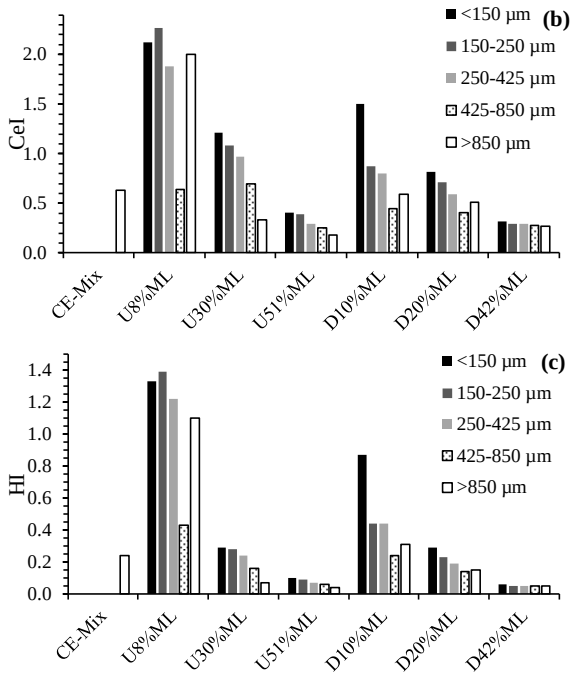

Figure 2.10. Plots showing changes in (a) carbonyl index (CI), (b) cellulose index (CeI), and (c) hydroxyl index (HI) for ground screened fractions (<150 µm, 150<x<250 µm, 250<x<425 µm, 425<x<850 µm, and >850 µm) of torrefied densified (D) and un-densified (U) material

For example, in the 30% mass loss torrefied material the CI decreased from 1.78 to 0.49 going from <150 µm to >850 µm particle size. For the low to moderate level of torrefaction (8-20% mass loss) the >850 µm fraction the higher CI values could be associated with higher levels of PET plastic. Furthermore, the CI levels were also shown to decrease, associated with cleavage of the ester linkages in PET/acrylates and removal of the volatile degradation products (Cepeliogullar and Putun, 2014), with the extent of torrefaction. Generally, for both CeI (Figure 2.10b) and HI (Figure 2.10c) decreased for all torrefied materials as screened particle size increased (<150 µm to >850 µm), suggesting that the cellulose fiber was mainly in the finer screened fractions. For example, in the 30% mass loss torrefied material the CeI and HI respectively decreased from 1.21 to 0.33 and 0.29 to 0.07 going from <150 µm to >850 µm particle size. Again, at low-moderate torrefaction levels (8-20% mass loss), the CeI and HI levels were high, suggesting that undegraded paper fragments were collected in the >850 µm fraction. Moreover, Both CeI and HI were shown to decrease as torrefaction severity increased. These findings support that the cellulose content decreased relative to plastic with the extent of torrefaction as a result of dehydration and degradation reactions (Wang et al. 2014).

2.5.5 Energy Content

The energy content was originally measured for un-sifted pulverized samples; however, it was discovered that scooping a sample of 1 g for the heat content test from a 200 g of the pulverized material gave very large scatter in the measured value. This was because the

pulverized material has a large size distribution (as observed above) and the scooping did not necessarily give uniform size distribution. Therefore, it was decided to measure the heat content for five size fractions: x<150 µm, 150<x<250 µm, 250<x<425 µm, 425<x<850 µm, and x>850 µm separately. Although the heat content for all sifted samples in these size fractions, for the sake of brevity heat content was shown for the following consolidated fractions: x<150 µm, 150<x<850 µm, x>850 µm, and the calculated total heat content (from the fraction and heat content for each fraction). Heat content results presented here are the dry- ash-free basis.

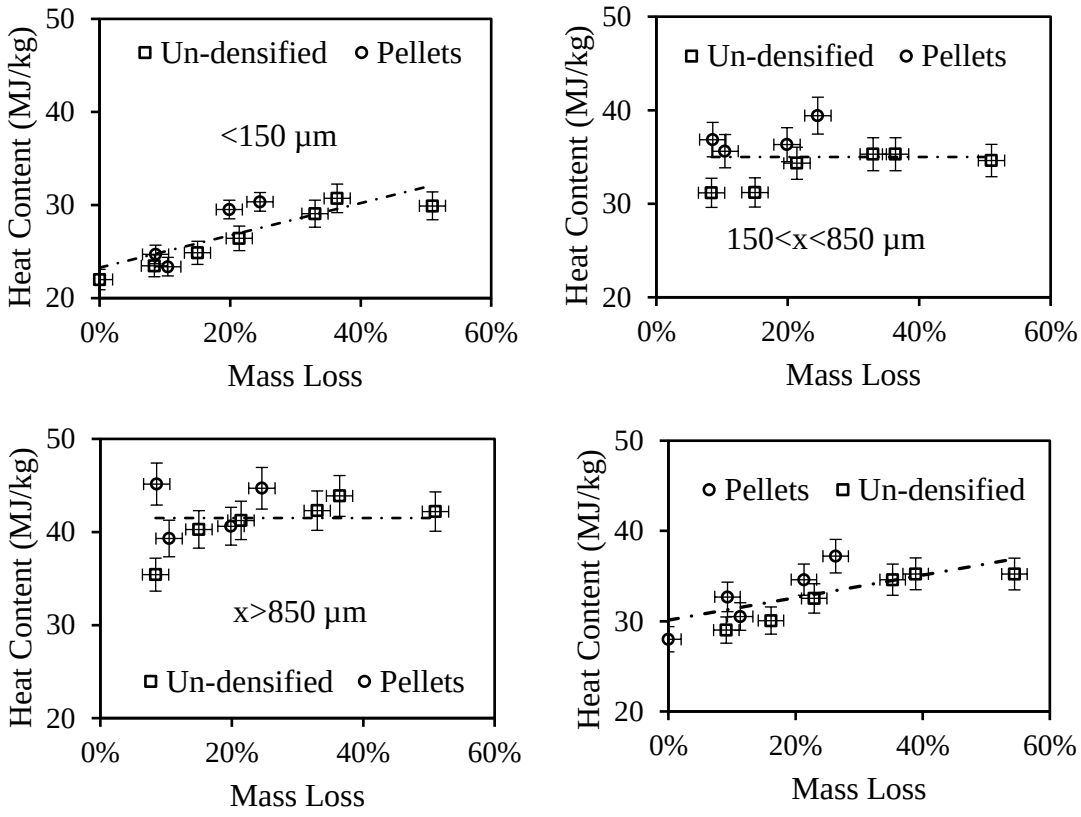

Figure 2.11. Top left. The heat content of the size fraction x<150 µm. Top right, same for 150<x<850 µm. Bottom left. Same for x>850 µm. Bottom right. Total heat content.

Figure 2.11 Top-left is a plot of the heat content of the x<150 µm fraction as a function of mass loss. The point at zero mass loss is the heat content of the blend prior to torrefaction and the dashed line is a linear trend line to lead the eye. Clearly, the main source of this fraction was pulp fibers that increase heat content with an increase in the mass loss as predicted by Klinger et al. (Klinger, Bar-Ziv & Shonnard, 2013; Klinger, Bar-Ziv, & Shonnard, 2015; Klinger et al, 2015). Figure 2.11 Top-right is a plot of the heat content of the 150 µm<x<850 µm fraction as a function of mass loss. The heat content does not seem to change with mass loss and has an average heat content of 35±3 MJ/kg; this value was lower than that of plastic and it was assumed as a combination of fiber and plastic materials. Figure 2.11 bottom-left is a plot of the heat content of the x>850 µm fraction as a function

of mass loss. The heat content does not seem to change with mass loss and has an average heat content of 41.5±3.0 MJ/kg; this value was similar to most of the plastic material (Sonawane, Shindikar, & Khaladkar, 2013) and thus was attributed as plastic. Figure 2.11 bottom-right is a plot of the total heat content, as calculated from all fractions, as a function of mass loss. The slope of heat content increase was identical to that of the fiber.

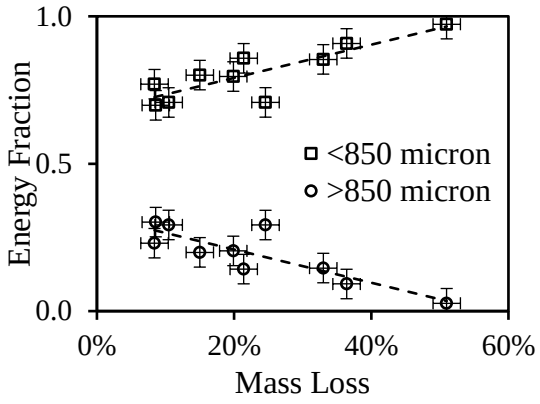

Figure 2.12. The energy contribution of the above and under 850 µm size fractions to the total heat content of both un-densified material and pellets as a function of mass loss.

Although the entire sample was pulverized, two materials (fibers and plastics) clearly retain their original structure which is indicated by the size distribution as shown above and the heat content as shown here. However, this material distinction diminishes as the torrefaction reaction proceeds (seen from the decrease of fraction x>850 µm). To further quantify this process, a plot of the contribution of the <850 µm fraction, which is a combination of torrefied material (from fibers) and fibers and the fraction >850 µm, which was entirely from plastic. Figure 2.12 shows results of the contribution to the total energy from each fraction, showing that the contribution from plastics was about 20% at about 5-8% mass loss and became zero at 50% mass loss, where the plastic lost its original integrity.

2.6 Conclusions

In the present study blends of fiber and plastic wastes at a ratio of 60:40 (fiber-to-plastic) were used as feedstock for torrefaction. Both the un-densified material and pellets were torrefied at 300 ºC with different time periods. It was observed that the two forms have significantly different torrefaction dynamics. Un-densified material takes less time to start torrefaction compared to the pellets, which is due to the faster heat transfer to the un-densified material. The torrefied samples were characterized by moisture content, grindability, particle size distribution, energy content, molecular functional structure, and chlorine content. It was shown that although torrefaction dynamics of the two forms differs significantly from each other, their properties depend on the mass loss. The fiber content was shown to decrease relative to plastic with the extent of torrefaction (mass loss) as determined by FTIR spectroscopy. Further, chemical (cellulose, hydroxyl, and carbonyl) changes were also shown to progressively decrease by torrefaction mass loss. Grinding characteristics, size distribution after grinding gave similar results as a function of mass

loss during torrefaction, for the forms of material. Further, the torrefied product demonstrates a similar grinding behavior to PRB coal. The heat content of the material with size x>850 μm is much higher than that of size x<150 μm; the former attributed to the plastic material, whereas the latter was attributed to the fibers. The total heat content was shown to increase with mass loss. Chlorine in the torrefied samples was removed by a high shear mixing in aqueous solution showing that 5 minutes was sufficient to remove all chlorine after 30% mass loss. Overall, the waste blends studied in this paper showed that they can be used as a drop-in fuel in coal power generation facilities since this fuel is low-cost, it also meets the environmental regulation standard.

2.7 Works Cited

Balogun, A., Sotoudehniakarani, F., McDonald, A.G. (2017). Thermo-kinetic, spectroscopic study of brewer's spent grains and characterization of their pyrolysis products. Journal of Analytical and Applied Pyrolysis. 127: 8-16. https://doi.org/10.1016/j.jaap.2017.09.009.

Bar-Ziv, E., and Saveliev, R. (2013). Torrefied-Biomass from Municipal Solid Waste for Power Production. ASME-Power2013-98044.

Bar-Ziv, E., Klinger, J., Zinchik, S., and Donepudi, Y. (2016). Torrefied-Biomass from Municipal Solid Waste for Power Production. ASME-PowerEnergy2016-59179.

Bates, R.B., and Ghoniem, A.F. (2013). Biomass torrefaction: Modeling of reaction thermochemistry. Bioresource Technology 134, 331-340.

Cepeliogullar, O., and Putun, A.E. (2014). A pyrolysis study for the thermal and kinetic characteristics of an agricultural waste with two different plastic wastes. Waste Management & Research 32(10), 971-979.

Demirbas, A. (1999). Physical properties of briquettes from waste paper and wheat straw mixtures. Energy Conversion & Management 40, 437-445.

De Rezende Pinho, A., De Almeida, M. B., Mendes, F. L., Casavechia, L. C., Talmadge, M. S., Kinchin, C. M., et al. (2017). Fast pyrolysis oil from pinewood chips co-processing with vacuum gas oil in an FCC unit for second generation fuel production. Fuel 188, 462-473.

Donepudi, Y. (2017) Impact of pretreatment methods on fast pyrolysis of biomass. [dissertation]. [Houghton (MI)]: Michigan Technological University

EPA, Environmental Protection Agency "Carbon Pollution Emission Guidelines for Existing Stationary Sources: Electric Utility Generating Units." Federal Register. Environmental Protection Agency, 18 June 2014. Web. 30 Nov. 2014.

EPA, Environmental Protection Agency, 2015, "Carbon pollution emission guidelines for existing stationary sources: electric utility generation units," EPA-HQ-OAR-2013-0602, 1560 pp., published 08-03-2015.

EPA, Environmental Protection Agency, "Assessing Trends in Material Generation, Recycling, Composting, Combustion with Energy Recovery and Landfilling in the United States," Report EPA530-R-17-01, 91 pp., November 2016.

Faix, O. (1992). Fourier transform infrared spectroscopy. In: Lin SY, Dence CW, editors. Methods in lignin chemistry. Berlin: Springer-Verlag. p. 83–132.

Funke, A., Henrich, E., Dahmen, N. and Sauer, J. (2017). Dimensional Analysis of Auger-Type Fast Pyrolysis Reactors. Energy Technology 5 (1): 119-129. doi:10.1002/ente.201600095

Helble, J.J., Srinivasachar, S. and Boni, A.A. (1990). Factors influencing the transformation of minerals during pulverized coal combustion. *Progress in Energy and Combustion Science*, *16*(4), pp.267-279.

Incropera, F.P., and DeWitt, D.P. (2002). Fundamentals of heat and mass transfer. New York: J. Wiley.

Iroba, K.L., Baik, O.D., and Tabil, L.G. (2017). Torrefaction of biomass from municipal solid waste fractions I: Temperature profiles, moisture content, energy consumption, mass yield, and thermochemical properties. Biomass and Bioenergy 106, 8-20. Biomass and Bioenergy 105 (2017a) 320-330.

Iroba, K.L., Baik, O.D., and Tabil, L.G. (2017). Torrefaction of biomass from municipal solid waste fractions II: Grindability characteristics, higher heating value, pelletability and moisture adsorption. Biomass and Bioenergy 106 (2017b) 8-20.

Khalsa, J., Leistner, D., Weller, N., Darvell, LI., and Dooley, B. (2016). Torrefied Biomass Pellets - Comparing Grindability in Different Laboratory Mills. Energies. Oct 4;9(10):1-16, doi:10.3390/en9100794

Kiel, J. (2011). Torrefaction for upgrading biomass into commodity fuel. In *Status and ECN Technology Development. EUBIONET III Workshop, Espoo, Finland* (Vol. 15).

Klinger, J., Bar-Ziv, E., and Shonnard, D. (2013). Kinetic study of aspen during torrefaction. Journal of analytical and applied pyrolysis, 104,146-152.

Klinger, J., Bar-Ziv, E., and Shonnard, D. (2015). Unified Kinetic Model for Torrefaction-Pyrolysis, Fuel Processing Technology, 138, 175-183.

Klinger, J., Bar-Ziv, E., Shonnard, D., Westover, T., and Emerson, R. (2015). Predicting Properties of Gas and Solid Streams by Intrinsic Kinetics of Fast Pyrolysis of Wood. Energy and Fuels 30 (1): 318-325. doi: 10.1021/acs.energyfuels.5b01877

Krimm, S. (1963). Infrared spectra and assignments for polyvinyl chloride and deuterated analogs. Journal of Polymer Science: Part A. 1: 2621-1650.

Kumar, L., Koukoulas, A.A., Mani, S., and Satyavolu, J. (2017). Integrating Torrefaction in the Wood Pellet Industry: A Critical Review. Energy Fuels, 31, 37-54.

Lédé, J. (2010). Biomass Pyrolysis: Comments on Some Sources of Confusions in the Definitions of Temperatures and Heating Rates. Energies 3 (4): 886-898. doi: 10.3390/en3040886

Luppens, J.A. (2011), A critical review of published coal quality data from the southwestern part of the Powder River Basin, Wyoming: U.S. Geological Survey Open-File Report 2011-1148, 23.

Mason, P.E., Darvell, L.I., Jones, J.M., and Williams, A. (2016). Comparative Study of the Thermal Conductivity of Solid Biomass Fuels. Energy and Fuels 30 (3): 2158-2163. doi: 10.1021/acs.energyfuels.5b02261

Mayo, D.W. (2004a). Characteristics of alkanes. In: Course Notes on the Interpretation of Infrared and Raman Spectra. Eds. Mayo, D.W; Miller, F.A.; Hannah, R.W., John Wiley & Sons, New Jersey. Pp 33-72.

Mayo, D.W. (2004b). Spectra of carbonyl compounds of all kinds (Factors affecting carbonyl group frequencies). In: Course Notes on the Interpretation of Infrared and Raman Spectra. Eds. Mayo, D.W; Miller, F.A.; Hannah, R.W., John Wiley & Sons, New Jersey. Pp 179-204.

McCabe, J.G. (2014). Addressing Biogenic Carbon Dioxide Emissions from Stationary Sources. United States Environmental Protection Agency.

McKendry, P. (2002). Energy production from biomass (part 2): conversion technologies. Bioresource Technology Volume 83, Issue 1, May 2002, 47-54.

Miller, F.A. (2004). Characteristic frequencies of alkenes (olefins). In: Course Notes on the Interpretation of Infrared and Raman Spectra. Eds. Mayo, D.W; Miller, F.A.; Hannah, R.W., John Wiley & Sons, New Jersey. Pp 73-84.

Miranda, R., Sosa-Blanco, C., Bustos-Martínez, D., and Vasile, C. (2007). Pyrolysis of textile waste I. Kinetics and yields. J. Anal. Appl. Pyrol., 80, 489-495.

Mumin, G.G., Prawisudha, P., Zaini, I.N., Aziz, M., and Pasek, A.D. (2017). Municipal solid waste processing and separation employing wet torrefaction for alternative fuel production and aluminum reclamation. Waste Management 67, 106-120.

Nakamura, D., and Mufson, S. (2014). China, U.S. Agree to Limit Greenhouse Gases. The Washington Post, 12.

Pandey, K.K. (1999). A study of chemical structure of soft and hardwood and wood polymers by FTIR spectroscopy. Journal of Applied Polymer Science. 71: 1969–75.

Patterson, J.E., Miers, R.J., and Carolina, N. (2010). The thermal conductivity of common tubing materials applied in a solar water heater collector, T. Sulbaran (Ed.), 46th ASC Annual International Conference, Wentworth Institute of Technology, Boston, Massachusetts.

Radics, R.I., Gonzales, R., Bilek, E.M., and Kelley, S.S. (2017). Systematic Review of Torrefied Wood Economics. BioResources 12 (3), 6868-6886.

Saleh, S.B., Flensborg, J.P., Shoulaifar, T.K., Sárossy, Z., Hansen, B.B., Egsgaard, H., et al. (2014). Release of Chlorine and Sulfur during Biomass Torrefaction and Pyrolysis. Energy and Fuels 28 (6): 3738-3746. doi: 10.1021/ef4021262

Sonawane, Y.B., Shindikar, M.R., and Khaladkar, M.Y. (2017). High Calorific Value Fuel from Household Plastic Waste by Catalytic Pyrolysis, Nature Environment and Pollution Technology, 16(3), 879.

Storm, R.F. (2009). " Blueprint" Your Pulverizer for Improved Performance. *Power*, *153*(3), pp.60-63.

Themelis, N.J., and Mussche, C. (2014). 2014 Energy and Economic Value of Municipal Solid Waste (MSW), Including Non-Recycled Plastics (NRP), Currently Landfilled in the Fifty States.

TRI, ThermoChem Recovery International, (2018). "Reforming gasification," 2017. http://tri-inc.net/steam-reforming-gasification/.

Unapumnuk, K., Keener, T.C., Lu, M., and Khang, S.J. (2006). Pyrolysis Behavior of Tire-Derived Fuels at Different Temperatures and Heating Rates. Journal of the Air & Waste Management Association, 56:5, 618-627, doi: 10.1080/10473289.2006.10464481

US-EIA, U.S. Energy Information Administration, based on U.S. Environmental Protection Agency, 2010 MSW Facts and Figures Factsheet. https://www.eia.gov/todayinenergy/detail.php?id=8010. Accessed 03-11-2018.

US-EIA, U.S. Energy Information Administration, "Monthly Energy Review," Chapter 6, February 2018, DOE/EIA-0035 (2018).

Wang, C., Li, M., and Fang, Y. (2016). Coprocessing of Catalytic-Pyrolysis-Derived Bio-Oil with VGO in a Pilot-Scale FCC Riser. Ind. Eng. Chem. Res. 55, 3525−3534.

Wang, L., Barta-Rajnai, E., Skreiberg, Ø., Khalil, R.A., Czégény, Z., Jakab, E., Barta, Z., et al. (2017). Impact of torrefaction on woody biomass properties.

Wang, Z., Pecha, B., Westerhof, R., Kersten, S., Li, C-Z., McDonald, A.G., Garcia-Perez, M. (2014). Effect of cellulose crystallinity on solid/liquid phase reactions responsible for the formation of carbonaceous residues during slow pyrolysis. Industrial & Engineering Chemistry Research. 53(8): 2940–2955.

Wei, L., McDonald, A.G., Freitag, C., and Morrell, J.J. (2013). Effects of wood fiber esterification on properties, weatherability and biodurability of wood plastic composites. Polymer Degradation & Stability. 98: 1348-1361.

White, E.D. (2014). The supreme court of the U.S., American Bar Association Journal 7.7 (1921): 341-343.

Yuan, H., Wang, Y., Kobayashi, N., Zhao, D., and Xing, S. (2015). Study of Fuel Properties of Torrefied Municipal Solid Waste, Energy Fuels 2015, 29, 4976-4980, doi: 10.1021/ef502277u

Zhao, W., Liu, D., and Zhang, Y., (2017). Study on the Influence of Pressure-Assisted Thermal Processing on PET/PE via the Change of Melting Enthalpy. Journal of Food Processing and Preservation, 41(5).

Zhu, Q. (2014). Coal sampling and analysis standards. IEA Clean Coal Centre, London, United Kingdom, 64-65.

Zinchik, S., J. L. Klinger., T. L. Westover., Y. Donepudi., S. Hernandez., J. D. Naber., et al. (2018). Evaluation of Fast Pyrolysis Feedstock Conversion with a Mixing Paddle Reactor. Fuel Processing Technology 171. Elsevier: 124-132. doi: 10.1016/j.fuproc

3 Properties of Pellets of Torrefied U.S. Waste Blends

This section is based on the following peer-reviewed paper:

Z. Xu, JW. Albrecht, SS. Kolapkar, S. Zinchik, E. Bar-Ziv. 2020. Chlorine Removal from US Solid Waste Blends through Torrefaction. Applied Sciences 10 (9), 3337.

doi.org/10.1016/j.wasman.2020.01.009

3.1 Abstract

With the continued growing U.S. population, solid waste generation will increase, which will lead to undesired and significant growth in landfilling. Thermal treatment can turn these high calorific value wastes into fuels that can be used in small-to-large power plants. This article focuses on using blends with 40% plastic and 60% fiber wastes and converting them into densified solid fuel by torrefaction and extrusion. The material was torrefied at 300 °C to obtain torrefied samples with different mass losses, ranging from 0% to a maximum of 51%. The torrefaction results showed a clear synergy between plastics and fibers. The torrefied material was then extruded into 9 mm diameter rods and the products were characterized by molecular functional group analysis, thermomechanical analysis, dynamic mechanical analysis, dynamic rheological measurement, density measurement, flexural testing, water absorption test, size distribution measurement, heat content test, and combustion test. The fiber content in the material decreased as mass loss increased, and the process reduced significantly the variability of the material. The heat content increased as the mass loss increased. The plastic in the feedstock acted as a process enabler as it imparted properties like bindability, water resistance, high heat content, and increased degradation reaction rate.

3.2 Introduction

The world is witnessing an unprecedented accumulation of solid wastes with significant, well-documented ecological, environmental, health, and economic consequences (El-Fadel et al., 1997, Arias et al., 2008). As population increases, the levels of wastes will continue to grow, especially the plastic waste levels that hugely impact landfilling and have been exacerbated by China's ban on plastic waste import (China Daily, 2018).

Western countries are witnessing a transition from current disposal of solid wastes in landfill to a zero-solid waste society (Bolton and Rousta, 2019). This grand challenge requires new technical approaches for the conversion and the valorization of the solid wastes into valuable products in order to create a circular economy (Paletta et al., 2019). Currently, commingled plastic-fiber wastes usually end up in the landfills since they are not suitable for recycling, creating challenges as well as opportunities for waste management. A thermal treatment (e.g. torrefaction) could turn this feedstock into a safe and low-cost drop-in fuel for the existing power plants. The current study is an attempt to provide one solution of converting plastic-fiber wastes into viable solid fuel.

Torrefied biomass has been proposed as a renewable substitute for coal in power generation (Van der Stelt et al., 2011), it complies with EPA regulations (US-EPA, 2015) as well as contributes to the reduction of greenhouse gases (GHG) (Tsalidis, et al., 2014; Nunes et al., 2014). Fibers in comingled wastes originate from biomass, hence can be considered as a source of renewable energy (Rodríguez-Monroy et al., 2018). Torrefaction technology has reached a level of maturity that it can be commercially used, however, it has not yet moved to the market. Three major hindrances in the commercialization of this technology have been identified: (1) the high cost associated with woody biomass feedstock (Kumar et al., 2017; Radics et al., 2017), (2) the degradation of lignin during torrefaction (Park et al., 2013), hence lack of a binder for compaction, and (3) the high reactivity of torrefied biomass, as self-heating of the material due to slow oxidization, that imposes tremendous safety risks during the process, transportation, storage and the operation in the power plant (Arias et al., 2008, Ceballos et al., 2015). In this study, we used blends of plastic and fiber wastes as a feedstock, which overcome the above hindrances.

Although recycling should be the prioritized for currently landfilled wastes, there is large volume of non-recyclable wastes along with portion of recyclable waste that ends up in landfill. These end-of-life wastes have an existing collection and transportation systems as well as tipping fees that make them economically attractive. These wastes can be used as a high calorific value fuel for power applications (US-EIA, 2010).

Torrefied biomass is densified by two main methods; (1) pelletization (Stelte et al., 2012) and (2) briquetting (Tumuluru et al., 2011). These methods, however, have some challenges: (1) they may require a binder, which adds cost to the final product, and (2) the pellets/briquettes of the torrefied biomass show clear propensity for oxidation at ambient temperatures (Donepudi, 2017), and therefore may cause safety hazards (Arias et al., 2017) in transportation, storage, and operation at the power plant (Stelte et al., 2016). These two challenges were overcome by the addition of plastic to the biomass (fiber) mix. As plastic is blended with fiber, we realized that extrusion can be used for densification, as this is a common densification technology make biochar-plastic composites (Hanaffi Mohd Fuad et al., 2018; Wang et al. 2019).

Recently, Xu et al., carried a comprehensive torrefaction study on fiber-plastic (60%/40%) waste blend and detailed waste composition was provided (Xu et al., 2018). The challenges and the advantages of using wastes as feedstock were discussed. They also reported properties of the produced torrefied material as a function of the extent of torrefaction and showed that this material can be pulverized like coal and have higher heat content than most coals. The current work deals with the densification of torrefied fiber-plastic (60%/40%) waste blends. Densification is carried out by extrusion and the produced pellet properties were characterized by a series of methods. The present study is a further development of Xu et al., 2018. work to produce a densified fuel.

3.3 Materials and Methods

3.3.1 Materials

The samples used in this study were fiber-plastic waste blend (40% plastic and 60% fiber) obtained from Convergen Energy LLC (CE). The wastes blends received by CE comprises of a large variety of paper, laminated papers, plastics, and fibers consisting of several impurities. CE has been tracking the properties of the waste blends for seven years, and the results are shown by Xu et al. (2018) CE removed any ferrous metals using a strong electric magnet, while non-ferrous were removed manually. The material was then shredded to 75-125 mm particle size by a shear grinder and then air-dried to 5-7% moisture content level (Xu et al., 2018).

3.3.2 Torrefaction

The sample was torrefied by introducing ~150 g of CE waste blends to an aluminum pan that was placed in the center of a muffle furnace (Lindenberg/Blue type BF51828C-1) heated to 300 oC for 3 to 60 min (Xu et al., 2018). An inert gas purge, either carbon dioxide or nitrogen, was purged at a rate of 30 L/min to avoid oxidation. In this study, mass loss was the dependent variable measured as a function of time.

Modeling of heat-transfer-torrefaction reaction has been developed by Xu et al., under the same conditions (i.e., small Biot number and Thermal Thiele Modulus) of the current study and has proven to fit the measured data rather accurately (Xu et al., 2018).

The model shows the relationships for the temperature and mass loss transients. Eq. (3.1) is the temperature transient (*T(t)*),

$$T(t) = T_w - (T_w - T_o)e^{-\frac{t}{\tau}} \tag{3.1}$$

where T_w and T_o are the temperatures of furnace wall and initial temperature of the particle, respectively, t is time and τ is a characteristic time given by Eq. (3.2)

$$\tau = \frac{mc_p}{hA} \tag{3.2}$$

This can be measured from sample mass (m), heat capacity (c_p), heat transfer coefficient of the furnace walls to the sample (h), and the surface area of sample (A).

The ratio of the sample mass (at a given time) to the initial sample mass is presented by α, and the reaction was assumed to be the first-order reaction, and the reaction rate ($R^{\dagger}$) was given by Eq. (3.3)

$$R^{\dagger} = \rho \frac{d\alpha(t)}{dt} = -\rho k \alpha(\mathrm{t}) \tag{3.3}$$

where *k(T)* is a rate coefficient given by Eq. (3.4)

$$k(T) = \frac{A^{\dagger}}{\rho} e^{-\frac{T_a}{T(t)}} \quad (3.4)$$

where ρ and $A^{\dagger}$ are the density of the sample and pre-exponential factor, respectively. T_a is a characteristic temperature given by $T_a=E_a/R$ where E_a and R, are activation energy and the gas constant, respectively. Commonly, mass loss, 1-α, is used to define the extent of torrefaction, which is presented by Eq. (3.5)

$$1 - \alpha = 1 - e^{-\int_0^t k dt} \quad (3.5)$$

Equations (3.1) and (3.2) enable us to calculate the temperature transient of a given sample in our furnace. By combining equations (3.3), (3.4) and fine-tuning the parameters T_a and $A^{\dagger}$, *1-*α (measured mass loss) could fit the experimental results. This procedure has been applied successfully by Xu et al (Xu et al., 2018).

3.3.3 Densification by Extrusion

This study examined the use of extrusion to densify the torrefied fiber-plastic blend. An 18-mm co-rotating twin-screw extruder (Leistritz, L/D ratio of 40, 200 rpm, 4.7 kW motor, base torque 18%) has been used in this study. The extruded material exited from a 9 mm diameter die as rods and were cooled by forced air (Adefisan et al., 2017). The extruder is divided into 8 zones heated independently and controlled by the wall temperature (zone 1 is the inlet of the extruder). Samples of the torrefied/non-torrefied plastic-fiber waste blends (400 g each) were manually fed into the extruder.

3.3.4 Characterization

3.3.4.1 Fourier-Transform Infrared Spectroscopy (FTIR) Characterization

FTIR spectral analysis was performed for 30 pieces each randomly chosen from (i) plastic waste (ii) fiber waste; (iii) waste blend and (iv) sliced sections of extruded non-torrefied/ torrefied material with an FTIR spectrometer (Thermo-Scientific Nicolet-iS5), 64 scans, with an attenuated total reflectance accessory (ZnSe crystal, iD5). OMNIC v9.8 software and Aldrich, Hummel, and Nicolet spectral libraries were used to analyze the data. The following indices were used: Carbonyl index (CI), cellulose index (CeI), and hydroxyl index (HI). The indices were defined as a ratio of the band intensity (absorbance) at 1720 cm^{-1}, 1024 cm^{-1}, and 3342 cm^{-1}, respectively, to the band 2916 cm^{-1} for the -CH_2- groups (Wei et al. 2013).

3.3.4.2 Thermal Analysis

Thermomechanical analysis (TMA) was performed with Perkin Elmer TMA 7 instrument on sliced discs (0.5 mm x 9 mm Ø) from the extruded rod using the penetration probe (static force 10 mN) from 30 to 200 ^{o}C at 5 ^{o}C/min. Data were analyzed using Pyris v8 software to determine the onset softening temperature. Dynamic mechanical analysis (DMA) was carried out in 3-point bending mode (15 mm span) on hot-pressed extruded rod samples (2 x 5.5 x 20 mm^3) using a Perkin Elmer DMA-7 instrument (1 Hz and 0.5 %

strain) with refrigerated cooling from -50 to 120 ºC at a ramp rate of 3 ºC/min. We run DMA experiments in a temperature sweep (in the current DMA setup) from -50 °C to just below its melting temperature (around 100 °C). This provides information about how materials behave as a function of temperature. That is to observe if there are any thermal transitions occurring such as glass transition, which can be sub-ambient for common thermoplastics such as polypropylene.

3.3.4.3 Rheology

Dynamic rheological measurements (G′, G″, and η*) were carried out on a Bohlin CVO 100 rheometer, using serrated parallel plates (25 mm Ø), in an oscillating mode with an extended temperature control module on pressed disc (3 mm × 25 mm Ø) samples. Dynamic rheological result is the response of a molten material (waste plastic blend or composite) to a cyclic torsional load in order to determine properties such as complex viscosity, loss modulus and storage modulus. Experiments were performed in the linear viscoelastic region. Measurements were carried out at 180 °C in the frequency range of 0.01 to 100 Hz at an applied strain of 0.5% (Luo et al., 2016). Data were analyzed using the Bohlin rheology v6.51 software.

3.3.4.4 Density

The weight of the pellet was measured by two methods: (i) by using a scale (A&D HR-60) with the readability of 0.0001 g. Since the surface of the extruded pellets was very smooth, cylinder-shaped pellets were cut from them to calculate cylinder volume. The diameter (d) and length of the cylinder (l) were measured using caliper (Fowler Electronic Caliper) with a resolution of 0.01 mm. The density was obtained by calculating using the formula *mass/cylinder-volume*; (ii) the dry weight of the pellet, m, was measured using a scale (A&D HR-60) with the readability of 0.0001 g. A 100 ml graduated cylinder partially filled with distilled water was prepared, and the reading V_o was recorded. The pellet was placed into water. The volume reading with immersed pellet, V, was recorded. The density was obtained by calculating the ratio $m/(V\text{-}V_o)$.

3.3.4.5 Flexural Testing

The extruded rod samples (150 mm long) were hot-pressed (PHI hydraulic press, 300 x 300 mm^2) slowly at 140 ºC over 20 min to a thickness of 3.25 mm, then cooled to room temperature under load. The flattened material was cut into flexural specimens (3.25 x 16 x 60 mm^3). Three-point flexural tests (strength and modulus) were performed on the specimens (≥6 replicates) according to ASTM Standard D 790-07 with a crosshead speed of 1.31 mm/min, span of 52 mm, tested until specimen failure or 5% strain, whichever occurred first on an Instron 5500R-1132 universal test machine (5 kN load cell). Data were collected and processed using Bluehill v3 software (Instron).

3.3.4.6 Water Absorption

The extruded sample was put into a vial and then filled with distilled water until the sample was fully submerged or the vial was full. The original weight was recorded, the sample after a certain period was taken out, surface water wiped off using a dry cloth, and the net

weight was measured. Water absorption is defined as the net weight of the sample over the original weight.

3.3.4.7 Size Distribution Analysis

For the size distribution analysis, 200g of pellets were ground for 120s. During grinding the motor power was monitored (by Watts Up pro power analyzer and data logger). Grinding was done, up to 1,800s, until grinding power stabilized at an asymptotic value (Xu et al., 2018). The ground sample was then moved to a sieve shaker (W.S Tyler, RX-86) with four screens (sizes of 150 µm, 250 µm, 425 µm, and 850 µm). The sieve shaker was operated for an hour to obtain five different fractions. Each fraction was weighted to determine the material size distribution after grinding.

3.3.4.8 Heat Content

Previous experience has shown that the results of the material heat content have large variabilities if the sample was directly taken after grinding. This was due to the nature of the blend, as grinding generates particles of different sizes. To resolve this issue, the ground material was sifted into five different fractions (as discussed above). Each fraction from the size distribution was tested for heat content, measured using a bomb calorimeter (Parr 6100). For each measurement, a crucible containing ~1g of the sample was placed into a bomb filled with oxygen (~400 psi), and the bomb was submerged into a jacket filled with distilled water (2,000 g). The sample was ignited, and the heat released during the combustion was transferred to the water in the jacket. The heat content was calculated by calorimeter by monitoring the temperature difference of the water in the jacket before and after the combustion. After a full analysis of all fractions from the sifting, a weighted average was calculated to determine the heat content of the sample.

3.3.4.9 Combustion Test

The extruded rods with different mass losses were cut into equal dimension pellets (24.8 mm x 9.55 mm Ø, 2g) and were placed on a tared porcelain crucible (Fisher brand FB-965-G) then placed in a muffle furnace (Lindenberg/Blue type BF51828C-1) set at 900 °C. The experiments were done for different times starting from 1 min. After each experiment, the crucible was removed from the furnace and placed in the desiccator, the weight was recorded after it was cooled to room temperature. If there was >2 mg difference between the current and previous experiment, the crucible would be re-furnaced until the difference was <2 mg (ASTM D 5630-94).

3.4 Results and Discussion

3.4.1 Torrefaction

Fiber and plastic wastes were torrefied separately and as a blend. The original waste blend as well as selective torrefied material used for extrusion.

According to Eq. (3.2), the characteristic time for fiber, plastic and blend were $\tau_{fiber}=136$ (s), $\tau_{plastic}=300$ (s) and $\tau_{blend}=184$ (s), respectively. Figure 3.1a portrays temperature

transients calculated by Eq. (3.1) for the raw feedstock, including fiber, plastic and the blend, reaching 300 ^{o}C, and the size of the material was 25mm by 25mm and 1mm thick flakes. The differences between the three transients arise from differences in the properties of the three materials, as summarized by Xu et al., (Xu et al., 2018). Figure 3.1b shows measured mass loss for fiber, plastic, and blend torrefied at 300 ^{o}C. For the three materials, mass loss remained zero for 4-5 min then it started to increase gradually. The figure also includes model results for each material and the expected model behavior of the blend. Experimental results for the mass loss for the plastic waste (square symbols) show a slow increase with time, whereas the measured results for the fiber waste (circle symbols) show a much faster increase of mass loss with time. Each of the mass loss transients was also modeled (dashed lines in Figure 3.1b), showing perfect fit to experimental data, as explained above (see Eq. (3.5)) and the kinetic parameters were drawn from the fitting process.

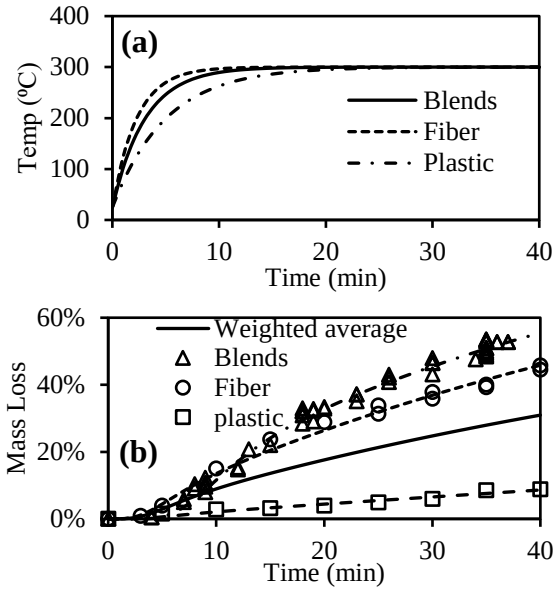

Figure 3.1. (a) Temperature transients calculated by Eq. (3.1) for the fiber, plastic, and the blend, reaching 300 °C; (b) a mass loss for the fiber, plastic, and the blend. The figure also shows model results for each component and the expected model behavior for the blend.

The parameters obtained by the fitting as follows: (i) *fiber:* $(A^{\dagger}/\rho)_{fiber} = 2{,}997$ and $(T_a)_{fiber} = 5{,}369\ (K)$, (ii) plastic: $(A^{\dagger}/\rho)_{plastic} = 2{,}558$ and $(T_a)_{plastic} = 6{,}383\ (K)$, *and* (iii) blend: $(A^{\dagger}/\rho)_{blend} = 1.2*10^{8}$ and $(T_a)_{blend} = 15{,}258\ (K)$. The important point is that these kinetic parameters were used to predict the mass loss behavior for the plastic-fiber waste blend, assuming each component does not influence the other. In this case, evidently, the resultant behavior should have been between the fiber and plastic transients, as shown by the solid line in the figure. However, the actual experimental data for the blend show much faster mass loss transients (triangle symbols) than expected. This is direct evidence that there is a strong reaction (synergy) between the fiber (mostly cellulose polymers) and the plastic material (mostly hydrocarbon polymers). Similar kinetic parameters were found for the un-densified torrefied blends as studied by Xu et al., 2018.

Although at this stage we did not carry out solid-state characterization measurements that might shed direct light on the reactions between the two polymers, it can be hypothesized that hydrogen atoms from the hydrocarbon polymer react with either, COOH, CO or OH groups in the cellulosic polymer and enhance the stripping of these groups, thus increasing the reaction rate of the degradation of the cellulosic polymer. Similar behavior was observed by Nallar and Wong, where the existence of high-density polyethylene accelerated the thermal degradation of the cellulose (Nallar and Wong, 2019).

3.4.2 Extruded Pellets

Samples of the non-torrefied waste blend (0% mass loss) and torrefied waste blend (11%, 32%, and 51% mass loss) were compounded and extruded into rods. Compounding homogenized both the non-torrefied and torrefied materials into a uniform extrudate. The molten plastic encapsulated the fiber to form a consistent/uniform extruded rod. After the extruded pellets cooled down, the plastic acted as a binder.

Note that the extruder barrel temperature was decreased by at least 10 ^{o}C for the torrefied material than the original waste blend, as stated above, to minimize surface cracking. The smoothness of the extrudate surface depended strongly on the die temperature that had to be adjusted to get the desired surface quality.

3.4.3 FTIR Spectroscopy

Despite the differences in the relative standard deviations, important information regarding the material in the blend can be obtained. FTIR spectroscopy was employed to examine the major chemical changes that occurred in the waste blend samples upon torrefaction (Balogun et al., 2017). FTIR measurements were performed on samples prior to and after the torrefaction. Details on FTIR measurements and consequent conclusions regarding the chemical changes during torrefaction are given below.

The feedstock used was a blend of 40% plastic and 60% fiber wastes. FTIR experiments were done 30 times for both fiber waste and plastic waste to determine the chemical identity before blending. Figure 3.2a shows that plastic wastes mainly consist of low-density polyethylene, polyethylene, polyethylene terephthalate, polyamide-nylon, polyvinyl, polypropylene, and some other materials. Figure 3.2b shows that there are silopren, polyester with kaolin filler, acrylate/paper mix together with cellophane/cellulose in the fiber wastes. The results from Figure 3.2a and Figure 3.2b indicated the large variability in the feedstock.

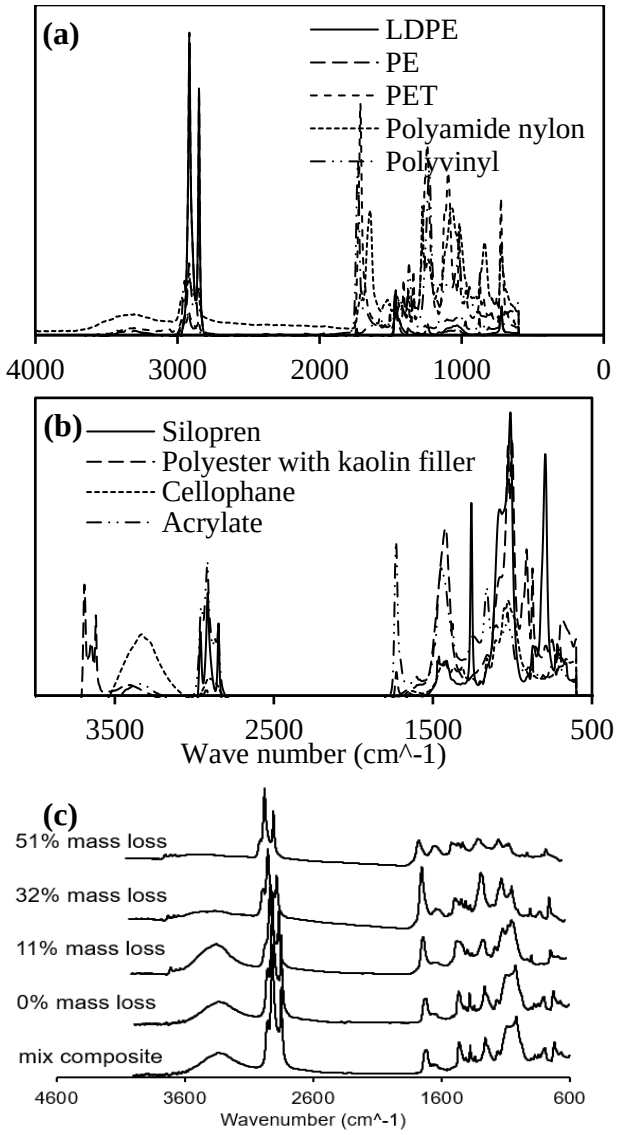

Figure 3.2. (a) Plastics materials identified from feedstock; (b) fibers materials identified from feedstock; (c) FTIR of a composite average of 30 waste blend pieces, extruded mixed plastic waste (0% mass loss) and extruded torrefied (11%, 32% and 51% mass loss) material.

Figure 3.2 (c) shows FTIR spectra of a composite average of 30 waste blend pieces, extruded mixed plastic waste (0% mass loss) and extruded torrefied (11%, 32%, and 51% mass loss) material. C -H stretching bands were observed in every sample and were attributed to methyl (2960 cm^{-1} and 2870 cm^{-1}) and methylene (2916 cm^{-1} and 2850 cm^{-1}) groups (Mayo, 2004). The two methylene bands were of comparable intensity for all samples and the methyl group decreased with the extent of torrefaction. It was observed that there exists O-H stretching band in all the samples at the region between 3100 and 3600 cm^{-1} and the intensity gradually reduced as mass loss increased. At 1690-1750 cm^{-1},

a broad carbonyl (C=O) band was detected mainly assigned to (i) an ester in linkage in PET and acrylate, and (ii) amide linkage in nylon (Mayo, 2003). Paper was recognized due to a small band at 1505 cm^{-1}. Wood cellulose and hemicellulose were also identified at the region at 1000-1070 cm-1 (Pandey, 1999). Cis- band at 727 cm-1 and trans-vinylene bands at 974 cm-1 were found in all the samples (Miller, 2003).

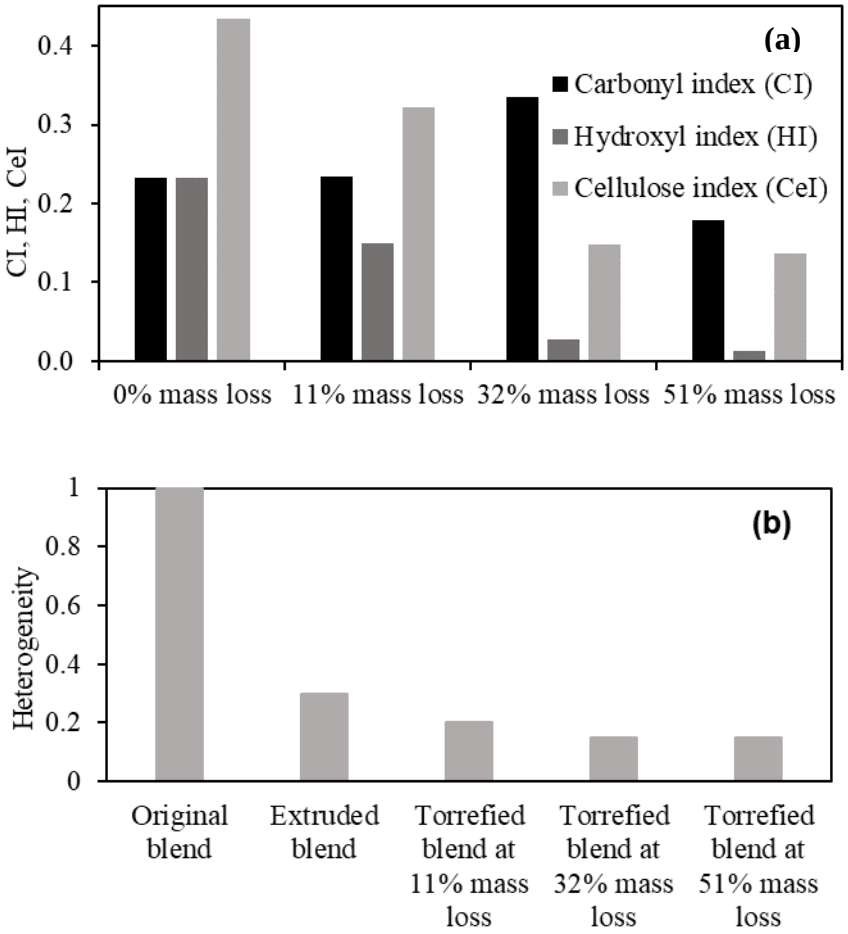

Figure 3.3 (a) Plot showing changes in hydroxyl (HI), carbonyl (CI) and cellulose (CeI) indices with the extent of torrefaction (mass loss); (b) Heterogeneity as defined by STD/IN of IR spectra measured.

The relative changes in hydroxyl, carbonyl, and cellulose that occurred during torrefaction were analyzed by calculating HI, CI, and CeI, respectively (Figure 3.3a). The CI, HI and CeI were obtained from the FTIR spectrum as explained in Section 2.4.1. The HI decreased from 0.27 to 0.02 in the mass loss region of 0-51%. In the same mass loss region, the CeI decreased from 0.51 to 0.20. These results support that the reduction in cellulose content was due to dehydration and degradation reactions (Wang et al. 2014). The CI increased from 0.26 to 0.34 at 32% mass loss then decreased to 0.21 at 51% mass loss and this change could not be explained. According to Ru et al., 2015, the effects of torrefaction on C═O groups is rather complex and depends strongly on the types of fibers. Harvey et al., also observed similar behavior for honey mesquite with the temperature range of 200-300 °C.

3.4.4 Material Variability and Homogeneity

FTIR spectroscopy shows that there exist large variabilities in the raw feedstock Figure 3.2. Perhaps one of the most important roles of extrusion and torrefaction of samples containing plastic is the ability to significantly reduce the heterogeneity of the initial waste blend. To note, a Heterogeneity parameter was defined as the ratio of standard deviation and intensity (STD/In) of the 30 IR spectra measured. The larger the term the greater is the heterogeneity of the blend. Figure 3.3b shows the normalized heterogeneity for the various samples: from left to right is the original fiber-plastic blend, followed by same blend that was extruded, which reduced the heterogeneity by ~70%, followed by the 10% mass loss blend, which reduced another 10% of heterogeneity and the number finally stabilized at ~15% after the mass loss reached 32%. The combination of torrefaction followed by the extrusion process decreased the heterogeneity of the original blend by a factor of 7. This indicated that the extrusion process reduced the variabilities of the material since the plastics were melted and the feedstock was well-mixed inside the extruder before getting extruded.

3.4.5 Thermomechanical Analysis (TMA)

TMA was performed on the extruded torrefied material to determine the materials' softening point (Figure 3.4). The softening temperature observed were as follows: for 0% mass loss, two softening temperatures (T_{s-1} and T_{s-2}), 102°C and 164°C were observed. For 11% and 32% mass loss, only one softening temperature (T_{s-1}) was observed at 120°C and 112°C respectively. Three softening temperatures ($T_{s-1,}$ $T_{s-2,}$ and T_{s-3}) were observed for 51% mass loss at 109°C, 123°C, and 142°C.

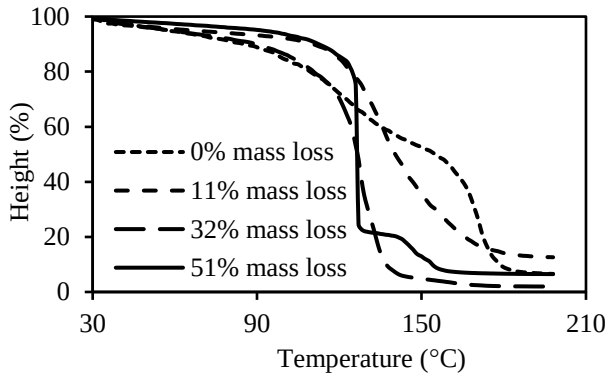

Figure 3.4. TMA thermograms of the extruded torrefied (0% to 51% mass loss) samples

The waste blend was shown to have two, gradual, softening temperatures (T_{s-1} and T_{s-2}) at 102 ^{o}C and 164 ^{o}C and these coincide with the melting temperatures of low-density polyethylene (LDPE) (98-115 ^{o}C) and polypropylene (160-175 ^{o}C) (Harper, 1999). The gradual change in probe height during the thermal transition is likely due to the reinforcing effect of cellulose/paper in the sample. As the waste blend was torrefied (11% mass loss), T_{s-1} increased slightly to 120 ^{o}C then progressively decreased to 109 ^{o}C (51% mass loss). Furthermore, the 51% mass loss torrefied material had two other transitions (T_{s-2} and T_{s-3})

at 123 °C (sharp) and 142 °C. The changes in the softening temperature are a combination of the following: (i) depolymerization of polymers in the mix as a result of torrefaction; (ii) changes in material properties due to differential thermal decomposition of certain components in the mixture (e.g. fiber).

3.4.6 Dynamic Rheological Results

Dynamic rheological measurements were also obtained on the extruded torrefied melts. Figure 3.5 shows the dynamic elastic (G') and viscous (G") moduli and complex viscosity (η*) as a function of frequency at 180 °C. For all melt samples G' and G" were shown to increase with angular frequency (Figure 3.5a and Figure 3.5b).

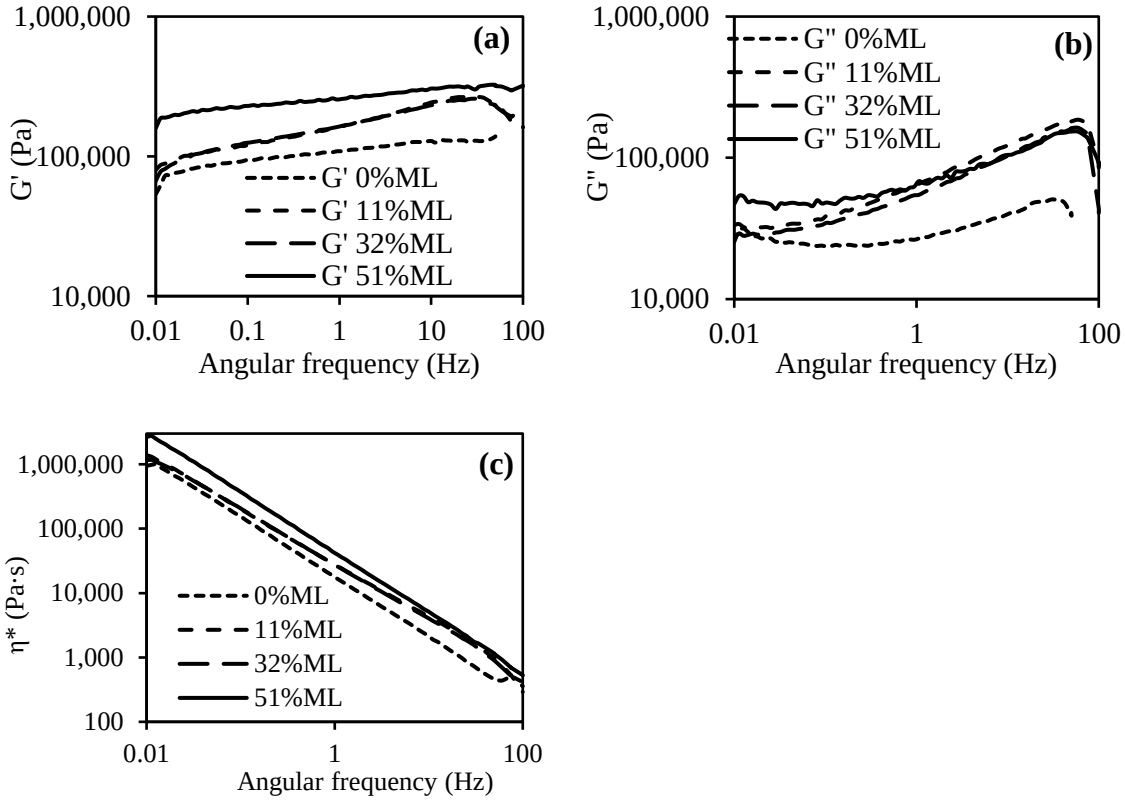

Figure 3.5. Dynamic rheology showing (a) elastic moduli (G'); (b) viscous moduli (G"); (c) complex viscosity (η*) as a function of frequency for torrefied waste blend extrudates at 180 °C.

Torrefaction of the waste blend to 51% mass loss was shown to increase both G' and G" >2-fold (at 1 Hz). Over the angular frequency range examined, the G' was higher than G", indicating an elastic response predominated at 180 °C. The η* was shown to decrease with an increase in angular frequency, showing a shear-thinning behavior for the melts and this trend has been observed in reprocessed mixed plastic wastes (Hamad et al. 2013) (Figure 3.5c). The η* (at 1 Hz) was also shown to increase from 16,800 Pa·s for the waste blend extrudate to 40,000 Pa·s for the 51% mass loss torrefied extrudate. As mass loss increases, an increase in complex viscosity and storage modulus (G') is observed, possibly due to (i)

improved compatibilization between the fiber and plastic matrix and (ii) long-chain branching (cross-linking) between the fiber-plastic and plastic-plastic which would increase viscosity.

3.4.7 Density and Flexural Testing

The densities of various mass loss samples, measured by the two methods detailed above, were found close to each other, with an average density of 1143 kg/m^3 with standard deviation of 44 kg/m^3, this value was determined from 10 measurements.

Flexural tests were carried out for four samples, at 0% mass loss, for a reference, 11%, 32, and 51% mass loss. Due to the inhomogeneous nature of the material, the results were somewhat scattered, however, clear trends were observed.

Figure 3.6a and b present results for the flexural modulus and flexural strength, showing mild decrease with mass loss, indicating mild propensity for decrease in durability as a function of extent of torrefaction. The modulus of these materials was comparable to polypropylene (1,170-1,720 MPa) (Shah, 1998). The mean flexural strength for the extruded torrefied samples (0 to 51% mass loss) was between 7.66 MPa and 10.94 MPa and has a lower strength than LDPE (12 MPa) (Kormin et al. 2017). We provided some comparative data of the torrefied material (that has been thermally degraded) relative to common plastics seen in the waste plastic mix.

Figure 3.6c presents results for the storage modulus (E' at 20 °C), showing a clear increase with mass loss. A similar trend has been found existing on natural fiber polypropylene composites (Tajvidi et al., 2006). This might be due to the lower fiber content at a higher mass loss, while the reinforcement imparted by the fiber could allow stress transfer from the matrix to the fiber (Rana et al., 1999).

DMA analysis was performed on the extruded material. Figure 3.6d presents results for tan(δ) (at 20 °C), showing a clear increase with mass loss, which indicates that the material has more energy dissipation potential as the mass loss increases.

Figure 3.6e presents the temperature of the maximum loss modulus (E”), showing a clear decrease from about 100 °C to 50 °C with an increase in mass loss from 0 to 51%. This indicates that the severity of torrefaction softens the material at the lower temperatures. This may be due to (i) a reduction in fiber length (due to extended torrefaction) and thus lower its reinforcement ability or (ii) a change in the torrefied material’s structure such as molar mass.

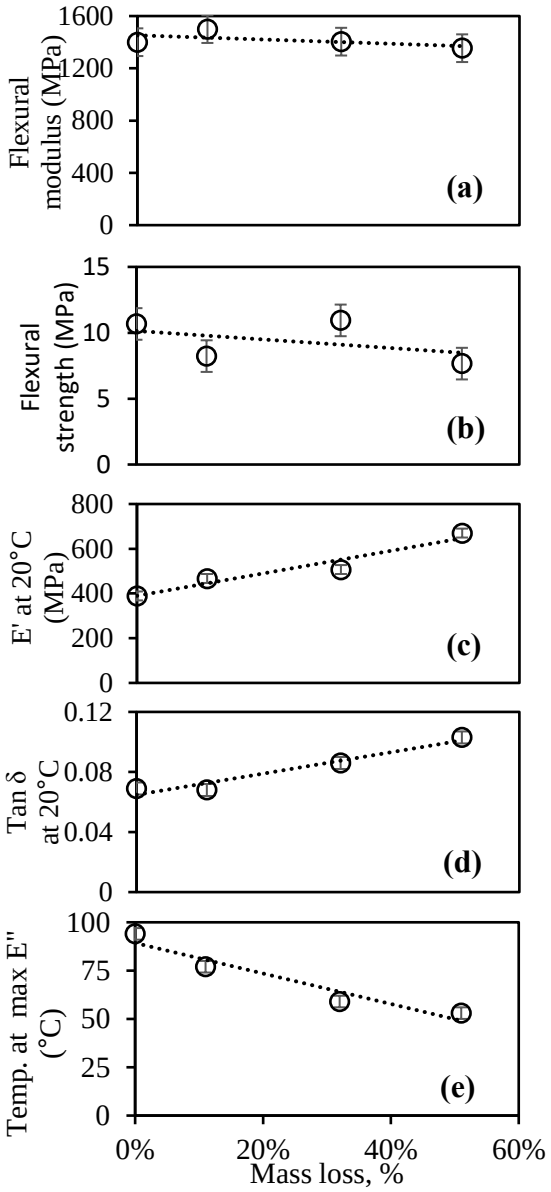

Figure 3.6**.** Various properties of extruded pellets vs. mass loss during torrefaction

3.4.8 Water Resistance

A sample of torrefied (20% mass loss) and extruded material was used in the water absorption experiment. The samples were submerged in water for 30 days. Samples were taken out for water intake measurements after 1,3,11,25 and 30 days. Material disintegration was not observed. The results show water intake (as the weight difference, in percent) reached an asymptotic value after 5 days to 0.7%, indicating that these extruded pellets did not absorb water (water resistance has been measured for all samples with similar results). This can be attributed to the plastic melted around the fiber. In addition, it can be hypothesized that the protective layer prevents oxygen from accessing the active sites created by the degradation of the cellulosic polymers.

3.4.9 Size Distribution

As shown by Xu et al., 2018, the fractions above and below 850 µm represent the changes in the material structure (physical and structural) as the mass loss increases. Figure 3.7a shows the size distribution of the extruded torrefied pellets with 0% 11%, 32%, and 51% mass loss. It was clear that after grinding, the size fraction below 850 µm went up as mass loss increased and it almost reached 100% at 51% mass loss, and size fraction above 850 µm went down accordingly. According to Wang et al., the increase in the size fraction under 850 µm can be attributed to weakening of cell walls of fibers after torrefaction (Wang et al., 2011). The ability to reduce the average size is essential for pulverized fuel combustion as smaller particles have faster combustion rate (Smith, 1982).

3.4.10 Heat Content

To avoid sampling issues the material was ground and sifted to 5 different fractions. The heat content of each size fractions was measured, and the total heat content was calculated based on the weighted average. Figure 3.7b-g shows the heat content for the pellets with the function of mass loss. The heat content increased from 28.1 MJ/kg to 35.2 MJ/kg as the mass loss increased to 51%. Combustion test

The extruded pellets produced can be burned as is in stokers, moving grates and other boilers (Taulbee et al., 2010) without grinding. In this case, it is essential to study the combustion behavior of the pellets. When the pellets are heated up, the volatile matter is first released and burned in the gas phase at a fast rate, then the fixed carbon burns at a much slower rate; this behavior is comparable to that of biomass and coal combustion.

The two-stage combustion behavior is expected to behave according to the following equation $\alpha = a_1\left(1 - e^{-\frac{t}{\tau_1}}\right) + a_2\left(1 - e^{-\frac{t}{\tau_2}}\right)$ where α is the fraction of the burned material (pellet), a_1 and a_2 are the fraction of volatile and fixed carbon, respectively. The characteristic times τ_1 and τ_2 represent the volatile burning and fixed carbon burning, respectively. The values of a_1 and a_2 were measured for each mass loss (Twin Port Testing, 2019). The values τ_1 and τ_2 were fitted from experimental data and were kept identical in all the cases (all the mass loss values). Figure 3.7b shows measured volatile content and fixed carbon as a function of mass loss. It has shown that the volatile matter of the material decreases with the extent of torrefaction, and the fixed carbon increases accordingly. Figure 3.7c-g show combustion test results, plotted as mass loss fraction vs. time, for non-torrefied pellets (Figure 3.7c) and for torrefied pellets with mass losses in the rage of 10-51% (Figure 3.7d-f). The characteristic times for the volatile matter and fixed carbon was found to be 1.49 min and 15.62 min, respectively.

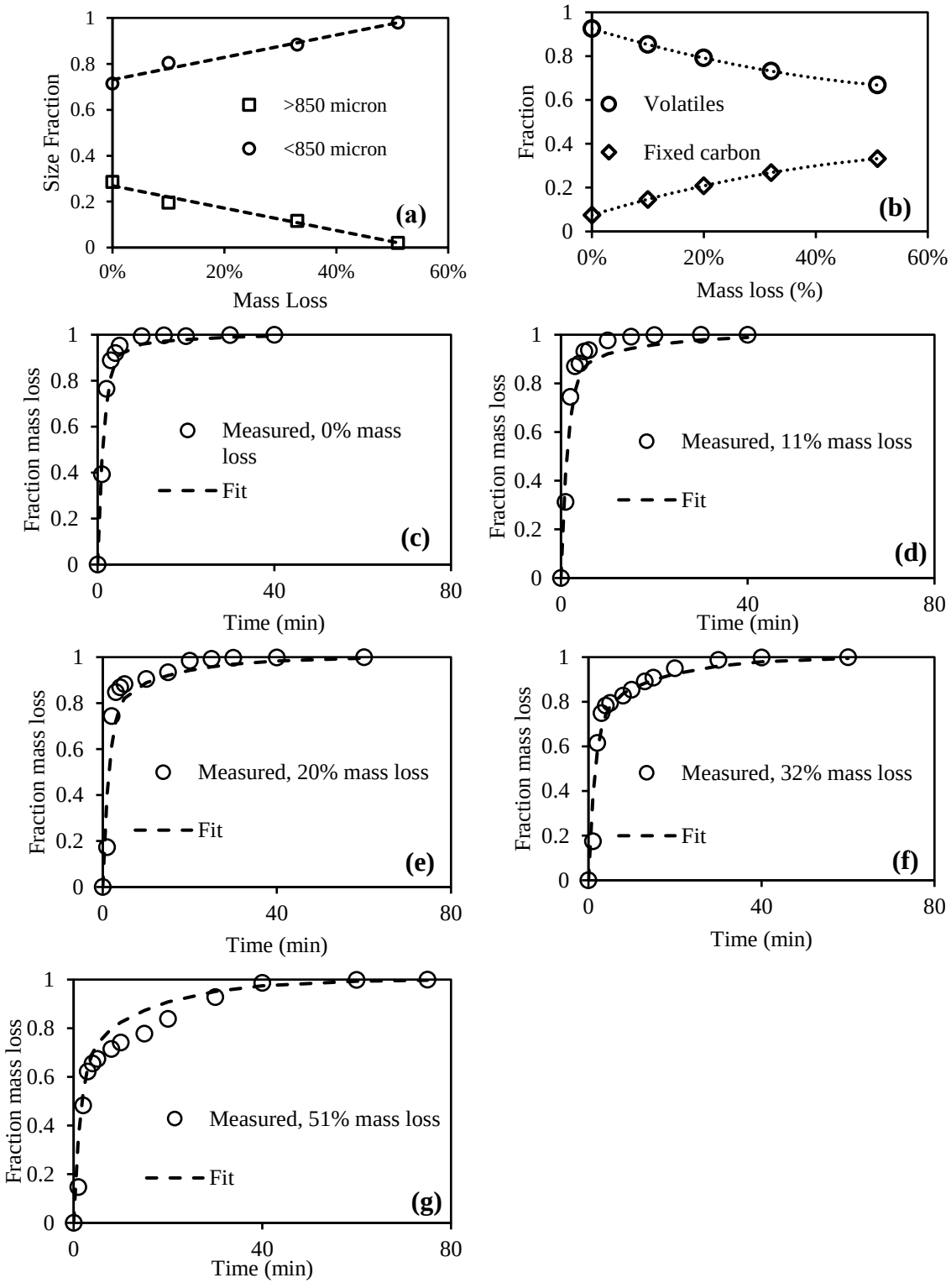

Figure 3.7. (a) Size fractions of the extruded pellets after grinding; (b) Volatile content and fixed carbon as measured as a function of torrefaction mass loss; (c) Combustion tests, plotted as mass loss fraction vs time for non-torrefied pellets; (d-g) torrefied

3.5 Summary and Conclusions

In this study, waste blends consisting of 40% plastic and 60% fiber were torrefied at 300°C in the range 0-51% mass loss. Samples were extruded into pellets, and the properties of the pellets were characterized. The following characteristics can be concluded:

Synergy. Torrefaction showed synergistic effects between the fiber (mostly cellulose polymers) and the plastic material (mostly hydrocarbon polymers).

Plastic. Acts as a binder in and the molten plastic encapsulated the fiber to form more consistent and uniform material.

Inhomogeneity. Extrusion and torrefaction enhanced significantly the uniformity.

Density and water resistance. After extrusion to density reached intrinsic values and the samples were water resistant.

Heat content. Was increased with extent of torrefaction.

Thermal and mechanical properties. Durability of the pellets is mildly affected by torrefaction.

Rheology. Elasticity improves with extent of torrefaction.

Grindability. The torrefied material becomes more brittle with extent of torrefaction.

Combustion. Combustion rate of the pellets decreases with extent of torrefaction due to loss of volatiles.

The overall conclusions is that the extruded torrefied pellets enhance the properties of the original plastic-fiber blends and could be a drop-in solid fuel for power generation.

Acknowledgements

We acknowledge the support from (1) Battelle/Idaho National Laboratory (INL) Grant contract number 209856; (2) M.J. Murdock Charitable Trust for the purchase of the twin-screw extruder.

3.6 Works Cited

Adefisan, O.O., Wei, L., & McDonald, A.G. (2017) Evaluation of plastic composites made with Laccosperma secundiflorum and Eremospatha macrocarpa canes. *Maderas Ciencia tecnologia.* 19(4): 517-524.

Arias, B., Pevida, C., Fermoso, J., Plaza, M. G., Rubiera, F., & Pis, J. J. (2008). Influence of torrefaction on grindability and reactivity of biomass. *Fuel Processing Technology*, 89(2), 169-175.

ASTM International (ASTM D 790-07). 2008. Standard test method for flexural properties of unreinforced and reinforced plastics and electrical insulating materials. *In Annual book of ASTM standards. Vol 08(01*). West Conshohocken, PA.

ASTM International (ASTM D 5630-13). 2001. Standard test method for ash content in plastics. *In Annual book of ASTM standards, Vol 08.03*. West Conshohocken, PA.

Ayomoh, M. K. O., Oke, S. A., Adedeji, W. O., & Charles-Owaba, O. E. (2008). An approach to tackling the env. and health impacts of MSW disposal in developing countries. *Journal of Environmental Management*, 88(1), 108-114.

Balogun, A., Sotoudehniakarani, F., & McDonald, A.G. (2017). Thermo-kinetic, spectroscopic study of brewer's spent grains and characterization of their pyrolysis products. *Journal of Analytical and Applied Pyrolysis*. 127: 8-16. https://doi.org/10.1016/j.jaap.2017.09.009.

Bar-Ziv, E., & Klinger, J. (2016). Logistics and storage of torrefied biomass Safety aspects, Safety Consideration in Biomass Torrefaction. *Energy-Tech Magazine*, Online, October 2016. Retrieved from http://www.energy-tech.com/fuels/.

Bolton, K., & Rousta, K. (2019). Solid Waste Management Toward Zero Landfill: A Swedish Model. In *Sustainable Resource Recovery and Zero Waste Approaches* (pp. 53-63).

Ceballos, D. C. C., Hawboldt, K., & Hellleur, R. (2015). Effect of production conditions on self-heating propensity of torrefied sawmill residues. *Fuel*, 160, 227-237.

China Daily. (2018). "China announces import ban on 32 types of solid waste". Retrieved from www.chinadaily.com.cn/a/201804/19/WS5ad83620a3105cdcf65194db.html.

Donepudi, Y. (2017) Impact of pretreatment methods on fast pyrolysis of biomass. [dissertation]. [Houghton (MI)]: Michigan Technological University

El-Fadel, M., Findikakis, A. N., & Leckie, J. O. (1997). Environmental impacts of solid waste landfilling. *Journal of Environmental Management*, *50*(1), 1-25.

EPA, Environmental Protection Agency. (2014) "Carbon Pollution Emission Guidelines for Existing Stationary Sources: Electric Utility Generating Units." Federal Register.

EPA, Environmental Protection Agency. (2015) Carbon pollution emission guidelines for existing stationary sources: electric utility generation units, EPA-HQ-OAR-2013-0602, pp1560.

Faix, O. (1992) Fourier transform infrared spectroscopy. In: Lin SY, Dence CW, editors. Methods in lignin chemistry. (pp. 83-132). Berlin: Springer-Verlag.

Harper, C.A. (1999) *Modern Plastics Handbook: Modern Plastics*. (pp. C41-C49). McGraw-Hill. N.Y.

Hamad, K., Kaseem, M., & Deri, F. (2013) Recycling of waste from polymer materials: An overview of the recent works. *Polymer Degradation and Stability*. 98: 2801-2812.

Hanaffi Mohd Fuad, M. A., Faizal, H. M., Rahman, M. R. A., & Latiff, Z. A. (2018). Torrefaction of densified empty fruit bunches with addition of plastics waste. *Biofuels*, 1-11.

Harvey, O. R., Herbert, B. E., Kuo, L. J., & Louchouarn, P. (2012). Generalized two-dimensional perturbation correlation infrared spectroscopy reveals mechanisms for the development of surface charge and recalcitrance in plant-derived biochars. *Environmental science & technology*, *46*(19), 10641-10650.

Iroba, K.L., Baik, O.D., & Tabil, L.G. (2017). Torrefaction of biomass from municipal solid waste fractions I: Temperature profiles, moisture content, energy consumption, mass yield, and thermochemical properties. *Biomass and Bioenergy*, *105*, 320-330.

Iroba, K.L., Baik, O.D., & Tabil, L.G. (2017). Torrefaction of biomass from municipal solid waste fractions II: Grindability characteristics, higher heating value, pelletability and moisture adsorption. *Biomass and Bioenergy*, *106*, 8-20.

Jacob, R., & Isac, J. (2017). Dynamic mechanical analysis and thermal degradation of jute fiber reinforced BSFT (Ba0. 6Sr0. 4FexTi (1-x) O3-δ), (x= 0.1)-polypropylene composite. *Indian Journal of Pure & Applied Physics (IJPAP)*, *55*(7), 497-502.

Kiel, J. (2011). Torrefaction for upgrading biomass into commodity fuel. In *Status and ECN Technology Development. EUBIONET III Workshop, Espoo, Finland* (Vol. 15).

Klinger, J., Bar-Ziv, E., & Shonnard, D. (2015). Unified kinetic model for torrefaction–pyrolysis. *Fuel Processing Technology*, *138*, 175-183.

Klinger, J., Klemetsrud, B., Bar-Ziv, E., & Shonnard, D. (2014). Temperature dependence of aspen torrefaction kinetics. *Journal of Analytical and Applied Pyrolysis*, *110*, 424-429.

Kormin S., Kormin, F., Beg, M.D.H., & Piah, M.B.M. (2017) Physical and mechanical properties of LDPE incorporated with different starch sources. IOP Conf. Series: Materials Science and Engineering 226: 1-9. DOI:10.1088/1757-899X/226/1/012157.

Kumar, L., Koukoulas, A.A., Mani, S., & Satyavolu, J. (2017). Integrating Torrefaction in the Wood Pellet Industry: A Critical Review. *Energy Fuels*, 31, 37-54.

Luo, S., Cao, J., & McDonald, A. G. (2016). Interfacial improvements in a green biopolymer alloy of poly (3-hydroxybutyrate-co-3-hydroxyvalerate) and lignin via in situ reactive extrusion. *ACS Sustainable Chemistry & Engineering*, *4*(6), 3465-3476.

Mayo, D.W., Miller, F. A., & Hannah, R. W. (2004). *Course notes on the interpretation of infrared and Raman spectra*. (pp 33-72). New York: Wiley-Interscience.

Mayo, D.W. (2003). Spectra of carbonyl compounds of all kinds (factors affecting carbonyl group frequencies). In *Course notes on the interpretation of infrared and Raman spectra*. (pp. 199-224). John Wiley & Sons, Inc. Hoboken, New Jersey.

Miller, F.A. (2003). Characteristic frequencies of alkenes (olefins). *Course Notes on the Interpretation of Infrared and Raman Spectra.* (pp. 73-84). John Wiley & Sons, New York.

Nallar, M., & Wong, H. W. (2019). Enhanced Levoglucosan Yields from the Co-pyrolysis of Cellulose and High-Density Polyethylene. *ACS Sustainable Chemistry & Engineering*.

Nunes, L. J. R., Matias, J. C. O., & Catalão, J. P. S. (2014). A review on torrefied biomass pellets as a sustainable alternative to coal in power generation. *Renewable and Sustainable Energy Reviews*, *40*, 153-160.

Paletta, A., Leal Filho, W., Balogun, A. L., Foschi, E., & Bonoli, A. (2019). Barriers and challenges to plastics valorisation in the context of a circular economy: Case studies from Italy. *Journal of Cleaner Production*, *241*, 118149.

Pandey, K.K. (1999) A study of chemical structure of soft and hardwood and wood polymers by FTIR spectroscopy. *Journal of Applied Polymer Science*. 71: 1969–75.

Park, J., Meng, J., Lim, K. H., Rojas, O. J., & Park, S. (2013). Transformation of lignocellulosic biomass during torrefaction. *Journal of Analytical and Applied Pyrolysis*, *100*, 199-206.

Radics, R.I., Gonzales, R., Bilek, E.M., & Kelley, S.S. (2017). Systematic Review of Torrefied Wood Economics. BioResources 12 (3), 6868-6886.

Rana, A. K., Mitra, B. C., & Banerjee, A. N. (1999). Short jute fiber ‐ reinforced polypropylene composites: Dynamic mechanical study. Journal of Applied Polymer Science, 71(4), 531-539.

Rodríguez-Monroy, C., Mármol-Acitores, G., & Nilsson-Cifuentes, G. (2018). Electricity generation in Chile using non-conventional renewable energy sources–A focus on biomass. *Renewable and Sustainable Energy Reviews*, 81, 937-945.

Ru, B., Wang, S., Dai, G., & Zhang, L. (2015). Effect of torrefaction on biomass physicochemical characteristics and the resulting pyrolysis behavior. *Energy & Fuels*, *29*(9), 5865-5874.

Smith, I. W. (1982). The combustion rates of coal chars: A review. *Symposium (International) on Combustion*, 19(1), 1045–1065. https://doi.org/10.1016/S0082-0784(82)80281-6.

Stelte, W., Bar-Ziv, E., & Klinger, J. (2016). Logistics and storage of torrefied biomass Safety aspects, Safety Consideration in Biomass Torrefaction. Energy-Tech Magazine, Online, October 2016. Retrieved from http://www.energy-tech.com/fuels/.

Stelte, W., Sanadi, A. R., Shang, L., Holm, J. K., Ahrenfeldt, J., & Henriksen, U. B. (2012). Recent developments in biomass pelletization–A review. *BioResources*, *7*(3), 4451-4490.

Shah, V (1998). *In* Handbook of Plastics Testing Technology, 2nd Ed (pp. 509). Wiley Interscience, NY.

Tajvidi, M., Falk, R. H., & Hermanson, J. C. (2006). Effect of natural fibers on thermal and mechanical properties of natural fiber polypropylene composites studied by dynamic mechanical analysis. *Journal of Applied Polymer Science*, *101*(6), 4341-4349.

Taulbee, D., Neathery, J., Patil, D., Sowder, N., O'Daniel, B., & Montross, M. (2010). Combustion of Briquettes and Fuels Pellets Prepared from Blends of Biomass and Fine Coal. In *International Coal Preparation Congress 2010 Conference Proceedings* (pp. 161-170). SME.

Tsalidis, G. A., Joshi, Y., Korevaar, G., & de Jong, W. (2014). Life cycle assessment of direct co-firing of torrefied and/or pelletised woody biomass with coal in The Netherlands. *Journal of Cleaner Production*, *81*, 168-177.

Tumuluru, J. S., Wright, C. T., Hess, J. R., & Kenney, K. L. (2011). A review of biomass densification systems to develop uniform feedstock commodities for bioenergy application. *Biofuels, Bioproducts and Biorefining*, *5*(6), 683-707.

Twin Port Testing. (2019, Feb 26). Retrieved from https://www.twinportstesting.com/.

US-EIA, U.S. Energy Information Administration, based on U.S. Environmental Protection Agency. (2010) 2010 MSW Facts and Figures Factsheet. Retrieved from https://www.eia.gov/todayinenergy/detail.php?id=8010.

Van der Stelt, M. J. C., Gerhauser, H., Kiel, J. H. A., & Ptasinski, K. J. (2011). Biomass upgrading by torrefaction for the production of biofuels: A review. *Biomass and bioenergy*, *35*(9), 3748-3762.

Wang, C., Li, M., & Fang, Y. (2016). Coprocessing of catalytic-pyrolysis-derived bio-oil with VGO in a pilot-scale FCC riser. Industrial & Engineering Chemistry Research, 55(12), 3525-3534.

Wang, G., Luo, Y., Deng, J., Kuang, J., & Zhang, Y. (2011). Pretreatment of biomass by torrefaction. *Chinese Science Bulletin*, *56*(14), 1442-1448.

Wang, X., Yu, Z., & McDonald, A.G. (2019) The effect of biochar as reinforcing filler on the properties of wood plastic composites. Journal of Bionic Engineering. 16(2): 337-353. https://doi.org/10.1007/s42235-019-0029-0.

Wang, Z., Pecha, B., Westerhof, R., Kersten, S., Li, C-Z., McDonald, A.G., & Garcia-Perez, M. (2014) Effect of cellulose crystallinity on solid/liquid phase reactions responsible for the formation of carbonaceous residues during slow pyrolysis. *Industrial & Engineering Chemistry Research*. 53(8): 2940–2955. dx.doi.org/10.1021/ie4014259

Wei, L., McDonald, A.G., Freitag, C., & Morrell, J.J. (2013) Effects of wood fiber esterification on properties, weatherability and biodurability of wood plastic composites. *Polymer Degradation & Stability*. 98: 1348-1361.

Xu, Z., Zinchik, S., Kolapkar, S. S., Conn, D., Hansen, T., Bar-Ziv, E., & McDonald, A. G. (2018). Properties of Torrefied US Waste Blends. *Frontiers in Energy Research, 6,* 65. doi.org/10.3389/fenrg.2018.00065.

4 Kinetic Study of Paper Waste Thermal Degradation

This section is based on the following paper that is currently in preparation:

Z. Xu, S. Zinchik, SS. Kolapkar, E. Bar-Ziv, J. Klinger, E. Fillerup, K. Schaller, C. Pilgrim. 2021. In preparation to be submitted to Polymer Degradation and Stability Elsevier

4.1 Abstract

The amount of paper waste generation has been increasing with a significant amount being landfilled. These non-recyclable paper wastes can be treated with thermal processes to turn into energy sources, which has been proven to be carbon neutral. These wastes contain mainly cellulose, hemicellulose, lignin, and some minerals. The thermal decomposition of cellulose, hemicellulose, and lignin have been extensively studied, however, the knowledge of thermal degradation of paper wastes at lower temperatures, which are more practical for industrial applications are still lacking. In this study, paper wastes have been characterized and thermogravimetric analyses were performed from 200 °C to 400 °C and the char produced were analyzed by nuclear magnetic resonance (NMR) spectroscopy. Two kinetic approaches were taken while developing the kinetic model of paper waste thermal degradation: (i) reconstructing the TGA results of paper waste thermal degradation by an additive law of the degradation of cellulose, hemicellulose and lignin; (ii) considering paper waste as one material and develop a multi-step consecutive reaction mechanism that focuses on solid products at different temperatures. It was found that there are interactions between cellulose, hemicellulose and lignin during paper waste degradation. Therefore, the second approach was concluded to be more plausible, and the kinetic parameters were determined according to the experimental results at different temperatures. These results provided insights into the degradation kinetic mechanism and solid product distribution of the paper waste. It was found that the first reaction was due to dehydration of cellulose and the 6^{th} and 7^{th} reaction can be attributed to the thermal degradation of lignin.

4.2 Introduction

The amount of waste generated across the world has been increasing, and paper waste is one of the major contributors to this growth. For instance, U.S. alone produced about 67 million tons of paper waste in 2017, with 18.4 million tons been landfilled (US EPA, 2017). These landfilled paper wastes are usually mixed with different materials, which makes them economically prohibitive to recycle. The landfill approach is not only inefficient in utilizing resources, but it would also produce greenhouse gases during the decomposition process. A potential alternative is treating these non-recyclable wastes with a thermal process and turn them into energy sources, which has been proven to be carbon-neutral (McCabe, 2014).

The paper wastes used in this study mainly consists of used paper and cardboard, which contain mostly cellulose, with lower level of hemicellulose, lignin, and inorganic material analyzed as ash content (Eichhorn et al., 2001; Ma et al., 2016). In order to study the thermal degradation of paper, it is essential to understand the behavior of cellulose, hemicellulose, and lignin during thermal degradation. The following provides a review of

the kinetics of thermal degradation of cellulose hemicellulose and lignin. Since cellulose hemicellulose and lignin have been extensively studied by many researchers, we restricted our review to a few studies.

Bradbury et al., proposed a mechanism for cellulose thermal degradation (Broido-Shafizadeh mechanism) (Bradbury et al., 1979). The mechanism suggests that the cellulose first produces active cellulose, during which the cellulose does not lose any mass. This reaction will subsequently go through two pathways, with one reaction producing volatiles, another decomposing into char and gases.

Cabrales and Abidi have studied the thermal degradation of cellulose of cotton fibers (Cabrales and Abidi, 2010). Reaction rate was calculated by the Arrhenius equation and activation energy was modeled as a function of the conversion level. It was stated that the thermal degradation of cellulose was a multi-step process, and the results showed that this process was governed by the slowest. Mamleev et al., studied the kinetics of cellulose thermal decomposition and focused on the main step of mass loss (Mamleev et al., 2007). A two-step reaction mechanism was proposed, and the kinetic parameters were obtained; this study focused on 300 °C.

The hemicellulose thermal degradation was also well investigated in the literature (Shen et al., 2010; Collard and Blin, 2014). The studies included different steps and product distributions during the degradation process. It was also found that hemicellulose is easier to degrade compared to cellulose. Hemicellulose produced more CO_2, which can be attributed to its higher carboxyl content; and cellulose had higher CO yield, due to the existence of carboxyl and carbonyl.

The lignin decomposes slower at the studied temperature range (200 °C-400 °C) in comparison to cellulose and hemicellulose (Brebu and Vasile, 2010). It has been found that lignin thermal degradation has two reaction rate peaks below 400 °C. The first one is at the range of 100-180 °C, due to the elimination of moisture, and the second from 375-400 °C. In addition, the reactions at around 400 °C produce mainly aromatic hydrocarbons, such as hydroxy phenolics and phenolics(Alén et al., 1996; Rodrigues et al., 2001). These studies shed some light on the products of the lignin thermal degradation.

Although the thermal degradation of cellulose, hemicellulose and lignin has been well documented, the existence of interactions between the three components in mixtures has been controversial. Some researchers did not observe interactions between cellulose and lignin during thermal degradation(Alén et al., 1996; Raveendran, 1996; Biagini et al., 2006; Yang et al., 2006), while others reported notable interactions (Hilbers et al., 2015; Wu et al., 2016; Volpe et al., 2018; Zhao et al., 2018). Zhang et al., studied the interactions between native (plant biomass) and non-native (physical mixture) cellulose-hemicellulose mixture and cellulose-lignin mixture (Zhang et al., 2015). They found that are no significant interactions between the physical mixture of cellulose-lignin, cellulose-hemicellulose and woody native cellulose-lignin samples. However, the interactions were observed in native cellulose−lignin mixture, as the levoglucosan yield decreased and the low molecular weight compounds and furans yield increased. Recently, Yang et al., found

that the volatiles produced from hemicellulose at 280 °C could interact with cellulose and lignin and promote their decomposition (Yang et al., 2020). In addition, it was observed that the volatiles produced from cellulose at 315 °C were captured by lignin to form aromatic rings. There are other studies that are not reviewed here, however, they further emphasized the controversy of existence of interactions between the three components. In order to understand paper waste degradation at the temperature range of 225 °C-400 °C, it is essential to study if there are potential interactions between cellulose, hemicellulos and lignin that are the main constituents in papers. If there are no interactions, paper degradation can be described by a simple additive rule of the three components. If there are such interactions during thermal degradation, paper wastes should be treated as one material, such as done in kinetics of biomass (that is also mainly consist of cellulose, hemicellulose and lignin) degradation at these temperatures; for example, see references (Várhegyi et al., 1997; Klinger et al., 2013, 2014; Zhou et al., 2015) and references cited therein.

Although both biomass and paper wastes mainly consist of cellulose, hemicellulose and lignin, the two material have different chemical structures. For example, the cellulose in the biomass is usually a relatively long thread that is the main structural material which formed plant cell wall (Pasangulapati et al., 2012). However, during paper making processes, especially pulping, drying and printing, the structure of cellulosic fibers can undergo significant changes (Hubbe et al., 2007). Further, paper wastes also contains various chemical additives (Farhat et al., 2017).

In this paper, we present comprehensive study of paper thermal degradation in the temperature range of 225 °C to 400 °C, that comprises experimental TGA measurements of paper waste and the individual cellulose, hemicellulose and lignin components. We attempted to analyze and interpret the experimental results by two kinetic approaches: (i) reconstructing the TGA results of paper waste thermal degradation by an additive law of the degradation of cellulose, hemicellulose and lignin; (ii) consider paper waste as one material and develop a multi-step consecutive reaction mechanism that focuses on solid products at different temperatures. It was found that there are interactions between cellulose, hemicellulose and lignin during paper degradation. Therefore, we took second approach mentioned above. This approach can both provide more insights in paper wastes thermal degradation and can effectively help to design paper waste thermal treating processes for the industrial systems.

4.3 Material and Methods

4.3.1 Material

The materials used in this study were non-recyclable industrial paper waste, cellulose powder (Avicel PH-101, Fluka), hemicellulose (extracted xylan). The paper waste consists of paper, cardboard, carton, wax papers and laminated paper residuals. Details of the paper waste has been covered in the previous work (Xu et al., 2018, 2020a). The paper wastes went through three stages of downsizing and the final size is 2 by 2 mm sized to reduce

heterogeneity of the original material. No additional treatment was performed for the commercial cellulose, hemicellulose and lignin.

4.3.2 Experimental Methods

4.3.2.1 Thermal properties analysis

Thermal conductivity was measured by ThermTest Inc. TPS15000. The samples are placed in an oven and two multimeters with 100nV accuracy were used. The results were analyzed with a custome build Vitual Instrument in Labview. As the interface temperature changes, the sample thermal diffusivity is fitted to match changes in resistance. The voltage potential across the sensor was used to calculate the sensor transient resistance.

4.3.2.2 Molecular Weight

Waste paper and Avicel®PH 101 were characterized for molecular weight distributions as described in previous work (Patkar and Panzade, 2016). The materials were prepared for molecular weight analysis using N, N-dimethylacetamide (HPLC grade, Sigma-Aldrich) and lithium chloride (99.9% Bioextra, Sigma-Aldrich) as solvents after fine milling the solids to less than 200 microns. The molecular weight distribution was determined using an Agilent 1200 HPLC (Agilent Technologies Inc., Santa Clara, CA) with a refractive index detector. Chromatographic conditions were: 2 in-line PLgel 20µm Mixed-A LS 300 X 7.5 mm columns and guard column; refractive index detector temperature 35°C; column temperature 70°C; 0.5% LiCl in N,N-dimethylacetamide mobile phase at a flow rate of 1.0mL/min. Cellulose standards (Pullulan standards, Agilent) of varying molecular weight from 180 to 640,000 g/mol were prepared in the same mobile phase and were used to calibrate the column and compared to retention times of samples. From this calibration, the retention times and retention time distributions of the primary eluent peaks indicated the molecular weight distribution of the solids.

4.3.2.3 Thermogravimetric Analysis (TGA)

A LECO TGA 701 was used to carry out thermogravimetric analysis. The oven temperature reaches 110 °C after the experiments started and will maintain this temperature until all the moisture is eliminated. The temperature will then increase to the set temperature with 16 °C/min (highest heating rate for this instrument). The sample mass was by a balance with 0.0001g readability.

4.4 Results and Discussion

In order to study the kinetics of paper waste thermal degradation, it is essential to determine if the temperature of the samples is uniform during the TGA experiments. The following section provides heat transfer modeling of a crucible within the TGA analyzer.

The heat transfer regime of the system was determined by calculating Biot Number (*Bi*) and Thermal Thiele Modulus (*M*), which are defined as:

$$Bi = \frac{h}{\lambda / L_c} \qquad (4.1)$$

$$M = \frac{R^{\dagger}}{\lambda/(c_p L_c^2)} \tag{4.2}$$

It is essential to determine the thermal conductivity of the paper waste since it contains both paper waste and cardboard. Similar analysis was done for the same experimental setup in our previous study. The parameters used to calculate *Bi* and *M* are summarized in Table 4.1 below.

Table 4.1. Estimated values for the parameters to determine the Bi and M.

Parameter	**Value**	**Source**
h, W/m^2-K	10	Free convection
λ for paper waste, W/m-K	0.25	Measured in this study
ρ (apparent), kg/m^3	1200	Measured in this study
c_p (apparent), J/kg-K	1340	(Mahdavi Nejad, 2019)
L_c diameter, m	0.0005	Measured in this study

According to Eq. 4.1, it was assumed that the h and λ are not dependent on temperature, therefore, *Bi* was calculated to yield 0.04, which means the heat convection from the oven walls to the sample surface is significantly slower than the heat transfer from the surface into the core of the sample, and the sample temperature is uniform during the experiments.

In order to calculate *M*, the reaction rate as a function of temperature has to be known. In this study, the measured reaction rate is shown in Figure 4.1 in the temperature range of 225 °C – 400 °C. It shows that the maximum mass loss rate increases as temperatures and at temperature higher than 300 °C, the paper waste thermal degradations reach highest rate at around 1,100 s.

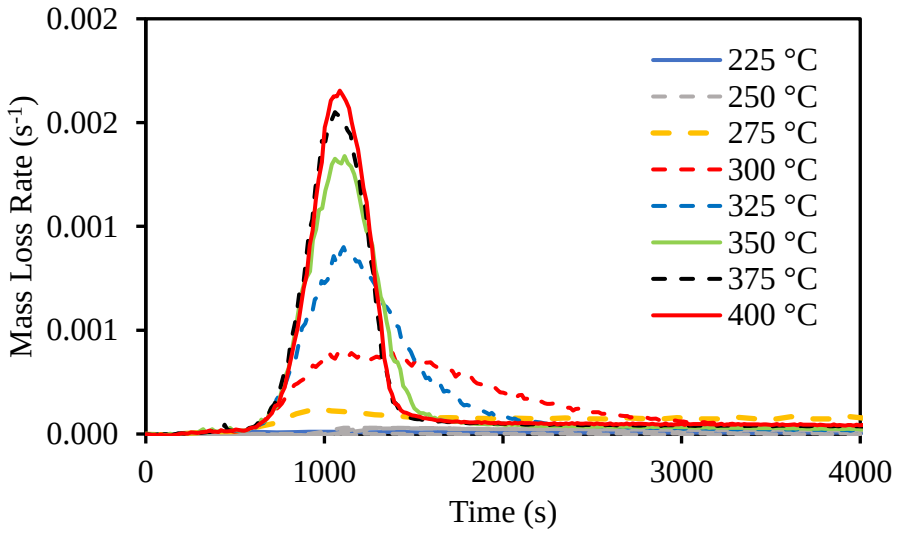

Figure 4.1. Measured mass loss rate at different temperatures vs. time.

From Eq. 4.2, assuming c_p is also constant, only $R^{\dagger}$ changes significantly with temperature. Therefore, the highest $R^{\dagger}$ can yield largest value of M, which is the worst-case scenario. Table 3 shows the maximum reaction rates of the material during experiments determined from Figure 4.1, and $R^{\dagger}$ was calculated by multiplying the maximum reaction rate with the density of the sample (see Table 2). The values of M at different temperatures are shown in Table 4.2. As shown in the table, the value of Ms vary in the range of $1.4x10^{-5}$ to $2.6x10^{-3}$ are significantly smaller than 1. This indicate that reaction rate is dominated by the heat from oven to the sample surface and the sample temperature is uniform and equals to the measured gas temperature.

Table 4.2. M at various temperatures

Temp (°C)	Rate (s^{-1})	$R^{\dagger}$ (kg/m^3-s)	M
225	8.6E-06	0.01	$1.4x10^{-5}$
250	8.6E-05	0.10	$1.4x10^{-4}$
275	3.9E-04	0.47	$6.3x10^{-4}$
300	4.0E-04	0.48	$6.4x10^{-4}$
325	9.0E-04	1.08	$1.4x10^{-3}$
350	1.3E-03	1.56	$2.1x10^{-3}$
375	1.5E-03	1.80	$2.4x10^{-3}$
400	1.6E-03	1.94	$2.6x10^{-3}$

4.4.1 Thermal Degradation of Cellulose, Hemicellulose, and Lignin

To study the thermal degradation behavior of paper waste, it is essential to analyze the experimental results of cellulose, hemicellulose and lignin degradation. TGA experiments were performed with cellulose, hemicellulose, and lignin individually. Figure 4.2 shows the mass loss rates and mass loss versus time of cellulose, hemicellulose and lignin degradation at 325 °C and 400 °C. From Figure 4.2 (a1), it can be found that at 325 °C, the degradation of hemicellulose started at around 240 °C and the mass loss rate of increased rapidly and reached maximum value at around 880 s; the rate of cellulose degradation increased slower but it has a wider time range; the rate of lignin thermal degradation at this temperature is much lower compared to cellulose and hemicellulose. Similar degradation behaviors were also observed in the literature (Brebu and Vasile, 2010; Chen et al., 2019; Yeo et al., 2019). Figure 4.2 (a2) depicts the mass loss transient of cellulose, hemicellulose and lignin during degradation. Although hemicellulose has higher maximum mass loss rate, the mass loss of cellulose (74.1%) after 8,000s was slightly higher compared to hemicellulose (70.2%), and the lignin mass loss at the same time only reached 28.7%. Figure 4.2 (b1) shows the temperature transient and the mass loss rate of cellulose, hemicellulose and lignin torrefaction at 400 °C. The degradation of hemicellulose started at around 240 °C and the rate reached peak value at around 375 °C; the degradation of cellulose started at around 275 °C and its highest mass loss rate is slightly higher than hemicellulose; the lignin started degrading at around 350 °C its maximum mass loss rate was very close to hemicellulose. Although hemicellulose started degrading at lower

temperature compared to cellulose, its mass loss (81.2%) after 8,000 s was lower than cellulose (87.3%), and the mass loss of lignin after 8,000 s reached 81.1%.

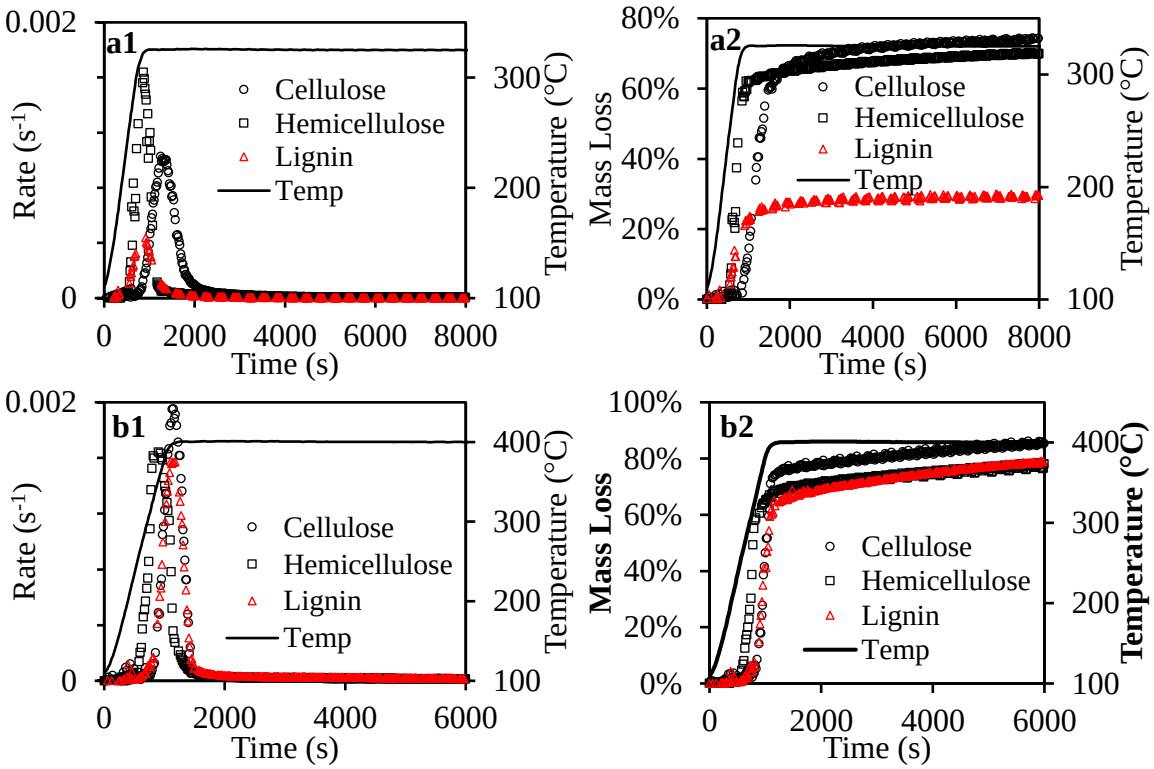

Figure 4.2. Mass loss rate of cellulose, hemicellulose and lignin at 325°C (a1) and 400°C (b1); mass loss of cellulose, hemicellulose and lignin at 325°C (a2) and 400°C (b2).

Figure 4.3 depicts typical measured results of paper waste TGA at 325 °C and 400 °C for (a) the degradation rate and (b) the integrated mass loss (Paper_exp). Figure 4.3 also shows the reconstructed rate and mass loss denoted by (Paper_cal) through combining the individual results for cellulose, hemicellulose and lignin. The measured mass loss for paper waste at 325 °C after 8,000 s was 71.4%, while the calculated was only 64.9%. At 400 °C, it can also be observed that the measured data for mass loss after 6,000 s is 90.6%, which is higher than the calculated results of 80.6%. This difference is indictive to potential synergistic effects between cellulose, hemicellulose and lignin. This is an important finding because it indicates that it is not practical to predict the paper thermal degradation by reconstructing the paper waste thermal degradation model by combining the model of cellulose, hemicellulose and lignin. Therefore, in order to develop the kinetic model of the paper waste thermal degradation, it is essential to treat paper waste as one material.

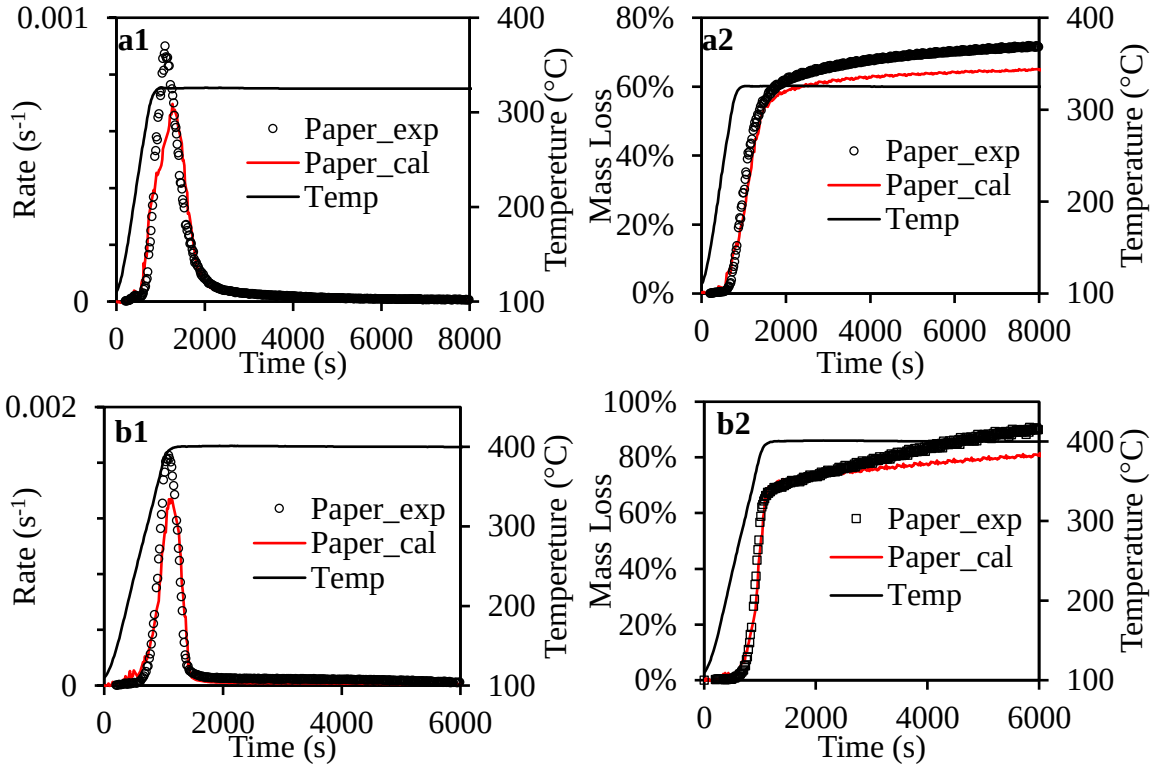

Figure 4.3. Mass loss rate of cellulose, hemicellulose and lignin at 325°C (a1) and 400°C (b1); mass loss of cellulose, hemicellulose and lignin at 325°C (a2) and 400°C.

4.4.2 Kinetic Modeling

In order to study the kinetics of the paper waste thermal degradation, a multi-consecutive reaction mechanism was proposed. Since the TGA only measures the weight of the solids during the experiments, this model focuses on solid products and as follows.

$$Paper \xrightarrow{k_1} S_1 + gas \qquad \text{Reaction 1}$$

$$S_1 \xrightarrow{k_2} S_2 + gas \qquad \text{Reaction 2}$$

$$\cdots\cdots$$

$$S_{i-1} \xrightarrow{k_i} S_i + gas \qquad \text{Reaction i}$$

$$\cdots$$

$$S_n \xrightarrow{k_{n+1}} Carbon + gas \qquad \text{Reaction n+1}$$

Paper and S_i denote paper and the solid product of the i^{th} reaction, respectively, and *Carbon* is the final product of the thermal degradation of paper waste. The mass loss results were based on dry-ash-free basis, and the number of reactions would differ with different degradation temperatures (Klinger et al., 2014, 2015). The reaction rate of all the solids are:

$$\frac{dx_{Paper}}{dt} = -k_1 x_{Paper} \tag{4.3}$$

…… (4.4)

$$\frac{dx_{S_{i-1}}}{dt} = \alpha_{i-1} k_{i-1} x_{S_{i-2}} - k_i x_{S_{i-1}}$$

$$\frac{dx_{S_n}}{dt} = \alpha_n k_n x_{S_{n-1}} \tag{4.5}$$

Where $x_{Paper} = \frac{m_{Paper}}{M_{Paper}}$, $x_{S_i} = \frac{m_{S_i}}{M_{S_i}}$, $\alpha_i = \frac{M_{S_i}}{M_{S_{i-1}}}$.

Assuming the thermal degradation reaction of paper to be first-order and the reaction rate k_i depends on the temperature and follows Arrhenius function:

$$k_i = A_i \exp\left(-\frac{T_{C_i}}{T(t)}\right) \tag{4.6}$$

Where A_i is the pre-exponential factor and T_{C_i} is the characteristic temperature that equals $\frac{E_{a_i}}{R}$ (E_{a_i}denotes the activation energy of the specific reaction and R is the gas constant). According the heat transfer model above, the temperature of the sample was uniform and equals to the temperature of the gas. Since the above reaction rate equation only represent the results in molar fraction, while the TGA were measuring the weight of the material, it is essential to transform the above equations into weight fraction.

For Eqs. 4.3-4.6, the following can be obtained by multiplying $\frac{m_{S_i}}{m_{Paper}}$:

$$\frac{dy_{Paper}}{dt} = -k_1 y_{Paper} \tag{4.7}$$

……

$$\frac{dy_{S_{i-1}}}{dt} = \alpha_{i-1} k_{i-1} y_{S_{i-2}} - k_i y_{S_{i-1}} \tag{4.8}$$

$$\frac{dy_{s_i}}{dt} = \alpha_i k_i y_{S_{i-1}} \tag{4.9}$$

Where y_{Paper} and y_{s_i} are the mass fractions of paper and s_i, respectively. By integrating the reaction rate from Eqs. 4.7-4.9, the mass fraction of the solids can be obtained, and the mass loss β, can be calculated by:

$$\beta = 1 - (y_{Paper} + y_1 + \cdots + y_i) \tag{4.10}$$

The molar weight ratios between each solid product and initial material can be obtained as follows:

$$\alpha_1 = \frac{M_{S_1}}{M_{Paper}} \tag{4.11}$$

$$\alpha_1 \alpha_2 \ldots \alpha_n = \frac{M_{S_n}}{M_{Paper}} \quad (4.12)$$

Equation 10 was fitted to the experimental data by adjusting A_i, T_{c_i} and α_i to achieve the best fit, and Figure 4.4a shows the mass loss rate vs. time and Figure 4.4b shows the temperature transient and mass loss vs. time. As shown in the figure, the fit between the model and experimental results are very good. Figure 4.4c depicts the trend of the total mass and solids during the paper waste thermal degradation at 300 °C. It shows that the paper was fully decomposed after 3,800 s, S_1, and S_2 increased at the beginning and was then decomposed after 4,000 s, and S_3 did not fully decompose at 8,000 s and S_4 kept increasing even after 8,000 s.

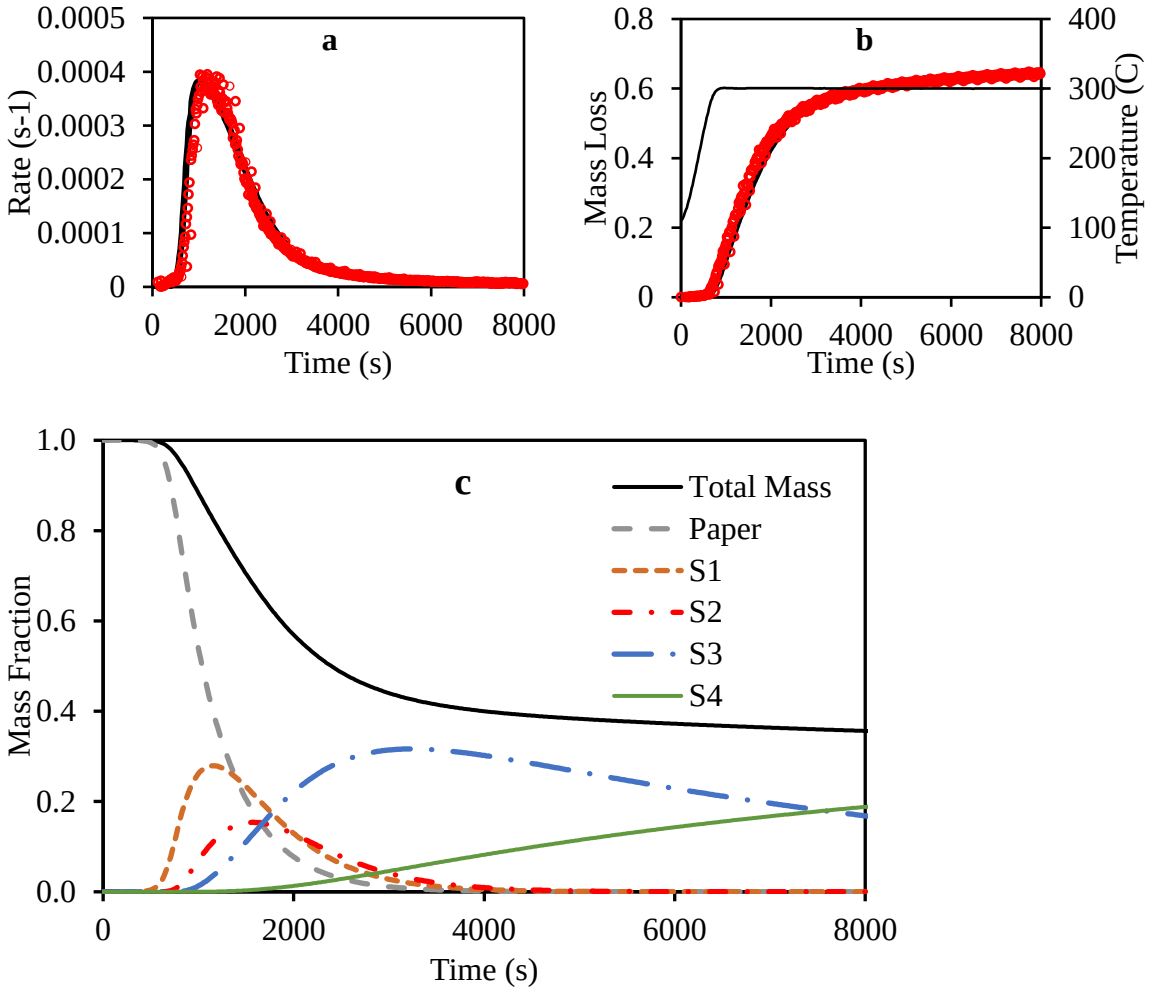

Figure 4.4. (a) Mass loss vs. time and temperature transient at 300 °C; (b) Mass loss vs. time at 300 °C; (c) Solid products mass fraction vs. time.

4.4.3 Modeling at Different Temperatures

Figure 4.5a shows the temperature transients and the mass loss vs. time results at temperatures from 225 °C to 400 °C, with the red symbol denoting experimental results and a black solid line showing the fitted model. Note that although x-axis was only labeled in the 400 °C plot, all of the plots share the same x-axis. The results at 200 °C were also carried out but not plotted here; the mass loss was rather insignificant (around 2% after four hours). Figure 4.5a showed an excellent fit between the experimental with the model results at various temperatures. The mass loss of paper wastes reached 7.24% at 225 °C after 15,000s, this value increased at the same time to 21.9% at 250 °C and 56.4% at 275 °C, showing that the extent of paper waste degradation increases with temperature. The mass loss increased much faster and reached an asymptotic value of 91.9% at 400 °C, which might indicate that there are more reactions at higher temperatures.

For Figure 4.5b, the black solid line, grey dashed line, orange dashed line, red dashed line, blue dash-dot line, green dash-dot line, blue solid line, orange solid line, red solid line and green solid line represent the mass fractions of total mass, paper, S_1, S_2, S_3, S_4, S_5, S_6, S_7 and S_8, respectively. It can be observed that at 225 °C, majority of the paper was degraded after 15,000s, and S_1 was the main solid product with a small fraction of paper waste left and S_2, S_3 produced. As temperature increases, paper waste was fully decomposed and more solid intermediate products were formed. The increase of temperature also increased the rate of paper waste degradation as well as the rate of the formation of all the intermediate solids. At temperatures above 300 °C, after the reaction started, the mass loss increases rather fast at the beginning, which can be mainly attributed to the dehydration reaction of cellulose, forming anhydrocellulose (Scheirs et al., 2001). The green dash-dot line, representing S_5, started to be produced at 275 °C. It increases with time at 300 °C, however, after temperature goes higher, it increased at the beginning and decreased with the extent of thermal decomposition, forming S_6; S_7 and S_8 was only observed at 400 °C.

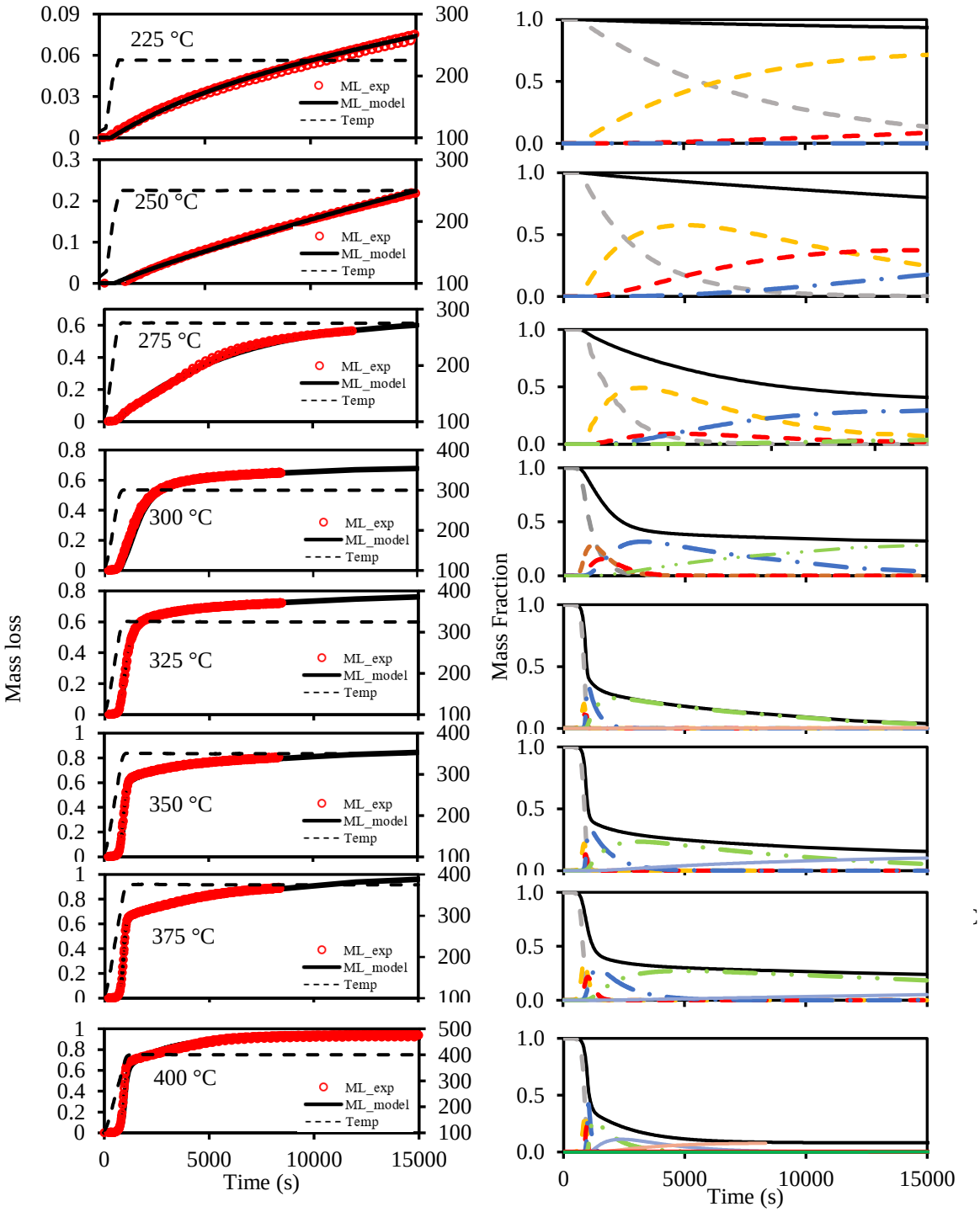

Figure 4.5. (a) Temperature transient and mass loss vs. time; (b) mass fractions of solids vs. time

4.4.4 Model Continuity

The reaction rate coefficient, k, is represented by the Arrhenius form (Eq. 6). At each temperature, we fitted the pre-exponential factor, A_i, the characteristic temperature, T_{ci}, and the molar weight ratio, a_i, to yield the best fit between the model results and mass loss experimental data. The activation energy, Ea_i, for each reaction at various temperatures is provided in Table 4.3. Ea_i should be the same for each reaction regardless of temperature (Kim et al., 2010), as indeed can be seen from Table 4.3. Figure 4.6 portrays the results of $ln(k)$ vs. $\frac{1}{T}$ for different ks at temperatures range from 225 °C to 400 °C. The activation energy can be obtained from the slope of each reaction rate coefficient as well, which is also summarized in Table 4, which fits well with the value fitted for the different temperatures.

Table 4.3. Activation energy of each reaction at various temperatures (kJ/mol)

	400 °C	**375 °C**	**350 °C**	**325 °C**	**300 °C**	**275 °C**	**From slope**
Reaction 1	113.1	111.5	111.5	111.5	111.5	111.5	110.9
Reaction 2	163.4	160.4	160.4	160.4	160.4	160.4	160.5
Reaction 3	160.9	170.9	162.6	162.6	162.6	161.5	155.3
Reaction 4	117.7	125.2	117.7	117.7	117.7	118.9	119.6
Reaction 5	201.7	193.4	185.1	185.1	-	-	188.2
Reaction 6	185.1	185.1	-	-	-	-	-
Reaction 7	183.4	-	-	-	-	-	-
Reaction 8	172.6	-	-	-	-	-	-

The average activation energy of the first reaction is 113.1 kJ/mol, which is comparable to the results of the activation energy value of cellulose dehydration (106.8 kJ/mol) (Alvarez and Vázquez, 2004). The 6th and 7th reactions that appeared at 375 °C and 400 °C, respectively could be mainly attributed to the degradation of lignin since the maximum degradation of lignin occurs at the temperature range of 375-400 °C (Brebu et al., 2013; Zhao et al., 2014). In addition, the activation energies of these two reactions are around 185 kJ/mol, which was comparable to the literature since lignin has a wide range of activation energy 120.7-197.3 kJ/mol (Ház et al., 2019). The reaction at this temperature range is mainly the demethylation of the dimethoxy- groups in lignin, which results in converting phenols into pyrocatechols (Brebu and Vasile, 2010; Chen et al., 2019).

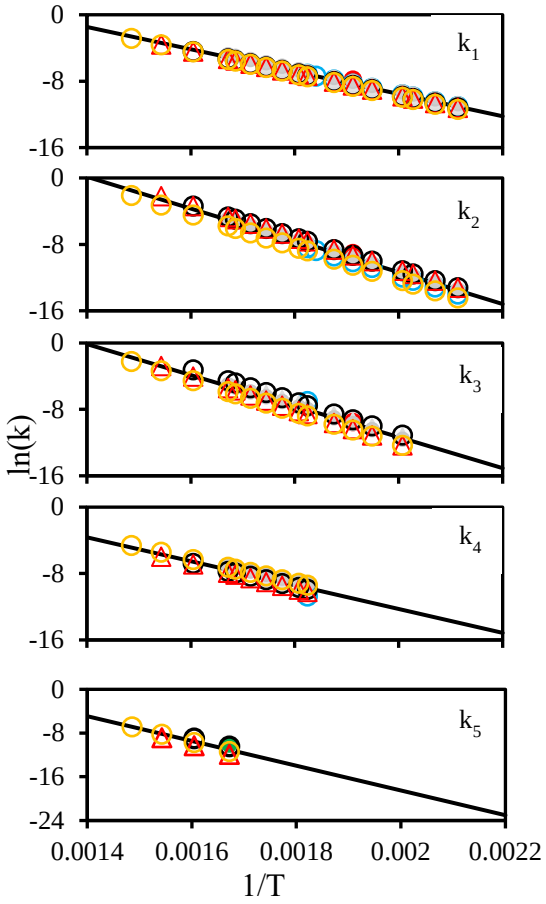

Figure 4.6. lnk vs. 1/T

4.4.5 Solid Product Distribution

As mentioned above, the stoichiometric parameters represent the molar weight ratios of the solid products. Therefore, the molar weight of the solid product of each reaction could be obtained given the initial molecular weight of the paper waste and the results from Table 4.4. Figure 4.7 shows the molar weight of the final product is around 59 g/mol.

Table 4.4. Molar weight ratios

Molar ratio	**Average**
α_1	0.81±0.02
$\alpha_1\alpha_2$	0.65±0.01
$\alpha_1\alpha_2\alpha_3$	0.42±0.004
$\alpha_1 \cdots \alpha_4$	0.31±0.01
$\alpha_1 \cdots \alpha_5$	0.13±0.01
$\alpha_1 \cdots \alpha_6$	0.05±0.02
$\alpha_1 \cdots \alpha_7$	0.02
$\alpha_1 \cdots \alpha_8$	0.002

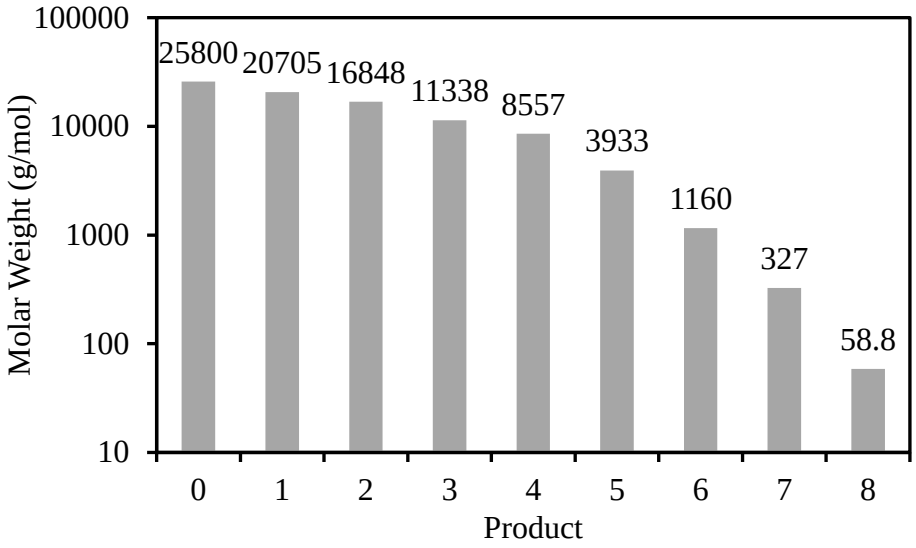

Figure 4.7. Molecular weight distribution of solid product after each reaction

4.5 Conclusions

Thermal degradation of paper waste was studied through thermogravimetric analysis at the temperature range of 200-400 °C. Two kinetic approaches were taken to develop the kinetic model for paper waste degradation: (i) reconstructing the TGA results of paper waste thermal degradation by an additive law of the degradation of cellulose, hemicellulose and lignin; (ii) considering paper waste as one material and develop a multi-step consecutive reaction mechanism that focuses on solid products at different temperatures. It was found that there exists synergistic effects between cellulose, hemicellulose and lignin during paper waste degradation. Therefore, this study took the second approach. The temperature transients were modeled, and the kinetic parameters were obtained through fitting to the TGA experimental results. The model showed: (i) the first reaction was mainly dehydration reaction of cellulose with anhydrocellulose as solid product; (ii) there are more reactions at higher temperatures; (iii) the activation energies of 6^{th} and 7^{th} reaction and the temperatures (375 °C and 400 °C) are comparable to the results of lignin thermal degradation in literature, thus can be attributed lignin thermal degradation. Theis model can not only provide chemical insights of the paper wastes thermal degradation, it also can be used to help with other mechanistic works.

4.6 Works Cited

Abbas, Z., Moghaddam, A. P., and Steenari, B. M. (2003). Release of salts from municipal solid waste combustion residues. *Waste Manag.* 23, 291–305. doi:10.1016/S0956-053X(02)00154-X.

Aboulkas, A., El harfi, K., and El Bouadili, A. (2010). Thermal degradation behaviors of polyethylene and polypropylene. Part I: Pyrolysis kinetics and mechanisms. *Energy Convers. Manag.* 51, 1363–1369. doi:10.1016/j.enconman.2009.12.017.

Adefisan, O. O., and McDonald, A. G. (2019). Evaluation of the strength, sorption and thermal properties of bamboo plastic composites. *Maderas Cienc. y Tecnol.* 21, 3–14. doi:10.4067/S0718-221X2019005000101.

Alén, R., Kuoppala, E., and Oesch, P. (1996). Formation of the main degradation compound groups from wood and its components during pyrolysis. *J. Anal. Appl. Pyrolysis* 36, 137–148. doi:10.1016/0165-2370(96)00932-1.

Alvarez, V. A., and Vázquez, A. (2004). Thermal degradation of cellulose derivatives/starch blends and sisal fibre biocomposites. *Polym. Degrad. Stab.* 84, 13–21. doi:10.1016/j.polymdegradstab.2003.09.003.

Anders, H., and Zimmermann, H. (1987). A comparison of the thermal degradation behaviours of poly(vinyl acetate), poly(vinyl alcohol) and poly(vinyl chloride). *Polym. Degrad. Stab.* 18, 111–122. doi:10.1016/0141-3910(87)90024-3.

Anuar Sharuddin, S. D., Abnisa, F., Wan Daud, W. M. A., and Aroua, M. K. (2016). A review on pyrolysis of plastic wastes. *Energy Convers. Manag.* 115, 308–326. doi:10.1016/J.ENCONMAN.2016.02.037.

Bacaloglu, R., and Fisch, M. (1995). Degradation and stabilization of poly (vinyl chloride). V. Reaction mechanism of poly(vinyl chloride) degradation. *Polym. Degrad. Stab.* 47, 33–57. doi:10.1016/0141-3910(94)00086-N.

Bach, Q. V., Chen, W. H., Eng, C. F., Wang, C. W., Liang, K. C., and Kuo, J. Y. (2019). Pyrolysis characteristics and non-isothermal torrefaction kinetics of industrial solid wastes. *Fuel* 251, 118–125. doi:10.1016/j.fuel.2019.04.024.

Bergman, T. L., Incropera, F. P., DeWitt, D. P., and Lavine, A. S. (2011). "Fundamentals of heat and mass transfer," in (New York: Wiley, pp. 983-1011), 56.

Biagini, E., Barontini, F., Tognotti, L., and Diotisal, V. (2006). Devolatilization of Biomass Fuels and Biomass Components Studied by TG / FTIR Technique. 4486–4493. doi:10.1021/ie0514049.

Bradbury, A. G. W., Sakai, Y., and Shafizadeh, F. (1979). A kinetic model for pyrolysis of cellulose. *J. Appl. Polym. Sci.* 23, 3271–3280. doi:10.1002/app.1979.070231112.

Braun, V. D., and Thallnaier, M. (1966). Zum mechanismus der thermischen chlorwassmtoffabspaltung aus polyvinylchlorid. 3. Mitt. Über die länge der polyensequenzen in partiell dehydrohalogenierten poiyvinylchloriden, polyvinylbromiden und vinylchlorid-copolymeren. *Die Makromol. Chemie* 99, 59–75. doi:10.1002/macp.1966.020990106.

Brebu, M., Tamminen, T., and Spiridon, I. (2013). Thermal degradation of various lignins by TG-MS/FTIR and Py-GC-MS. *J. Anal. Appl. Pyrolysis* 104, 531–539. doi:10.1016/j.jaap.2013.05.016.

Brebu, M., and Vasile, C. (2010). Thermal Degradation of Lignin-A Review. *Cellul. Chem. Technol.* 44, 353–363. Available at: https://www.semanticscholar.org/paper/THERMAL-DEGRADATION-OF-LIGNIN-A-

REVIEW-Brebu-Vasile/67fecec0d827e7ac1cbb5a4c6752b6d8ec6c1fef [Accessed August 7, 2020].

Burra, K. G., and Gupta, A. K. (2018). Synergistic effects in steam gasification of combined biomass and plastic waste mixtures. *Appl. Energy* 211, 230–236. doi:10.1016/j.apenergy.2017.10.130.

Cabrales, L., and Abidi, N. (2010). On the thermal degradation of cellulose in cotton fibers. *J Therm Anal Calorim* 102, 485–491. doi:10.1007/s10973-010-0911-9.

Cangialosi, F., Intini, G., Liberti, L., Notarnicola, M., and Stellacci, P. (2008). Health risk assessment of air emissions from a municipal solid waste incineration plant - A case study. *Waste Manag.* 28, 885–895. doi:10.1016/j.wasman.2007.05.006.

Chang, S.-S. (1977). Heat Capacity and Thermodynamic Properties of Poly(Vinyl Chloride). *J. Res. Natl. Bur. Stand. (1934).* 82, 9–18. doi:10.6028/jres.082.002.

Chattopadhyay, J., Kim, C., Kim, R., and Pak, D. (2008). Thermogravimetric characteristics and kinetic study of biomass co-pyrolysis with plastics. 25, 1047–1053.

Chen, R., Zhang, S., Cong, K., Li, Q., and Zhang, Y. (2020). Insight into synergistic effects of biomass-polypropylene co-pyrolysis using representative biomass constituents. *Bioresour. Technol.* 307, 123–243. doi:10.1016/j.biortech.2020.123243.

Chen, W. H., Wang, C. W., Ong, H. C., Show, P. L., and Hsieh, T. H. (2019). Torrefaction, pyrolysis and two-stage thermodegradation of hemicellulose, cellulose and lignin. *Fuel* 258, 116–168. doi:10.1016/j.fuel.2019.116168.

Chen, W., and Kuo, P. (2011). Isothermal torrefaction kinetics of hemicellulose , cellulose , lignin and xylan using thermogravimetric analysis. *Energy* 36, 6451–6460. doi:10.1016/j.energy.2011.09.022.

Chen, W., Peng, J., and Bi, X. T. (2015). A state-of-the-art review of biomass torrefaction , densi fi cation and applications. 44, 847–866. doi:10.1016/j.rser.2014.12.039.

Collard, F. X., and Blin, J. (2014). A review on pyrolysis of biomass constituents: Mechanisms and composition of the products obtained from the conversion of cellulose, hemicelluloses and lignin. *Renew. Sustain. Energy Rev.* 38, 594–608. doi:10.1016/j.rser.2014.06.013.

Conti, J., Holtberg, P., Diefenderfer, J., LaRose, A., Turnure, J. T., and Westfall, L. (2016). International Energy Outlook 2016 with Prokctions to 2040. Available at: https://www.eia.gov/outlooks/ieo/pdf/0484(2016).pdf.

Curling, S., Clausen, C. A., and Winandy, J. E. (2001). The effect of hemicellulose degradation on the mechanical properties of wood during brown rot decay. in *International Research Group on Wood Preservation 2011*, 1–10.

De Carvalho, G., Frollini, E., and Dos Santos, W. N. (1996). Thermal conductivity of polymers by hot-wire method. *J. Appl. Polym. Sci.* 62, 2281–2285. doi:10.1002/(sici)1097-4628(19961226)62:13<2281::aid-app12>3.3.co;2-t.

Dence, C. W. (1992). The Determination of Lignin. *Methods Lignin Chem.*, 33–61. Available at: https://link.springer.com/chapter/10.1007/978-3-642-74065-7_3.

Donepudi, Y. (2017). Impact of Pretreatment Methods on Fast Pyrolysis of Biomass. Available at: https://digitalcommons.mtu.edu/etdr/496.

Dupuis, D. P., Grim, R. G., Nelson, E., Tan, E. C. D., Ruddy, D. A., Hernandez, S., et al. (2019). High-Octane Gasoline from Biomass: Experimental, Economic, and Environmental Assessment. *Appl. Energy* 241, 25–33. doi:10.1016/j.apenergy.2019.02.064.

Eichhorn, S. J., Sirichaisit, J., and Young, R. J. (2001). Deformation mechanisms in cellulose fibres, paper and wood. *J. Mater. Sci.* 36, 3129–3135. doi:10.1023/A:1017969916020.

El-Fadel, M., Findikakis, A. N., and Leckie, J. O. (1997). Environmental impacts of solid waste landfilling. *J. Environ. Manage.* 50, 125.

Enviromental Protection Agency (2017). Advancing Sustainable Materials Management: 2017 Fact Sheet Assessing Trends in Material Generation, Recycling, Composting, Combustion with Energy Recovery and Landfilling in the United States. Available at: https://www.epa.gov/sites/production/files/2019-11/documents/2017_facts_and_figures_fact_sheet_final.pdf [Accessed November 11, 2020].

EPA Clean Air Act, 42 USC 7412(f) (1992). Available at: https://www.govinfo.gov/content/pkg/USCODE-2013-title42/html/USCODE-2013-title42-chap85-subchapI-partA-sec7412.htm [Accessed January 19, 2020].

Fabiyi, J. S., and McDonald, A. G. (2010). Effect of wood species on property and weathering performance of wood plastic composites. *Compos. Part A Appl. Sci. Manuf.* 41, 1434–1440. doi:10.1016/j.compositesa.2010.06.004.

Farhat, W., Venditti, R., Quick, A., Taha, M., Mignard, N., Becquart, F., et al. (2017). Hemicellulose extraction and characterization for applications in paper coatings and adhesives. *Ind. Crop. Prod.* 107, 370–377. doi:10.1016/j.indcrop.2017.05.055.

Fung, B. M., Khitrin, A. K., and Ermolaev, K. (2000). An Improved Broadband Decoupling Sequence for Liquid Crystals and Solids. *J. Magn. Reson.* 142, 97–101. doi:10.1006/jmre.1999.1896.

Funke, A., Henrich, E., Dahmen, N., and Sauer, J. (2017). Dimensional Analysis of Auger-Type Fast Pyrolysis Reactors. *Energy Technol.* 5, 119–129. doi:10.1002/ente.201600095.

Gao, Z., Kaneko, T., Amasaki, I., and Nakada, M. (2003). A kinetic study of thermal degradation of polypropylene. *Polym. Degrad. Stab.* 80, 269–274. doi:10.1016/S0141-3910(02)00407-X.

Gómez, M. A., Álvarez, M. A., Eguía, P., and Comesa, R. (2012). Thermochimica Acta Thermal lag analysis on a simulated TGA-DSC device. 547, 13–21.

Goorah, S. S. D., Esmyot, M. L. I., and Boojhawon, R. (2009). The health impact of nonhazardous solid waste disposal in a community: the case of the Mare Chicose landfill in Mauritius. *J. Environ. Health* 72, 48–55.

Han, B., Chen, Y., Wu, Y., and Hua, D. (2014). Co-pyrolysis behaviors and kinetics of plastics – biomass blends through thermogravimetric analysis. 227–235. doi:10.1007/s10973-013-3228-7.

Hatanaka, T., Imagawa, T., and Takeuchi, M. (2000). Formation of PCDD/Fs in artificial solid waste incineration in a laboratory-scale fluidized-bed reactor: Influence of contents and forms of chlorine sources in high-temperature combustion. *Environ. Sci. Technol.* 34, 3920–3924. doi:10.1021/es991258w.

Ház, A., Jablonský, M., Šurina, I., Kačík, F., Bubeníková, T., and Ďurkovič, J. (2019). Chemical composition and thermal behavior of kraft lignins. *Forests* 10, 1–12. doi:10.3390/f10060483.

He, Q., Ding, L., Gong, Y., Li, W., Wei, J., and Yu, G. (2019). Effect of torrefaction on pinewood pyrolysis kinetics and thermal behavior using thermogravimetric analysis. *Bioresour. Technol.* 280, 104–111. doi:10.1016/j.biortech.2019.01.138.

He, Q., Guo, Q., Ding, L., Gong, Y., Wei, J., and Yu, G. (2018). Co-pyrolysis Behavior and Char Structure Evolution of Raw/Torrefied Rice Straw and Coal Blends. *Energy and Fuels* 32, 12469–12476. doi:10.1021/acs.energyfuels.8b03469.

Hilbers, T. J., Wang, Z., Pecha, B., Westerhof, R. J. M., Kersten, S. R. A., Pelaez-samaniego, M. R., et al. (2015). Cellulose-Lignin interactions during slow and fast pyrolysis. *J. Anal. Appl. Pyrolysis* 114, 197–207. doi:10.1016/j.jaap.2015.05.020.

Hoornweg, D., and Bhada-Tata, P. (2012). What a Waste : A Global Review of Solid Waste Management. *Urban Dev. Ser. Pap. no. 15. World Bank, Washington, DC. © World Bank. Licens. CC BY 3.0 IGO."* 15, 8. doi:10.3970/cmes.2014.098.129.

Hu, J., Shen, D., Wu, S., Zhang, H., and Xiao, R. (2014). Effect of temperature on structure evolution in char from hydrothermal degradation of lignin. *J. Anal. Appl. Pyrolysis* 106, 118–124. doi:10.1016/j.jaap.2014.01.008.

Hubbe, M. A., Venditti, R. A., and Rojas, O. J. (2007). What happens to cellulosic fibers during papermaking and recycling? A review. *BioResources* 2, 739–788. doi:10.15376/biores.2.4.739-788.

Incroper, F. P., Dewitt, D. P., Bergman, T. L., and Lavine, A. S. (2011). *Fundamentals of Heat and Mass Transfer*. 7th ed. Wiley, pp. 983-1011 Available at: http://cds.cern.ch/record/1339915/files/9780471457282_TOC.pdf [Accessed July 30, 2019].

Indrawan, B., Prawisudhap, P., and Yoshikawa, K. (2011). Chlorine-free Solid Fuel Production from Municipal Solid Waste by Hydrothermal Process. *J. Japan Inst. Energy* 90, 1177–1182. doi:10.3775/jie.90.1177.

Inoue, T., Miyazaki, M., Kamitani, M., Kano, J., and Saito, F. (2004). Mechanochemical dechlorination of polyvinyl chloride by co-grinding with various metal oxides. *Adv. Powder Technol.* 15, 215–225. doi:10.1163/156855204773644445.

Ito, M., and Nagai, K. (2010). Thermal aging and oxygen permeation of Nylon-6 and Nylon-6/montmorillonite composites. *J. Appl. Polym. Sci.* 118, 928–935. doi:10.1002/app.32424.

Jacques Lédé (2010). Biomass Pyrolysis: Comments on Some Sources of Confusions in the Definitions of Temperatures and Heating Rates. *Energies* 3, 886–898. doi:doi:10.3390/en3040886.

Jiang, Y., Lu, M., Liu, S., Bao, C., and Liang, G. (2018). Deactivation by HCl of CeO2–MoO3/TiO2 catalyst for selective catalytic reduction of NO with NH3. 8, 17677–17684. doi:10.1039/c8ra00280k.

Jung, Y. G., Choi, S. C., Oh, C. S., and Paik, U. G. (1997). Residual stress and thermal properties of zirconia/metal (nickel, stainless steel 304) functionally graded materials fabricated by hot pressing. *J. Mater. Sci.* 32, 3841–3850. doi:10.1023/A:1018640126751.

Kim, U. J., Eom, S. H., and Wada, M. (2010). Thermal decomposition of native cellulose: Influence on crystallite size. *Polym. Degrad. Stab.* 95, 778–781. doi:10.1016/j.polymdegradstab.2010.02.009.

Kiran, N., Ekinci, E., and Snape, C. . (2000). Recyling of plastic wastes via pyrolysis. *Resour. Conserv. Recycl.* 29, 273–283. doi:10.1016/S0921-3449(00)00052-5.

Klinger, J., Bar-Ziv, E., and Shonnard, D. (2013). Kinetic study of aspen during torrefaction. *J. Anal. Appl. Pyrolysis* 104, 146–152. doi:10.1016/j.jaap.2013.08.010.

Klinger, J., Bar-Ziv, E., and Shonnard, D. (2015). Unified kinetic model for torrefaction-pyrolysis. *Fuel Process. Technol.* 138, 175–183. doi:10.1016/j.fuproc.2015.05.010.

Klinger, J., Bar-Ziv, E., Shonnard, D., Westover, T., and Emerson, R. (2016). Predicting Properties of Gas and Solid Streams by Intrinsic Kinetics of Fast Pyrolysis of Wood. *Energy and Fuels* 30, 318–325. doi:10.1021/acs.energyfuels.5b01877.

Klinger, J., Klemetsrud, B., Bar-Ziv, E., and Shonnard, D. (2014). Temperature dependence of aspen torrefaction kinetics. *J. Anal. Appl. Pyrolysis* 110, 424–429. doi:10.1016/j.jaap.2014.10.008.

Kotchen, M. J., and Mansur, E. T. (2014). How stringent are the US EPA's proposed carbon pollution standards for new power plants? *Rev. Environ. Econ. Policy* 8, 290–306. doi:10.1093/reep/reu003.

Kumar, L., Koukoulas, A. A., Mani, S., and Satyavolu, J. (2017). Integrating torrefaction in the wood pellet industry: A critical review. *Energy and Fuels* 31, 37–54. doi:10.1021/acs.energyfuels.6b02803.

Lauer, D., Motell, E. L., Traficante, D. D., and Maciel, G. E. (1972). Carbon-13 Chemical Shifts in Monoalkyl Benzenes and Some Deuterio Analogs. *J. Am. Chem. Soc.* 94, 5335–5338. doi:10.1021/ja00770a032.

Lavrykov, S. A., and Ramarao, B. V. (2012). Thermal Properties of Copy Paper Sheets. *Dry. Technol.* 30, 297–311. doi:10.1080/07373937.2011.638148.

Lin, X., Zhang, Z., Wang, Q., and Sun, J. (2020). Interactions between biomass-derived components and polypropylene during wood–plastic composite pyrolysis. *Biomass Convers. Biorefinery*, 1–13. doi:10.1007/s13399-020-00861-4.

Love, G. D., Snape, C. E., and Jarvis, M. C. (1998). Comparision of Leaf and Stem Cell-Wall Components in Barley Straw by Solid-State 13C NMR. *Phytochemistry* 49, 1191–1194.

Lu, P., Huang, Q., Bourtsalas, A. T., Themelis, N. J., Chi, Y., and Yan, J. (2019). Review on fate of chlorine during thermal processing of solid wastes. *J. Environ. Sci. (China)* 78, 13–28. doi:10.1016/j.jes.2018.09.003.

Luppens, J. A. (2011). A critical review of published coal quality data from the southwestern part of the Powder River Basin, Wyoming. Reston, Virginia Available at: https://pubs.usgs.gov/of/2011/1148/pdf/ofr20111148_072111.pdf.

Ma, Y., Hummel, M., Määttänen, M., Särkilahti, A., Harlin, A., and Sixta, H. (2016). Upcycling of waste paper and cardboard to textiles. *Green Chem.* 18, 858–866. doi:10.1039/c5gc01679g.

Mahdavi Nejad, A. (2019). Thermal Analysis of Paper Board Packaging with Phase Change Material: A Numerical Study. *J. Packag. Technol. Res.* 3, 181–192. doi:10.1007/s41783-019-00060-1.

Mamleev, V., Bourbigot, S., and Yvon, J. (2007). Kinetic analysis of the thermal decomposition of cellulose: The main step of mass loss. *J. Anal. Appl. Pyrolysis* 80, 151–165. doi:10.1016/j.jaap.2007.01.013.

Marongiu, A., Faravelli, T., Bozzano, G., Dente, M., and Ranzi, E. (2003). Thermal degradation of poly(vinyl chloride). *J. Anal. Appl. Pyrolysis* 70, 519–553. doi:10.1016/S0165-2370(03)00024-X.

Maunu, S. L. (2009). "13C CPMAS NMR Studies of Wood, Cellulose Fibers, and Derivatives," in *Characterization of Lignocellulosic Materials*, eds. Q. Thomas and Q. Hu (Hoboken: Blackwell), 227–248. doi:https://doi.org/10.1002/9781444305425.ch13.

Mayo, W. D., Miller, A. F., and Hannah, W. R. (2004). "Course Notes on the Interpretation of Infrared and Raman Spectra," in *Course Notes on the Interpretation of Infrared and Raman Spectra* (John Wiley & Sons), 33–72. doi:10.1002/0471690082.

McCabe, J. G. (2014). Addressing Biogenic Carbon Dioxide Emissions from Stationary Sources. United States Enviromental Protection Agency. Washington, D.C Available at: https://archive.epa.gov/epa/sites/production/files/2016-08/documents/biogenic-co2-emissions-memo-111914.pdf.

McNeill, I. C., Memetea, L., and Cole, W. J. (1995). A study of the products of PVC thermal degradation. *Polym. Degrad. Stab.* 49, 181–191. doi:10.1016/0141-3910(95)00064-S.

More recycling raises average energy content of waste used to generate electricity (2012). Available at: https://www.eia.gov/todayinenergy/detail.php?id=8010 [Accessed January 19, 2020].

Moreira, L. R. S., and Filho, E. X. F. (2008). An overview of mannan structure and mannan-degrading enzyme systems. *Appl. Microbiol. Biotechnol.* 79, 165–178. doi:10.1007/s00253-008-1423-4.

National Emission Standards for Hazardous Air Pollutants (NESHAP) (2017). Available at: https://www.epa.gov/stationary-sources-air-pollution/national-emission-standards-hazardous-air-pollutants-neshap-9 [Accessed July 29, 2019].

National Overview: Facts and Figures on Materials, Wastes and Recycling (2017). Available at: https://www.epa.gov/facts-and-figures-about-materials-waste-and-recycling/national-overview-facts-and-figures-materials#Landfilling [Accessed January 19, 2020].

Ni, Y., Zhang, H., Fan, S., Zhang, X., Zhang, Q., and Chen, J. (2009). Emissions of PCDD/Fs from municipal solid waste incinerators in China. *Chemosphere* 75, 1153–1158. doi:10.1016/j.chemosphere.2009.02.051.

Olajire, A., Zhi, C., Hanson, S., and Wai, C. (2014). Thermogravimetric analysis of the pyrolysis characteristics and kinetics of plastics and biomass blends. 128, 471–481. doi:10.1016/j.fuproc.2014.08.010.

Oyedun, A. O., Gebreegziabher, T., Ng, D. K. S., and Hui, C. W. (2014). Mixed-waste pyrolysis of biomass and plastics waste - A modelling approach to reduce energy usage. *Energy* 75, 127–135. doi:10.1016/j.energy.2014.05.063.

Pandey, K. K. (1999). A Study of Chemical Structure of Soft and Hardwood and Wood Polymers by FTIR Spectroscopy. *J. Appl. Polym. Sci.* 71, 1969–1975. doi:10.1002/(sici)1097-4628(19990321)71:12<1969::aid-app6>3.0.co;2-d.

Papadopoulou, M. P., Karatzas, G. P., and Bougioukou, G. G. (2007). Numerical modelling of the environmental impact of landfill leachate leakage on groundwater quality - A field application. *Environ. Model. Assess.* 12, 43–54. doi:10.1007/s10666-006-9050-x.

Pasangulapati, V., Ramachandriya, K. D., Kumar, A., Wilkins, M. R., Jones, C. L., and Huhnke, R. L. (2012). Effects of cellulose, hemicellulose and lignin on thermochemical conversion characteristics of the selected biomass. *Bioresour. Technol.* 114, 663–669. doi:10.1016/j.biortech.2012.03.036.

Patkar, S. N., and Panzade, P. D. (2016). Fast and efficient method for molecular weight analysis of cellulose pulp, in-process and finished product. *Anal. Methods* 8, 3210–3215. doi:10.1039/c5ay03012a.

Peterson, J. D., Vyazovkin, S., and Wight, C. A. (2001). Kinetics of the thermal and thermo-oxidative degradation of polystyrene, polyethylene and poly(propylene).

Macromol. Chem. Phys. 202, 775–784. doi:10.1002/1521-3935(20010301)202:6<775::AID-MACP775>3.0.CO;2-G.

Petre, A. L., Budrugeac, P., and Segal, E. (1999). Thermal Degradation of Polyvinyl Chloride. *J. Therm. Anal. Calorim.* 56, 1065–1070. doi:10.1023/A:1010136507843.

Pines, A., Gibby, M. G., and Waugh, J. S. (1972). Proton-enhanced nuclear induction spectroscopy. a method for high resolution nmr of dilute spins in solids. *J. Chem. Phys.* 56, 1776–1777. doi:10.1063/1.1677439.

Radics, R. I., Gonzalez, R., Bilek, E. M., and Kelley, S. S. (2017). Systematic review of torrefied wood economics. *BioResources* 12, 6868–6884. doi:10.15376/biores.12.3.6868-6884.

Raveendran, K. (1996). Pyrolysis characteristics of biomass and biomass components. *Fuel* 75, 987–998. doi:10.1016/0016-2361(96)00030-0.

Risby, T. H., Yergey, J. A., and Scocca, J. J. (1982). Linear Programmed Thermal Degradation Mass Spectrometry of Polystyrene and Poly(vinyl chloride). *Anal. Chem.* 54, 2228–2233. doi:10.1021/ac00250a022.

Ritchie and Roser (2018). *Plastic Pollution - Our World in Data*. Available at: https://ourworldindata.org/plastic-pollution?utm_source=newsletter&utm_medium=email&utm_campaign=sendto_newslettertest&stream=top [Accessed January 23, 2020].

Rodrigues, J., Graça, J., and Pereira, H. (2001). Influence of tree eccentric growth on syringyl/guaiacyl ratio in Eucalyptus globulus wood lignin assessed by analytical pyrolysis. *J. Anal. Appl. Pyrolysis* 58–59, 481–489. doi:10.1016/S0165-2370(00)00121-2.

Rojas, A., and Orozco, E. (2003). Measurement of the enthalpies of vaporization and sublimation of solids aromatic hydrocarbons by differential scanning calorimetry. 405, 93–107. doi:10.1016/S0040-6031(03)00139-4.

Salvilla, J. N. V., Ofrasio, B. I. G., Rollon, A. P., Manegdeg, F. G., Abarca, R. R. M., and de Luna, M. D. G. (2020). Synergistic co-pyrolysıs of polyolefin plastics with wood and agricultural wastes for biofuel production. *Appl. Energy* 279, 115668. doi:10.1016/j.apenergy.2020.115668.

Sánchez-Jiménez, P. E., Perejón, A., Criado, J. M., Diánez, M. J., and Pérez-Maqueda, L. A. (2010). Kinetic model for thermal dehydrochlorination of poly(vinyl chloride). *Polymer (Guildf).* 51, 3998–4007. doi:10.1016/J.POLYMER.2010.06.020.

Schaefer, J., Stejskal, E. O., and Buchdahl, R. (1975). High-Resolution Carbon-13 Nuclear Magnetic Resonance Study of Some Solid, Glassy Polymers. *Macromolecules* 8, 291–296. doi:10.1021/ma60045a010.

Scheirs, J., Camino, G., and Tumiatti, W. (2001). Overview of water evolution during the thermal degradation of cellulose. *Eur. Polym. J.* 37, 933–942. doi:10.1016/S0014-3057(00)00211-1.

Sharypov, V., Beregovtsova, N., Kuznetsov, B., Baryshnikov, S., Marin, N., and Weber, J. (2003). Light Hydrocarbon Liquids Production by Co-Pyrolysis of Polypropylene and Hydrolytic Lignin. *Chem. Sustain. Dev.* 11, 427–434.

Shen, D. K., Gu, S., and Bridgwater, A. V. (2010). Study on the pyrolytic behaviour of xylan-based hemicellulose using TG-FTIR and Py-GC-FTIR. *J. Anal. Appl. Pyrolysis* 87, 199–206. doi:10.1016/j.jaap.2009.12.001.

Shenoy, A. V. (1999). "Rheology of Filled Polymer Systems," in (Springer Science&Business Media Dordrecht), 54–111.

Sluiter, J., and Sluiter, A. (2011). Summative Mass Closure: Laboratory Analytical Procedure (LAP) Review and Integration: Feedstocks; Issue Date: April 2010; Revision Date: July 2011 (Version 07-08-2011). Available at: http://www.nrel.gov/biomass/analytical_procedures.html [Accessed October 16, 2020].

Solmaz, R., Kardaş, G., Çulha, M., Yazıcı, B., and Erbil, M. (2008). Investigation of adsorption and inhibitive effect of 2-mercaptothiazoline on corrosion of mild steel in hydrochloric acid media. *Electrochim. Acta* 53, 5941–5952. doi:10.1016/J.ELECTACTA.2008.03.055.

Subramanian, P. M. (2000). Plastics recycling and waste management in the US. *Resour. Conserv. Recycl.* 28, 253–263. doi:10.1016/S0921-3449(99)00049-X.

Tian, H. H., & Ouyang, N. (2003). Preliminary Investigaton on Dioxing Emission from MSW Incinerators. *Environ. Chem.* 22, 255–258.

Utschick, H., Ritz, M., Mallon, H.-J., Arnold, M., Ludwig, W., Kettrup, A., et al. (1994). Investigations on the thermal degradation of post-chlorinated polyvinyl chloride. *Thermochim. Acta* 234, 139–151. doi:10.1016/0040-6031(94)85140-9.

Várhegyi, G., Antal, M. J., Jakab, E., and Szabó, P. (1997). Kinetic modeling of biomass pyrolysis. *J. Anal. Appl. Pyrolysis* 42, 73–87. doi:10.1016/S0165-2370(96)00971-0.

Vikelsoe, J., Nielsen, P., Blinksbjerg, P., Madsen, H., & Manscher, O. (1990). Significance of chlorine sources for the generation of dioxins during incineration of MSW. *Organohalogen Compd.* 3, 193–196.

Volpe, R., Zabaniotou, A. A., and Skoulou, V. (2018). Synergistic Effects between Lignin and Cellulose during Pyrolysis of Agricultural Waste. doi:10.1021/acs.energyfuels.8b00767.

Wakeman, I. B., and Johnson, H. R. (1978). Vinyl chloride formation from the thermal degradation of poly(vinyl chloride). *Polym. Eng. Sci.* 18, 404–407. doi:10.1002/pen.760180512.

Wang, X., Sotoudehniakarani, F., Yu, Z., Morrell, J. J., Cappellazzi, J., and McDonald, A. G. (2019). Evaluation of corrugated cardboard biochar as reinforcing fiber on properties, biodegradability and weatherability of wood-plastic composites. *Polym. Degrad. Stab.* 168, 108955. doi:10.1016/j.polymdegradstab.2019.108955.

Wang, Z., Pecha, B., Westerhof, R. J. M., Kersten, S. R. A., Li, C. Z., McDonald, A. G., et al. (2014). Effect of cellulose crystallinity on solid/liquid phase reactions responsible for the formation of carbonaceous residues during pyrolysis. *Ind. Eng. Chem. Res.* 53, 2940–2955. doi:10.1021/ie4014259.

Wei, L., McDonald, A. G., Freitag, C., and Morrell, J. J. (2013). Effects of wood fiber esterification on properties, weatherability and biodurability of wood plastic composites. *Polym. Degrad. Stab.* 98, 1348–1361. doi:10.1016/j.polymdegradstab.2013.03.027.

What is U.S. electricity generation by energy source? (2020). Available at: https://www.eia.gov/tools/faqs/faq.php?id=427&t=3 [Accessed April 29, 2020].

Williams, C. L., Westover, T. L., Petkovic, L. M., Matthews, A. C., Stevens, D. M., and Nelson, K. R. (2017). Determining Thermal Transport Properties for Softwoods under Pyrolysis Conditions. *ACS Sustain. Chem. Eng.* 5, 1019–1025. doi:10.1021/acssuschemeng.6b02326.

Wimberley, J. W., Carel, A. B., and Cabbiness Conoco Inc., D. K. (1982). Automated Method for Measuring the Thermal Degradation of Polyvinyl Chloride. *Anal. Lett.* 15, 89–100. doi:10.1080/00032718208064366.

Wu, S., Shen, D., Hu, J., Zhang, H., and Xiao, R. (2016). Biomass and Bioenergy Cellulose-lignin interactions during fast pyrolysis with different temperatures and mixing methods. 90. doi:10.1016/j.biombioe.2016.04.012.

Xu, Z., Albrecht, J. W., Kolapkar, S. S., Zinchik, S., and Bar-Ziv, E. (2020a). Chlorine Removal from U.S. Solid Waste Blends through Torrefaction. *Appl. Sci.* 10, 3337. doi:10.3390/app10093337.

Xu, Z., Kolapkar, S., Zinchik, S., Bar-Ziv, E., and Mcdonald, A. (2020b). Comprehensive Kinetic Study of Thermal Degradation of Polyvinylchloride (PVC). *Polym. Degrad. Stab.* 176. doi:doi.org/10.1016/j.polymdegradstab.2020.109148.

Xu, Z., Zinchik, S., Kolapkar, S., Bar-ziv, E., Hansen, T., and Conn, D. (2018). Properties of Torrefied U . S . Waste Blends. *Front. Energy Res.* 6, 65. doi:doi.org/10.3389/fenrg.2018.00065.

Xue, Y., and Bai, X. (2018). Synergistic enhancement of product quality through fast co-pyrolysis of acid pretreated biomass and waste plastic. *Energy Convers. Manag.* 164, 629–638. doi:10.1016/j.enconman.2018.03.036.

Yang, H., Liu, M., Chen, Y., Xin, S., Zhang, X., Wang, X., et al. (2020). Vapor – solid interaction among cellulose , hemicellulose and lignin. *Fuel* 263. doi:10.1016/j.fuel.2019.116681.

Yang, H., Yan, R., Chen, H., Zheng, C., Lee, D. H., Uni, V., et al. (2006). In-Depth Investigation of Biomass Pyrolysis Based on Three Major Components : Hemicellulose , Cellulose and Lignin. 388–393. doi:10.1021/ef0580117.

Yeo, J. Y., Chin, B. L. F., Tan, J. K., and Loh, Y. S. (2019). Comparative studies on the pyrolysis of cellulose, hemicellulose, and lignin based on combined kinetics. *J. Energy Inst.* 92, 27–37. doi:10.1016/j.joei.2017.12.003.

Yin, R.-H., Zhang, R.-Z., and Luo, Y.-H. (2016). The Effect of Utilizing Homogeneous Conversion to Control the Formation of Chlorinated Hydrocarbons During PVC Pyrolysis. 35, 1012–1019. doi:10.1002/ep.12313.

Yu, J., Sun, L., Ma, C., Qiao, Y., and Yao, H. (2016). Thermal degradation of PVC: A review. *Waste Manag.* 48, 300–314. doi:10.1016/j.wasman.2015.11.041.

Yuan, H., Wang, Y., Kobayashi, N., Zhao, D., and Xing, S. (2015). Study of Fuel Properties of Torrefied Municipal Solid Waste. *Energy and Fuels* 29, 4976–4980. doi:10.1021/ef502277u.

Zhang, J., Choi, Y. S., Yoo, C. G., Kim, T. H., Brown, R. C., and Shanks, B. H. (2015). Cellulose−Hemicellulose and Cellulose−Lignin Interactions during Fast Pyrolysis. *ACS Sustain. Chem. Eng.* 3, 293–301. doi:doi.org/10.1021/sc500664h.

Zhang, X., Lei, H., Zhu, L., Zhu, X., Qian, M., Yadavalli, G., et al. (2016). Bioresource Technology Thermal behavior and kinetic study for catalytic co-pyrolysis of biomass with plastics. *Bioresour. Technol.* 220, 233–238. doi:10.1016/j.biortech.2016.08.068.

Zhao, J., Xiuwen, W., Hu, J., Liu, Q., Shen, D., and Xiao, R. (2014). Thermal degradation of softwood lignin and hardwood lignin by TG-FTIR and Py-GC/MS. *Polym. Degrad. Stab.* 108, 133–138. doi:10.1016/j.polymdegradstab.2014.06.006.

Zhao, S., Liu, M., Zhao, L., and Zhu, L. (2018). Influence of Interactions among Three Biomass Components on the Pyrolysis Behavior. *Ind. Eng. Chem. Res.* 57, 5241–5249. doi:10.1021/acs.iecr.8b00593.

Zhou, H., Long, Y., Meng, A., Chen, S., Li, Q., and Zhang, Y. (2015). A novel method for kinetics analysis of pyrolysis of hemicellulose, cellulose, and lignin in TGA and macro-TGA. *RSC Adv.* 5, 26509–26516. doi:10.1039/c5ra02715b.

Zhou, L., Wang, Y., Huang, Q., and Cai, J. (2006). Thermogravimetric characteristics and kinetic of plastic and biomass blends co-pyrolysis. *Fuel Process. Technol.* 87, 963–969. doi:10.1016/j.fuproc.2006.07.002.

Zinchik, S., Xu, Z., Kolapkar, S. S., Bar-Ziv, E., and McDonald, A. G. (2020). Properties of pellets of torrefied U.S. waste blends. *Waste Manag.* 104, 130–138. doi:10.1016/j.wasman.2020.01.009.

5 Bypassing Energy Barriers in Fiber-Polymer Torrefaction

This section is based on the following peer-reviewed paper:

Z Xu, SS Kolapkar, S Zinchik, E Bar-Ziv, L Ewurum, AG McDonald, J. Klinger, E. Fillerup, K. Schaller, C. Pilgrim. 2021. Bypassing Energy Barriers in Fiber-Polymer Torrefaction. Frontiers in Energy Research 9, 75.

doi: 10.3389/fenrg.2021.643371

5.1 Abstract

The amount of waste generation has been increasing with a significant amount being landfilled. These non-recyclable wastes contain large number of fiber and plastic wastes which can be treated with thermal processes to turn them into energy sources since they have high calorific values, are abundant and usually tipping fees are paid to handle them. This paper studied the torrefaction of non-recyclable paper (fiber) wastes, mixed plastic wastes (MPW) and their blends at different ratios in the temperature range of 250°C-400°C through thermogravimetric analysis (TGA). The solid residues after the experiments were analyzed by nuclear magnetic resonance (NMR) spectroscopy. Significant synergy between fiber and MPW were observed at the range 250°C-300°C, showing both increase in the reaction rate as well as the overall mass loss. At 250°C, the maximum mass loss rate was more than two times higher and the mass loss at the end of the experiments were also much higher compared to the expected results. In addition, synergy was weakened with an increase of temperature, disappearing at 400 °C. The existence of such interactions between fiber and plastic wastes indicates that the natural energy barriers during the individual torrefaction in paper waste or plastic waste could be bypassed, and the torrefaction of fiber and plastic blend can be achieved at lower temperatures and/or shorter residence times. The MPW and fiber wastes were also compounded by extrusion (to produce pellets) at 220 °C with different blend ratios. The fiber-MPW pellets from extrusion were characterized by IR spectroscopy, rheology, thermal analysis and flexural properties and showed significant chemical changes from the non-extruded blends at the same ratios. From IR characterization, it was found that there was significant increase in hydroxyl (OH) group on account of the carbonyl (C=O) and etheric (C-O-C) groups. The interaction between paper and MPW can be attributed to the plastic polymers acting as a hydrogen donor during the reactive extrusion process. Synergistic effects were also found from mechanical and rheological properties.

5.2 Introduction

The amount of waste generated across the world has been increasing, among which the paper and mixed plastic wastes (MPW) are the major contributors to this growth (paper waste and MPW are part of organic waste, which has other components). For instance, the U.S. alone produced 67 million tons of paper waste and 35.4 tons of MPW in 2017, with 18.4 million tons of paper wastes and 26.8 tons of MPW being sent landfilled

(Enviromental Protection Agency, 2017). Landfilling these wastes is not only an insufficient way of utilizing resources, but it also produces greenhouse gases along with other hazardous materials during the decomposition process (Papadopoulou et al., 2007). Since these wastes are abundant and usually have negative cost due to the tipping fees, a potential alternative is treating these wastes through torrefaction and turn them into an energy source.

Torrefaction has been proposed as a process for thermal chemical conversion of various feedstocks to increase the heating value and make the material more friable (Chen and Kuo, 2011; Chen et al., 2015, 2019; He et al., 2018, 2019; Xu et al., 2018). The synergies between biomass and plastics during thermochemical conversion have also been well explored in the past decades (Chattopadhyay et al., 2008; Han et al., 2014; Olajire et al., 2014; Zhang et al., 2016; Burra and Gupta, 2018; Chen et al., 2020). Sharypov et al. studied the effects of co-pyrolyzing polypropylene (PP) and hydrolytic lignin at 400 °C (Sharypov et al., 2003). It was found that with 30 wt% of lignin added to the PP sample, the light product yields reached 3 times compared to the results from only PP. The addition of the lignin also increased the olefin content in the heavy liquid products. However, since the study was limited to the interactions between lignin and PP, the results of treating both paper wastes and MPW are still lacking. Oyedun et al. conducted research on pyrolyzing biomass (bamboo) and polystyrene (PS) with different blend ratios (Oyedun et al., 2014). Synergistic effects were observed, and a mathematical model was developed to explain the data. The results showed that this synergy could reduce the overall energy usage by 6.2% with 25% of PS. The study also indicated that the synergy can be mainly attributed to the interaction between the lignin and plastic.

Zhou et al. studied the behaviors of co-pyrolysis of biomass (Chinese pine wood dust) and plastic (high density polyethylene (HDPE), low density polyethylene (LDPE) and PP) with TGA from room temperature up to 650 °C (Zhou et al., 2006). Significant synergies between biomass and plastics were found at high temperature region (530 – 650 °C). Furthermore, synergistic effects observed between the biomass with both HDPE and PP are higher compared to biomass with LDPE. The above two studies provided more details regarding the reduction of activation energy enabled by the interactions between biomass and mixed plastics.

Xue and Bai studied the synergistic effects through co-pyrolyzing polyethylene (PE) with acid pretreated corn stover (Xue and Bai, 2018). It was seen that the synergy was greatly enhanced compared to the results obtained by co-pyrolyzing raw corn stove and PE, which increased the oil yield with higher carbon content and lower oxygen content. A more recent study by Salvilla et al. investigated the synergistic co-pyrolysis of biomass (corn stover and wood waste) with pulverized plastics including PP, LDPE and HDPE using TGA (Salvilla et al., 2020). This synergy was observed at ~500 °C, and it was attributed to the hydrogen that was donated from the plastics during the co-pyrolysis. It was also observed that the activation energy of plastic decomposition was reduced. These studies were carried out at pyrolysis temperatures where the main product is liquid.

In this study, the focus was on lower temperature treatment, carried out at 250°C-400°C, referred to as torrefaction, with solid as the main product. Further, previous studies used various types of biomass, cellulose, hemicellulose, and lignin, while paper wastes consist of cellulose, hemicellulose, lignin, and various chemical additives (Hubbe et al., 2007). They differ significantly from natural biomass and its constituents including the additives (Farhat et al., 2017). The high temperature pyrolysis results are not applicable to the low temperature torrefaction of paper-MPW to produce solid fuels.

Therefore, it is essential to learn if similar interactions exist between paper and MPW, which is the objective of this study. Synergistic effects between the non-recyclable MPW and paper wastes during torrefaction were observed in a previous study (Zinchik et al., 2020), showing significant synergistic effect between fiber and MPW at 300°C with fiber-MPW (60%-40%). The current study expands to other blends and temperatures in the range of 250°C-400°C. Further, the effects of compound extrusion process were also investigated through studying the rheological and mechanical properties of the composites. This approach can help in designing mixed paper-MPW torrefaction processes for the industrial systems.

5.3 Material and Methods

5.3.1 Material

The materials in this study were waste industrial paper wastes, MPW and commercially available LDPE (Rainier Plastics), cellulose powder (Avicel PH-101, ~50µm particle size, Fluka) as well as hemicellulose (extracted xylan). The paper wastes and MPW have been described in detail in the prior studies (Xu et al., 2018, 2020a). The paper wastes are a mixture of paper, carton and cardboard, label matrix residuals, wax papers, and laminated non-recyclable papers; and the plastic wastes consist of LDPE, PE, polyethylene-terephthalate (PET), polyamide-nylon, polyvinylchloride (PVC), PP, and some other materials. These wastes were received and had been through a primary size reduction to a coarse size of < 100 mm. They were then passed through a low RPM, high-torque twin-shaft shredder (Taskmaster TM8500). The rotor blades were approximately 6 mm thick, and size reduced the material to fiber bundles approximately 6 mm x 12-25 mm. A final size reduction step was performed in a knife mill (Model 4 Wiley Mill, 800 RPM) and the material to pass through a 2 mm screen. This size enables homogenization of the sample, and therefore it is good representation of the heterogeneous feedstock.

5.3.2 Experimental Methods

5.3.2.1 Compositional Analysis

Compositional analysis for structural and extractive carbohydrates and lignin was performed following the Laboratory Analytical Procedures developed at NREL (Sluiter and Sluiter, 2011). The solids are initially prepared between 20 and 80 mesh followed by water and ethanol-based solvent extractions to determine non-structural carbohydrates, proteins, waxes, and resins, etc. The extracted material then goes to a two-stage sulfuric acid hydrolysis and insoluble Klason lignin determined gravimetrically and the acid-

insoluble lignin content determined by UV spectroscopy at 240 nm (extinction coefficient of 12 L g^{-1} cm^{-1}). The sugars were analyzed via high-performance liquid chromatography (HPLC).

5.3.2.2 Ultimate Analysis

Ultimate analysis was performed using a LECO TruSpec C/H/N and S add-on module, with a modified ASTM D5373-16 method to accommodate fiber wastes samples that use a slightly different burn profile of 4 slm for 40 s, 1 slm for 30 s, and 4 slm for 30 s of ultra-high purity O_2. ASTM D4239-17 was used to determine elemental sulfur content, and oxygen content was calculated by subtraction (Dupuis et al., 2019).

5.3.2.3 Thermal Properties Analysis

Thermal conductivity was measured in a transient plane source (ThermTest Inc. TPS15000 hot disc thermal constants analyzer) (Williams et al., 2017). The samples are housed in a heated oven (LF2 SP 3kW, Vecstar) during the tests. Power to the sensor was provided by a TSX3510P Aim TTi power supply. Gold tipped leads connected the power supply, thermal sensor (Mica 4921, radius of 9.719 mm, Themtest), thermistor, and reference resistor to two multimeters (0.002% accuracy to 100nV, up to 2000 Hz, Keithley). Outputs from the power supply and the multimeters were fed into a custom build Virtual Instrument (VI) constructed in Labview (National Instruments). During the tests, a current is sent through the resistive element sensor to generate heat. The thermal diffusivity of the sample is used as a fitting parameter to match the measured and theoretical change is resistance within the sensor as the interface temperature changes. The transient resistance of the sensor was determined by recording the voltage potential across the sensor and that of a 10.05 Ohm reference resistor. The temperature rise at the sensor-solid interface was targeted at approximately 1.0 °C to ensure good experimental resolution, in addition to maintaining an assumed semi-infinite medium and quiescent atmosphere in the sample chamber. For these tests, the pulse sequence was performed at 0.09 V for 100 s, then 1.0 V for 160 s, then 0.11 V for 100 s.

5.3.2.4 Extrusion

The MPW crumb and MPW/fiber crumb material (50/50 and 75/25) were blended in 0.5 kg batches using a Kitchen Aid mixer. The blended formulations (0.5 kg each) were each fed into the 18-mm co-rotating twin-screw extruder (Leistritz, L/D ratio of 40, 200 rpm, 4.7 kW motor, base torque 18%) using a mass loss twin screw feeder (K-Tron) at 0.5 kg/h. The extruded material exited from a 9 mm diameter die as rods and were cooled by forced air (Adefisan et al., 2017). The 8 heated extruder barrel zones were maintained at 220°C.

5.3.2.5 Thermomechanical Analysis and Differential Scanning Calorimetry

The softening point of the various extruded material formulations and LDPE was determined by thermomechanical analysis (TMA) on a Perkin Elmer TMA-7 instrument on thin sections (3 mm x 3 mm x 0.5 mm) from -25°C to 250°C at 5°C/min using a penetration probe. The melting temperature and degree of crystallization on the extruded

MPW (10 mg) was performed by differential scanning calorimetry (DSC) on a Perkin Elmer DSC-7 instrument from 25 to 300°C at 10°C/min.

5.3.2.6 Thermogravimetric Analysis (TGA)

The thermogravimetric analysis was performed in a LECO TGA 701. This unit has a 19-sample (approximately 1g) carrousel that is fully enclosed in a nitrogen-purged (10 slm) oven. For these tests, all 19 crucibles were loaded with either the wastepaper, commercial cellulose powder, and MPW for replication and the statistical significance of the extracted results. The samples were first heated at 110 °C to eliminate moisture and then the temperature increased to the set temperature with the rate of 16 °C/min. Over the experiment, the carousel rotated, and samples were weighted approximately every 15 s between the crucibles with full revolutions taking 5 min each. After the transient data were retrieved, the 19 sample traces were composited to obtain a TGA curve that is representative of the 0.07 Hz mass recording as well as the variability of the material and the technique. Mass was recorded to 0.0001g (0.01-0.05% of initial mass) by the thermally isolated, low-drift balance.

5.3.2.7 FTIR Spectroscopy

FTIR spectra were obtained using a Nicolet-iS5 FTIR spectrometer, 64 scans, with an attenuated total reflectance accessory (ZnSe crystal, iD5) and data analyzed and averaged with the OMNIC v9.8 software.

5.3.2.8 Solid-State $^{13}C\{^{1}H\}$-CP/MAS NMR Spectroscopy

Solid samples were mixed with 10% adamantane (by mass) to use as an internal standard to provide a basis to compare the different samples semi-quantitatively, as the densities of carbon species differed greatly as the torrefaction temperature was changed. The paper/adamantane mixtures were ground to a uniform particle size with a mortar and pestle and were then loaded into 4 mm ZrO rotors and capped with Kel-F rotor caps. The spectra were obtained using a standard Bruker HX magic-angle spinning (MAS) probe as part of a Bruker Avance III spectrometer with a field strength of 9.4 T (^{1}H ν = 400.03 MHz, ^{13}C ν = 100.59 MHz). The torrefied paper samples were spun at ν_R = 15 kHz. The standard cross-polarization (CP) experiment was used for these experiments (Pines et al., 1972; Schaefer et al., 1975). ^{1}H NMR spectra were recorded for each sample to determine the center of the excitation profile for the CP experiment. CP/MAS conditions were first optimized on the 325 °C torrefied paper sample and used for the remaining samples. Proton nutation frequency was set at 92.6 kHz with a decoupling field strength of 48.0 kHz (under the SPINAL64 decoupling program) (Fung et al., 2000). The Hartman-Hahn condition (contact time) was optimized at 1.8 msec. For the CP/MAS experiments the relaxation delay was set to 4 sec, the sweep width was set to 745 ppm, and the total number of transients per experiment was 3072. Also, the time domain of the free-induction decay (FID) consisted of 4004 points but due to that the quick relaxation of the FID the processed spectra was cut-off after 900 points, to reduce the amount of noise.

When processing the NMR data, care was taken to normalize the peak heights within the individual spectra to the adamantane peak at 36.4 ppm and to the mass percentage of the

sample. Spectra were then further normalized on a mass basis using mass loss values from TGA. Spectral deconvolutions of the 0-50 ppm region were run using MestReNova™ (Mestrelab Research) to provide the isolated peak heights for normalization.

5.3.2.9 Dynamic Rheology

Dynamic rheological measurements (complex viscosity, η*) were carried out on a Bohlin CVO 100 rheometer, using serrated parallel plates (25 mm Ø), in an oscillating mode with an extended temperature control module on compression molded discs (2.5 mm × 25 mm Ø) of extruded materials, LDPE, and MPW crumb samples at 180 °C (0.01 to 100 Hz at an applied strain of 0.25%). Data were analyzed using the Bohlin rheology v6.51 software.

5.3.2.10 Flexural Tests

The extruded rod samples, MPW crumb and LDPE (13 g) were hot-pressed (PHI hydraulic press, 300 x 300 mm^2) at 180 ^oC in a 75 mm Ø pellet die over 20 min and then cooled to room temperature. The flattened material was cut into flexural specimens (3 mm x 14 mm strips). Three-point flexural tests (strength and modulus) were performed on an Instron 5500R-1132 universal test machine (5 kN load cell) on specimens (≥6 replicates) according to ASTM Standard D 790 with a crosshead speed of 1.31 mm/min, span of 48 mm, and tested until specimen failure or 5% strain, whichever occurred first. Data were collected and processed using Bluehill v3.2 software (Instron).

5.4 Results and Discussion

5.4.1 Paper and MPW Compositional and Ultimate Analyses

The major constituents of paper waste were determined by compositional analysis. The results were obtained on a normalized and ash-free basis the carbohydrates and lignin, where balance was made of other unidentified material and other minor sugars. The paper wastes consist of 65.5% cellulose (glucan), 18.0% hemicellulose (xylan (13.8%), mannan (3.6%) and arabinan (0.6%)) and 14.3% lignin, and was similar to other reported values (Curling et al., 2001; Moreira and Filho, 2008).

Ultimate and compositional analyses were performed to help determine the elemental distribution and chemical changes the paper and MPW experienced through torrefaction. The inorganic content (measured as ash after combustion) was found to be 10.59 wt% and 6.51wt% for paper and MPW, respectively. Along with these values, the initial volatile matter and fixed carbon for paper waste were 77.5 wt% and 11.9 wt%, respectively; for MPW the volatile matter and fixed carbon were 90.6 wt% and 2.9 wt%, respectively. Ash-free elemental analysis of the major constituents of paper and MPW are shown in Table 5.1. Results are given in wt% with mol% in parenthesis. As is shown in the table, paper wastes contain much higher oxygen compared to MPW, and the hydrogen content in MPW is significantly higher than in paper waste.

Table 5.1. Ash-free elemental analysis of the major constituents of paper

	C (%)	H (%)	N (%)	O (%)
Paper waste	45.1 (28.7)	6.3 (48.1)	0.04 (0.02)	48.5 (23.1)
MPW	78.7 (32.5)	13.1 (65.0)	0.2 (0.06)	7.9 (2.4)

5.4.2 Heat Transfer Modeling

Biot Number (*Bi*) and Thermal Thiele Modulus (*M*) were calculated to determine the heat transfer regime of the experimental setup as follows:

$$Bi = \frac{h}{\lambda/L_c} \tag{5.1}$$

$$M = \frac{R^{\dagger}}{\lambda/(c_p L_c^2)} \tag{5.2}$$

It is essential to determine the thermal conductivity of the paper waste since it contains both paper waste and cardboard.

To calculate *M*, the reaction rate with a function of temperature has to be known. In this study, the measured reaction rate is shown in Figure 4.1, showing the mass loss rate vs. time at various temperatures. The maximum mass loss rate is approximately at the same time, however, the width in the mass loss rate is wider as the temperature decreases. Also, note that the thermal conductivity of the paper waste was measured at 25 °C with pressure of 1 atm. According to Lavrykov and Ramarao, the thermal conductivity of paper would increase as temperature increase (Lavrykov and Ramarao, 2012). Therefore, *Bi* was calculated with the smallest thermal conductivity and the maximum mass loss rate was selected for the calculation of *M*, as these would provide the worst-case scenario. Any larger thermal conductivity and smaller reaction rate would yield lower *Bi* and *M* values, respectively. To convert mass loss rate from units of s^{-1} to kg/m^3-s, it was multiplied by its density as measured in this study.

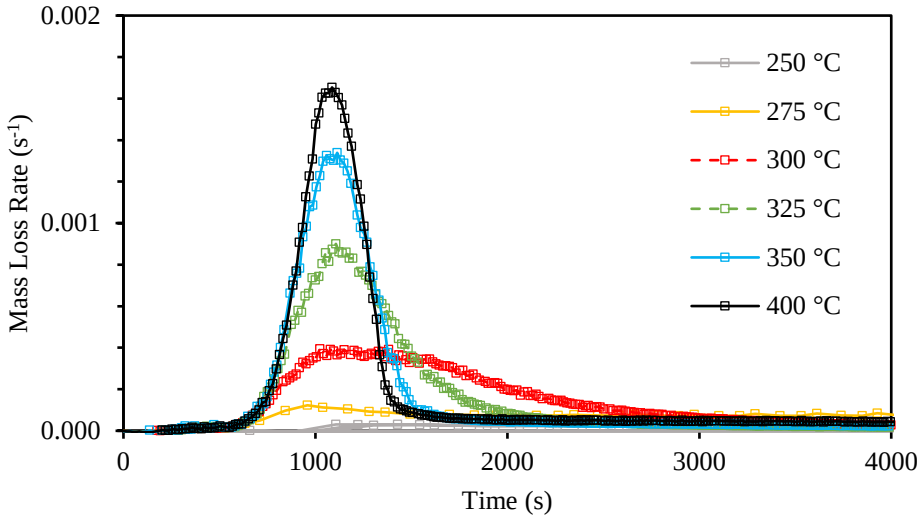

Figure 5.1. Measured mass loss rate at different temperatures vs. time.

With the parameter above, the *Bi* and *M* at different temperatures can be calculated and the results given in Table 5.2.

Table 5.2. *Bi* and *M* at various temperatures

Temp (°C)	**Rate (s^{-1})**	**R^{+} (kg/m^3-s)**	***M***	***Bi***
250	8.6E-05	0.10	1.3E-04	0.04
275	3.9E-04	0.47	6.0E-04	0.04
300	4.0E-04	0.48	6.2E-04	0.04
325	9.0E-04	1.08	1.4E-03	0.04
350	1.3E-03	1.56	2.0E-03	0.04
400	1.6E-03	1.94	2.5E-03	0.04

Since *Bi* equals 0.04, which is much smaller than 1, it indicates that the samples are thermally thin. Therefore, the heat convection from the oven to the sample surface is much slower than the heat conduction into the sample; for $M << 1$, it indicates that the heat conduction into the sample is much faster than the reaction rate. Thus, the particle temperature throughout was uniform and equals to the gas temperature (which is measured), and the reaction rate was governed by the heat convection from the oven to the surface of the sample (Xu et al., 2018).

5.4.3 Torrefaction of Paper Wastes

To study the torrefaction of the waste blends, it is essential to understand the torrefaction behavior of the paper wastes. Figure 5.2 depicts the experimental results of paper wastes torrefaction using TGA at 250 °C, 300 °C and 400 °C. From Figure 5.2 (a1 and a2), it was found that the maximum mass loss rate at 250 °C was only ~0.00003 (s^{-1}), the rate dropped to ~ 0.00001 after ~10,000 s and remained constant until the 15,000 s, while the mass loss

reached ~21%, with an almost linear increase after ~1,000 s. Figure 5.2 (b1 and b2) shows the results of mass loss rate and mass loss of paper waste torrefaction at 300 °C. The peak value of mass loss rate reached ~0.00034 (s^{-1}), which is much higher compared to the maximum rate of 250 °C. The mass loss had a two-stage behavior, it reached ~45% mass loss at ~2,000s and after which the reaction rate continues to slow down, and the mass loss reached ~60% mass loss after 8,000 s. The torrefaction behavior of paper wastes at 400 °C was similar to 300 °C, while it has higher maximum mass loss rate (~0.0018 s^{-1}) and the first stage ended at ~1,000 s, with mass loss of ~65% mass loss. The mass loss keeps rising with a lower rate and reached ~90% after 6,000 s. It was observed that the reaction rate depends on both temperature and the constituents of the paper wastes, detailed discussion is provided in the end of this section.

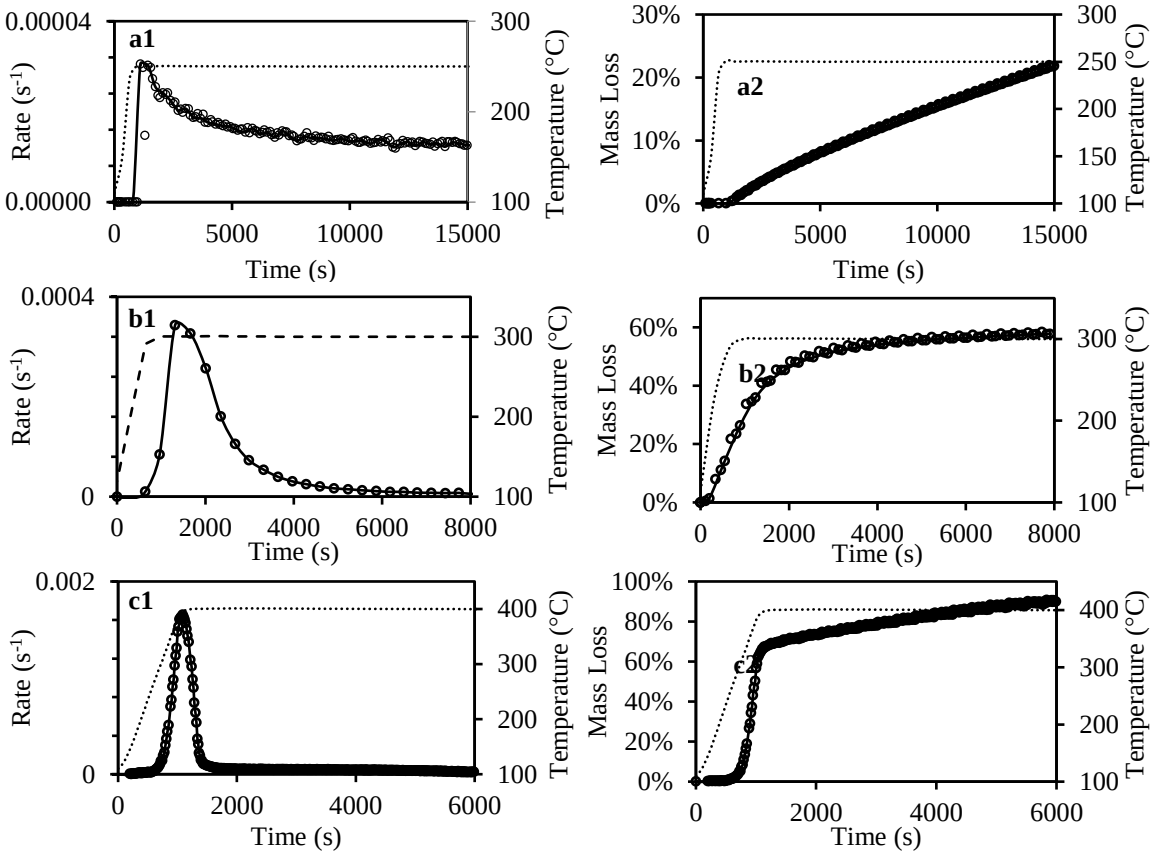

Figure 5.2. Mass loss rate of paper wastes torrefaction at: 250 °C (a1), 300 °C (b1), 400 °C (c1); mass loss of paper torrefaction at: 250 °C (a2), 300 °C (b2), 400 °C (c2).

To further understand the chemical changes occurred during the paper waste torrefaction, NMR spectroscopy was performed on the solid residues after the TGA experiments at various temperatures. In the ^{13}C NMR spectra of the low-temperature torrefaction processes (<275 °C), the peaks present between 50 and 100 ppm correspond to the carbons within the cellulosic framework of the material (Figure 5.3a) (Maunu, 2009). As the torrefaction temperature increased, a steady decline in the cellulose content was observed until it is fully converted at temperatures above 300 °C. The broad peak centered at 127

ppm during the same span (Figure 5.3b), shows very little reduction in intensity at these lower temperatures, though it too disappears by the final torrefaction temperature of this study. This broad peak is largely comprised of lignin signals that lie in the aromatic region of the ^{13}C NMR spectrum (Lauer et al., 1972). The NMR spectral data suggests that cellulosic carbon decomposes more readily at increasing temperatures through carbonization. As indicated in Hu *et al.* lignin retains its structure at temperatures below 280 °C, starts to slowly degrade and increase surface area between 310 and 330 °C, and past the critical temperature of 365 °C it turns into an aromatic hydrocarbon framework (Hu et al., 2014). The thermal decomposition of a constituent at ~31 ppm is also observed (Figure 5.3c) which begins to degrade at 250 °C. In biomass, this peak is often associated with the waxy cutin component (Love et al., 1998), however, in this case it is likely waxy aliphatic finish present on components of the wastepaper.

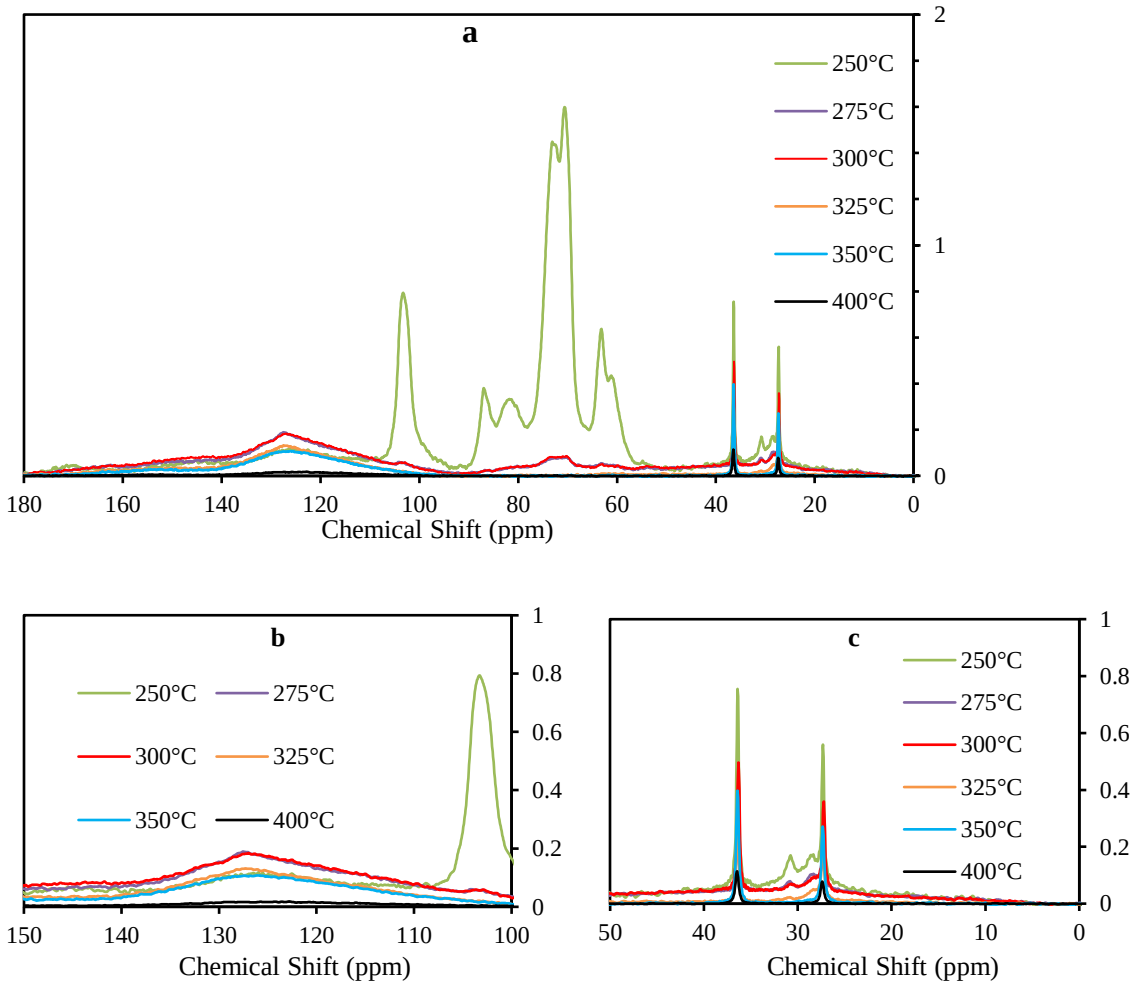

Figure 5.3. (a)$^{13}C\{^{1}H\}$ CP/MAS NMR spectrum of torrefied paper at temperatures from 200-400 °C showing asymmetric degradation of carbon species at increasing temperatures; (b) $^{13}C\{^{1}H\}$ CP/MAS NMR spectrum of torrefied paper centered around 127 ppm showing degradation of aromatic carbon throughout the temperature regime; (c) $^{13}C\{^{1}H\}$ CP/MAS NMR spectrum of torrefied paper in the aliphatic region showing thermal decomposition

of peak at 31 ppm. The peaks at 36.5 and 27.4 ppm are from the adamantane standard used for peak normalization.

5.4.4 Torrefaction of MPW

The torrefaction of MPW was also studied as shown in Figure 5.4. FTIR analysis of 30 random MPW pieces identified the mix to be 39% PE, 27% poly(ethylene-co-vinylacetate) (PEVA), 27% PET, 3% polyamide-nylon, and 3% PP. Our previous study has characterized these MPW, and it was found that these wastes are mainly consist of LDPE, PE, PET, PP, polyamide-nylon, PVC and other materials (Zinchik et al., 2020). From Figure 5.4 (a1 and a2), it was observed that the maximum mass loss rate at 250 °C was ~0.00002 (s^{-1}) and the rate remained constant until 8,000 s with mass loss reaching ~14%. This was due mainly to content of PP and nylon which degrade with relatively low rate at this temperature (Peterson et al., 2001; Ito and Nagai, 2010). Figure 5.4 (b1 and b2) show the results of mass loss rate and mass loss of MPW torrefaction at 300 °C. The peak value of mass loss rate reached ~0.00034 s^{-1}, which was much higher compared to the maximum rate of 250 °C. It reached ~45% mass loss at ~2,000 s and after which the reaction rate continued to slow down, and the mass loss reached ~60% after 8,000 s. The MPW torrefaction behavior at 400 °C (Figure 5.4 c1 and c2) were rather different compared to 250 °C and 300 °C. It has a higher maximum mass loss rate (~0.0016 s^{-1}) and the rate decreased after it reached a peak value. The mass loss keeps rising and reached an asymptotic value of ~40% after 8,000 s. This behavior was consistent with other literature findings, as LDPE, PE and PP would require higher temperature to degrade (Gao et al., 2003; Aboulkas et al., 2010).

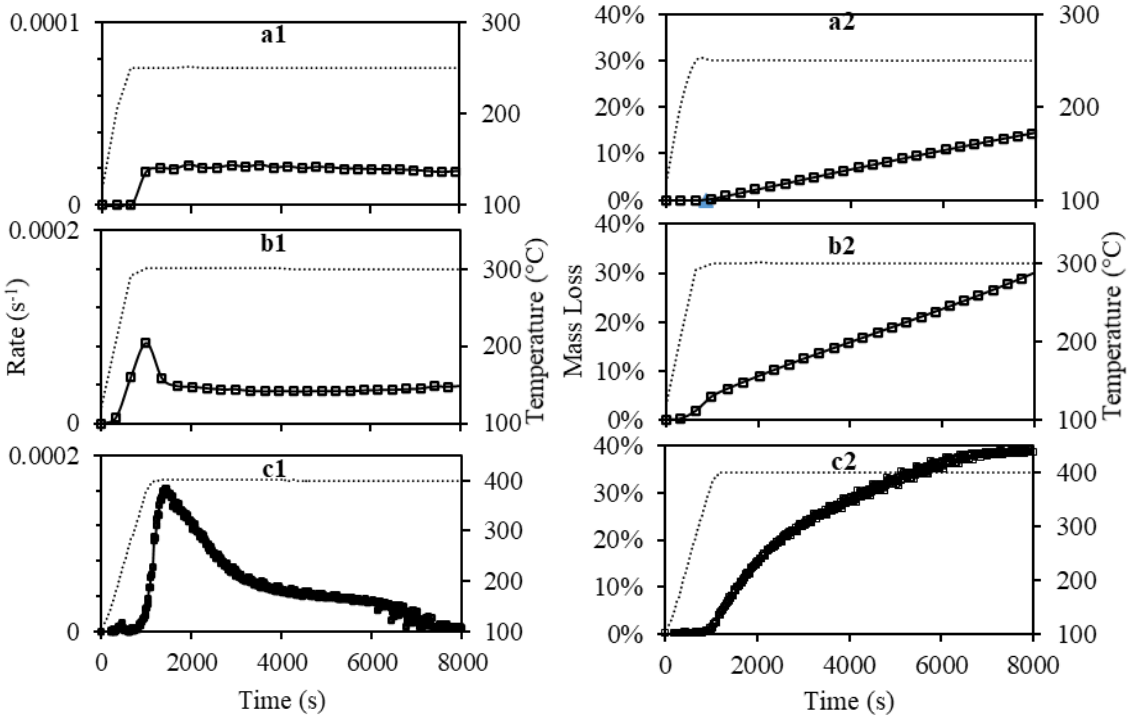

Figure 5.4. Mass loss rate of MPW torrefaction at: 250 °C (a1), 300 °C (b1), 400 °C (c1); mass loss of paper torrefaction at: 250 °C (a2), 300 °C (b2), 400 °C (c2).

5.4.5 Extrusion of MPW-Fiber Blends

In this study we examined both extruded and non-extruded MPW-fiber blends to determine the impact of loose blend mixtures compared to a more uniformly extruded material. Compounding extrusion of the MPW-fiber waste was initially performed at 160 ^{o}C and showed that the material was not consistent showing unmolten particles (nylon and PET) distributed throughout the extrudate. To alleviate this problem, compounding extrusion was then performed at 220 ^{o}C and resulted in a homogenized uniform extrudate and this temperature was used for MPW-fiber formulations.

The extruded MPW rod was analyzed by differential scanning calorimetry DSC (Figure 5.5 a) and 5 melting peaks were observed at 101 ^{o}C, 117 ^{o}C and 121 ^{o}C, 175 ^{o}C, and 252 °C and assigned (based on standards) to PEVA, LDPE, HDPE, PP and PET, respectively. This MPW composition is in general agreement with FTIR analysis of 30 random plastic pieces, except for nylon.

The softening temperature (T_s) of the extruded MPW, MPW-fiber formulations and LDPE were determined by TMA (Figure 5.5 b). Two T_s's were recorded for LDPE at 33 and 113 °C. While the mixed extruded MPW had a T_s of 111 ^{o}C and the addition of fiber increased this slightly to 116 ^{o}C (25% fiber) and 118 ^{o}C (50% fiber). The softening point of the mixture was dominated by PE as the major component of the mix.

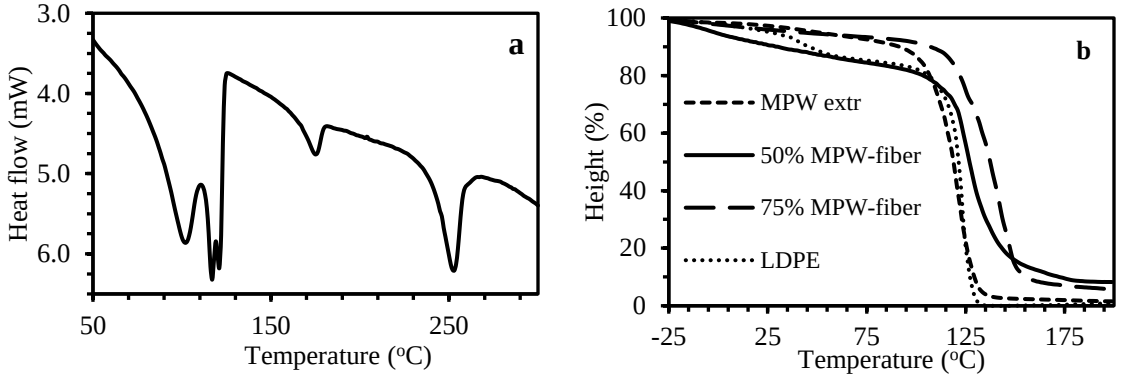

Figure 5.5. (a) DSC thermogram of extruded MPW; (b) TMA thermograms of extruded MPW, extruded MPW-fiber (50/50 and 75/25), and LDPE.

5.4.6 Synergy Effect in Torrefaction of Fiber-MPW

TGA experiments were performed at different temperatures with various blend ratios to study the interactions between paper and MPW, and the results are shown below in Figure 5.6 and Figure 5.7. Similar to section 3.4, "_exp" denotes the experimental results and the "_cal" denotes the reconstructed results according to linear mixing rules. The MPW-fiber weight ratio of the blend is also noted in each plot. Figure 5.6 (a, b, c) represents the results at 250 °C, Figure 5.7 (a, b, c) shows the results at 300 °C and 400 °C results are depicted in Figure 5.7 (d).

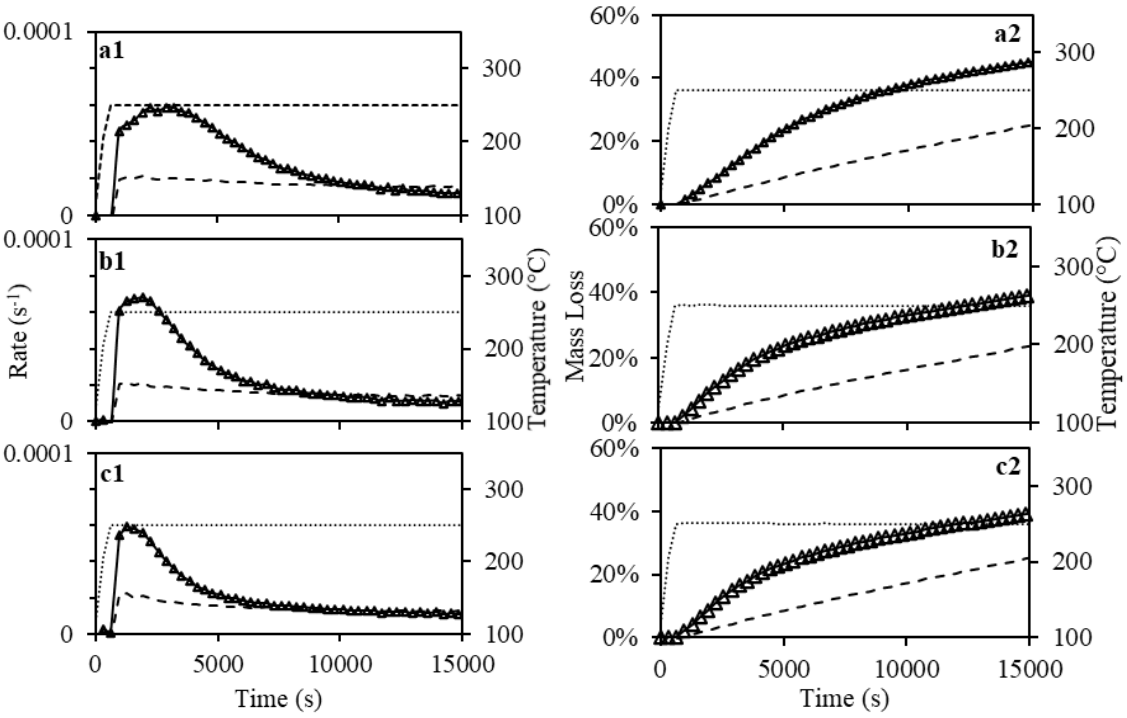

Figure 5.6. Mass loss rate of paper-MPW torrefaction at 250 °C with paper-MPW blend ratio of (a1, 3:1), (b1, 1:1), (c1, 1:3); Mass loss of paper-MPW torrefaction at 250 °C with paper-MPW ratio of (a2, 3:1), (b2, 1:1), (c2, 1:3).

Figure 5.6 (a, b c) show significant synergistic effects between paper and MPW during torrefaction at 250 °C. In all three experiments with different ratios, it can be found that the maximum mass loss rate was more than doubled and the mass loss at the end of the experiments were also much higher compared to the expected results. It can also be observed that different blend ratios have impacts on the significance of the synergistic effects. For instance, the mass loss of the paper-MPW ratio 1:3 sample reached ~43% after 15,000 s (Figure 5.6 a2), while the sample of the lowest MPW composition (25%) only reached ~38% mass loss after the same time (Figure 5.6 c2). At 300 °C, although the reaction rates are faster and the mass losses are higher than 250 °C, the overall synergistic effects were less significant. In addition, the blend ratio has a larger impact on the synergistic effects. For instance, the effects of the synergy on the mass loss rate with paper-MPW ratio of 1:3 and 1:1 are less significant compared to 250 °C (Figure 5.7 a1, b1), while the final mass loss after 8,000 s were still much higher than expected values. This finding was close to another previous study with paper-MPW ratio of 3:2, which were thermally treated at 300 °C (Zinchik et al., 2020). However, with paper-MPW ratio of 3:1 at 300 °C, the synergistic effects were almost insignificant. And at higher temperature (400 °C) with paper MPW ratio 1:1, there were no synergistic effects observed as shown in Figure 5.7 (d).

From the results of Figure 5.6 and Figure 5.7, it can be concluded that synergistic effects depend inversely on temperature, where the strongest effect is observed at 250°C. Additionally, higher MPW composition leads to more synergistic effects. As seen from Table 5.1, MPW has significantly higher hydrogen than paper waste, which leads us to hypothesize that MPW is acting as a hydrogen donor during torrefaction. It has been hypothesized by Lin et al. that the radicals derived from paper wastes during the process also intensified the scission of the polymer chain, participated in polymer radical terminations, and inhibited polymer intermolecular hydrogen transfer reactions; which increases the overall reaction rate (Lin et al., 2020). The interactions could be also due to crosslinking, which has been suggested between polymers (Tillet et al., 2011) and between wood flour and polyethylene (Bengtsson et al., 2005). These interactions between material components act to enhance the global degredation rates while the decomposition is relatively slow (low temperatures), but are obscured by the increased rate of the torrefaction chemistries at higher temperatures.

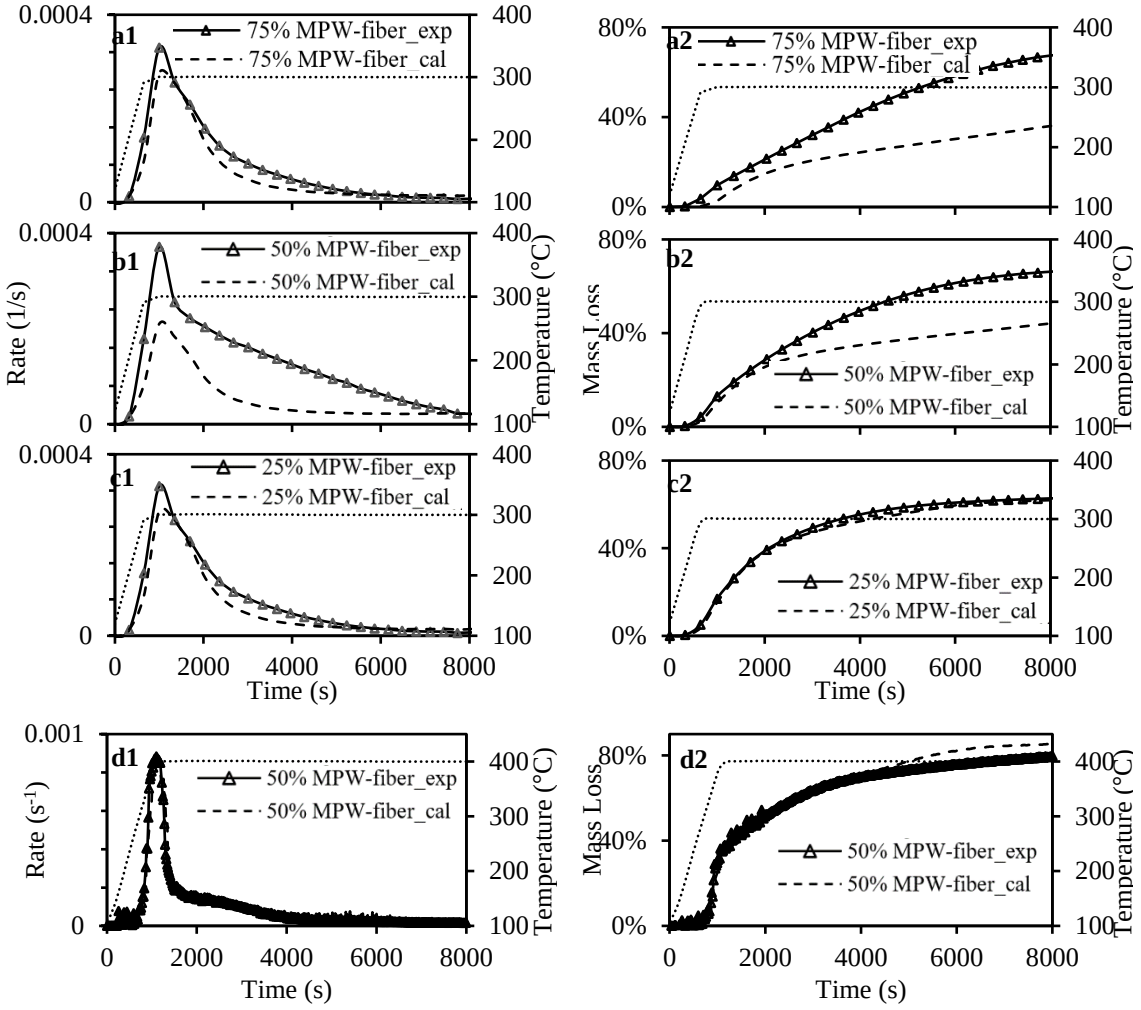

Figure 5.7. Mass loss rate of paper-MPW torrefaction at 300 °C with paper-MPW ratio of (a1, 3:1), (b1, 1:1), (c1, 1:3); 400 °C with paper-MPW ratio of (d1, 1:1); Mass loss of paper-MPW torrefaction at: 300 °C with paper-MPW ratio of (a2, 3:1), (b2, 1:1), (c2, 1:3).

The existence of interactions between fiber and MPW indicates that the natural energy barriers during the individual torrefaction in paper waste or MPW could be bypassed, and the torrefaction of fiber and MPW blend can be achieved at lower temperatures and/or shorter residence times. This is clearly observed from the *r*esults of Figure 5.6 and Figure 5.7, which indicate that there are significant impacts to the degradation trajectory that are not explainable by simple linear component mixing laws. This enhanced degradation offers an opportunity in industrial processing, through bypassing the natural energy barriers during the torrefaction chemistry in waste plastic-paper or waste plastic alone. For example, if torrefaction is sought as a method of creating an enhanced solid fuel or to making biomass fibers more compatible to matrix with plastics in composites, the degradation can be achieved at a much low temperature and/or lower reactor residence time. As discussed above, the content of carbon is significantly enriched in the fiber chars around 40-50% mass loss. At 250 °C, this extent of reaction is not realizable even at the

extended reaction times in the analytical techniques studied here and the maximum mass loss values based on individual components was not expected to be much higher than 20%. Indeed, for the fiber content these values were not observed until 300 °C and residence times approaching 60 min. Through taking advantage of the interactions of the paper and plastic components, similar results are realizable at either lower temperatures (250 °C, similar residence time of 60-90 min) or lower residence times (300 °C, 30 min). Identifying such interactions could lead to operating reactors at lower temperatures with less energy input or even greater energy export as co-product, less thermal losses, or a lower residence time that could substantially reduce capital investment or increase throughput. Further, operating the thermal reactor at lower temperatures offers less expensive and exotic reactor and materials of construction options. For example, inexpensive silicon-based seals can be continuously exposed to reaction temperatures around 250 °C, whereas more expensive and less resilient graphite or vermiculite seals are often used above 280 °C. Lower reaction temperatures can also decrease any corrosion effects from formed organic acids, or halogens present in waste plastics (such as chlorine that would evolve as HCl). As another example (and further evidenced by the composite testing that follows), Wang et al. demonstrated how waste fiber degradation between 25-70% mass loss enhanced the ability of fibers to reinforce plastic composites, improve weatherability, and resist microbial action (Wang et al., 2019). Future work will quantify the energy barriers and process kinetics and evaluate these potential economical benefits in schemes for producing a solid fuel as well as biomaterials. As mentioned above, biomass and plastic synergistic effects were observed at high temperature pyrolysis, where liquids are the main products of degradation. From this study, which focuses on low temperature torrefaction with the major product being solid fuel, shown synergistic effects were observed, which differ significantly from the high temperature pyrolysis studies.

5.4.7 Further Synergistic Evidence

To further study the synergistic effect between fiber and plastic polymers, the pellets produced from fiber-MPW by reactive extrusion were characterized by various methods.

5.4.7.1 IR Spectroscopy

Figure 5.8 (a, b) show an FTIR spectrum of paper-MPW without extrusion and with extrusion at 1:1 ratio. C-H stretching bands were observed in all the samples at 2916 cm^{-1} and 2850 cm^{-1} , which can be attributed to methylene groups (Mayo et al., 2004). O-H stretching band also exists between 3100 cm^{-1} to 3600 cm^{-1} in all the samples (Wang et al., 2014). Broad carbonyl (C=O) band at was found in all the samples 1690-1750 cm^{-1}, which can be attributed to ester in linkage in PET and amide linkage in nylon (Mayo et al., 2004). Paper was also identified at 1505 cm^{-1} with a small band associated with lignin (Dence, 1992). In addition, C–O stretching in wood cellulose and hemicellulose was observed in region between 1000 and 1070 cm^{-1}; cis- bands at 727 cm^{-1} and trans-vinylene bands at 974 cm^{-1} were found in all the samples as well (Pandey, 1999; Mayo et al., 2004). We observe slight differences between the non-extruded samples and the extruded ones. Similar results were obtained for other blend ratios as well.

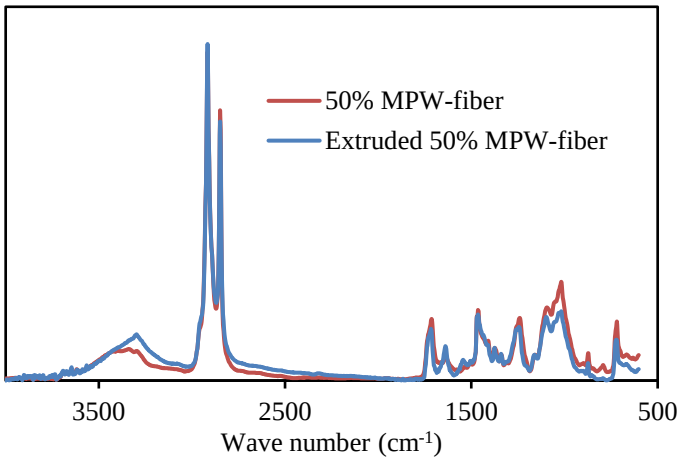

Figure 5.8. FTIR spectrum of non-extruded and extruded 50/50 MPW-fiber ratio.

In order to study the chemical changes occurred during the reactive extrusion, the following indices were used: Carbonyl index (CI), cellulose index (CeI), and hydroxyl index (HI). The indices were defined as a ratio of the band intensity at 1720 cm^{-1}, 1024 cm^{-1}, and 3342 cm^{-1}, respectively, to the band 2916 cm^{-1} for the -CH_2- groups (Wei et al., 2013). The relative changes in hydroxyl, carbonyl, and cellulose that occurred during torrefaction were analyzed by calculating CI, CeI, and HI respectively (Zinchik et al., 2020).

To show the changes in CI, CeI, and HI we defined the following relative indices:

$$(CI)_{rel} = \frac{(CI)_{extrud}}{(CI)_{non-extrud}}$$

$$(CeI)_{rel} = \frac{(CeI)_{extrud}}{(CeI)_{non-extrud}}$$

$$(HI)_{rel} = \frac{(HI)_{extrud}}{(HI)_{non-extrud}}$$

These new variables will show the relative change of each of these indices because of the reactive extrusion process. Figure 5.9 shows these indices for two MPW-fiber (50/50 and 75/25, fiber to MPW ratios); the line at unity depicts no change in the index. The HI increases after extrusion by ~27% for both blends, whereas, the CI are reduced by 30% and the CeI is reduced by ~27%. It can be concluded that the increase in HI (the hydroxyl group) was on account of the reduction of the CeI and CI. This is indicative to transfer of hydrogen atoms to the C=O and C-O-C groups and as a consequent the increase of the OH group. It also indicates that the reduction in cellulose content was due to dehydration and degradation reactions (Wang et al., 2014).

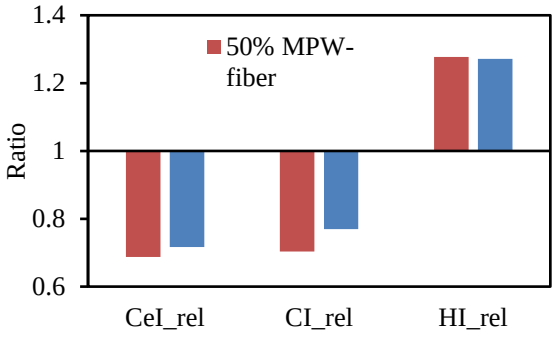

Figure 5.9. CeI_{rel}, CI_{rel} and HI_{rel} of MPW-fiber with ratio of 50/50 and 75/25

5.4.7.2 Dynamic Rheology

Dynamic rheological measurements were also obtained on the extruded materials, compression molded MPW crumb, and LDPE. Figure 5.10 shows the complex viscosity (η*) of all melt samples to decrease with shear rate at 180 °C. This behavior is indicative of shear-thinning of non-Newtonian fluids such as polymer melts (Shenoy, 1999). The η* (at 1 s^{-1}) for LDPE (reference material) was low at 2,760 Pa·s. The compression molded and extruded MPW waste materials respectively, have η* of 8,260 Pa.s and 19,200 Pa·s. By compounding the MPW in an extruder, good dispersion, distribution, and interaction of the various plastics was achieved strengthening the polymer melt resulting in a two-fold higher viscosity. The two plastic mixed samples had a higher viscosity that LDPE alone. The addition of 25% and 50% fiber to MPW increased its η* approximately 2- and 4-fold, respectively. The entangled fibers reinforced the polymer matrix as well as enhanced interactions between the two, thus increased its viscosity (Shenoy, 1999; Wang et al., 2019). This trend is also observed in wood plastic composite systems (Adefisan and McDonald, 2019).

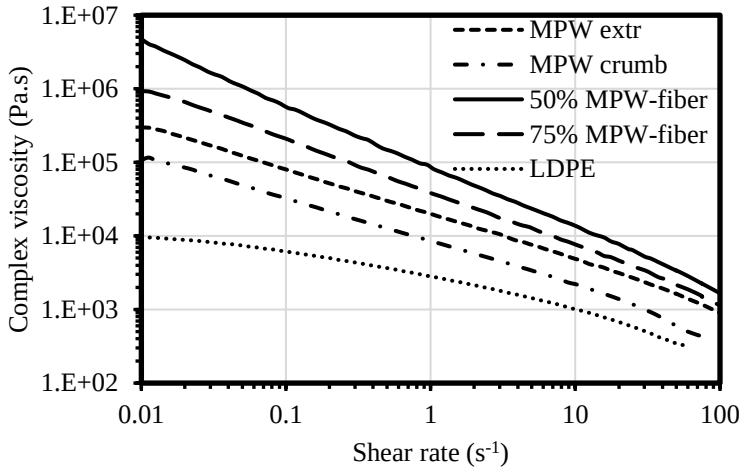

Figure 5.10. Flow curves (complex viscosity vs shear rate) at 180 °C of extruded MPW, extruded MPW-fiber (50/50 and 75/25), compression molded MPW crumb and LDPE.

Figure 5.11 shows the complex viscosity at shear rate of 1 s^{-1}, for of LDPE, MPW crumbs, extruded MPW, extruded MPW-fiber (50/50 and 75/25). It is to be noted that the complex viscosity of MPW crumbs is higher than that of LDPE (a major component in MPW). The important part is that when MPW is extruded, it has complex viscosity 7 times higher than that of LDPE and 2.3 times more than non-extruded MPW. This is a direct evidence of the synergistic effects within plastic components themselves. When fiber is added to MPW and extruded, the complex viscosity increases significantly over non-extruded and extruded MPW, with strong effect of the fiber content in the blend.

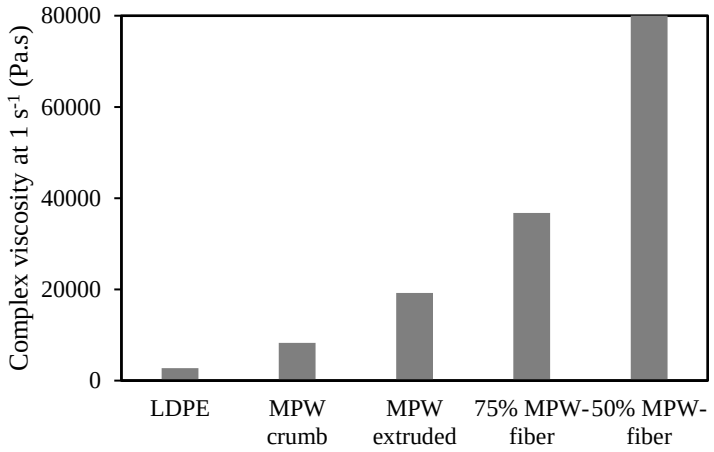

Figure 5.11. Complex viscosity at 1 s^{-1} shear rate at 180 °C of LDPE, MPW crumbs, extruded MPW, extruded MPW-fiber (50/50 and 75/25).

5.4.7.3 Flexural Testing

Flexural tests were carried out for extruded MPW, extruded MPW-fiber (50/50 and 75/25), compression molded MPW crumb and LDPE. Figure 5.12 a shows the flexural modulus for the same samples shown in Figure 5.11. The LDPE and MPW have similar values for the flexural modulus, 213±10 MPa and 195±10 MPa, respectively. When the MPW is extruded, it increases flexural modulus by 40% to 278±10 MPa, which is a strong indication of the synergy between the various polymer components in MPW. When fiber is added to MPW and extruded, the flexural modulus increases significantly; the 75%MPW-25%fiber blend shows increase of almost a factor of 3 and the 50%MPW-50%fiber blend increases further by a factor of 6 over the non-extruded MPW. The flexural strength shows a similar behavior, though less pronounced, as seen in Figure 5.12 (b). This improvement in mechanical properties by addition of fibers is also observed in wood plastic composite systems (Fabiyi and McDonald, 2010; Adefisan and McDonald, 2019; Wang et al., 2019).

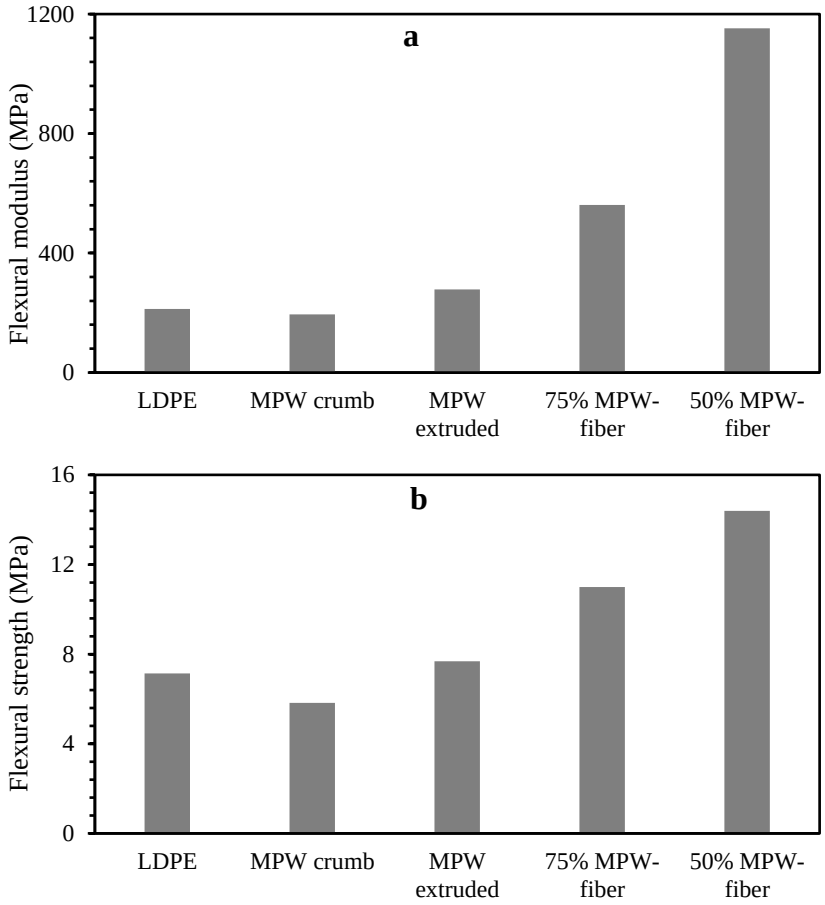

Figure 5.12. (a) Flexural modulus and (b) Flexural strength of LDPE, MPW crumb, extruded MPW, extruded MPW-fiber (50/50 and 75/25).

5.5 Summary and Conclusions

In this study, the torrefaction of paper wastes, MPW and paper-MPW blends at various temperatures were studied. Synergistic effects were observed between paper plastic wastes during torrefaction. It was also found that at lower temperatures (250 °C), the maximum mass loss rate was more than doubled and the mass loss at the end of the experiments were also much higher compared to the expected results (if there are no interactions). In addition, with higher plastic content, the effects are more significant, both increasing the reaction rate as well as the overall mass loss. However, there is no synergy observed at higher temperature (400 °C). The existence of such interactions between fiber and plastic wastes indicates that the natural energy barriers during the individual torrefaction in paper waste or plastic waste could be bypassed, and the torrefaction of fiber and plastic blend can be achieved at lower temperatures and/or shorter residence times. The reactive extrusion at 220 °C also showed there exists chemical changes during the process, which reduces the C-O and carbonyl index and increased hydroxyl content. The interaction between paper and plastic wastes during torrefaction can be attributed to the plastic acting as a hydrogen donor during the torrefaction of the paper, and the radicals derived from paper wastes also intensified the scission of the polymer chain, initiating the scission of the polymer chain,

which increases the overall reaction rate and mass loss. It was also found that complex viscosity of the extruded MWP-fiber blends is 7 times higher than LDPE and 2.3 times more than non-extruded MPW. The results of flexural testing indicated that there exist synergistic effects not only between the MPW and fiber wastes, but also with the MPW. These synergistic effects can greatly help to design the process parameters to valorize mixed paper-plastic wastes.

Acknowledgements

We acknowledge the support from (1) Battelle/Idaho National Laboratory (INL) Grant contract number 209856; (2) National Science Foundation grant number 1827364; (3) the M.J. Murdock Charitable Trust for their support in the purchase of the twin-screw extruder; and (4) supported by the U.S. Department of Energy (DOE), Office of Energy Efficiency and Renewable Energy (EERE), Bioenergy Technologies Office (BETO), under DOE Idaho Operations Office Contract DE-AC07-05ID14517.

Author Contributions Statement

ZX analyzed the data and wrote the manuscript. SK and SZ helped in data analysis and manuscript review. LE and AM performed the extrusion experiments, analyzed the extruded pellets and contributed to the manuscript in the appropriate sections. EF, KS, and CP characterized the feedstock, carried out the TGA, analyzed the char samples and contributed to the related sections in manuscript writing. EBZ and JK supervised the entire work, analyzed the data and helped in manuscript writing.

5.6 Works Cited

Abbas, Z., Moghaddam, A. P., and Steenari, B. M. (2003). Release of salts from municipal solid waste combustion residues. *Waste Manag.* 23, 291–305. doi:10.1016/S0956-053X(02)00154-X.

Aboulkas, A., El harfi, K., and El Bouadili, A. (2010). Thermal degradation behaviors of polyethylene and polypropylene. Part I: Pyrolysis kinetics and mechanisms. *Energy Convers. Manag.* 51, 1363–1369. doi:10.1016/j.enconman.2009.12.017.

Adefisan, O. O., and McDonald, A. G. (2019). Evaluation of the strength, sorption and thermal properties of bamboo plastic composites. *Maderas Cienc. y Tecnol.* 21, 3–14. doi:10.4067/S0718-221X2019005000101.

Alén, R., Kuoppala, E., and Oesch, P. (1996). Formation of the main degradation compound groups from wood and its components during pyrolysis. *J. Anal. Appl. Pyrolysis* 36, 137–148. doi:10.1016/0165-2370(96)00932-1.

Alvarez, V. A., and Vázquez, A. (2004). Thermal degradation of cellulose derivatives/starch blends and sisal fibre biocomposites. *Polym. Degrad. Stab.* 84, 13–21. doi:10.1016/j.polymdegradstab.2003.09.003.

Anders, H., and Zimmermann, H. (1987). A comparison of the thermal degradation behaviours of poly(vinyl acetate), poly(vinyl alcohol) and poly(vinyl chloride). *Polym. Degrad. Stab.* 18, 111–122. doi:10.1016/0141-3910(87)90024-3.

Anuar Sharuddin, S. D., Abnisa, F., Wan Daud, W. M. A., and Aroua, M. K. (2016). A review on pyrolysis of plastic wastes. *Energy Convers. Manag.* 115, 308–326. doi:10.1016/J.ENCONMAN.2016.02.037.

Bacaloglu, R., and Fisch, M. (1995). Degradation and stabilization of poly (vinyl chloride). V. Reaction mechanism of poly(vinyl chloride) degradation. *Polym. Degrad. Stab.* 47, 33–57. doi:10.1016/0141-3910(94)00086-N.

Bach, Q. V., Chen, W. H., Eng, C. F., Wang, C. W., Liang, K. C., and Kuo, J. Y. (2019). Pyrolysis characteristics and non-isothermal torrefaction kinetics of industrial solid wastes. *Fuel* 251, 118–125. doi:10.1016/j.fuel.2019.04.024.

Bengtsson, M., Gatenholm, P., and Oksman, K. (2005). The effect of crosslinking on the properties of polyethylene/wood flour composites. *Compos. Sci. Technol.* 65, 1468–1479. doi:10.1016/j.compscitech.2004.12.050Bergman, T. L., Incropera, F. P., DeWitt, D. P., and Lavine, A. S. (2011). "Fundamentals of heat and mass transfer," in (New York: Wiley, pp. 983-1011), 56.

Biagini, E., Barontini, F., Tognotti, L., and Diotisal, V. (2006). Devolatilization of Biomass Fuels and Biomass Components Studied by TG / FTIR Technique. 4486–4493. doi:10.1021/ie0514049.

Bradbury, A. G. W., Sakai, Y., and Shafizadeh, F. (1979). A kinetic model for pyrolysis of cellulose. *J. Appl. Polym. Sci.* 23, 3271–3280. doi:10.1002/app.1979.070231112.

Braun, V. D., and Thallnaier, M. (1966). Zum mechanismus der thermischen chlorwassmtoffabspaltung aus polyvinylchlorid. 3. Mitt. Über die länge der polyensequenzen in partiell dehydrohalogenierten poiyvinylchloriden, polyvinylbromiden und vinylchlorid-copolymeren. *Die Makromol. Chemie* 99, 59–75. doi:10.1002/macp.1966.020990106.

Brebu, M., Tamminen, T., and Spiridon, I. (2013). Thermal degradation of various lignins by TG-MS/FTIR and Py-GC-MS. *J. Anal. Appl. Pyrolysis* 104, 531–539. doi:10.1016/j.jaap.2013.05.016.

Brebu, M., and Vasile, C. (2010). Thermal Degradation of Lignin-A Review. *Cellul. Chem. Technol.* 44, 353–363. Available at: https://www.semanticscholar.org/paper/THERMAL-DEGRADATION-OF-LIGNIN-A-REVIEW-Brebu-Vasile/67fecec0d827e7ac1cbb5a4c6752b6d8ec6c1fef [Accessed August 7, 2020].

Burra, K. G., and Gupta, A. K. (2018). Synergistic effects in steam gasification of combined biomass and plastic waste mixtures. *Appl. Energy* 211, 230–236. doi:10.1016/j.apenergy.2017.10.130.

Cabrales, L., and Abidi, N. (2010). On the thermal degradation of cellulose in cotton fibers. *J Therm Anal Calorim* 102, 485–491. doi:10.1007/s10973-010-0911-9.

Cangialosi, F., Intini, G., Liberti, L., Notarnicola, M., and Stellacci, P. (2008). Health risk assessment of air emissions from a municipal solid waste incineration plant - A case study. *Waste Manag.* 28, 885–895. doi:10.1016/j.wasman.2007.05.006.

Chang, S.-S. (1977). Heat Capacity and Thermodynamic Properties of Poly(Vinyl Chloride). *J. Res. Natl. Bur. Stand. (1934).* 82, 9–18. doi:10.6028/jres.082.002.

Chattopadhyay, J., Kim, C., Kim, R., and Pak, D. (2008). Thermogravimetric characteristics and kinetic study of biomass co-pyrolysis with plastics. 25, 1047–1053.

Chen, R., Zhang, S., Cong, K., Li, Q., and Zhang, Y. (2020). Insight into synergistic effects of biomass-polypropylene co-pyrolysis using representative biomass constituents. *Bioresour. Technol.* 307, 123–243. doi:10.1016/j.biortech.2020.123243.

Chen, W. H., Wang, C. W., Ong, H. C., Show, P. L., and Hsieh, T. H. (2019). Torrefaction, pyrolysis and two-stage thermodegradation of hemicellulose, cellulose and lignin. *Fuel* 258, 116–168. doi:10.1016/j.fuel.2019.116168.

Chen, W., and Kuo, P. (2011). Isothermal torrefaction kinetics of hemicellulose , cellulose , lignin and xylan using thermogravimetric analysis. *Energy* 36, 6451–6460. doi:10.1016/j.energy.2011.09.022.

Chen, W., Peng, J., and Bi, X. T. (2015). A state-of-the-art review of biomass torrefaction , densi fi cation and applications. 44, 847–866. doi:10.1016/j.rser.2014.12.039.

Collard, F. X., and Blin, J. (2014). A review on pyrolysis of biomass constituents: Mechanisms and composition of the products obtained from the conversion of cellulose, hemicelluloses and lignin. *Renew. Sustain. Energy Rev.* 38, 594–608. doi:10.1016/j.rser.2014.06.013.

Conti, J., Holtberg, P., Diefenderfer, J., LaRose, A., Turnure, J. T., and Westfall, L. (2016). International Energy Outlook 2016 with Prokctions to 2040. Available at: https://www.eia.gov/outlooks/ieo/pdf/0484(2016).pdf.

Curling, S., Clausen, C. A., and Winandy, J. E. (2001). The effect of hemicellulose degradation on the mechanical properties of wood during brown rot decay. in *International Research Group on Wood Preservation 2011*, 1–10.

De Carvalho, G., Frollini, E., and Dos Santos, W. N. (1996). Thermal conductivity of polymers by hot-wire method. *J. Appl. Polym. Sci.* 62, 2281–2285. doi:10.1002/(sici)1097-4628(19961226)62:13<2281::aid-app12>3.3.co;2-t.

Dence, C. W. (1992). The Determination of Lignin. *Methods Lignin Chem.*, 33–61. Available at: https://link.springer.com/chapter/10.1007/978-3-642-74065-7_3.

Donepudi, Y. (2017). Impact of Pretreatment Methods on Fast Pyrolysis of Biomass. Available at: https://digitalcommons.mtu.edu/etdr/496.

Dupuis, D. P., Grim, R. G., Nelson, E., Tan, E. C. D., Ruddy, D. A., Hernandez, S., et al. (2019). High-Octane Gasoline from Biomass: Experimental, Economic, and Environmental Assessment. *Appl. Energy* 241, 25–33. doi:10.1016/j.apenergy.2019.02.064.

Eichhorn, S. J., Sirichaisit, J., and Young, R. J. (2001). Deformation mechanisms in cellulose fibres, paper and wood. *J. Mater. Sci.* 36, 3129–3135. doi:10.1023/A:1017969916020.

El-Fadel, M., Findikakis, A. N., and Leckie, J. O. (1997). Environmental impacts of solid waste landfilling. *J. Environ. Manage.* 50, 125.

Enviromental Protection Agency (2017). Advancing Sustainable Materials Management: 2017 Fact Sheet Assessing Trends in Material Generation, Recycling, Composting, Combustion with Energy Recovery and Landfilling in the United States. Available at: https://www.epa.gov/sites/production/files/2019-11/documents/2017_facts_and_figures_fact_sheet_final.pdf [Accessed November 11, 2020].

EPA Clean Air Act, 42 USC 7412(f) (1992). Available at: https://www.govinfo.gov/content/pkg/USCODE-2013-title42/html/USCODE-2013-title42-chap85-subchapI-partA-sec7412.htm [Accessed January 19, 2020].

Fabiyi, J. S., and McDonald, A. G. (2010). Effect of wood species on property and weathering performance of wood plastic composites. *Compos. Part A Appl. Sci. Manuf.* 41, 1434–1440. doi:10.1016/j.compositesa.2010.06.004.

Farhat, W., Venditti, R., Quick, A., Taha, M., Mignard, N., Becquart, F., et al. (2017). Hemicellulose extraction and characterization for applications in paper coatings and adhesives. *Ind. Crop. Prod.* 107, 370–377. doi:10.1016/j.indcrop.2017.05.055.

Fung, B. M., Khitrin, A. K., and Ermolaev, K. (2000). An Improved Broadband Decoupling Sequence for Liquid Crystals and Solids. *J. Magn. Reson.* 142, 97–101. doi:10.1006/jmre.1999.1896.

Funke, A., Henrich, E., Dahmen, N., and Sauer, J. (2017). Dimensional Analysis of Auger-Type Fast Pyrolysis Reactors. *Energy Technol.* 5, 119–129. doi:10.1002/ente.201600095.

Gao, Z., Kaneko, T., Amasaki, I., and Nakada, M. (2003). A kinetic study of thermal degradation of polypropylene. *Polym. Degrad. Stab.* 80, 269–274. doi:10.1016/S0141-3910(02)00407-X.

Gómez, M. A., Álvarez, M. A., Eguía, P., and Comesa, R. (2012). Thermochimica Acta Thermal lag analysis on a simulated TGA-DSC device. 547, 13–21.

Goorah, S. S. D., Esmyot, M. L. I., and Boojhawon, R. (2009). The health impact of nonhazardous solid waste disposal in a community: the case of the Mare Chicose landfill in Mauritius. *J. Environ. Health* 72, 48–55.

Han, B., Chen, Y., Wu, Y., and Hua, D. (2014). Co-pyrolysis behaviors and kinetics of plastics – biomass blends through thermogravimetric analysis. 227–235. doi:10.1007/s10973-013-3228-7.

Hatanaka, T., Imagawa, T., and Takeuchi, M. (2000). Formation of PCDD/Fs in artificial solid waste incineration in a laboratory-scale fluidized-bed reactor: Influence of

contents and forms of chlorine sources in high-temperature combustion. *Environ. Sci. Technol.* 34, 3920–3924. doi:10.1021/es991258w.

Ház, A., Jablonský, M., Šurina, I., Kačík, F., Bubeníková, T., and Ďurkovič, J. (2019). Chemical composition and thermal behavior of kraft lignins. *Forests* 10, 1–12. doi:10.3390/f10060483.

He, Q., Ding, L., Gong, Y., Li, W., Wei, J., and Yu, G. (2019). Effect of torrefaction on pinewood pyrolysis kinetics and thermal behavior using thermogravimetric analysis. *Bioresour. Technol.* 280, 104–111. doi:10.1016/j.biortech.2019.01.138.

He, Q., Guo, Q., Ding, L., Gong, Y., Wei, J., and Yu, G. (2018). Co-pyrolysis Behavior and Char Structure Evolution of Raw/Torrefied Rice Straw and Coal Blends. *Energy and Fuels* 32, 12469–12476. doi:10.1021/acs.energyfuels.8b03469.

Hilbers, T. J., Wang, Z., Pecha, B., Westerhof, R. J. M., Kersten, S. R. A., Pelaez-samaniego, M. R., et al. (2015). Cellulose-Lignin interactions during slow and fast pyrolysis. *J. Anal. Appl. Pyrolysis* 114, 197–207. doi:10.1016/j.jaap.2015.05.020.

Hoornweg, D., and Bhada-Tata, P. (2012). What a Waste : A Global Review of Solid Waste Management. *Urban Dev. Ser. Pap. no. 15. World Bank, Washington, DC. © World Bank. Licens. CC BY 3.0 IGO."* 15, 8. doi:10.3970/cmes.2014.098.129.

Hu, J., Shen, D., Wu, S., Zhang, H., and Xiao, R. (2014). Effect of temperature on structure evolution in char from hydrothermal degradation of lignin. *J. Anal. Appl. Pyrolysis* 106, 118–124. doi:10.1016/j.jaap.2014.01.008.

Hubbe, M. A., Venditti, R. A., and Rojas, O. J. (2007). What happens to cellulosic fibers during papermaking and recycling? A review. *BioResources* 2, 739–788. doi:10.15376/biores.2.4.739-788.

Incroper, F. P., Dewitt, D. P., Bergman, T. L., and Lavine, A. S. (2011). *Fundamentals of Heat and Mass Transfer*. 7th ed. Wiley, pp. 983-1011 Available at: http://cds.cern.ch/record/1339915/files/9780471457282_TOC.pdf [Accessed July 30, 2019].

Indrawan, B., Prawisudhap, P., and Yoshikawa, K. (2011). Chlorine-free Solid Fuel Production from Municipal Solid Waste by Hydrothermal Process. *J. Japan Inst. Energy* 90, 1177–1182. doi:10.3775/jie.90.1177.

Inoue, T., Miyazaki, M., Kamitani, M., Kano, J., and Saito, F. (2004). Mechanochemical dechlorination of polyvinyl chloride by co-grinding with various metal oxides. *Adv. Powder Technol.* 15, 215–225. doi:10.1163/156855204773644445.

Ito, M., and Nagai, K. (2010). Thermal aging and oxygen permeation of Nylon-6 and Nylon-6/montmorillonite composites. *J. Appl. Polym. Sci.* 118, 928–935. doi:10.1002/app.32424.

Jacques Lédé (2010). Biomass Pyrolysis: Comments on Some Sources of Confusions in the Definitions of Temperatures and Heating Rates. *Energies* 3, 886–898. doi:doi:10.3390/en3040886.

Jiang, Y., Lu, M., Liu, S., Bao, C., and Liang, G. (2018). Deactivation by HCl of CeO2–MoO3/TiO2 catalyst for selective catalytic reduction of NO with NH3. 8, 17677–17684. doi:10.1039/c8ra00280k.

Jung, Y. G., Choi, S. C., Oh, C. S., and Paik, U. G. (1997). Residual stress and thermal properties of zirconia/metal (nickel, stainless steel 304) functionally graded materials fabricated by hot pressing. *J. Mater. Sci.* 32, 3841–3850. doi:10.1023/A:1018640126751.

Kim, U. J., Eom, S. H., and Wada, M. (2010). Thermal decomposition of native cellulose: Influence on crystallite size. *Polym. Degrad. Stab.* 95, 778–781. doi:10.1016/j.polymdegradstab.2010.02.009.

Kiran, N., Ekinci, E., and Snape, C. . (2000). Recyling of plastic wastes via pyrolysis. *Resour. Conserv. Recycl.* 29, 273–283. doi:10.1016/S0921-3449(00)00052-5.

Klinger, J., Bar-Ziv, E., and Shonnard, D. (2013). Kinetic study of aspen during torrefaction. *J. Anal. Appl. Pyrolysis* 104, 146–152. doi:10.1016/j.jaap.2013.08.010.

Klinger, J., Bar-Ziv, E., and Shonnard, D. (2015). Unified kinetic model for torrefaction-pyrolysis. *Fuel Process. Technol.* 138, 175–183. doi:10.1016/j.fuproc.2015.05.010.

Klinger, J., Bar-Ziv, E., Shonnard, D., Westover, T., and Emerson, R. (2016). Predicting Properties of Gas and Solid Streams by Intrinsic Kinetics of Fast Pyrolysis of Wood. *Energy and Fuels* 30, 318–325. doi:10.1021/acs.energyfuels.5b01877.

Klinger, J., Klemetsrud, B., Bar-Ziv, E., and Shonnard, D. (2014). Temperature dependence of aspen torrefaction kinetics. *J. Anal. Appl. Pyrolysis* 110, 424–429. doi:10.1016/j.jaap.2014.10.008.

Kotchen, M. J., and Mansur, E. T. (2014). How stringent are the US EPA's proposed carbon pollution standards for new power plants? *Rev. Environ. Econ. Policy* 8, 290–306. doi:10.1093/reep/reu003.

Kumar, L., Koukoulas, A. A., Mani, S., and Satyavolu, J. (2017). Integrating torrefaction in the wood pellet industry: A critical review. *Energy and Fuels* 31, 37–54. doi:10.1021/acs.energyfuels.6b02803.

Lauer, D., Motell, E. L., Traficante, D. D., and Maciel, G. E. (1972). Carbon-13 Chemical Shifts in Monoalkyl Benzenes and Some Deuterio Analogs. *J. Am. Chem. Soc.* 94, 5335–5338. doi:10.1021/ja00770a032.

Lavrykov, S. A., and Ramarao, B. V. (2012). Thermal Properties of Copy Paper Sheets. *Dry. Technol.* 30, 297–311. doi:10.1080/07373937.2011.638148.

Lin, X., Zhang, Z., Wang, Q., and Sun, J. (2020). Interactions between biomass-derived components and polypropylene during wood–plastic composite pyrolysis. *Biomass Convers. Biorefinery*, 1–13. doi:10.1007/s13399-020-00861-4.

Love, G. D., Snape, C. E., and Jarvis, M. C. (1998). Comparision of Leaf and Stem Cell-Wall Components in Barley Straw by Solid-State 13C NMR. *Phytochemistry* 49, 1191–1194.

Lu, P., Huang, Q., Bourtsalas, A. T., Themelis, N. J., Chi, Y., and Yan, J. (2019). Review on fate of chlorine during thermal processing of solid wastes. *J. Environ. Sci. (China)* 78, 13–28. doi:10.1016/j.jes.2018.09.003.

Luppens, J. A. (2011). A critical review of published coal quality data from the southwestern part of the Powder River Basin, Wyoming. Reston, Virginia Available at: https://pubs.usgs.gov/of/2011/1148/pdf/ofr20111148_072111.pdf.

Ma, Y., Hummel, M., Määttänen, M., Särkilahti, A., Harlin, A., and Sixta, H. (2016). Upcycling of waste paper and cardboard to textiles. *Green Chem.* 18, 858–866. doi:10.1039/c5gc01679g.

Mahdavi Nejad, A. (2019). Thermal Analysis of Paper Board Packaging with Phase Change Material: A Numerical Study. *J. Packag. Technol. Res.* 3, 181–192. doi:10.1007/s41783-019-00060-1.

Mamleev, V., Bourbigot, S., and Yvon, J. (2007). Kinetic analysis of the thermal decomposition of cellulose: The main step of mass loss. *J. Anal. Appl. Pyrolysis* 80, 151–165. doi:10.1016/j.jaap.2007.01.013.

Maunu, S. L. (2009). "13C CPMAS NMR Studies of Wood, Cellulose Fibers, and Derivatives," in *Characterization of Lignocellulosic Materials*, eds. Q. Thomas and Q. Hu (Hoboken: Blackwell), 227–248. doi:https://doi.org/10.1002/9781444305425.ch13.

Mayo, W. D., Miller, A. F., and Hannah, W. R. (2004). "Course Notes on the Interpretation of Infrared and Raman Spectra," in *Course Notes on the Interpretation of Infrared and Raman Spectra* (John Wiley & Sons), 33–72. doi:10.1002/0471690082.

McCabe, J. G. (2014). Addressing Biogenic Carbon Dioxide Emissions from Stationary Sources. United States Enviromental Protection Agency. Washington, D.C Available at: https://archive.epa.gov/epa/sites/production/files/2016-08/documents/biogenic-co2-emissions-memo-111914.pdf.

More recycling raises average energy content of waste used to generate electricity (2012). Available at: https://www.eia.gov/todayinenergy/detail.php?id=8010 [Accessed January 19, 2020].

Moreira, L. R. S., and Filho, E. X. F. (2008). An overview of mannan structure and mannan-degrading enzyme systems. *Appl. Microbiol. Biotechnol.* 79, 165–178. doi:10.1007/s00253-008-1423-4.

National Emission Standards for Hazardous Air Pollutants (NESHAP) (2017). Available at: https://www.epa.gov/stationary-sources-air-pollution/national-emission-standards-hazardous-air-pollutants-neshap-9 [Accessed July 29, 2019].

National Overview: Facts and Figures on Materials, Wastes and Recycling (2017). Available at: https://www.epa.gov/facts-and-figures-about-materials-waste-and-recycling/national-overview-facts-and-figures-materials#Landfilling [Accessed January 19, 2020].

Ni, Y., Zhang, H., Fan, S., Zhang, X., Zhang, Q., and Chen, J. (2009). Emissions of PCDD/Fs from municipal solid waste incinerators in China. *Chemosphere* 75, 1153–1158. doi:10.1016/j.chemosphere.2009.02.051.

Olajire, A., Zhi, C., Hanson, S., and Wai, C. (2014). Thermogravimetric analysis of the pyrolysis characteristics and kinetics of plastics and biomass blends. 128, 471–481. doi:10.1016/j.fuproc.2014.08.010.

Oyedun, A. O., Gebreegziabher, T., Ng, D. K. S., and Hui, C. W. (2014). Mixed-waste pyrolysis of biomass and plastics waste - A modelling approach to reduce energy usage. *Energy* 75, 127–135. doi:10.1016/j.energy.2014.05.063.

Pandey, K. K. (1999). A Study of Chemical Structure of Soft and Hardwood and Wood Polymers by FTIR Spectroscopy. *J. Appl. Polym. Sci.* 71, 1969–1975. doi:10.1002/(sici)1097-4628(19990321)71:12<1969::aid-app6>3.0.co;2-d.

Papadopoulou, M. P., Karatzas, G. P., and Bougioukou, G. G. (2007). Numerical modelling of the environmental impact of landfill leachate leakage on groundwater quality - A field application. *Environ. Model. Assess.* 12, 43–54. doi:10.1007/s10666-006-9050-x.

Pasangulapati, V., Ramachandriya, K. D., Kumar, A., Wilkins, M. R., Jones, C. L., and Huhnke, R. L. (2012). Effects of cellulose, hemicellulose and lignin on thermochemical conversion characteristics of the selected biomass. *Bioresour. Technol.* 114, 663–669. doi:10.1016/j.biortech.2012.03.036.

Patkar, S. N., and Panzade, P. D. (2016). Fast and efficient method for molecular weight analysis of cellulose pulp, in-process and finished product. *Anal. Methods* 8, 3210–3215. doi:10.1039/c5ay03012a.

Peterson, J. D., Vyazovkin, S., and Wight, C. A. (2001). Kinetics of the thermal and thermo-oxidative degradation of polystyrene, polyethylene and poly(propylene). *Macromol. Chem. Phys.* 202, 775–784. doi:10.1002/1521-3935(20010301)202:6<775::AID-MACP775>3.0.CO;2-G.

Petre, A. L., Budrugeac, P., and Segal, E. (1999). Thermal Degradation of Polyvinyl Chloride. *J. Therm. Anal. Calorim.* 56, 1065–1070. doi:10.1023/A:1010136507843.

Pines, A., Gibby, M. G., and Waugh, J. S. (1972). Proton-enhanced nuclear induction spectroscopy. a method for high resolution nmr of dilute spins in solids. *J. Chem. Phys.* 56, 1776–1777. doi:10.1063/1.1677439.

Radics, R. I., Gonzalez, R., Bilek, E. M., and Kelley, S. S. (2017). Systematic review of torrefied wood economics. *BioResources* 12, 6868–6884. doi:10.15376/biores.12.3.6868-6884.

Raveendran, K. (1996). Pyrolysis characteristics of biomass and biomass components. *Fuel* 75, 987–998. doi:10.1016/0016-2361(96)00030-0.

Risby, T. H., Yergey, J. A., and Scocca, J. J. (1982). Linear Programmed Thermal Degradation Mass Spectrometry of Polystyrene and Poly(vinyl chloride). *Anal. Chem.* 54, 2228–2233. doi:10.1021/ac00250a022.

Ritchie and Roser (2018). *Plastic Pollution - Our World in Data*. Available at: https://ourworldindata.org/plastic-pollution?utm_source=newsletter&utm_medium=email&utm_campaign=sendto_newslettertest&stream=top [Accessed January 23, 2020].

Rodrigues, J., Graça, J., and Pereira, H. (2001). Influence of tree eccentric growth on syringyl/guaiacyl ratio in Eucalyptus globulus wood lignin assessed by analytical pyrolysis. *J. Anal. Appl. Pyrolysis* 58–59, 481–489. doi:10.1016/S0165-2370(00)00121-2.

Rojas, A., and Orozco, E. (2003). Measurement of the enthalpies of vaporization and sublimation of solids aromatic hydrocarbons by differential scanning calorimetry. 405, 93–107. doi:10.1016/S0040-6031(03)00139-4.

Salvilla, J. N. V., Ofrasio, B. I. G., Rollon, A. P., Manegdeg, F. G., Abarca, R. R. M., and de Luna, M. D. G. (2020). Synergistic co-pyrolysıs of polyolefin plastics with wood and agricultural wastes for biofuel production. *Appl. Energy* 279, 115668. doi:10.1016/j.apenergy.2020.115668.

Sánchez-Jiménez, P. E., Perejón, A., Criado, J. M., Diánez, M. J., and Pérez-Maqueda, L. A. (2010). Kinetic model for thermal dehydrochlorination of poly(vinyl chloride). *Polymer (Guildf).* 51, 3998–4007. doi:10.1016/J.POLYMER.2010.06.020.

Schaefer, J., Stejskal, E. O., and Buchdahl, R. (1975). High-Resolution Carbon-13 Nuclear Magnetic Resonance Study of Some Solid, Glassy Polymers. *Macromolecules* 8, 291–296. doi:10.1021/ma60045a010.

Scheirs, J., Camino, G., and Tumiatti, W. (2001). Overview of water evolution during the thermal degradation of cellulose. *Eur. Polym. J.* 37, 933–942. doi:10.1016/S0014-3057(00)00211-1.

Sharypov, V., Beregovtsova, N., Kuznetsov, B., Baryshnikov, S., Marin, N., and Weber, J. (2003). Light Hydrocarbon Liquids Production by Co-Pyrolysis of Polypropylene and Hydrolytic Lignin. *Chem. Sustain. Dev.* 11, 427–434.

Shen, D. K., Gu, S., and Bridgwater, A. V. (2010). Study on the pyrolytic behaviour of xylan-based hemicellulose using TG-FTIR and Py-GC-FTIR. *J. Anal. Appl. Pyrolysis* 87, 199–206. doi:10.1016/j.jaap.2009.12.001.

Shenoy, A. V. (1999). "Rheology of Filled Polymer Systems," in (Springer Science&Business Media Dordrecht), 54–111.

Sluiter, J., and Sluiter, A. (2011). Summative Mass Closure: Laboratory Analytical Procedure (LAP) Review and Integration: Feedstocks; Issue Date: April 2010; Revision Date: July 2011 (Version 07-08-2011). Available at: http://www.nrel.gov/biomass/analytical_procedures.html [Accessed October 16, 2020].

Solmaz, R., Kardaş, G., Çulha, M., Yazıcı, B., and Erbil, M. (2008). Investigation of adsorption and inhibitive effect of 2-mercaptothiazoline on corrosion of mild steel in hydrochloric acid media. *Electrochim. Acta* 53, 5941–5952. doi:10.1016/J.ELECTACTA.2008.03.055.

Subramanian, P. M. (2000). Plastics recycling and waste management in the US. *Resour. Conserv. Recycl.* 28, 253–263. doi:10.1016/S0921-3449(99)00049-X.

Tian, H. H., & Ouyang, N. (2003). Preliminary Investigaton on Dioxing Emission from MSW Incinerators. *Environ. Chem.* 22, 255–258.

Tillet, G., Boutevin, B., and Ameduri, B. (2011). Chemical reactions of polymer crosslinking and post-crosslinking at room and medium temperature. *Prog. Polym. Sci.* 36, 191–217. doi:10.1016/j.progpolymsci.2010.08.003.Utschick, H., Ritz, M., Mallon, H.-J., Arnold, M., Ludwig, W., Kettrup, A., et al. (1994). Investigations on the thermal degradation of post-chlorinated polyvinyl chloride. *Thermochim. Acta* 234, 139–151. doi:10.1016/0040-6031(94)85140-9.

Várhegyi, G., Antal, M. J., Jakab, E., and Szabó, P. (1997). Kinetic modeling of biomass pyrolysis. *J. Anal. Appl. Pyrolysis* 42, 73–87. doi:10.1016/S0165-2370(96)00971-0.

Vikelsoe, J., Nielsen, P., Blinksbjerg, P., Madsen, H., & Manscher, O. (1990). Significance of chlorine sources for the generation of dioxins during incineration of MSW. *Organohalogen Compd.* 3, 193–196.

Volpe, R., Zabaniotou, A. A., and Skoulou, V. (2018). Synergistic Effects between Lignin and Cellulose during Pyrolysis of Agricultural Waste. doi:10.1021/acs.energyfuels.8b00767.

Wakeman, I. B., and Johnson, H. R. (1978). Vinyl chloride formation from the thermal degradation of poly(vinyl chloride). *Polym. Eng. Sci.* 18, 404–407. doi:10.1002/pen.760180512.

Wang, X., Sotoudehniakarani, F., Yu, Z., Morrell, J. J., Cappellazzi, J., and McDonald, A. G. (2019). Evaluation of corrugated cardboard biochar as reinforcing fiber on properties, biodegradability and weatherability of wood-plastic composites. *Polym. Degrad. Stab.* 168, 108955. doi:10.1016/j.polymdegradstab.2019.108955.

Wang, Z., Pecha, B., Westerhof, R. J. M., Kersten, S. R. A., Li, C. Z., McDonald, A. G., et al. (2014). Effect of cellulose crystallinity on solid/liquid phase reactions responsible for the formation of carbonaceous residues during pyrolysis. *Ind. Eng. Chem. Res.* 53, 2940–2955. doi:10.1021/ie4014259.

Wei, L., McDonald, A. G., Freitag, C., and Morrell, J. J. (2013). Effects of wood fiber esterification on properties, weatherability and biodurability of wood plastic composites. *Polym. Degrad. Stab.* 98, 1348–1361. doi:10.1016/j.polymdegradstab.2013.03.027.

What is U.S. electricity generation by energy source? (2020). Available at: https://www.eia.gov/tools/faqs/faq.php?id=427&t=3 [Accessed April 29, 2020].

Williams, C. L., Westover, T. L., Petkovic, L. M., Matthews, A. C., Stevens, D. M., and Nelson, K. R. (2017). Determining Thermal Transport Properties for Softwoods under Pyrolysis Conditions. *ACS Sustain. Chem. Eng.* 5, 1019–1025. doi:10.1021/acssuschemeng.6b02326.

Wimberley, J. W., Carel, A. B., and Cabbiness Conoco Inc., D. K. (1982). Automated Method for Measuring the Thermal Degradation of Polyvinyl Chloride. *Anal. Lett.* 15, 89–100. doi:10.1080/00032718208064366.

Wu, S., Shen, D., Hu, J., Zhang, H., and Xiao, R. (2016). Biomass and Bioenergy Cellulose-lignin interactions during fast pyrolysis with different temperatures and mixing methods. 90. doi:10.1016/j.biombioe.2016.04.012.

Xu, Z., Albrecht, J. W., Kolapkar, S. S., Zinchik, S., and Bar-Ziv, E. (2020a). Chlorine Removal from U.S. Solid Waste Blends through Torrefaction. *Appl. Sci.* 10, 3337. doi:10.3390/app10093337.

Xu, Z., Kolapkar, S., Zinchik, S., Bar-Ziv, E., and Mcdonald, A. (2020b). Comprehensive Kinetic Study of Thermal Degradation of Polyvinylchloride (PVC). *Polym. Degrad. Stab.* 176. doi:doi.org/10.1016/j.polymdegradstab.2020.109148.

Xu, Z., Zinchik, S., Kolapkar, S., Bar-ziv, E., Hansen, T., and Conn, D. (2018). Properties of Torrefied U . S . Waste Blends. *Front. Energy Res.* 6, 65. doi:doi.org/10.3389/fenrg.2018.00065.

Xue, Y., and Bai, X. (2018). Synergistic enhancement of product quality through fast co-pyrolysis of acid pretreated biomass and waste plastic. *Energy Convers. Manag.* 164, 629–638. doi:10.1016/j.enconman.2018.03.036.

Yang, H., Liu, M., Chen, Y., Xin, S., Zhang, X., Wang, X., et al. (2020). Vapor – solid interaction among cellulose , hemicellulose and lignin. *Fuel* 263. doi:10.1016/j.fuel.2019.116681.

Yang, H., Yan, R., Chen, H., Zheng, C., Lee, D. H., Uni, V., et al. (2006). In-Depth Investigation of Biomass Pyrolysis Based on Three Major Components : Hemicellulose , Cellulose and Lignin. 388–393. doi:10.1021/ef0580117.

Yeo, J. Y., Chin, B. L. F., Tan, J. K., and Loh, Y. S. (2019). Comparative studies on the pyrolysis of cellulose, hemicellulose, and lignin based on combined kinetics. *J. Energy Inst.* 92, 27–37. doi:10.1016/j.joei.2017.12.003.

Yin, R.-H., Zhang, R.-Z., and Luo, Y.-H. (2016). The Effect of Utilizing Homogeneous Conversion to Control the Formation of Chlorinated Hydrocarbons During PVC Pyrolysis. 35, 1012–1019. doi:10.1002/ep.12313.

Yu, J., Sun, L., Ma, C., Qiao, Y., and Yao, H. (2016). Thermal degradation of PVC: A review. *Waste Manag.* 48, 300–314. doi:10.1016/j.wasman.2015.11.041.

Yuan, H., Wang, Y., Kobayashi, N., Zhao, D., and Xing, S. (2015). Study of Fuel Properties of Torrefied Municipal Solid Waste. *Energy and Fuels* 29, 4976–4980. doi:10.1021/ef502277u.

Zhang, J., Choi, Y. S., Yoo, C. G., Kim, T. H., Brown, R. C., and Shanks, B. H. (2015). Cellulose−Hemicellulose and Cellulose−Lignin Interactions during Fast Pyrolysis. *ACS Sustain. Chem. Eng.* 3, 293–301. doi:doi.org/10.1021/sc500664h.

Zhang, X., Lei, H., Zhu, L., Zhu, X., Qian, M., Yadavalli, G., et al. (2016). Bioresource Technology Thermal behavior and kinetic study for catalytic co-pyrolysis of

biomass with plastics. *Bioresour. Technol.* 220, 233–238. doi:10.1016/j.biortech.2016.08.068.

Zhao, J., Xiuwen, W., Hu, J., Liu, Q., Shen, D., and Xiao, R. (2014). Thermal degradation of softwood lignin and hardwood lignin by TG-FTIR and Py-GC/MS. *Polym. Degrad. Stab.* 108, 133–138. doi:10.1016/j.polymdegradstab.2014.06.006.

Zhao, S., Liu, M., Zhao, L., and Zhu, L. (2018). Influence of Interactions among Three Biomass Components on the Pyrolysis Behavior. *Ind. Eng. Chem. Res.* 57, 5241–5249. doi:10.1021/acs.iecr.8b00593.

Zhou, H., Long, Y., Meng, A., Chen, S., Li, Q., and Zhang, Y. (2015). A novel method for kinetics analysis of pyrolysis of hemicellulose, cellulose, and lignin in TGA and macro-TGA. *RSC Adv.* 5, 26509–26516. doi:10.1039/c5ra02715b.

Zhou, L., Wang, Y., Huang, Q., and Cai, J. (2006). Thermogravimetric characteristics and kinetic of plastic and biomass blends co-pyrolysis. *Fuel Process. Technol.* 87, 963–969. doi:10.1016/j.fuproc.2006.07.002.

Zinchik, S., Xu, Z., Kolapkar, S. S., Bar-Ziv, E., and McDonald, A. G. (2020). Properties of pellets of torrefied U.S. waste blends. *Waste Manag.* 104, 130–138. doi:10.1016/j.wasman.2020.01.009.

6 Comprehensive Kinetic Study of Thermal Degradation of Polyvinylchloride (PVC)

This section is based on the following peer-reviewed paper:

Z. Xu, SS. Kolapkar, S. Zinchik, E. Bar-Ziv, AG. McDonald. 2020. Comprehensive kinetic study of thermal degradation of polyvinylchloride (PVC). Polymer Degradation and Stability, 109148.

doi.org/10.1016/j.polymdegradstab.2020.109148

6.1 Abstract

The plastic waste accumulation has been increasing and a solution other than landfilling is required. Due to the high cost of recycling, thermal treatment could be an option. However, the existence of polyvinyl chloride (PVC) would release hydrochloric acid which would cause emission problems as well as damage to the reactor systems. The thermal degradation of PVC has been studied over the years. However, the mechanism of the PVC thermal degradation is not fully developed. Specifically, the mechanism of the PVC thermal degradation at medium temperatures, which is more practical for industries, is still lacking. A degradation temperature of 300^{o}C was used to study the dehydrochlorination behavior of PVC. A rather comprehensive mechanism with four consecutive reactions has been developed based on the micro-pyrolysis experiments and has been validated and proved by predicting the mass loss, chlorine content, heat content and elemental composition with high precision experimental data in different reactors with/without heat transfer coupling.

6.2 Introduction

There is an unprecedented accumulation of plastic wastes that calls for an urgent need to find solutions other than disposal in landfills (Ritchie and Roser, 2018). As recycling is a costly option (Subramanian, 2000), other methods for upcycling into products are being sought (Kiran et al., 2000). In most applications that require thermal treatment of the plastic wastes, such as waste-to-energy or waste-to-chemical, hydrochloric acid (HCl) is released from chlorinated compound (mostly polyvinyl chloride - PVC) in the waste materials (Anuar Sharuddin et al., 2016). For these energy and chemical applications, hydrochloric acid must be removed, or reduced drastically as it is corrosive (Solmaz et al., 2008), can degrade catalysts (Jiang et al., 2018), and its emission is strictly controlled by EPA (National Emission Standards for Hazardous Air Pollutants (NESHAP), 2017). As the source of chlorine is mostly from PVC, understanding of its behavior at high temperatures is rather critical for these applications. The current paper presents a comprehensive kinetic study at 300^{o}C, including a plausible mechanism, for the thermal degradation of PVC.

In the current study, a short review will be provided on kinetic mechanisms and modeling of PVC thermal degradation. Thermal degradation of PVC has been studied extensively as early as the sixties by Braun et al. (Braun and Thallnaier, 1966). Wakeman and Johnson were probably the first to observe gaseous species such as aromatic and chlorinated

compounds, which led the way the various PVC degradation mechanisms were proposed later (Wakeman and Johnson, 1978). Wimberley et al., carried out low temperature degradation of PVC (120-150^{o}C) by thermogravimetry with samples collected at specific time intervals and later analysed by gas chromatography-mass spectrometry (GC-MS) (Wimberley et al., 1982). They focused on the development of methods for analysis of HCl which was the primary product in the first stage of the degradation. Due to the low temperatures, each experiment required several hours of reaction time.

Risby et al., were the first to observe the production of polyaromatic compounds in the gas phase (in addition to HCl) from thermal degradation of PVC (Risby et al., 1982). They correlated the production of these aromatic compounds with the temperature at which the degradation process was studied. This important study showed a plausible chemical mechanism of degradation of PVC. Anders and Zimmermann, observed double bond formation during the thermal degradation of PVC and concluded that this depends strongly on the chemical structure of the parent molecule (Anders and Zimmermann, 1987). Utschick et al., continued the investigation of PVC thermal degradation using thermogravimetry, mass-spectrometry, and pyrolysis gas chromatography and provided insights into the gas composition and further observing HCl, aromatic and chlorinated compounds (Utschick et al., 1994). This study continued to provide insights into expected gas composition.

Petre et al., studied the thermal degradation of PVC by thermogravimetry and observed two regions, first attributed to HCl release and the second to aromatics (mostly benzene) (Petre et al., 1999). They proposed a simple two-step kinetic model and fitted the data to yield pre-exponential factor as well as activation energies. Due to lack of gaseous composition, kinetic insights are rather limited from this study. Marongiu et al., made the first attempt to develop a very comprehensive kinetic mechanism that comprises 40 solid and gaseous species, both stable molecules and radicals, and 250 reactions (Marongiu et al., 2003). The study used thermogravimetric analysis as the source of experimental data for model validation. The mechanism proposed include production of HCl, double carbon bonds, and all the way to polyaromatic structures. The lack of experimental data on the gaseous products in this study limits the insight that one can gain from such a detailed mechanism. However, it provides an excellent start that provides guidance on compounds that should be looked for in other experimental studies.

Sanchez-Jimenez et al., studied PVC degradation using a custom-built thermogravimetric analyzer, on two different molecular weight (MW) (80,000 and 233,000 g/mol) PVC samples, where mass loss was measured at various temperatures (Sánchez-Jiménez et al., 2010). This study included a model that comprised both mass and heat transports and a one-chemical reaction mechanism (including pre-exponential constant, activation energy, and a partial order). Experiments were done at (i) different heating rates and (ii) isothermal conditions. Through a parameter fitting procedure, values for the above kinetic model parameters were determined. This study provides useful information regarding the mechanism; however, it lacks insight into the product distribution and its dynamic behavior.

Yin et al., carried out pyrolysis of PVC rods in a temperature-controlled reactor equipped with GC-MS on-line analysis. They found many gaseous species, starting from H_2, light hydrocarbons (such as CH_4, C_2H_4, and C_3H_6), polyaromatics, chlorinated hydrocarbons and aromatics (Yin et al., 2016). This study shed light into the chemical composition however, no kinetic information can be drawn from the results. A recent review by Yu et al., summarized the knowledge on the thermal degradation of PVC (Yu et al., 2016).

From the above reviews, it can be seen that further elucidation of the degradation mechanism of PVC is required, specifically transient data for the gaseous products as well as the remaining solid, at various temperatures. From such data, one may develop a comprehensive kinetic model for PVC degradation. In this study, we carried out PVC degradation in various reactors (reactors with no heat transport limitation, all the way to reactors with strongly coupled heat-transport-reaction). Gas species as well as the properties of the remaining solid were characterized. This study is limited to 300^{o}C, however, it enabled us to develop a rather comprehensive mechanism that showed a predictive power of all measured properties in all reactors used. The temperature selected here enabled a measurable PVC degradation rate, that can be of practical importance in industrial systems for chlorine removal. However, higher temperature experiments are planned in the near future.

6.3 Materials and Methods

The PVC resin used in the experiments was from Shintech Inc. (grade SE-950, density = 1.4 g/cm^3). The sample was used without any modification.

In this study, three types of experiments (detailed following) for kinetic investigation of PVC thermal degradation were carried out as follows:

1. Micro-pyrolysis using 50-100 µg sample, where the gas stream were measured continuously.
2. In-house tubular reactor with 0.25 mm thick wall and 2.5 g of material holding capacity, where mass loss, heat and chlorine contents were measured at the end of each run.
3. Thermogravimetric measurements under isothermal conditions with heating rates of 200^{o}C/min, using 5 mg sample, where weight were measured continuously.

6.3.1 Micro-pyrolysis

Analytical pyrolysis on PVC samples (50-100 µg) was performed at 300°C using a Pyrojector II unit (SGE Analytical Science) coupled to a GC-MS (Focus-ISQ, Thermo Scientific). Helium was used as the carrier gas at 1.2 mL/min. The products were separated either on (i) ZB-5 capillary column (5 m × 0.25 mm Ø, Phenomenex) held isothermally at 300°C (30 min) for kinetic studies or (ii) ZB-5 capillary column (30 m × 0.25 mm Ø, Phenomenex) from 50 (1 min) to 250°C (10 min) at 5°C min^{-1} and the eluted compounds were identified by their mass spectra, authentic standards, and NIST 2017 library matching. Figure 6.1 showed the schematics of the micro-pyrolysis-GCMS system. The results measured by the mass spectrometer are proportional to the rates at which the species are

produced. According to Lattimer and Kroenke, secondary reactions of the volatiles produced during pyrolysis are negligible in our conditions (Lattimer and Kroenke, 1982). For instance, the PVC pyrolysis experiment conducted by Lattimer and Kroenke was done at 600 °C with ~40 µg of PVC sample, and it was found that the secondary reaction was insignificant. Since the current study used similar amount of sample with much lower temperature, it can be concluded that the secondary reactions in our study are negligible.

To calibrate the measurements, 5 µl aliquots of HCl, benzene, and naphthalene were headspace injected in the micro-pyrolysis reactor where the PVC samples was placed, and the mass spectrum signals were measured and are shown in Figure 6.2: HCl at m/z = 35-38, Benzene at m/z = 78, and naphthalene at m/z = 128 are shown. As observed, the signals appear at around 8.5 s after the injection and have widths of about 2.3 s. The signals can be perceived as the transfer function that convolute the actual signals of the various species. In other words, when the gas species reach the mass spectrometer detector they are convoluted. It was not possible to inject an aliquot of anthracene in the headspace since the vaporization temperature is 225°C (Rojas and Orozco, 2003). As HCl, benzene and naphthalene have similar results, it is appropriate to assume a similar behavior of gas anthracene to that of gas naphthalene.

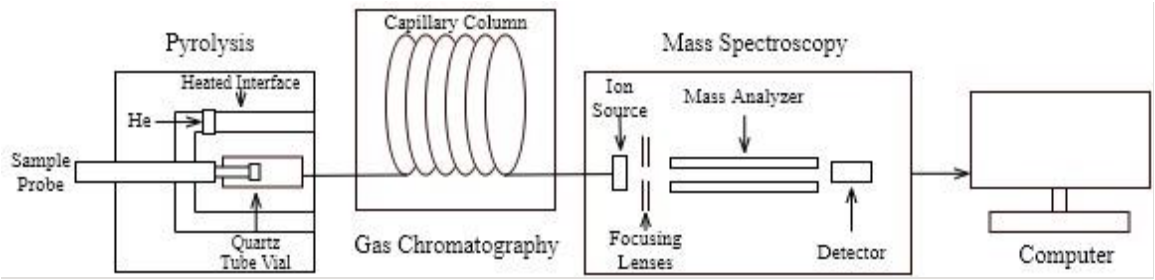

Figure 6.1. Schematics of micro-pyrolysis-GCMS system.

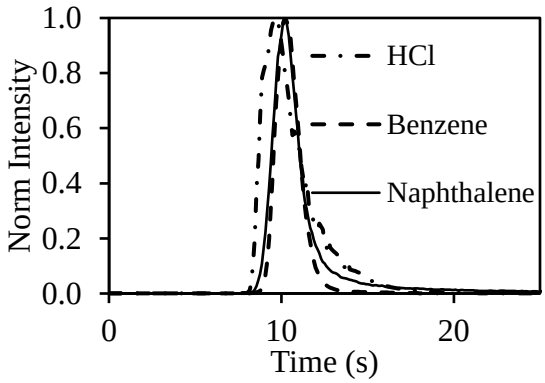

Figure 6.2. Normalized intensity of headspace injected HCl, benzene and naphthalene.

6.3.2 Thermogravimetric Analysis

Thermogravimetric analysis (TGA) was conducted using a Perkin Elmer TGA 7 instrument. PVC samples (5-6 mg) was analyzed at from 30°C to 300°C with the heating

rate of 200°C/min and remained isothermal for 60 min in a nitrogen atmosphere (30 mL/min). The results were analyzed by the Pyris v13 software (Perkin Elmer). The mass loss up to 300°C was negligible change and therefore it was decided to set reaction time to zero when the temperature reached the set temperature.

6.3.3 In-house Tubular Reactor

Figure 6.3 is the schematics of the torrefaction system. The PVC sample was placed in the bottom of a stainless-steel tube 127 mm long, 9.5 mm OD and 0.25 mm wall thickness. The tube was sealed by a cap at the bottom and fiber ceramic was filled inside the cap to avoid any PVC sample falling into the cap, which would create non-uniform heat transfer rate. The tube reactor was connected to another stainless-steel pipe with the same diameter, and the exhaust gas would be transferred to the furnace. A clamp was used to hold the instrument to ensure that the reactor stayed in the middle of the furnace.

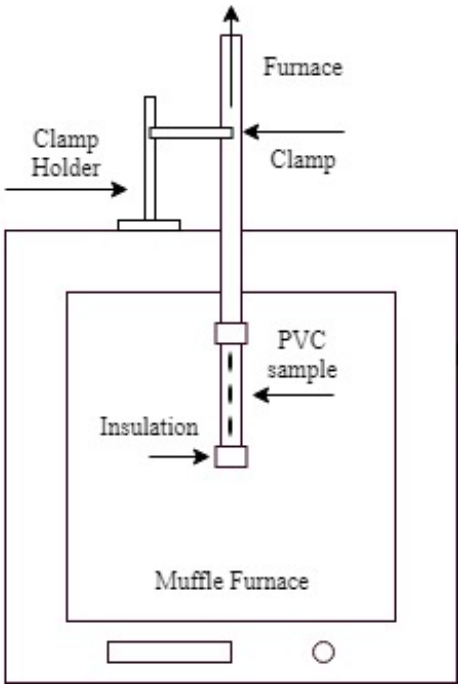

Figure 6.3. Schematics of the torrefaction system.

A PVC sample (2.5 g) was inserted in the tubular reactor as described above. The reactor with the sample was weighed. The reactor was placed in the furnace at 300°C for a given time. The reactor was then removed from the furnace and cooled quickly by air until it reached ambient temperature. The reactor with sample was weighed again and from the weight difference the mass loss was calculated. The experiment was repeated in 1 min time intervals for up to 50 min and the mass loss was plotted vs. time. As noted, the temperature in this tubular reactor was not measured, however, the temperature from heat transfer considerations as described in section 6.4.2 was calculated.

6.3.4 Heat Content and Chlorine Content

Heat content of the samples was measured by bomb calorimeter (Parr 6100) according to ASTM standard D5865-04. For each measurement, a crucible containing the sample (1.0 g) was placed into a bomb filled with oxygen (~400 psi).

Chlorine content was measured according to ASTM standard D4208-18. Torrefied PVC sample (1.0 g) was combusted in the bomb calorimeter, as described above, and 5 ml of 2% Na_2CO_3 was added to capture the HCl. After the combustion, the vessel was opened slowly (the release of gas requires no less than 2 min), rinsed thoroughly several times with distilled water totally ~90 mL The chloride content of the aqueous solution was measured using an ion meter (Oakton ion 700) with chloride ion-selective electrode. The electrode was calibrated with 1000 ppm chloride standard solution that was serially diluted (100 ppm and 10 ppm).

6.3.5 C/H/Cl Elemental Composition Analysis

The C/H elemental composition was determined by a Costech ECS 4010 CHNSO Analyzer. The sample was placed in a tin capsule, weighed and dropped into the combustion reactor of the Analyzer, prior to the flow of oxygen (in excess). The sample was combusted at 1700^{o}C to 1800^{o}C and helium was used to carry the CO_2 and H_2O produced during the combustion. The extra oxygen was absorbed by the copper reduction column. The gases flown through a GC column and are detected by the Thermoconductivity Detector (TCD). The TCD generates a signal, which is proportional to the amount of element in the sample, consequently, carbon and hydrogen contents were determined. As PVC has only C/H/Cl, chlorine was determined by subtraction.

6.4 Results and Discussion

6.4.1 Micro-pyrolysis Measurements

The PVC sample was micro-pyrolyzed at 300^{o}C with heating time ~ 1 s and the products were analyzed by GC-MS (ramped and isothermal runs). The identity of the PVC pyrolysis products was determined from the ramped GC-MS runs where full mass spectra for each compound was obtained (data not shown). From the averaged mass spectrum (Figure 6.4) of the isothermal experiment, the following species could be observed temporally: HCl (m/z 35-38), benzene (m/z 78), naphthalene (m/z 128), and anthracene (m/z 178). These products were also found by other researchers to be produced directly during the degradation of PVC as part of aromatic ring formation due to generation of consecutive double bonds (Risby et al., 1982; McNeill et al., 1995; Marongiu et al., 2003). Nitrogen (m/z 28) and oxygen (m/z 32) were also detected and due to trace air introduced when the sample was loaded into the pyrolysis-GC-MS system.

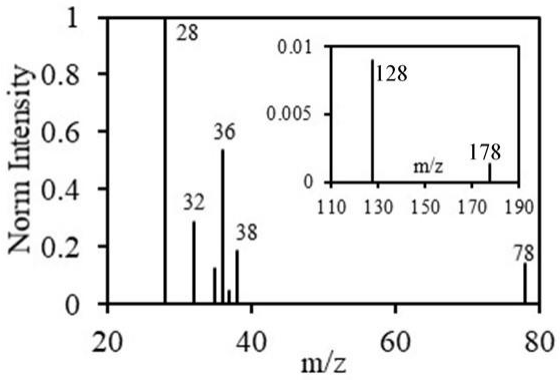

Figure 6.4. Mass spectral regions of m/z 0 to 80 and the inset shows m/z 110 to 190, for pyrolyzed PVC at 300°C.

From these spectra, we were able to obtain kinetic data for each of these species. In the next section we will present a kinetic model and a comparison to the experimental data obtained in this study.

6.4.2 Kinetic Modeling

Kinetic modeling is based on the micro-pyrolysis results. It should be noted that the gaseous products from this study span over many species. For the modeling, focus is on the main species, i.e., HCl, benzene, naphthalene, and anthracene. As noted in the Introduction section, this study is limited to 300°C (with residence times in the range of 500-1500 s). A four-consecutive reaction model was found to be sufficient for describing the PVC degradation as follows.

$$PVC(s) \xrightarrow{k_1} S_1(s) + \alpha_{1,1}HCl(g) + \alpha_{1,2}B(g) + \alpha_{1,3}N(g) + \alpha_{1,4}A(g) \qquad \text{Reaction 1}$$

$$S_1(s) \xrightarrow{k_2} S_2(s) + \alpha_{2,1}HCl(g) + \alpha_{2,2}B(g) + \alpha_{2,3}N(g) + \alpha_{2,4}A(g) \qquad \text{Reaction 2}$$

$$S_2(s) \xrightarrow{k_3} S_3(s) + \alpha_{3,1}HCl(g) + \alpha_{3,2}B(g) + \alpha_{3,3}N(g) + \alpha_{3,4}A(g) \qquad \text{Reaction 3}$$

$$S_3(s) \xrightarrow{k_4} S_4(s) + \alpha_{4,1}HCl(g) + \alpha_{4,2}B(g) + \alpha_{4,3}N(g) + \alpha_{4,4}A(g) \qquad \text{Reaction 4}$$

S_1, S_2, S_3 and S_4 are solid products of the PVC degradation; the symbols *s* and *g* denote, solid and gas phase, respectively; k_1, k_2, k_3 and k_4 are the respective reaction coefficients, and α-s are the stoichiometric parameters for the various products; *B*, *N*, and *A*, denote benzene, naphthalene, and anthracene, respectively.

The reaction rates for all species, both in the solid and gas phases, are:

$$\frac{dx_{HCl}}{dt} = \alpha_{1,1}x_{PVC} + \alpha_{2,1}x_{S_1} + \alpha_{3,1}x_{S_2} + \alpha_{4,1}x_{S_3} \quad (6.1)$$

$$\frac{dx_B}{dt} = \alpha_{1,2}x_{PVC} + \alpha_{2,2}x_{S_1} + \alpha_{3,2}x_{S_2} + \alpha_{4,2}x_{S_3} \quad (6.2)$$

$$\frac{dx_N}{dt} = \alpha_{1,3}x_{PVC} + \alpha_{2,3}x_{S_1} + \alpha_{3,3}x_{S_2} + \alpha_{4,3}x_{S_3} \quad (6.3)$$

$$\frac{dx_A}{dt} = \alpha_{1,4}x_{PVC} + \alpha_{2,4}x_{S_1} + \alpha_{3,4}x_{S_2} + \alpha_{4,4}x_{S_3} \quad (6.4)$$

Where $x_{PVC} = \frac{c_{PVC}}{c_{PVC,o}}$, and $x_{S_i} = \frac{c_{S_i}}{c_{PVC,o}}x_{S_2}$

$$\frac{dx_{PVC}}{dt} = k_1 x_{PVC} \quad (6.5)$$

$$\frac{dx_{S_1}}{dt} = k_1 x_{PVC} - k_2 x_{S_1} \quad (6.6)$$

$$\frac{dx_{S_2}}{dt} = k_2 x_{S_1} - k_3 x_{S_2} \quad (6.7)$$

$$\frac{dx_{S_3}}{dt} = k_3 x_{S_2} - k_4 x_{S_3} \quad (6.8)$$

$$\frac{dx_{S_4}}{dt} = k_4 x_{S_3} \quad (6.9)$$

As noted in Section 6.3.1, the measured signals are convoluted, therefore in order to compare them with the modeling results, the latter must be convoluted as well. Convolution is defined by Eq (6.10).

$$(f * g)(x) = \int_{-\infty}^{\infty} f(x) * g(\tau - x)\, d\tau \tag{6.10}$$

where, *f(x)* is the intensity of headspace injected as shown Figure 6.2 and *g(x)* represents the modeling results for each of the gas species. The final convolution for each species was used for the fitting process.

As noted above, the results generated by TCD are proportional to the rates at which the species are produced, therefore model reaction rates of the gas species Eqs (6.1-6.4) were fitted to the experimental data, by varying the *k*-s and the α-s, to obtain the best fit between the measured transients of HCl, benzene, naphthalene, and anthracene to the model results. This comparison is summarized in Figure 3.5, the values were normalized to the peak of HCl which was set at unity, showing an excellent fit between experiment and model.

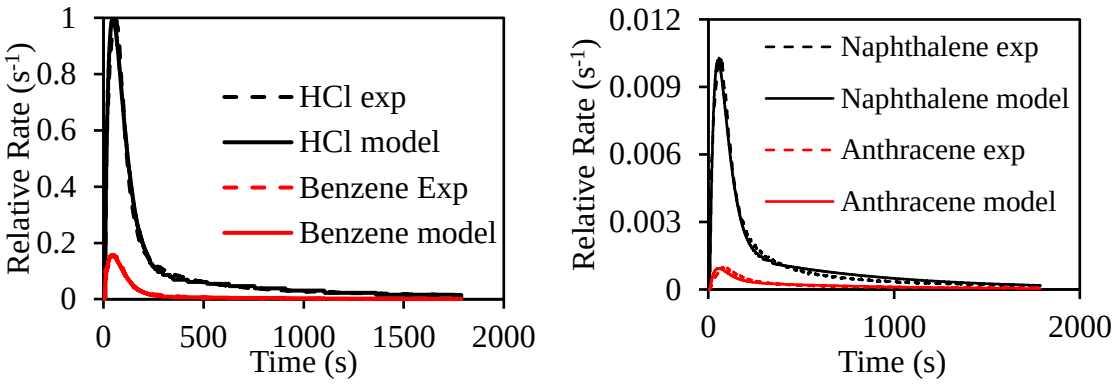

Figure 6.5. Experimental and modeling reaction rates for the production of HCl, benzene, naphthalene, and anthracene from pyrolysis of PVC at 300°C.

The parameters, the *k*-s and the α-s related to the fits shown in Figure 3.5, are summarized in Table 6.1, which includes a total of 20 parameters and the question is whether these values have any physical significance, or they are mere fitting parameters. To answer this question, one should indicate that each of the experimental transients (for HCl, benzene, naphthalene, and anthracene) included 17,190 data points, and a total of 68,670 data points for the 4 species, using the same values of the rate coefficients (k_1, k_2, k_3 and k_4) for the four reactions. Further, the measurements in the micro-pyrolysis reactor were repeated 4-5 times to show the reproducibility of the measurements (1-2%). With such a data set in comparison to the number of parameters fitted, one would expect that each of the obtained parameters indeed has a significance. To strengthen this claim, one should indicate that all parameters used here are scalars and do not appear in power or polynomial form. In Table 6.1, α are the respective stoichiometric parameters showing the relative stoichiometric parameters for the PVC degradation model at 300°C. The stoichiometric parameters for all the solid products were assumed to be unity and the summation of total HCl being produced was adjusted to unity, and the parameters for benzene, naphthalene, and anthracene are adjusted accordingly. It would require further study to obtain the actual stoichiometric

parameters. Note that for the first reaction, the α–s for naphthalene and anthracene were zero and for the fourth reaction, the α–s for HCl, benzene and naphthalene were zero. Which indicated that there were no naphthalene and anthracene in the first reaction and no HCl, benzene and naphthalene were produced in the fourth reaction.

Table 6.1. The reaction rate coefficients (k_1, k_2, k_3 and k_4) and the stoichiometric parameters for the PVC degradation reactions model at 300°C

Reaction	k (s^{-1})	α_{HCL}	α_B	α_N	α_A
1	0.24619	0.1225	0.0307	0	0
2	0.24615	0.8423	0.2254	0.0126	0.0011
3	0.0013	0.0352	0.0061	0.0007	0.0002
4	0.00098	0	0	0	4.24E-06
Sum	–	1.000	0.262	0.013	0.001

The parameters in Table 6.1 were used to calculate the solid materials produced during the reaction and presented the results in Figure 6.6, which depicts the normalized reaction rate transient of the solid material with the extent of the torrefaction. As is shown in the Figure 6.6. Normalized reaction rate of PVC, S1, S2, S3 and S4 torrefied at 300°C, PVC was fully decomposed after ~250 s and S_1 was decomposed after ~330 s. S_2 and S_3 require ~3000 s to fully decompose and S_4 did not reach its maximum even at 3000 s.

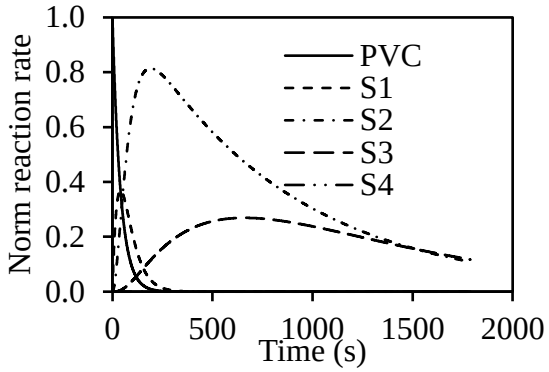

Figure 6.6. Normalized reaction rate of PVC, S1, S2, S3 and S4 torrefied at 300°C

6.4.3 Kinetic Model Validation

Since the heating rate of the TGA experiment was 200°C/min and the small characteristic size (~1 mm) of the sample. Using the heat transfer model developed in section below, we also found that the heat transfer issues in this case can be negligible. The developed kinetic model and parameters determined above were directly used for the TGA experiments. The mass loss, β, from the kinetic model can be determined by calculating the reaction rates of the solid products (*PVC*, S_1, S_2, S_3, and S_4), Eqs (6.5-6.9), by using the values of k_1, k_2, k_3 and k_4 (Table 6.1) and integrating over time, to yield:

$$\beta = 1 - \left(x_{PVC} + x_{S_1} + x_{S_2} + x_{S_3} + x_{S_4}\right) \tag{6.11}$$

Equation (6.11) provides the transient of the mass loss, however, a scalar is needed to adjust the values to the measured ones, as the parameters for the solid materials in Table 6.1 were normalized in reference to the first reaction. Figure 6.7 shows TGA results with model data, portraying a good fit between the two. This good fit provides a validation of the kinetic model developed above.

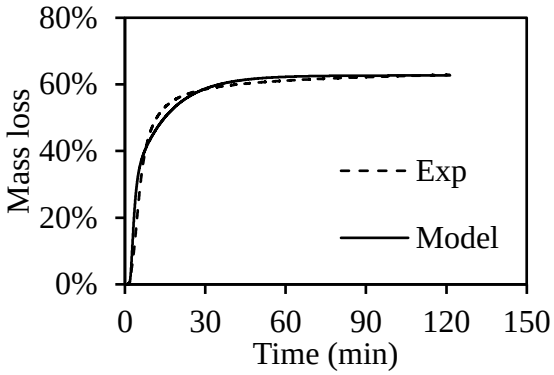

Figure 6.7. Mass loss vs. time in TGA experiments of PVC at 300°C, using a 5 mg sample.

6.4.4 Kinetic Model Application

The above kinetic model has been developed where there were no heat and mass transfer limitations. However, in the methods section 6.3.3 where 2.5 g of sample (with a characteristic length of 10 mm) were also used to study PVC degradation, this sample size would result in coupling between the chemical reaction with heat transfer processes. Therefore, heat transfer calculations for the experimental configuration (tubular reactor in the furnace) were used to study the kinetics for this sample size. From the heat transfer calculations, the temperature transient of the samples will be determined and the reaction rate would be modeled accordingly, using the above kinetic model. Success of predicting the experimental measurements from the coupled processes, with the large size samples, would provide further validation to this kinetic model, but most importantly to apply this kinetic model in other systems.

6.4.4.1 Heat Transfer Model

Figure 6.8 shows schematics of the tubular reactor and a sample within the reactor. The reactor and sample are placed in the center of the furnace and heat is transferred convectively from the furnace walls. Previous experience with this furnace has helped us develop the heat transfer model for this specific experimental setup (Xu et al., 2018).

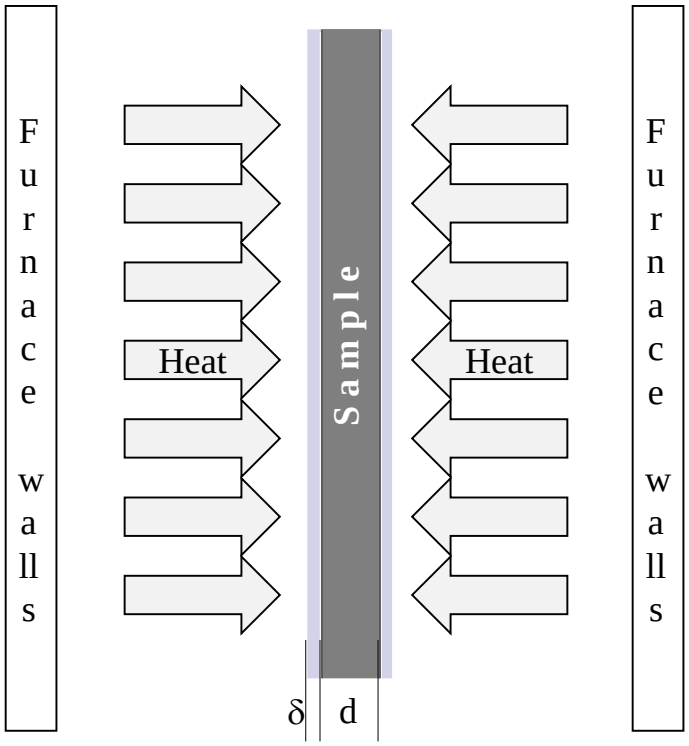

Figure 6.8. Schematics of the tubular reactor in the furnace.

The heat transfer regime can be determined from the values of the Biot number (*Bi*) and thermal Thiele modulus (*M*); *Bi* relates to the heating regime and *M* relates to the reaction propagation within the sample. *Bi* and *M* are defined by:

$$Bi = \frac{h}{\lambda / L_c} \tag{6.12}$$

$$M = \frac{R^{\dagger}}{\lambda / (c_p L_c^2)} \tag{6.13}$$

where h is the convective heat transfer coefficient, λ is the thermal conductivity of PVC, L_c is the characteristic length of the sample, $R^{\dagger}$ is the degradation reaction rate of PVC, c_p is heat capacity of the sample, and ρ is the density of the sample. It is noted that the analysis should include the stainless-steel shell as well as the sample. The parameters required for the stainless are easily obtained, whereas the properties for PVC depend on the porosity, molecular weight and temperature and therefore, its properties are estimate. The stainless-steel thermal conductivity (Jung et al., 1997) is two order of magnitudes larger than that of PVC (De Carvalho et al., 1996), hence it shell reaches the surroundings temperature much faster than the PVC sample, thus *Bi* and *M* were determined from the PVC properties only. Table 6.2 summarizes the properties and parameters required for the calculations for the

PVC in this study, and the determined values for *Bi* and *M* to be 0.32 and 0.05, respectively. The value for *Bi* indicates that the convection heat transfer rate is smaller than the conduction heat transfer rate into the sample. The value of *M* indicates that the reaction rate is significantly smaller than the conduction heat transfer, thus the sample equilibrates its temperature faster than the reaction rate. These two values indicate that the sample temperature becomes uniform faster than the reaction rate.

Table 6.2. Estimated values for the parameters to determine the Bi and M.

Parameter	**Value**	**Source**
h, W/m^2-K	10	(Bergman et al., 2011)
λ for PVC, W/m-K	0.15	(De Carvalho et al., 1996)
$R^{\prime}$ for PVC, kg/m^3-s	0.5	Approximated in this study
ρ (apparent), kg/m^3	600	Approximated in this study
c_p (apparent), J/kg-K	700	(Chang, 1977)
L_c diameter, m	0.005	Measured in current study
Bi	0.32	Current result
M	0.05	Current result

The above analysis indicated that the PVC degradation reaction rate in the tubular reactor is governed by the convective heat transfer from the furnace walls to the sample surface. Therefore, the sample has uniform temperature at all times. For the TGA experiment mentioned above, the Biot number was calculated to be 0.1 using Eq. (6.12), which also indicting that the temperature is uniform at all times (Gómez et al., 2012). As noted, the sample temperature was not measured, however, it can be calculated as a function of time by

$$\frac{dQ(t)}{dt} = hA[T_w - T_s(t)] \tag{6.14}$$

here $dQ(t)/dt$ is the heat rate from the furnace walls, T_w is the temperature of the wall and $T_s(t)=T(t)$ represents sample surface temperatures and the heat required to increase the sample temperature is indicated by $Q(t)$, or

$$Q(t) = mc_p[T(t) - T_o] + mh_r \tag{6.15}$$

where m and c_p are sample mass and specific heat capacity, respectively, T_o is the temperature at the core of the sample, which equals to the initial temperature of the sample and h_r is reaction enthalpy. As the value for h_r is 99.4 J/kg (Bacaloglu and Fisch, 1995) and with a 2.5 g sample, the heat required to heat the sample is 1000 larger, therefore the h_r term in Eq. (6.14) was ignored. Thus, introducing Eq. (6.15), assuming h_r=0, into Eq. (6.14) and integration from T_w to $T(t)$ yields

$$Q\frac{T_w - T(t)}{T_w - T_o} = e^{-t/\tau} \tag{6.16}$$

where τ is a characteristic time, defined as

$$\tau = \frac{mc_p}{hA} \tag{6.17}$$

For the sample in the cylinder, $\tau_{cyl}=d\rho c_p/4h$, where d is diameter of the cylinder, and ρ is the density of the sample. Rearrangement of Eq. (6.16) yields

$$T(t) = T_w - (T_w - T_o)e^{-t/\tau} \tag{6.18}$$

Table 6.2 summarized the values that were used to determining τ. Introducing these values in Eq. (6.17) yields $\tau_{cyl} \sim 100$ (s).

The calculated temperature is given below together with the mass loss transient.

6.4.4.2 Mass Loss

The mass loss of the 2.5 g experiments was modeled by the same method described above (Eq. 6.11). The dotted line in Figure 6.9 shows temperature transients from the heat transfer model. Figure 6.9 also portrays the experimental mass loss transient. It indicated that there was no measurable mass loss until the sample reached ~296°C (indicated by the dashed line), which is only 4°C less than the maximum temperature. Therefore, the changes of the activation energy were negligible. The mass loss model obtained based on both the heat transfer calculation and the kinetic model shows good fit with the experimental results. It was possible to predict the mass loss results measured by two different methods by this model, strengthen the argument that the current model developed provides a good description of the real reaction for PVC degradation.

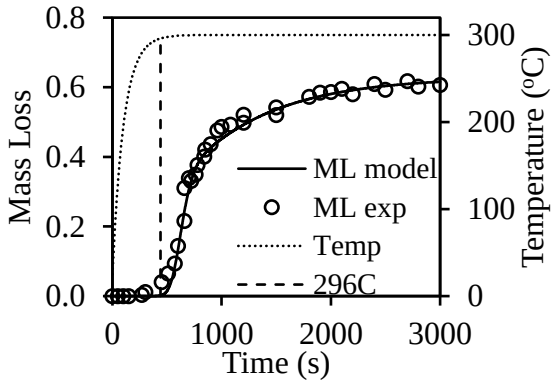

Figure 6.9. Mass loss vs time in the tubular reactor for torrefaction of PVC at 300°C, using 2.5 g sample.

6.4.4.3 Chlorine Content

Since HCl is the only source of the chlorine in the gas phase and there is one mole of chlorine atom in one mole of HCl, the removal of chlorine was also modeled based on the developed kinetic model and parameters acquired from above. Figure 6.10 showed that the model was also able to predict the chlorine removal behavior of PVC with time during torrefaction.

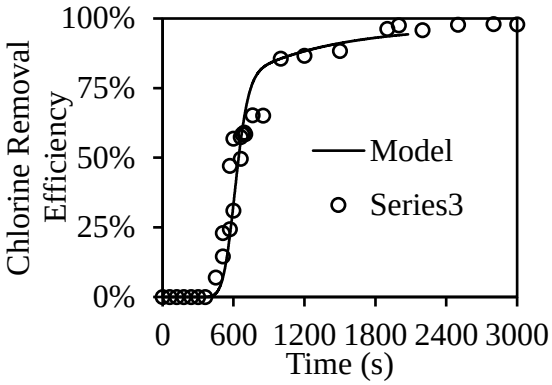

Figure 6.10. Normalized chlorine in gas vs. time during PVC torrefaction at 300°C.

In various torrefaction systems the time variable was replaced by mass loss with the notion that mass loss can be a universal variable that would depict a degradation behavior irrespective of residence time and temperature (Klinger et al., 2016). This presentation might apply to PVC as well. The experimental results of Figure 6.10 were replotted as a function of mass loss (Figure 6.11). On the other hand, the kinetic model above, enables the description of chlorine removal as a function of mass loss; i.e., calculate x_{HCl} (by integration of Eq. 3.1) and plot it vs. β (Eq. 3.11). The solid line in Figure 6.11 shows an excellent agreement between the model and experimental results.

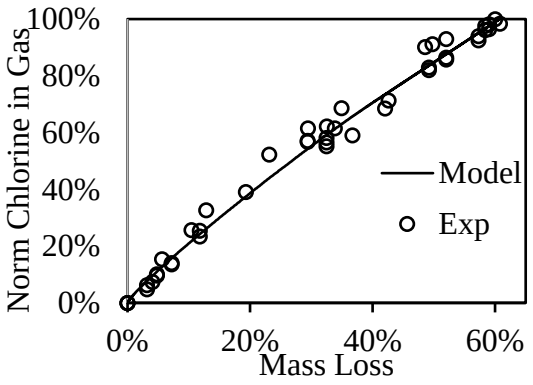

Figure 6.11. Normalized chlorine in gas vs. mass loss during PVC torrefaction at 300°C.

6.4.4.4 Elemental Composition Modeling

As noted in Section 6.3.5, C/H were measured, and Cl was calculated by difference. To note in Section 6.3.4, Cl was measured directly. Comparison between the chlorine content by the two methods showed a perfect fit to each other within the experimental error. On the other hand, the kinetic model can also provide C/H/Cl (by use of the parameters of Table 6.1) as follows: (i) The amount of HCl, benzene, naphthalene and anthracene can be calculated from which C/H/Cl can be determined; (ii) since one mole of HCl consists of one mole of hydrogen (H) and one mole of chlorine (Cl); one mole of benzene consists of 6 moles of carbon (C) and 6 moles of hydrogen; one mole of naphthalene consists of 10 moles of carbon and 8 moles of hydrogen; and one mole of anthracene consists of 14 moles of carbon and 10 moles of hydrogen; and (iii) accordingly, the amounts of C, H and Cl can be determined from the model. To note that a scalar is required to convert the normalized values of the gaseous products to actual molar fractions. Figure 6.12 shows the elemental composition of PVC thermal degradation gas product at different mass losses. It showed that the release of hydrogen and chlorine was almost at the same speed when the mass loss was lower than 15%. After 15% mass loss, carbon started to be released into the gas phase as hydrocarbons. These behaviors were also predicted by the kinetic mode mentioned above, as HCl was proposed to be the main product at the initial stage of the reaction, since 1 mole of HCl contains 1 mole of hydrogen and chlorine, it explained the same speed of the release of hydrogen and chlorine. And according to the model, hydrocarbons are produced along with HCl at later stage, indicating the increase of carbon release as well as the faster release of hydrogen into gaseous.

6.4.4.5 Heat Content Modeling

The heat content (HC) of PVC degraded samples is not obtainable through enthalpies of formations as the remaining solid material is not defined. Therefore, a correlation of the HC versus the C/H/Cl composition was measured and modeled. From the numerous experiments of PVC degradation in the tubular reactor, the HC of each sample was measured and enabled us to obtain a correlation between HC and C/H/Cl. The correlation found is given by Eq. (6.19)

$$HC = (a_C x_C + a_H x_H + a_{Cl} x_{Cl})/(1-\beta) \qquad (6.19)$$

Since the elemental composition results obtained from the experiments were weight basis, they were transformed into molar fractions according to their own molar weight, where $a_C = 13.96$, $a_H = 4.27$, and $a_{Cl} = 0.23$ (MJ/kg).

The HC can be also modeled using Eq. (3.19) and the elemental composition determined by the model as described in Section 6.4.2. Figure 6.13 shows experimental results for HC as a function of mass loss (symbols) as well as the HC determined by the model, showing a good fit between the two.

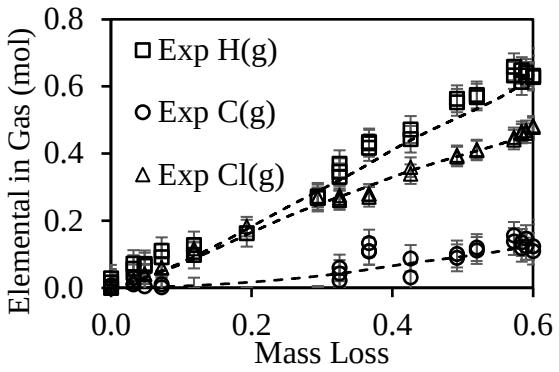

Figure 6.12. Elemental composition of H, C and Cl for PVC torrefaction at 300°C vs. mass loss

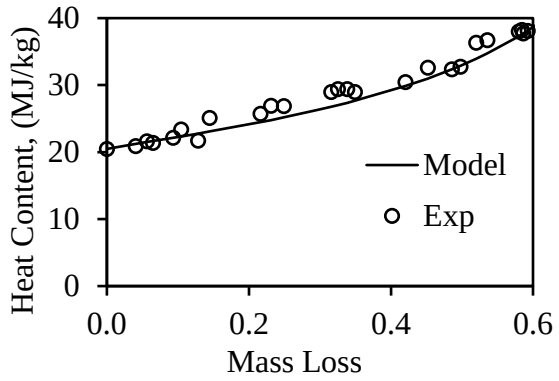

Figure 6.13. Heat content (HC) of torrefied PVC at 300°C vs. mass loss.

6.5 Conclusion

A comprehensive study of the kinetics of the PVC thermal degradation at 300°C has been carried out and was based on detailed measured in a micro-pyrolysis reactor, with no heat and mass transfer limitation. It has been shown that the thermal degradation of PVC at this temperature requires four consecutive reactions. Different hydrocarbons (mostly aromatics) were produced along with HCl in the gas phase. The model showed: (i) HCl and benzene were produced only by the first three reactions; (ii) naphthalene was produced by second and third reactions only; and (iii) anthracene was produced mostly by the second and third reaction, with some produced in the fourth reaction. This model has been validated and proved by predicting the mass loss, chlorine content, heat content and elemental composition with high precision experimental data in different reactors with/without heat transfer coupling. It is expected, however, that for higher temperatures, this model needs to be improved by adding more consecutive reactions and other products.

Declaration of competing interest

The authors do not have any competing interest.

CRediT authorship contribution statement

Xu: Methodology, Investigation and Writing Original Draft; Kolapkar: Investigation and Writing Review and Editing; Zinchik: Investigation and Writing Review and Editing; Bar-Ziv: Conceptualization and Supervision; McDonald: Supervision and Investigation.

Acknowledgements

The authors acknowledge the support from the National Science Foundation grant number 1827364.

6.6 Work Cited

Anders, H., and Zimmermann, H. (1987). A comparison of the thermal degradation behaviours of poly(vinyl acetate), poly(vinyl alcohol) and poly(vinyl chloride). *Polym. Degrad. Stab.* 18, 111–122. doi:10.1016/0141-3910(87)90024-3.

Anuar Sharuddin, S. D., Abnisa, F., Wan Daud, W. M. A., and Aroua, M. K. (2016). A review on pyrolysis of plastic wastes. *Energy Convers. Manag.* 115, 308–326. doi:10.1016/J.ENCONMAN.2016.02.037.

Bacaloglu, R., and Fisch, M. (1995). Degradation and stabilization of poly (vinyl chloride). V. Reaction mechanism of poly(vinyl chloride) degradation. *Polym. Degrad. Stab.* 47, 33–57. doi:10.1016/0141-3910(94)00086-N.

Bergman, T. L., Incropera, F. P., DeWitt, D. P., and Lavine, A. S. (2011). "Fundamentals of heat and mass transfer," in (New York: Wiley, pp. 983-1011), 56.

Braun, V. D., and Thallnaier, M. (1966). Zum mechanismus der thermischen chlorwassmtoffabspaltung aus polyvinylchlorid. 3. Mitt. Über die länge der polyensequenzen in partiell dehydrohalogenierten poiyvinylchloriden, polyvinylbromiden und vinylchlorid-copolymeren. *Die Makromol. Chemie* 99, 59–75. doi:10.1002/macp.1966.020990106.

Chang, S.-S. (1977). Heat Capacity and Thermodynamic Properties of Poly(Vinyl Chloride). *J. Res. Natl. Bur. Stand. (1934).* 82, 9–18. doi:10.6028/jres.082.002.

De Carvalho, G., Frollini, E., and Dos Santos, W. N. (1996). Thermal conductivity of polymers by hot-wire method. *J. Appl. Polym. Sci.* 62, 2281–2285. doi:10.1002/(sici)1097-4628(19961226)62:13<2281::aid-app12>3.3.co;2-t.

Gómez, M. A., Álvarez, M. A., Eguía, P., and Comesa, R. (2012). Thermochimica Acta Thermal lag analysis on a simulated TGA-DSC device. 547, 13–21.

Jiang, Y., Lu, M., Liu, S., Bao, C., and Liang, G. (2018). Deactivation by HCl of CeO2–MoO3/TiO2 catalyst for selective catalytic reduction of NO with NH3. 8, 17677–17684. doi:10.1039/c8ra00280k.

Jung, Y. G., Choi, S. C., Oh, C. S., and Paik, U. G. (1997). Residual stress and thermal properties of zirconia/metal (nickel, stainless steel 304) functionally graded

materials fabricated by hot pressing. *J. Mater. Sci.* 32, 3841–3850. doi:10.1023/A:1018640126751.

Kiran, N., Ekinci, E., and Snape, C. . (2000). Recyling of plastic wastes via pyrolysis. *Resour. Conserv. Recycl.* 29, 273–283. doi:10.1016/S0921-3449(00)00052-5.

Klinger, J., Bar-Ziv, E., Shonnard, D., Westover, T., and Emerson, R. (2016). Predicting Properties of Gas and Solid Streams by Intrinsic Kinetics of Fast Pyrolysis of Wood. *Energy and Fuels* 30, 318–325. doi:10.1021/acs.energyfuels.5b01877.

Lattimer, R. P., and Kroenke, W. J. (1982). Mechanisms of formation of volatile aromatic pyrolyzates from poly(vinyl chloride). J. Appl. Polym. Sci. 27, 1355–1366. doi:10.1002/app.1982.070270425.

Marongiu, A., Faravelli, T., Bozzano, G., Dente, M., and Ranzi, E. (2003). Thermal degradation of poly(vinyl chloride). *J. Anal. Appl. Pyrolysis* 70, 519–553. doi:10.1016/S0165-2370(03)00024-X.

McNeill, I. C., Memetea, L., and Cole, W. J. (1995). A study of the products of PVC thermal degradation. *Polym. Degrad. Stab.* 49, 181–191. doi:10.1016/0141-3910(95)00064-S

National Emission Standards for Hazardous Air Pollutants (NESHAP) (2017). Available at: https://www.epa.gov/stationary-sources-air-pollution/national-emission-standards-hazardous-air-pollutants-neshap-9 [Accessed July 29, 2019].

Petre, A. L., Budrugeac, P., and Segal, E. (1999). Thermal Degradation of Polyvinyl Chloride. *J. Therm. Anal. Calorim.* 56, 1065–1070. doi:10.1023/A:1010136507843.

Risby, T. H., Yergey, J. A., and Scocca, J. J. (1982). Linear Programmed Thermal Degradation Mass Spectrometry of Polystyrene and Poly(vinyl chloride). *Anal. Chem.* 54, 2228–2233. doi:10.1021/ac00250a022.

Ritchie and Roser (2018). *Plastic Pollution - Our World in Data*. Available at: https://ourworldindata.org/plastic-pollution?utm_source=newsletter&utm_medium=email&utm_campaign=sendto_newslettertest&stream=top [Accessed January 23, 2020].

Rojas, A., and Orozco, E. (2003). Measurement of the enthalpies of vaporization and sublimation of solids aromatic hydrocarbons by differential scanning calorimetry. 405, 93–107. doi:10.1016/S0040-6031(03)00139-4.

Sánchez-Jiménez, P. E., Perejón, A., Criado, J. M., Diánez, M. J., and Pérez-Maqueda, L. A. (2010). Kinetic model for thermal dehydrochlorination of poly(vinyl chloride). *Polymer (Guildf).* 51, 3998–4007. doi:10.1016/J.POLYMER.2010.06.020.

Solmaz, R., Kardaş, G., Çulha, M., Yazıcı, B., and Erbil, M. (2008). Investigation of adsorption and inhibitive effect of 2-mercaptothiazoline on corrosion of mild steel in hydrochloric acid media. *Electrochim. Acta* 53, 5941–5952. doi:10.1016/J.ELECTACTA.2008.03.055.

Subramanian, P. M. (2000). Plastics recycling and waste management in the US. *Resour. Conserv. Recycl.* 28, 253–263. doi:10.1016/S0921-3449(99)00049-X.

Utschick, H., Ritz, M., Mallon, H.-J., Arnold, M., Ludwig, W., Kettrup, A., et al. (1994). Investigations on the thermal degradation of post-chlorinated polyvinyl chloride. *Thermochim. Acta* 234, 139–151. doi:10.1016/0040-6031(94)85140-9.

Wakeman, I. B., and Johnson, H. R. (1978). Vinyl chloride formation from the thermal degradation of poly(vinyl chloride). *Polym. Eng. Sci.* 18, 404–407. doi:10.1002/pen.760180512.

Wimberley, J. W., Carel, A. B., and Cabbiness Conoco Inc., D. K. (1982). Automated Method for Measuring the Thermal Degradation of Polyvinyl Chloride. *Anal. Lett.* 15, 89–100. doi:10.1080/00032718208064366.

Xu, Z., Zinchik, S., Kolapkar, S., Bar-ziv, E., Hansen, T., and Conn, D. (2018). Properties of Torrefied U . S . Waste Blends. *Front. Energy Res.* 6, 65. doi:doi.org/10.3389/fenrg.2018.00065.

Yin, R.-H., Zhang, R.-Z., and Luo, Y.-H. (2016). The Effect of Utilizing Homogeneous Conversion to Control the Formation of Chlorinated Hydrocarbons During PVC Pyrolysis. 35, 1012–1019. doi:10.1002/ep.12313.

Yu, J., Sun, L., Ma, C., Qiao, Y., and Yao, H. (2016). Thermal degradation of PVC: A review. *Waste Manag.* 48, 300–314. doi:10.1016/j.wasman.2015.11.041.

7 Chlorine Removal from U.S. Solid Waste Blends through Torrefaction

This section is based on the following peer-reviewed paper:

Z. Xu, JW. Albrecht, SS. Kolapkar, S. Zinchik, E. Bar-Ziv. 2020. Chlorine Removal from US Solid Waste Blends through Torrefaction. Applied Sciences 10 (9), 3337.

doi.org/10.3390/app10093337

7.1 Abstract

The amount of solid waste generated annually is increasing around the world. Although the waste has high calorific value, one major obstacle may prevent it from becoming a feedstock for power applications is the existence of polyvinyl chloride (PVC), which causes corrosion and emission issues after combustion due to its high chlorine content. Torrefaction is known to release hydrochloric acid, thus it has been applied in this study for the reduction of chlorine from potential waste feedstocks. Fiber-plastic (60%-40%) waste blends, with different chlorine content levels, as well as PVC were used in the current study. Torrefaction was conducted at 400 °C. Chlorine and heat content were measured. Experimental results showed that organically bonded chlorine was reduced during torrefaction as a function of mass loss. The chlorine removal efficiency was only dependent on temperature and residence time, not chlorine level. The heat content of the sample increased with mass loss up to a maximum of ~34 MJ/kg at ~45% mass loss. It was also observed that at ~30% mass loss, the organic chlorine content per unit heat content reduced ~90%, while the heat content is ~32 MJ/kg and ~90% energy was retained.

7.2 Introduction

Solid waste generation is increasing across the world, and this trend is growing as the population grows (Hoornweg and Bhada-Tata, 2012). Due to reasons like cost and poor quality of material, much of these wastes cannot be feasibly recycled and were instead landfilled (Subramanian, 2000). For instance, the United States alone landfilled 139 million tons of municipal solid waste in the year of 2017 (National Overview: Facts and Figures on Materials, Wastes and Recycling, 2017). The practice of landfilling is known to cause significant environmental damage and negative health impact (El-Fadel et al., 1997; Goorah et al., 2009). Moreover, landfilling is economically destructive by wasting a precious, energy-intensive resource. Closely following population and economic growth, global energy demand is expected to increase 48% from 2012 to 2040 (Conti et al., 2016), requiring investment into safe, low cost, and clean energy sources. Furthermore, in a highly competitive and increasingly regulated sector, existing coal power plants are facing more stringent regulations (Kotchen and Mansur, 2014). These issues can be reconciled by utilizing a thermal treatment process to convert the solid waste into a low-cost and clean fuel source.

Torrefaction, a thermochemical treatment process with the purpose of improving the feedstock characteristics for later use in pyrolysis, gasification, or combustion. This has long been studied as key to development the use of woody biomass, a renewable energy source, to help replace fossil fuels (Yuan et al., 2015). Although the technology is well-established, biomass has not yet taken on as a major energy source in the market, contributing to just 1.5% of US energy production (What is U.S. electricity generation by energy source?, 2020). Among many obstructions to the commercialization of technology for biomass torrefaction (Xu et al., 2018), prohibitive high cost is the most prominent (Kumar et al., 2017; Radics et al., 2017).

Solid waste is a more recently proposed candidate for the use in the torrefaction process as more sustainable alternative to coal (More recycling raises average energy content of waste used to generate electricity, 2012). It solves many of the challenges associated with woody biomass (Xu et al., 2018), but most importantly, the source is ubiquitous and readily available. With waste disposal tipping fees, the waste feedstock often has a negative price, helping the economic issues associated with biomass feedstocks.

The use of raw solid waste in waste-to-energy (WTE) plants has been long considered, with 12.7% of U.S. Municipal Solid Waste (MSW) currently being combusted with some energy recovery in the year of 2017 (National Overview: Facts and Figures on Materials, Wastes and Recycling, 2017). A major reason this idea has failed to take hold is the poor properties of the untreated mixed solid wastes such as energy density, moisture content and the high costs associated with the high chlorine in the flue gas treatment (Xu et al., 2018). However, a simple torrefaction process of the solid waste is being increasingly studied and shown to be an inexpensive and reliable method of improving the feedstock quality (Zinchik et al., 2020). Additionally, using heat-treated MSW has been shown to be carbon-neutral due to the reduction in methane and CO_2 emissions from landfills (McCabe, 2014).

Xu et al., 2018 have previously shown that torrefied solid waste has similar characteristics to the common Powder River Basin (PRB) coal and can be used to replace it in existing plants (Xu et al., 2018). Using heat-treated solid waste in existing coal-fired plants, full economic advantage of the available resources can be taken, while simultaneously curbing the use of heavily polluting coal and reducing the accumulation of waste. The same team also studied the characteristics of extruded wastes produced by the same feedstock, which addressed multiple properties including densification, grindability, water resistance, durability, heat content and combustion behaviors (Zinchik et al., 2020).

A major hurdle solid waste faces as a potential solid fuel is the chlorine released from PVC waste during combustion. This chlorine is known to cause corrosion and emission issues (Solmaz et al., 2008). Hatanaka et al., 2000 found that the higher the chlorine level of the waste, more polychlorinated dibenzo-p-dioxins and dibenzofurans (PCDD/Fs) emission will be produced(Hatanaka et al., 2000). Vikelsoe et al., 1990 also studied the effect of PVC content on the PCDD emissions during MSW combustion. The results showed that doubling the PVC content of MSW would increase PCDD emissions during combustion by 32%(Vikelsoe, J., Nielsen, P., Blinksbjerg, P., Madsen, H., & Manscher, 1990). A study done by Tian and Ouyang, 2003 has found that there exists MSW incinerators that emit

dioxins higher than nation standard in China, while later study done by Ni et al., 2009 showed the dioxin emissions form the new generation MSW incinerators met the national standard (Tian, H. H., & Ouyang, 2003; Ni et al., 2009). Cangialosi et al., 2007 carried out a case study of air pollutants for a MSW incineration plant in Italy (Cangialosi et al., 2008). The results showed their PCDD/Fs emission levels have rather small health impact for the surrounding population. However, they also indicated that the source of the waste and the technology used for the incineration would affect the final results. EPA also has stringent guidelines for PCDD emissions, which requiring the risk factor to be lower than 10^{-6} (one occurrence per one million people) (EPA Clean Air Act, 42 USC 7412(f), 1992). Since the source of the solid waste is mostly unknown, it is essential to removal the chlorine to reduce the potential PCDD/Fs emission.

Chlorine removal from wastes has been studied extensively over the years. Takeshita et al., 2004 reported a method of hydrothermally treating PVC waste in subcritical and supercritical regions. They were able to decompose the PVC without producing any harmful chlorinated organics. However, the behavior of chlorine removal from mixed waste was still lacking since this study focused on just PVC waste. Inoue et al., 2008 carried out a mechano-chemical method of de-chlorination by co-grinding the PVC with various metal oxides using a planetary ball mill. The ground product was dispersed in water to extract the inorganic chlorine compounds, and the release of chlorine was found to increase as the grinding time and additive ration increased. However, the PVC used in this study was in powder form, and therefore does not apply for existing PVC waste (Inoue et al., 2004).

Indrawan et al., 2011 introduced hydrothermal process to produce chlorine-free solid fuels from MSW. This process used saturated steam at ~200 °C with a pressure of 2 MPa on a 1-ton batch feedstock and they were able to produce chlorine-free solid fuels. However, the product additionally required water washing to remove the inorganic chlorine produced during the hydrothermal treatment. For sufficient chlorine removal weight ratio of water used to MSW cleaned was 3:1 (Indrawan et al., 2011).

Xu et al., 2018 investigated the method of chlorine removal from the solid waste in the previous study (Xu et al., 2018), however, it was done at 300 °C, which requires relatively long residence times of torrefaction involved with high-shear mixing with water. In the recent study, Xu et al., 2020 studied the mechanism and kinetics of de-chlorination of pure PVC (Xu et al., 2020b). It investigated the products of Torrefaction and proposed a comprehensive mechanism of PVC degradation at 300 °C, which provides insight for the process of PVC de-chlorination.

With the goal of improving solid waste feedstock quality, this study more closely investigates the issue of chlorine as a contaminant in potential feedstocks. Since waste as a feedstock contains variety of components which may widely affect the initial chlorine levels, it is essential to study PVC chlorine removal at different chlorine levels in order to apply this method to other types of wastes compositions.

The present paper deals with two aspects: (1) determination of appropriate torrefaction process parameters that can maximize the retained energy and minimize the chlorine levels; (2) the effect of different chlorine levels of material on the PVC de-chlorination behavior.

7.3 Materials and Methods

7.3.1 Materials

Convergen Energy, LLC (CE) supplied the mixed solid waste used in this study which was shredded to 75-125 mm size. Both the "Low Chlorine" (LC) and "High Chlorine" (HC) materials used were blends of 40% plastic and 60% fiber waste, with chlorine content of ~1,100 ppm and 16,000 ppm, respectively. The properties of these materials have been well documented over the past seven years and have been shown to be consistent (Xu et al., 2018). Both types contain a variety of mixed materials, including non-recyclable plastic and paper flakes, cartoon, cardboard, laminated papers, fibers and different types of plastics. The major difference between the two types of material is the increase in the chlorine concentration for the HC material, due to higher content of PVC. Throughout this study it was observed that, as a whole, the HC material contains approximately 15 times the concentration of chlorine as the LC material.

To improve the grindability of the sample, the materials were placed in a Lindberg/Blue BF51828C-1 muffle furnace at 300 °C for 2 minutes in ~100 g batches. Two of these 100 g "reference" samples were made for both LC and HC materials. The mass losses of the samples from this process were negligible. The material became more brittle after the process and was ground in a Col-Int Tech CIT-FW-800 High-Speed Rotor Mill/Grinder for 1-2 minutes to decrease particle size and increase homogeneity for further testing.

Even with the well-ground 100 g reference samples, some heterogeneity was observed. It was found that the error could be reduced significantly by taking ~4 g samples for each test, mixing them well, and testing 1 g of that 4 g sample as a reference to compare to any tests from the remaining 3 g sample. This method was employed for most of the tests, but due to the inherent heterogeneity of the mixed waste, variability in the results still exists.

The PVC used in Section 3.3 for the comparison with results of solid waste was procured from Shintech Inc. with grade SE-950 and density = 1,400 kg/m^3.

7.3.2 Torrefaction

For each torrefaction test, a 203 mm long, 9.5 mm outer diameter (OD) and 0.25 mm wall thickness stainless-steel tube reactor was assembled with insulation separating the material from the bottom of the sealed cap. A stainless-steel tube with same diameter was connected to the reactor to guide the produced gaseous to an Induced Draft (ID) Fan. The torrefaction experimental setup was identical to the one used in the previous study (Xu et al., 2020b). Before each test, the reactor's mass was taken on an A&D EJ-410 scale (readability of 0.01 g) to get a value for m_1 from Eq.(7.1). The reactor was then filled with 1.3-1.4 g of material from a well-mixed 4 g sample of one of the 100 g CE batches and weighed again for m_2.

The reactor filled with tested material was attached to a long pipe inserted into a ventilation system to remove any gas produced by the torrefaction process. The pipe and reactor were then lowered into the furnace (Lindberg/Blue type BF51828C-1 Muffle Furnace) and held for a set time, ranging from 1 to 75 min. The furnace was kept at 400 °C for every test in this study in order to increase the reaction rate and reduce the residence time. The same practice was also done for a few PVC torrefaction experiments at 400 °C.

After the set time, the reactor was immediately removed from the furnace and quenched in a container of water to rapidly cool down the temperature of the reactor. To ensure no water entered the reactor pipe, metal seals were placed on each end. This water was completely dried off with a paper towel before any mass measurements were taken. After the reactor was fully dried, the mass of all the constituents was taken to obtain m_3. The total mass loss was calculated according to Eq. (7.1),

$$ML(t) = \frac{m_2 - m_3(t)}{m_2 - m_1} \tag{7.1}$$

where m_1 is the reactor vessel mass, m_2 is the reactor mass with test material, and $m_3(t)$ is the reactor mass with test material after torrefaction. After measuring the mass loss, the sample would be removed for further testing.

7.3.3 Characterization

7.3.3.1 Moisture Content

The moisture contents of HC and LC materials were tested before the experiments. For each test, 1 g samples were tested in the HFT 1000 Moisture Analyzer by Data Support Co. Inc. The moisture analyzer worked by heating up the material to 120 °C and continuously weighing the material placed inside the analyzer until the sample weight stabilizes. The moisture content was calculated by measuring the percent change of the total weight. The moisture contents for the LC and HC material were measured to be 3.4% and 3.1%, respectively. To avoid moisture buildup, the sample was kept in a SHEL LAB SMO28-2 Forced Air Oven prior to be dried at 80°C at all times after being taken out of the furnace.

7.3.3.2 Heat Content

Heat content of all samples was measured with a Parr-6100 bomb calorimeter. A small metal crucible was filled with 0.5-1 g of material for each test. Test material was weighed in the crucible on an A&D HR-60 scale. This crucible was then placed inside the calorimeter's bomb and a cotton thread was used to help the ignition of the sample. Five ml of 2% Na_2CO_3 was added to capture any HCl released for later chlorine testing. The bomb was then sealed and injected with 400 Psi compressed oxygen to permit complete combustion. The bomb was submerged in a 2,000 g bath of distilled water, and the calorimeter calculated the sample heat content based on the temperature increase of the water after the test sample was ignited. The error caused by the extra 2% Na_2CO_3 in the

bomb (5 ml) was neglected, since it was insignificant compared to the total water (2000 ml) in the bucket.

7.3.3.3 Chlorine Content

Chloride concentration was measured using chloride ion-selective electrode with the Oakton Ion 700 Cl-meter, calibrated using 1, 10, and 100 ppm dilutions from a 1000 ppm Cl- standard solution. For this study, all chlorine originated from the solid phase, and the sample to be measured was prepared in accordance with ASTM standard D4208-18. After the combustion was complete, the bomb was opened and the pressure was then released at a steady rate, taking at least 2 minutes to avoid disturbing the contents. After the bomb was opened, all interior parts were washed thoroughly with distilled water and collected in a 140 ml beaker for testing. The total volume of liquid was kept between 80-90 ml. Liquid mass was next taken on an A&D EK-15KL scale (readability of 0.1 g). Finally, prior to measuring the chlorine content, 2 ml of 5M $NaNO_3$ ionic strength adjustor (ISA) were added to the solution.

The Oakton Cl-meter determines the chloride concentration by measuring electric potential across a liquid and converting to a concentration value in ppm. During measurements, a magnetic stirrer was used to keep the solution homogeneous and ambient temperature was maintained for each test. Since the aqueous chloride concentration provided by the measurement is given respective to mass, the chlorine concentration of the original solid can be calculated according to Eq. (7.2):

$$C_{Cl,sample} = \frac{C_{Cl,aq} M_{aq}}{M_{sample}} \tag{7.2}$$

where $C_{Cl,sample}$ and $C_{Cl,aq}$ are the chlorine/chloride concentrations in ppm of the material sample and aqueous solution, respectively. M_{sample} and M_{aq} are the respective masses of the material sample and aqueous solution.

7.4 Results and Discussion

7.4.1 Torrefaction

As mentioned, all the experiments were carried out by placing the tubular reactor in the muffle furnace set at 400 °C. In order to determine the heat transfer regime of the system behavior, the Biot Number (*Bi*), which relates to the heating regime of the material, and the Thermal Thiele Modulus (*M*), relating to the propagation of the reaction within the sample were determined as:

$$Bi = \frac{h}{\lambda / L_c} \tag{7.3}$$

$$M = \frac{R^{\dagger}}{\lambda / (c_p L_c^2)} \tag{7.4}$$

The parameters are summarized in Table 7.1 below.

Table 7.1. Estimated values for the parameters to determine the Bi and M.

Parameter	**Value**	**Source**
h, W/m^2-K	10	(Incroper et al., 2011)
λ for CE material, W/m-K	0.2	(De Carvalho et al., 1996)
ρ (apparent), kg/m^3	1150	Measured in this study
c_p (apparent), J/kg-K	1600	(Incroper et al., 2011)
L_c diameter, m	0.003	Measured in this study
Bi	0.15	Current result
M	0.009	Current result

Note that as thermal conductivity for stainless-steel is significantly greater than the value for CE material (Jung et al., 1997), and the diameter of the reactor is significantly smaller compared to the size of the furnace chamber, the influence of the stainless-steel tube on the heat convection from the furnace wall to the sample surface was neglected. The *Bi* and *M* for this experimental setup were obtained for the CE material. Since *Bi* equals 0.15, which is smaller than 1, it indicates that the samples are thermally thin, and the heat conduction into the sample is much faster than the heat convection from the furnace wall to the sample surface; for *M* equaling to 0.009, it indicates that the reaction rate was much smaller than the heat conduction into the sample. Therefore, the reaction rate was governed by the heat convection from the furnace to the sample surface, after which the temperature of the particle became uniform instantly.

The analysis of the same experimental setup was done by Xu et al., 2020 and the temperature of the sample particle could be defined as:

$$\frac{T_w - T(t)}{T_w - T_o} = e^{-t/\tau} \tag{7.5}$$

where Tw, T_o and τ represents the furnace wall temperature, initial temperature of the sample and the characteristic time, respectively (Xu et al., 2020b). And τ can be defined as:

$$\tau = \frac{mc_p}{hA} \tag{7.6}$$

For this specific experiment setup, the characteristic time was calculated to be 120.3 s. Since the waste consists of both fiber and plastics, and previous study showed fiber and plastic behave differently during the torrefaction (Zinchik et al., 2020). In order to obtain a preliminary correlation to study the behavior of the torrefaction behavior of this waste

material, we assumed two first order reactions, which is rather common in biomass and plastic torrefaction representing the degradation of fiber and plastic for the torrefaction experiment (Jacques Lédé, 2010; Funke et al., 2017; Bach et al., 2019). Similar correlation has been developed and implemented successfully by Xu et al., 2018 (Xu et al., 2018).The correlation between mass loss and time was represented by the following equation:

$$\alpha = 1 - (a_1 A_1^* e^{-\frac{T_{a_1}}{T(t)}} + a_2 A_2^* e^{-\frac{T_{a_2}}{T(t)}}) \quad (7.7)$$

Where α, a, A^* and T_a are the mass loss, pre-exponential factor and characteristic time, respectively. The values of the parameters were determined by fitting Eq. 7.6 to the experimental results and the results are shown in Table 7.2.

Table 7.2. Fitted parameter values used in Equation 7

a_1	0.39	a_2	0.61
A_1^*	2.81×10^7	A_2^*	7.58×10^5
T_{a_1}	1.53×10^4	T_{a_2}	1.55×10^4

With the model developed above, the temperature transient as well as the mass loss were plotted as function of time as shown in Figure 7.1. The dotted line indicates the correlation between mass loss of the material and time. The two vertical dashed lines represent the time when the sample reaches 340 °C and 400 °C, respectively. It indicates that the mass loss started at ~340 °C and increased to ~30% at 400 °C after ~12 minutes. The mass loss later gradually increased and reached ~55% after 60 minutes. According to Zinchik et al., 2020, relatively fast increase in mass loss at early stage can mainly be attributed to the decomposition of the fibers, while the later slow increase in mass loss can mainly be attributed to torrefaction of the plastics (Zinchik et al., 2020). The results show that the mass loss behavior as a function of time was similar for both LC and HC materials. However, this mass loss behavior is unique to this material blend (40% plastic and 60% fiber).

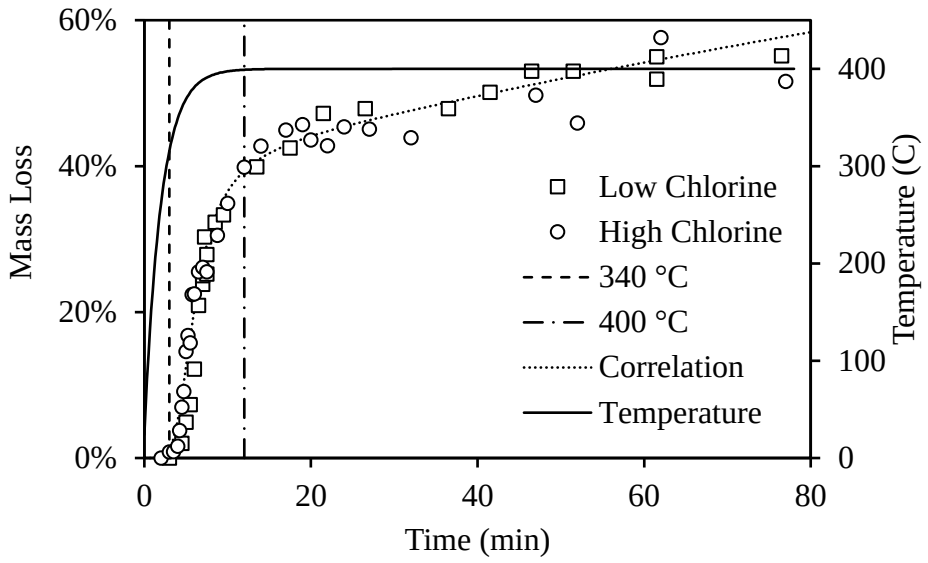

Figure 7.1. Mass loss and temperature transient vs. time.

7.4.2 Chlorine Content

Chlorine content is one of the major considerations for use of wastes as a feedstock for energy production. In this study, the chlorine content of the waste at different extents of torrefaction was measured and the results are shown below in Figure 7.2a. The term "CE material" represents both LC and HC materials since they have similar behavior for chlorine removal efficiency. The release of chlorine started at ~340 °C, which also aligns with the findings of the mass loss behavior in Section 7.4.1, since the PVC would release chlorine in the form of hydrochloric acid (HCl) during the torrefaction process (Anuar Sharuddin et al., 2016). The results show chlorine reaching asymptotic value at ~80% removal efficiency after 20 minutes of torrefaction at 400 °C.

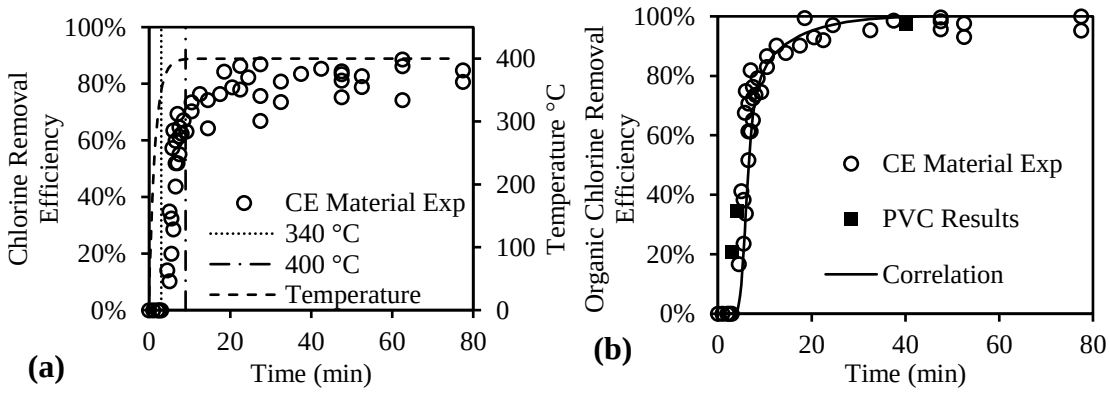

Figure 7.2. (a) Chlorine removal efficiency (from waste) and temperature vs. time; (b) Organic chlorine removal efficiency from waste and from PVC vs. time.

Previous study has shown that the chlorine removal efficiency through torrefaction of PVC would increase as the residence time increases, eventually reaching 100% (Xu et al., 2020b). However, we noticed that the chlorine removal efficiency of the waste material did not reach 100%, which contradicts with previous results if PVC was the only source of chlorine in the waste.

Since the chlorine removal efficiency reached an asymptotic value of ~80%, it indicated that all the chlorine from PVC was removed while the rest 20% was from an unknown source. The organic chlorine reduction efficiency of CE material through torrefaction was calculated by normalizing the results to its peak value and denoted as organic chlorine removal efficiency. The de-chlorination reaction of chlorine from PVC was assumed to be first order reaction and the organic chlorine removal efficiency was determined by the following equation:

$$\alpha = 1 - A_3^* e^{-\frac{T_{a_3}}{T(t)}} \tag{7.8}$$

Where A_3^* = 1.11×10^9, and T_{a_3}= 1.51×10^4. The results are shown in Figure 7.2b, denoted as correlation. To compare the chlorine removal behavior of PVC to the solid waste, torrefied PVC samples at 400 °C with different times were also characterized. Figure 7.2b also presents results of organic chlorine removal efficiency from waste and from PVC vs. time, showing that the chlorine release from PVC was not affect by the composition difference. This indicates that chlorine removal from PVC and waste materials, containing PVC, during torrefaction depends on temperature and residence time, not on the waste composition. It also shows that chlorine removal behavior is independent of the initial chlorine levels and removal of chlorine is not affected by the presence of other waste components in the surrounding during the process.

It is also essential to identify the sources of the remaining 20% of chlorine. Ma et al., 2010 studied the existence of inorganic chlorine in the waste that was found to release in temperature range of 700 °C to 1000 °C using thermal treatment. According to Lu et al., 2018, alkali chlorides (salt, e.g. KCl, NaCl) are the main sources of the inorganic chlorine in the waste.(Lu et al., 2019) The method of measuring the chlorine content in the current study was by analyzing the HCl in gaseous form after combustion of the sample with combustion temperature of the waste over 850 °C (Abbas et al., 2003). Therefore, based on the temperature range indicated, it can be hypothesized that the remaining chlorine from the CE material originates from inorganic sources, as this chlorine did not release during torrefaction at 400 °C. To prove this hypothesis, we used the method by Donepudi, 2017, who showed that inorganic compounds containing chlorine are very brittle and therefore can be well pulverized in order to be separated through sifting (Donepudi, 2017). Therefore, we took a sample of the waste, pulverized it in a high-shear grinder (24,000 rpm with stainless steel blades) and sifted it using various mesh screens. Preliminary results show that sifting with a 425-micron size screen can remove the inorganic chlorine. However, more comprehensive study is needed to have conclusive results on removal of inorganic chlorine by sifting.

7.4.3 Correlation between Chlorine Removal and Mass Loss

To study the correlation between chlorine removal and the mass loss, the results of the organic chlorine removal efficiency were plotted using correlation developed above. Figure 7.3 shows that the efficiency increased as the mass loss increased, and all the chlorine from PVC was released after the mass loss reached ~40%. The behavior in Figure 7.3 is unique to the specific waste blend, i.e., the chlorine removal efficiency vs. mass loss, will depend on the waste composition. As noted above, chlorine removal depends only on the temperature and residence time. However, for a given blend, the results of Figure 7.3 are useful as they provide a predictive behavior that can be used for design considerations.

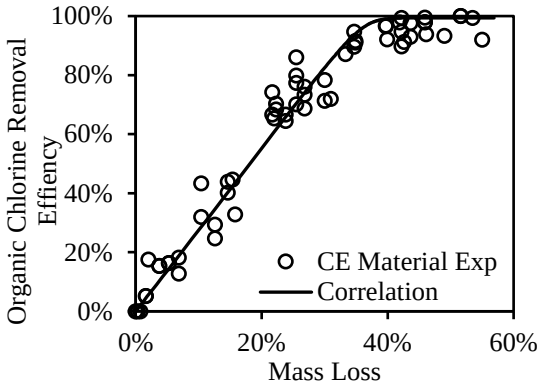

Figure 7.3. Organic chlorine removal efficiency vs. mass loss.

7.4.4 Heat Content

Figure 7.4 shows the heat content of the sample at different mass losses. It demonstrates that the LC and HC samples have similar behavior with the extent of torrefaction. Although there exists some scatter in the results (due to the heterogeneity natural of the sample), it clearly indicates a trend that heat content of both LC and HC sample increases due to the release of volatiles as the mass loss increases, reaching a maximum of ~34 MJ/kg at ~45% mass loss. After 45% mass loss, the heat content started decreasing as the mass loss increased, due to the formation of fixed carbon, and it reached ~32 MJ/kg at ~58% mass loss. As compared to PRB coal with a heat content of ~ 17 to 19 MJ/kg (Luppens, 2011), these numbers are rather encouraging. In order to help further study the behavior of the effect on the heat content of the material, the experimental results were fitted mathematically, showing in Figure 7.4. Heat content vs. mass loss.. It is essential to note that Figure 7.4 is only applicable to this specific blend of material since different composition will have different heat content. If we would like to produce chlorine-free solid fuels, predicting the heat content of such fuel is essential. After all the organic chlorine was removed, the remaining inorganic chlorine (salts) could potentially be removed through mechanical process (pulverizing and sifting). Since the calorific value of inorganic chlorine is negligible, and the mechanical processes do not affect the calorific value of other materials in the waste, we could assume that the heat content of fully dechlorinated waste is comparable to the one after all the organic chlorine is removed.

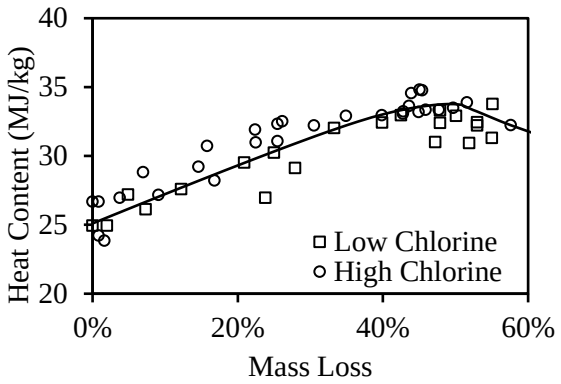

Figure 7.4. Heat content vs. mass loss.

Since the torrefaction process releases volatiles, which also contain some energy, it is essential to understand the energy retained at different extent of torrefaction compared to the initial amount. Figure 7.5 shows the normalized retained energy vs. mass loss, which indicates that the energy retained for both LC and HC samples have similar behavior with the extent of torrefaction. The retained energy decreases as the mass loss increases to a final value of ~ 50% of retained energy at ~ 58% mass loss.

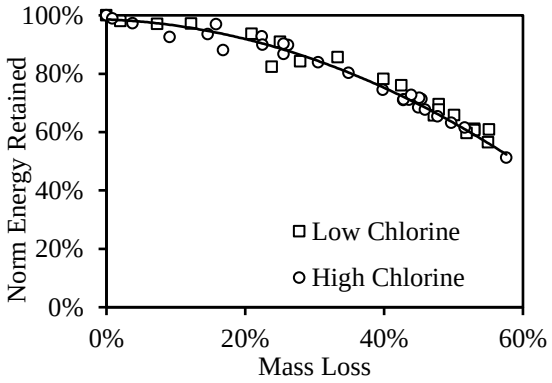

Figure 7.5. Normalized retained energy vs. mass loss.

7.4.5 Chlorine Removal per Unit Energy

In order to further study the relationship between the chlorine content and energy content, the following normalized properties (normalized according to their initial values) were calculated from the developed correlations above: (i) heat content (Norm HC), (ii) organic chlorine content (Norm Cl), (iii) retained energy (Norm Retained Energy), and (iv) organic chlorine per unit heat content (Norm Cl/HC), and were plotted in Figure 7.6. It indicates that as the mass loss increases, the organic chlorine per unit heat content reduces faster compared to the chlorine content. This suggests that we would need less residence time if we consider reducing the chlorine emission levels from Cl/HC point of view. For instance, at ~30% mass loss, the organic chlorine content per unit heat content reduced ~90%, while the heat content is ~32 MJ/kg and ~90% energy was retained. This could help to predict the properties and optimize the process parameters for treating this type of waste blends.

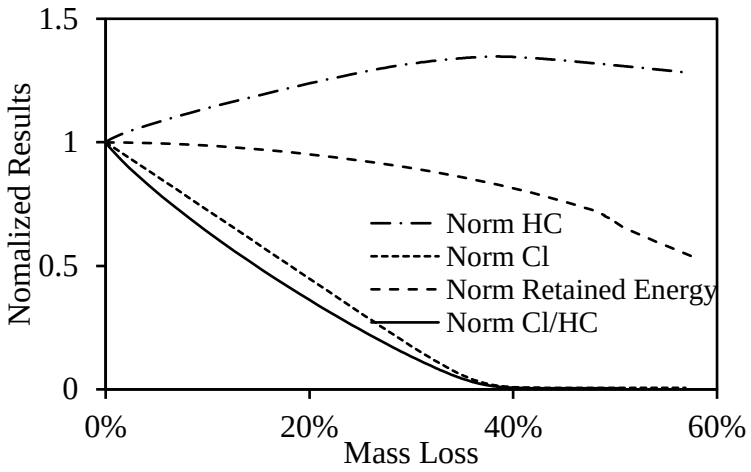

Figure 7.6. Chlorine removal per unit energy vs. mass loss.

7.5 Summary and Conclusions

In the present study, two types of fiber and plastic waste blends with a ratio of 60:40, including LC and HC material were torrefied at 400 °C with different residence times. It was found that although these two types contain different chlorine content, the torrefaction behaviors were comparable, and their heat contents and chlorine removal efficiencies were also similarly correlated to torrefaction. The mass losses both started at ~340 °C and reached ~55% after 60 minutes. The mass losses increased relatively faster at the early stage, which can be mainly attributed to the decomposition of the fiber, while slower increase at later stage was mainly due to torrefaction of the plastics. The heat content of the CE material was found to increase as the mass loss increased due to the release of volatiles. It reached a peak value (~34 MJ/kg) at ~45% mass loss and gradually decreased as mass loss increased due to the formation of fixed carbon. However, the behaviors of the mass loss and heat content only apply to this specific type of material. The chlorine removal efficiency increased as mass loss increased, reaching an asymptotic value of ~80% after ~20 minutes at ~ 40% mass loss, while the remaining 20% of chlorine can be attributed to inorganic sources (mainly alkali chlorides such as KCl, NaCl). The results indicated that the behavior of organic chlorine removal efficiency over time from PVC at 400 °C is universal regardless of its composition. It was also observed that the chlorine content per unit heat content reduced as the mass loss increased and the lowest value was obtained at ~40% mass loss. However, if we consider reaching high chlorine removal efficiency while avoiding losing too much energy, it was found that at ~30% mass loss, the organic chlorine content per unit heat content reduced ~90%, while the heat content is ~32 MJ/kg and ~90% energy was retained**.** Understanding how torrefaction would affect mechanical processing (pulverizing and sifting) in removal of inorganic chlorine could be a topic to be investigated in future work.

Acknowledgments

This research was supported under the MTRAC Program by the State of Michigan 21st Century Jobs Fund received through the Michigan Strategic Fund and administered by the Michigan Economic Development Corporation, grant number RC109248.

7.6 Works Cited

Abbas, Z., Moghaddam, A. P., and Steenari, B. M. (2003). Release of salts from municipal solid waste combustion residues. *Waste Manag.* 23, 291–305. doi:10.1016/S0956-053X(02)00154-X.

Aboulkas, A., El harfi, K., and El Bouadili, A. (2010). Thermal degradation behaviors of polyethylene and polypropylene. Part I: Pyrolysis kinetics and mechanisms. *Energy Convers. Manag.* 51, 1363–1369. doi:10.1016/j.enconman.2009.12.017.

Adefisan, O. O., and McDonald, A. G. (2019). Evaluation of the strength, sorption and thermal properties of bamboo plastic composites. *Maderas Cienc. y Tecnol.* 21, 3–14. doi:10.4067/S0718-221X2019005000101.

Alén, R., Kuoppala, E., and Oesch, P. (1996). Formation of the main degradation compound groups from wood and its components during pyrolysis. *J. Anal. Appl. Pyrolysis* 36, 137–148. doi:10.1016/0165-2370(96)00932-1.

Alvarez, V. A., and Vázquez, A. (2004). Thermal degradation of cellulose derivatives/starch blends and sisal fibre biocomposites. *Polym. Degrad. Stab.* 84, 13–21. doi:10.1016/j.polymdegradstab.2003.09.003.

Anders, H., and Zimmermann, H. (1987). A comparison of the thermal degradation behaviours of poly(vinyl acetate), poly(vinyl alcohol) and poly(vinyl chloride). *Polym. Degrad. Stab.* 18, 111–122. doi:10.1016/0141-3910(87)90024-3.

Anuar Sharuddin, S. D., Abnisa, F., Wan Daud, W. M. A., and Aroua, M. K. (2016). A review on pyrolysis of plastic wastes. *Energy Convers. Manag.* 115, 308–326. doi:10.1016/J.ENCONMAN.2016.02.037.

Bacaloglu, R., and Fisch, M. (1995). Degradation and stabilization of poly (vinyl chloride). V. Reaction mechanism of poly(vinyl chloride) degradation. *Polym. Degrad. Stab.* 47, 33–57. doi:10.1016/0141-3910(94)00086-N.

Bach, Q. V., Chen, W. H., Eng, C. F., Wang, C. W., Liang, K. C., and Kuo, J. Y. (2019). Pyrolysis characteristics and non-isothermal torrefaction kinetics of industrial solid wastes. *Fuel* 251, 118–125. doi:10.1016/j.fuel.2019.04.024.

Bergman, T. L., Incropera, F. P., DeWitt, D. P., and Lavine, A. S. (2011). "Fundamentals of heat and mass transfer," in (New York: Wiley, pp. 983-1011), 56.

Biagini, E., Barontini, F., Tognotti, L., and Diotisal, V. (2006). Devolatilization of Biomass Fuels and Biomass Components Studied by TG / FTIR Technique. 4486–4493. doi:10.1021/ie0514049.

Bradbury, A. G. W., Sakai, Y., and Shafizadeh, F. (1979). A kinetic model for pyrolysis of cellulose. *J. Appl. Polym. Sci.* 23, 3271–3280. doi:10.1002/app.1979.070231112.

Braun, V. D., and Thallnaier, M. (1966). Zum mechanismus der thermischen

chlorwassmtoffabspaltung aus polyvinylchlorid. 3. Mitt. Über die länge der polyensequenzen in partiell dehydrohalogenierten poiyvinylchloriden, polyvinylbromiden und vinylchlorid-copolymeren. *Die Makromol. Chemie* 99, 59–75. doi:10.1002/macp.1966.020990106.

Brebu, M., Tamminen, T., and Spiridon, I. (2013). Thermal degradation of various lignins by TG-MS/FTIR and Py-GC-MS. *J. Anal. Appl. Pyrolysis* 104, 531–539. doi:10.1016/j.jaap.2013.05.016.

Brebu, M., and Vasile, C. (2010). Thermal Degradation of Lignin-A Review. *Cellul. Chem. Technol.* 44, 353–363. Available at: https://www.semanticscholar.org/paper/THERMAL-DEGRADATION-OF-LIGNIN-A-REVIEW-Brebu-Vasile/67fecec0d827e7ac1cbb5a4c6752b6d8ec6c1fef [Accessed August 7, 2020].

Burra, K. G., and Gupta, A. K. (2018). Synergistic effects in steam gasification of combined biomass and plastic waste mixtures. *Appl. Energy* 211, 230–236. doi:10.1016/j.apenergy.2017.10.130.

Cabrales, L., and Abidi, N. (2010). On the thermal degradation of cellulose in cotton fibers. *J Therm Anal Calorim* 102, 485–491. doi:10.1007/s10973-010-0911-9.

Cangialosi, F., Intini, G., Liberti, L., Notarnicola, M., and Stellacci, P. (2008). Health risk assessment of air emissions from a municipal solid waste incineration plant - A case study. *Waste Manag.* 28, 885–895. doi:10.1016/j.wasman.2007.05.006.

Chang, S.-S. (1977). Heat Capacity and Thermodynamic Properties of Poly(Vinyl Chloride). *J. Res. Natl. Bur. Stand. (1934).* 82, 9–18. doi:10.6028/jres.082.002.

Chattopadhyay, J., Kim, C., Kim, R., and Pak, D. (2008). Thermogravimetric characteristics and kinetic study of biomass co-pyrolysis with plastics. 25, 1047–1053.

Chen, R., Zhang, S., Cong, K., Li, Q., and Zhang, Y. (2020). Insight into synergistic effects of biomass-polypropylene co-pyrolysis using representative biomass constituents. *Bioresour. Technol.* 307, 123–243. doi:10.1016/j.biortech.2020.123243.

Chen, W. H., Wang, C. W., Ong, H. C., Show, P. L., and Hsieh, T. H. (2019). Torrefaction, pyrolysis and two-stage thermodegradation of hemicellulose, cellulose and lignin. *Fuel* 258, 116–168. doi:10.1016/j.fuel.2019.116168.

Chen, W., and Kuo, P. (2011). Isothermal torrefaction kinetics of hemicellulose , cellulose , lignin and xylan using thermogravimetric analysis. *Energy* 36, 6451–6460. doi:10.1016/j.energy.2011.09.022.

Chen, W., Peng, J., and Bi, X. T. (2015). A state-of-the-art review of biomass torrefaction , densi fi cation and applications. 44, 847–866. doi:10.1016/j.rser.2014.12.039.

Collard, F. X., and Blin, J. (2014). A review on pyrolysis of biomass constituents: Mechanisms and composition of the products obtained from the conversion of cellulose, hemicelluloses and lignin. *Renew. Sustain. Energy Rev.* 38, 594–608. doi:10.1016/j.rser.2014.06.013.

Conti, J., Holtberg, P., Diefenderfer, J., LaRose, A., Turnure, J. T., and Westfall, L. (2016). International Energy Outlook 2016 with Prokctions to 2040. Available at: https://www.eia.gov/outlooks/ieo/pdf/0484(2016).pdf.

Curling, S., Clausen, C. A., and Winandy, J. E. (2001). The effect of hemicellulose degradation on the mechanical properties of wood during brown rot decay. in *International Research Group on Wood Preservation 2011*, 1–10.

De Carvalho, G., Frollini, E., and Dos Santos, W. N. (1996). Thermal conductivity of polymers by hot-wire method. *J. Appl. Polym. Sci.* 62, 2281–2285. doi:10.1002/(sici)1097-4628(19961226)62:13<2281::aid-app12>3.3.co;2-t.

Dence, C. W. (1992). The Determination of Lignin. *Methods Lignin Chem.*, 33–61. Available at: https://link.springer.com/chapter/10.1007/978-3-642-74065-7_3.

Donepudi, Y. (2017). Impact of Pretreatment Methods on Fast Pyrolysis of Biomass. Available at: https://digitalcommons.mtu.edu/etdr/496.

Dupuis, D. P., Grim, R. G., Nelson, E., Tan, E. C. D., Ruddy, D. A., Hernandez, S., et al. (2019). High-Octane Gasoline from Biomass: Experimental, Economic, and Environmental Assessment. *Appl. Energy* 241, 25–33. doi:10.1016/j.apenergy.2019.02.064.

Eichhorn, S. J., Sirichaisit, J., and Young, R. J. (2001). Deformation mechanisms in cellulose fibres, paper and wood. *J. Mater. Sci.* 36, 3129–3135. doi:10.1023/A:1017969916020.

El-Fadel, M., Findikakis, A. N., and Leckie, J. O. (1997). Environmental impacts of solid waste landfilling. *J. Environ. Manage.* 50, 125.

Enviromental Protection Agency (2017). Advancing Sustainable Materials Management: 2017 Fact Sheet Assessing Trends in Material Generation, Recycling, Composting, Combustion with Energy Recovery and Landfilling in the United States. Available at: https://www.epa.gov/sites/production/files/2019-11/documents/2017_facts_and_figures_fact_sheet_final.pdf [Accessed November 11, 2020].

EPA Clean Air Act, 42 USC 7412(f) (1992). Available at: https://www.govinfo.gov/content/pkg/USCODE-2013-title42/html/USCODE-2013-title42-chap85-subchapI-partA-sec7412.htm [Accessed January 19, 2020].

Fabiyi, J. S., and McDonald, A. G. (2010). Effect of wood species on property and weathering performance of wood plastic composites. *Compos. Part A Appl. Sci. Manuf.* 41, 1434–1440. doi:10.1016/j.compositesa.2010.06.004.

Farhat, W., Venditti, R., Quick, A., Taha, M., Mignard, N., Becquart, F., et al. (2017). Hemicellulose extraction and characterization for applications in paper coatings and adhesives. *Ind. Crop. Prod.* 107, 370–377. doi:10.1016/j.indcrop.2017.05.055.

Fung, B. M., Khitrin, A. K., and Ermolaev, K. (2000). An Improved Broadband Decoupling Sequence for Liquid Crystals and Solids. *J. Magn. Reson.* 142, 97–101. doi:10.1006/jmre.1999.1896.

Funke, A., Henrich, E., Dahmen, N., and Sauer, J. (2017). Dimensional Analysis of Auger-Type Fast Pyrolysis Reactors. *Energy Technol.* 5, 119–129. doi:10.1002/ente.201600095.

Gao, Z., Kaneko, T., Amasaki, I., and Nakada, M. (2003). A kinetic study of thermal degradation of polypropylene. *Polym. Degrad. Stab.* 80, 269–274. doi:10.1016/S0141-3910(02)00407-X.

Gómez, M. A., Álvarez, M. A., Eguía, P., and Comesa, R. (2012). Thermochimica Acta Thermal lag analysis on a simulated TGA-DSC device. 547, 13–21.

Goorah, S. S. D., Esmyot, M. L. I., and Boojhawon, R. (2009). The health impact of nonhazardous solid waste disposal in a community: the case of the Mare Chicose landfill in Mauritius. *J. Environ. Health* 72, 48–55.

Han, B., Chen, Y., Wu, Y., and Hua, D. (2014). Co-pyrolysis behaviors and kinetics of plastics – biomass blends through thermogravimetric analysis. 227–235. doi:10.1007/s10973-013-3228-7.

Hatanaka, T., Imagawa, T., and Takeuchi, M. (2000). Formation of PCDD/Fs in artificial solid waste incineration in a laboratory-scale fluidized-bed reactor: Influence of contents and forms of chlorine sources in high-temperature combustion. *Environ. Sci. Technol.* 34, 3920–3924. doi:10.1021/es991258w.

Ház, A., Jablonský, M., Šurina, I., Kačík, F., Bubeníková, T., and Ďurkovič, J. (2019). Chemical composition and thermal behavior of kraft lignins. *Forests* 10, 1–12. doi:10.3390/f10060483.

He, Q., Ding, L., Gong, Y., Li, W., Wei, J., and Yu, G. (2019). Effect of torrefaction on pinewood pyrolysis kinetics and thermal behavior using thermogravimetric analysis. *Bioresour. Technol.* 280, 104–111. doi:10.1016/j.biortech.2019.01.138.

He, Q., Guo, Q., Ding, L., Gong, Y., Wei, J., and Yu, G. (2018). Co-pyrolysis Behavior and Char Structure Evolution of Raw/Torrefied Rice Straw and Coal Blends. *Energy and Fuels* 32, 12469–12476. doi:10.1021/acs.energyfuels.8b03469.

Hilbers, T. J., Wang, Z., Pecha, B., Westerhof, R. J. M., Kersten, S. R. A., Pelaez-samaniego, M. R., et al. (2015). Cellulose-Lignin interactions during slow and fast pyrolysis. *J. Anal. Appl. Pyrolysis* 114, 197–207. doi:10.1016/j.jaap.2015.05.020.

Hoornweg, D., and Bhada-Tata, P. (2012). What a Waste : A Global Review of Solid Waste Management. *Urban Dev. Ser. Pap. no. 15. World Bank, Washington, DC. © World Bank. Licens. CC BY 3.0 IGO."* 15, 8. doi:10.3970/cmes.2014.098.129.

Hu, J., Shen, D., Wu, S., Zhang, H., and Xiao, R. (2014). Effect of temperature on structure evolution in char from hydrothermal degradation of lignin. *J. Anal. Appl. Pyrolysis* 106, 118–124. doi:10.1016/j.jaap.2014.01.008.

Hubbe, M. A., Venditti, R. A., and Rojas, O. J. (2007). What happens to cellulosic fibers during papermaking and recycling? A review. *BioResources* 2, 739–788. doi:10.15376/biores.2.4.739-788.

Incroper, F. P., Dewitt, D. P., Bergman, T. L., and Lavine, A. S. (2011). *Fundamentals of*

Heat and Mass Transfer. 7th ed. Wiley, pp. 983-1011 Available at: http://cds.cern.ch/record/1339915/files/9780471457282_TOC.pdf [Accessed July 30, 2019].

Indrawan, B., Prawisudhap, P., and Yoshikawa, K. (2011). Chlorine-free Solid Fuel Production from Municipal Solid Waste by Hydrothermal Process. *J. Japan Inst. Energy* 90, 1177–1182. doi:10.3775/jie.90.1177.

Inoue, T., Miyazaki, M., Kamitani, M., Kano, J., and Saito, F. (2004). Mechanochemical dechlorination of polyvinyl chloride by co-grinding with various metal oxides. *Adv. Powder Technol.* 15, 215–225. doi:10.1163/156855204773644445.

Ito, M., and Nagai, K. (2010). Thermal aging and oxygen permeation of Nylon-6 and Nylon-6/montmorillonite composites. *J. Appl. Polym. Sci.* 118, 928–935. doi:10.1002/app.32424.

Jacques Lédé (2010). Biomass Pyrolysis: Comments on Some Sources of Confusions in the Definitions of Temperatures and Heating Rates. *Energies* 3, 886–898. doi:doi:10.3390/en3040886.

Jiang, Y., Lu, M., Liu, S., Bao, C., and Liang, G. (2018). Deactivation by HCl of CeO2–MoO3/TiO2 catalyst for selective catalytic reduction of NO with NH3. 8, 17677–17684. doi:10.1039/c8ra00280k.

Jung, Y. G., Choi, S. C., Oh, C. S., and Paik, U. G. (1997). Residual stress and thermal properties of zirconia/metal (nickel, stainless steel 304) functionally graded materials fabricated by hot pressing. *J. Mater. Sci.* 32, 3841–3850. doi:10.1023/A:1018640126751.

Kim, U. J., Eom, S. H., and Wada, M. (2010). Thermal decomposition of native cellulose: Influence on crystallite size. *Polym. Degrad. Stab.* 95, 778–781. doi:10.1016/j.polymdegradstab.2010.02.009.

Kiran, N., Ekinci, E., and Snape, C. . (2000). Recyling of plastic wastes via pyrolysis. *Resour. Conserv. Recycl.* 29, 273–283. doi:10.1016/S0921-3449(00)00052-5.

Klinger, J., Bar-Ziv, E., and Shonnard, D. (2013). Kinetic study of aspen during torrefaction. *J. Anal. Appl. Pyrolysis* 104, 146–152. doi:10.1016/j.jaap.2013.08.010.

Klinger, J., Bar-Ziv, E., and Shonnard, D. (2015). Unified kinetic model for torrefaction-pyrolysis. *Fuel Process. Technol.* 138, 175–183. doi:10.1016/j.fuproc.2015.05.010.

Klinger, J., Bar-Ziv, E., Shonnard, D., Westover, T., and Emerson, R. (2016). Predicting Properties of Gas and Solid Streams by Intrinsic Kinetics of Fast Pyrolysis of Wood. *Energy and Fuels* 30, 318–325. doi:10.1021/acs.energyfuels.5b01877.

Klinger, J., Klemetsrud, B., Bar-Ziv, E., and Shonnard, D. (2014). Temperature dependence of aspen torrefaction kinetics. *J. Anal. Appl. Pyrolysis* 110, 424–429. doi:10.1016/j.jaap.2014.10.008.

Kotchen, M. J., and Mansur, E. T. (2014). How stringent are the US EPA's proposed carbon pollution standards for new power plants? *Rev. Environ. Econ. Policy* 8, 290–306. doi:10.1093/reep/reu003.

Kumar, L., Koukoulas, A. A., Mani, S., and Satyavolu, J. (2017). Integrating torrefaction in the wood pellet industry: A critical review. *Energy and Fuels* 31, 37–54. doi:10.1021/acs.energyfuels.6b02803.

Lauer, D., Motell, E. L., Traficante, D. D., and Maciel, G. E. (1972). Carbon-13 Chemical Shifts in Monoalkyl Benzenes and Some Deuterio Analogs. *J. Am. Chem. Soc.* 94, 5335–5338. doi:10.1021/ja00770a032.

Lavrykov, S. A., and Ramarao, B. V. (2012). Thermal Properties of Copy Paper Sheets. *Dry. Technol.* 30, 297–311. doi:10.1080/07373937.2011.638148.

Lin, X., Zhang, Z., Wang, Q., and Sun, J. (2020). Interactions between biomass-derived components and polypropylene during wood–plastic composite pyrolysis. *Biomass Convers. Biorefinery*, 1–13. doi:10.1007/s13399-020-00861-4.

Love, G. D., Snape, C. E., and Jarvis, M. C. (1998). Comparision of Leaf and Stem Cell-Wall Components in Barley Straw by Solid-State 13C NMR. *Phytochemistry* 49, 1191–1194.

Lu, P., Huang, Q., Bourtsalas, A. T., Themelis, N. J., Chi, Y., and Yan, J. (2019). Review on fate of chlorine during thermal processing of solid wastes. *J. Environ. Sci. (China)* 78, 13–28. doi:10.1016/j.jes.2018.09.003.

Luppens, J. A. (2011). A critical review of published coal quality data from the southwestern part of the Powder River Basin, Wyoming. Reston, Virginia Available at: https://pubs.usgs.gov/of/2011/1148/pdf/ofr20111148_072111.pdf.

Ma, Y., Hummel, M., Määttänen, M., Särkilahti, A., Harlin, A., and Sixta, H. (2016). Upcycling of waste paper and cardboard to textiles. *Green Chem.* 18, 858–866. doi:10.1039/c5gc01679g.

Mahdavi Nejad, A. (2019). Thermal Analysis of Paper Board Packaging with Phase Change Material: A Numerical Study. *J. Packag. Technol. Res.* 3, 181–192. doi:10.1007/s41783-019-00060-1.

Mamleev, V., Bourbigot, S., and Yvon, J. (2007). Kinetic analysis of the thermal decomposition of cellulose: The main step of mass loss. *J. Anal. Appl. Pyrolysis* 80, 151–165. doi:10.1016/j.jaap.2007.01.013.

Marongiu, A., Faravelli, T., Bozzano, G., Dente, M., and Ranzi, E. (2003). Thermal degradation of poly(vinyl chloride). *J. Anal. Appl. Pyrolysis* 70, 519–553. doi:10.1016/S0165-2370(03)00024-X.

Maunu, S. L. (2009). "13C CPMAS NMR Studies of Wood, Cellulose Fibers, and Derivatives," in *Characterization of Lignocellulosic Materials*, eds. Q. Thomas and Q. Hu (Hoboken: Blackwell), 227–248. doi:https://doi.org/10.1002/9781444305425.ch13.

Mayo, W. D., Miller, A. F., and Hannah, W. R. (2004). "Course Notes on the Interpretation of Infrared and Raman Spectra," in *Course Notes on the Interpretation of Infrared and Raman Spectra* (John Wiley & Sons), 33–72. doi:10.1002/0471690082.

McCabe, J. G. (2014). Addressing Biogenic Carbon Dioxide Emissions from Stationary

Sources. United States Enviromental Protection Agency. Washington, D.C Available at: https://archive.epa.gov/epa/sites/production/files/2016-08/documents/biogenic-co2-emissions-memo-111914.pdf.

McNeill, I. C., Memetea, L., and Cole, W. J. (1995). A study of the products of PVC thermal degradation. *Polym. Degrad. Stab.* 49, 181–191. doi:10.1016/0141-3910(95)00064-S.

More recycling raises average energy content of waste used to generate electricity (2012). Available at: https://www.eia.gov/todayinenergy/detail.php?id=8010 [Accessed January 19, 2020].

Moreira, L. R. S., and Filho, E. X. F. (2008). An overview of mannan structure and mannan-degrading enzyme systems. *Appl. Microbiol. Biotechnol.* 79, 165–178. doi:10.1007/s00253-008-1423-4.

National Emission Standards for Hazardous Air Pollutants (NESHAP) (2017). Available at: https://www.epa.gov/stationary-sources-air-pollution/national-emission-standards-hazardous-air-pollutants-neshap-9 [Accessed July 29, 2019].

National Overview: Facts and Figures on Materials, Wastes and Recycling (2017). Available at: https://www.epa.gov/facts-and-figures-about-materials-waste-and-recycling/national-overview-facts-and-figures-materials#Landfilling [Accessed January 19, 2020].

Ni, Y., Zhang, H., Fan, S., Zhang, X., Zhang, Q., and Chen, J. (2009). Emissions of PCDD/Fs from municipal solid waste incinerators in China. *Chemosphere* 75, 1153–1158. doi:10.1016/j.chemosphere.2009.02.051.

Olajire, A., Zhi, C., Hanson, S., and Wai, C. (2014). Thermogravimetric analysis of the pyrolysis characteristics and kinetics of plastics and biomass blends. 128, 471–481. doi:10.1016/j.fuproc.2014.08.010.

Oyedun, A. O., Gebreegziabher, T., Ng, D. K. S., and Hui, C. W. (2014). Mixed-waste pyrolysis of biomass and plastics waste - A modelling approach to reduce energy usage. *Energy* 75, 127–135. doi:10.1016/j.energy.2014.05.063.

Pandey, K. K. (1999). A Study of Chemical Structure of Soft and Hardwood and Wood Polymers by FTIR Spectroscopy. *J. Appl. Polym. Sci.* 71, 1969–1975. doi:10.1002/(sici)1097-4628(19990321)71:12<1969::aid-app6>3.0.co;2-d.

Papadopoulou, M. P., Karatzas, G. P., and Bougioukou, G. G. (2007). Numerical modelling of the environmental impact of landfill leachate leakage on groundwater quality - A field application. *Environ. Model. Assess.* 12, 43–54. doi:10.1007/s10666-006-9050-x.

Pasangulapati, V., Ramachandriya, K. D., Kumar, A., Wilkins, M. R., Jones, C. L., and Huhnke, R. L. (2012). Effects of cellulose, hemicellulose and lignin on thermochemical conversion characteristics of the selected biomass. *Bioresour. Technol.* 114, 663–669. doi:10.1016/j.biortech.2012.03.036.

Patkar, S. N., and Panzade, P. D. (2016). Fast and efficient method for molecular weight

analysis of cellulose pulp, in-process and finished product. *Anal. Methods* 8, 3210–3215. doi:10.1039/c5ay03012a.

Peterson, J. D., Vyazovkin, S., and Wight, C. A. (2001). Kinetics of the thermal and thermo-oxidative degradation of polystyrene, polyethylene and poly(propylene). *Macromol. Chem. Phys.* 202, 775–784. doi:10.1002/1521-3935(20010301)202:6<775::AID-MACP775>3.0.CO;2-G.

Petre, A. L., Budrugeac, P., and Segal, E. (1999). Thermal Degradation of Polyvinyl Chloride. *J. Therm. Anal. Calorim.* 56, 1065–1070. doi:10.1023/A:1010136507843.

Pines, A., Gibby, M. G., and Waugh, J. S. (1972). Proton-enhanced nuclear induction spectroscopy. a method for high resolution nmr of dilute spins in solids. *J. Chem. Phys.* 56, 1776–1777. doi:10.1063/1.1677439.

Radics, R. I., Gonzalez, R., Bilek, E. M., and Kelley, S. S. (2017). Systematic review of torrefied wood economics. *BioResources* 12, 6868–6884. doi:10.15376/biores.12.3.6868-6884.

Raveendran, K. (1996). Pyrolysis characteristics of biomass and biomass components. *Fuel* 75, 987–998. doi:10.1016/0016-2361(96)00030-0.

Risby, T. H., Yergey, J. A., and Scocca, J. J. (1982). Linear Programmed Thermal Degradation Mass Spectrometry of Polystyrene and Poly(vinyl chloride). *Anal. Chem.* 54, 2228–2233. doi:10.1021/ac00250a022.

Ritchie and Roser (2018). *Plastic Pollution - Our World in Data*. Available at: https://ourworldindata.org/plastic-pollution?utm_source=newsletter&utm_medium=email&utm_campaign=sendto_newslettertest&stream=top [Accessed January 23, 2020].

Rodrigues, J., Graça, J., and Pereira, H. (2001). Influence of tree eccentric growth on syringyl/guaiacyl ratio in Eucalyptus globulus wood lignin assessed by analytical pyrolysis. *J. Anal. Appl. Pyrolysis* 58–59, 481–489. doi:10.1016/S0165-2370(00)00121-2.

Rojas, A., and Orozco, E. (2003). Measurement of the enthalpies of vaporization and sublimation of solids aromatic hydrocarbons by differential scanning calorimetry. 405, 93–107. doi:10.1016/S0040-6031(03)00139-4.

Salvilla, J. N. V., Ofrasio, B. I. G., Rollon, A. P., Manegdeg, F. G., Abarca, R. R. M., and de Luna, M. D. G. (2020). Synergistic co-pyrolysıs of polyolefin plastics with wood and agricultural wastes for biofuel production. *Appl. Energy* 279, 115668. doi:10.1016/j.apenergy.2020.115668.

Sánchez-Jiménez, P. E., Perejón, A., Criado, J. M., Diánez, M. J., and Pérez-Maqueda, L. A. (2010). Kinetic model for thermal dehydrochlorination of poly(vinyl chloride). *Polymer (Guildf).* 51, 3998–4007. doi:10.1016/J.POLYMER.2010.06.020.

Schaefer, J., Stejskal, E. O., and Buchdahl, R. (1975). High-Resolution Carbon-13 Nuclear Magnetic Resonance Study of Some Solid, Glassy Polymers. *Macromolecules* 8, 291–296. doi:10.1021/ma60045a010.

Scheirs, J., Camino, G., and Tumiatti, W. (2001). Overview of water evolution during the thermal degradation of cellulose. *Eur. Polym. J.* 37, 933–942. doi:10.1016/S0014-3057(00)00211-1.

Sharypov, V., Beregovtsova, N., Kuznetsov, B., Baryshnikov, S., Marin, N., and Weber, J. (2003). Light Hydrocarbon Liquids Production by Co-Pyrolysis of Polypropylene and Hydrolytic Lignin. *Chem. Sustain. Dev.* 11, 427–434.

Shen, D. K., Gu, S., and Bridgwater, A. V. (2010). Study on the pyrolytic behaviour of xylan-based hemicellulose using TG-FTIR and Py-GC-FTIR. *J. Anal. Appl. Pyrolysis* 87, 199–206. doi:10.1016/j.jaap.2009.12.001.

Shenoy, A. V. (1999). "Rheology of Filled Polymer Systems," in (Springer Science&Business Media Dordrecht), 54–111.

Sluiter, J., and Sluiter, A. (2011). Summative Mass Closure: Laboratory Analytical Procedure (LAP) Review and Integration: Feedstocks; Issue Date: April 2010; Revision Date: July 2011 (Version 07-08-2011). Available at: http://www.nrel.gov/biomass/analytical_procedures.html [Accessed October 16, 2020].

Solmaz, R., Kardaş, G., Çulha, M., Yazıcı, B., and Erbil, M. (2008). Investigation of adsorption and inhibitive effect of 2-mercaptothiazoline on corrosion of mild steel in hydrochloric acid media. *Electrochim. Acta* 53, 5941–5952. doi:10.1016/J.ELECTACTA.2008.03.055.

Subramanian, P. M. (2000). Plastics recycling and waste management in the US. *Resour. Conserv. Recycl.* 28, 253–263. doi:10.1016/S0921-3449(99)00049-X.

Tian, H. H., & Ouyang, N. (2003). Preliminary Investigaton on Dioxing Emission from MSW Incinerators. *Environ. Chem.* 22, 255–258.

Utschick, H., Ritz, M., Mallon, H.-J., Arnold, M., Ludwig, W., Kettrup, A., et al. (1994). Investigations on the thermal degradation of post-chlorinated polyvinyl chloride. *Thermochim. Acta* 234, 139–151. doi:10.1016/0040-6031(94)85140-9.

Várhegyi, G., Antal, M. J., Jakab, E., and Szabó, P. (1997). Kinetic modeling of biomass pyrolysis. *J. Anal. Appl. Pyrolysis* 42, 73–87. doi:10.1016/S0165-2370(96)00971-0.

Vikelsoe, J., Nielsen, P., Blinksbjerg, P., Madsen, H., & Manscher, O. (1990). Significance of chlorine sources for the generation of dioxins during incineration of MSW. *Organohalogen Compd.* 3, 193–196.

Volpe, R., Zabaniotou, A. A., and Skoulou, V. (2018). Synergistic Effects between Lignin and Cellulose during Pyrolysis of Agricultural Waste. doi:10.1021/acs.energyfuels.8b00767.

Wakeman, I. B., and Johnson, H. R. (1978). Vinyl chloride formation from the thermal degradation of poly(vinyl chloride). *Polym. Eng. Sci.* 18, 404–407. doi:10.1002/pen.760180512.

Wang, X., Sotoudehniakarani, F., Yu, Z., Morrell, J. J., Cappellazzi, J., and McDonald, A. G. (2019). Evaluation of corrugated cardboard biochar as reinforcing fiber on

properties, biodegradability and weatherability of wood-plastic composites. *Polym. Degrad. Stab.* 168, 108955. doi:10.1016/j.polymdegradstab.2019.108955.

Wang, Z., Pecha, B., Westerhof, R. J. M., Kersten, S. R. A., Li, C. Z., McDonald, A. G., et al. (2014). Effect of cellulose crystallinity on solid/liquid phase reactions responsible for the formation of carbonaceous residues during pyrolysis. *Ind. Eng. Chem. Res.* 53, 2940–2955. doi:10.1021/ie4014259.

Wei, L., McDonald, A. G., Freitag, C., and Morrell, J. J. (2013). Effects of wood fiber esterification on properties, weatherability and biodurability of wood plastic composites. *Polym. Degrad. Stab.* 98, 1348–1361. doi:10.1016/j.polymdegradstab.2013.03.027.

What is U.S. electricity generation by energy source? (2020). Available at: https://www.eia.gov/tools/faqs/faq.php?id=427&t=3 [Accessed April 29, 2020].

Williams, C. L., Westover, T. L., Petkovic, L. M., Matthews, A. C., Stevens, D. M., and Nelson, K. R. (2017). Determining Thermal Transport Properties for Softwoods under Pyrolysis Conditions. *ACS Sustain. Chem. Eng.* 5, 1019–1025. doi:10.1021/acssuschemeng.6b02326.

Wimberley, J. W., Carel, A. B., and Cabbiness Conoco Inc., D. K. (1982). Automated Method for Measuring the Thermal Degradation of Polyvinyl Chloride. *Anal. Lett.* 15, 89–100. doi:10.1080/00032718208064366.

Wu, S., Shen, D., Hu, J., Zhang, H., and Xiao, R. (2016). Biomass and Bioenergy Cellulose-lignin interactions during fast pyrolysis with different temperatures and mixing methods. 90. doi:10.1016/j.biombioe.2016.04.012.

Xu, Z., Albrecht, J. W., Kolapkar, S. S., Zinchik, S., and Bar-Ziv, E. (2020a). Chlorine Removal from U.S. Solid Waste Blends through Torrefaction. *Appl. Sci.* 10, 3337. doi:10.3390/app10093337.

Xu, Z., Kolapkar, S., Zinchik, S., Bar-Ziv, E., and Mcdonald, A. (2020b). Comprehensive Kinetic Study of Thermal Degradation of Polyvinylchloride (PVC). *Polym. Degrad. Stab.* 176. doi:doi.org/10.1016/j.polymdegradstab.2020.109148.

Xu, Z., Zinchik, S., Kolapkar, S., Bar-ziv, E., Hansen, T., and Conn, D. (2018). Properties of Torrefied U . S . Waste Blends. *Front. Energy Res.* 6, 65. doi:doi.org/10.3389/fenrg.2018.00065.

Xue, Y., and Bai, X. (2018). Synergistic enhancement of product quality through fast co-pyrolysis of acid pretreated biomass and waste plastic. *Energy Convers. Manag.* 164, 629–638. doi:10.1016/j.enconman.2018.03.036.

Yang, H., Liu, M., Chen, Y., Xin, S., Zhang, X., Wang, X., et al. (2020). Vapor – solid interaction among cellulose , hemicellulose and lignin. *Fuel* 263. doi:10.1016/j.fuel.2019.116681.

Yang, H., Yan, R., Chen, H., Zheng, C., Lee, D. H., Uni, V., et al. (2006). In-Depth Investigation of Biomass Pyrolysis Based on Three Major Components : Hemicellulose , Cellulose and Lignin. 388–393. doi:10.1021/ef0580117.

Yeo, J. Y., Chin, B. L. F., Tan, J. K., and Loh, Y. S. (2019). Comparative studies on the pyrolysis of cellulose, hemicellulose, and lignin based on combined kinetics. *J. Energy Inst.* 92, 27–37. doi:10.1016/j.joei.2017.12.003.

Yin, R.-H., Zhang, R.-Z., and Luo, Y.-H. (2016). The Effect of Utilizing Homogeneous Conversion to Control the Formation of Chlorinated Hydrocarbons During PVC Pyrolysis. 35, 1012–1019. doi:10.1002/ep.12313.

Yu, J., Sun, L., Ma, C., Qiao, Y., and Yao, H. (2016). Thermal degradation of PVC: A review. *Waste Manag.* 48, 300–314. doi:10.1016/j.wasman.2015.11.041.

Yuan, H., Wang, Y., Kobayashi, N., Zhao, D., and Xing, S. (2015). Study of Fuel Properties of Torrefied Municipal Solid Waste. *Energy and Fuels* 29, 4976–4980. doi:10.1021/ef502277u.

Zhang, J., Choi, Y. S., Yoo, C. G., Kim, T. H., Brown, R. C., and Shanks, B. H. (2015). Cellulose−Hemicellulose and Cellulose−Lignin Interactions during Fast Pyrolysis. *ACS Sustain. Chem. Eng.* 3, 293–301. doi:doi.org/10.1021/sc500664h.

Zhang, X., Lei, H., Zhu, L., Zhu, X., Qian, M., Yadavalli, G., et al. (2016). Bioresource Technology Thermal behavior and kinetic study for catalytic co-pyrolysis of biomass with plastics. *Bioresour. Technol.* 220, 233–238. doi:10.1016/j.biortech.2016.08.068.

Zhao, J., Xiuwen, W., Hu, J., Liu, Q., Shen, D., and Xiao, R. (2014). Thermal degradation of softwood lignin and hardwood lignin by TG-FTIR and Py-GC/MS. *Polym. Degrad. Stab.* 108, 133–138. doi:10.1016/j.polymdegradstab.2014.06.006.

Zhao, S., Liu, M., Zhao, L., and Zhu, L. (2018). Influence of Interactions among Three Biomass Components on the Pyrolysis Behavior. *Ind. Eng. Chem. Res.* 57, 5241–5249. doi:10.1021/acs.iecr.8b00593.

Zhou, H., Long, Y., Meng, A., Chen, S., Li, Q., and Zhang, Y. (2015). A novel method for kinetics analysis of pyrolysis of hemicellulose, cellulose, and lignin in TGA and macro-TGA. *RSC Adv.* 5, 26509–26516. doi:10.1039/c5ra02715b.

Zhou, L., Wang, Y., Huang, Q., and Cai, J. (2006). Thermogravimetric characteristics and kinetic of plastic and biomass blends co-pyrolysis. *Fuel Process. Technol.* 87, 963–969. doi:10.1016/j.fuproc.2006.07.002.

Zinchik, S., Xu, Z., Kolapkar, S. S., Bar-Ziv, E., and McDonald, A. G. (2020). Properties of pellets of torrefied U.S. waste blends. *Waste Manag.* 104, 130–138. doi:10.1016/j.wasman.2020.01.009.

8 Conclusion and Future Work

This work focused on two main aspects: (i) studying the properties of waste blends after torrefaction at various conditions; (ii) researching the dechlorination of wastes through torrefaction. Initially two types of waste blends (densified and un-densified) with 60% fiber and 40% plastic were torrefied at 300 °C with different time periods; (iii) investigate the decomposition chemistry of mixed paper and plastic waste under torrefaction conditions through advanced vapor- and solid-phase characterization. Present lumped pseudo-mechanism model to predict changes in solid composition and properties. It was found that although torrefaction dynamics of the two forms differs significantly from each other, their properties depend only on the mass loss. Grinding characteristics, size distribution after grinding gave similar results as a function of mass loss during torrefaction, for the forms of material. Further, the torrefied product demonstrates a similar grinding behavior to PRB coal. The total heat content was shown to increase with mass loss. Overall, the torrefied waste blends studied in this paper showed that they can be used as a drop-in fuel in coal power generation facilities since this fuel is low-cost, it also meets the environmental regulation standard.

After studying the properties of the torrefied waste blends, these materials were extruded into 9 mm diameter pellets and the products were characterized. It was found that there exist synergistic effects between the fiber and plastics during torrefaction. The results also showed that extrusion could significantly increase the homogeneity, durability and water resistance of the material. The overall conclusions is that the extruded torrefied pellets enhance the properties of the original plastic-fiber blends and could be a drop-in solid fuel for power generation.

In order to further study the synergy with the waste blends, the kinetic study of the paper waste during torrefaction at the temperature range of 200-400 °C was carried out. It was found that there exists synergistic effects between cellulose, hemicellulose and lignin during paper waste degradation. Therefore, paper waste was considered as one material and a multi-step consecutive reaction mechanism that focuses on solid products at different temperatures was developed. The temperature transients were modeled, and the kinetic parameters were obtained through fitting to the TGA experimental results. The model showed: (i) the first reaction was mainly dehydration reaction of cellulose with anhydrocellulose as solid product; (ii) there are more reactions at higher temperatures; (iii) the activation energies of 6^{th} and 7^{th} reaction and the temperatures (375 °C and 400 °C) are comparable to the results of lignin thermal degradation in literature, thus can be attributed lignin thermal degradation. This model can not only provide chemical insights of the paper wastes thermal degradation, it also can be used to help with other mechanistic works.

The study then focused on the interactions between fiber and plastic wastes during torrefaction. Synergistic effects were observed between paper plastic wastes during torrefaction. It was also found that at lower temperatures (250 °C), the maximum mass loss rate was more than doubled and the mass loss at the end of the experiments were also much higher compared to the expected results. In addition, with higher plastic content, the effects are more significant, both increasing the reaction rate as well as the overall mass loss.

However, there is no synergy observed at higher temperature (400 °C). The existence of such interactions between fiber and plastic wastes indicates that the natural energy barriers during the individual torrefaction in paper waste or plastic waste could be bypassed, and the torrefaction of fiber and plastic blend can be achieved at lower temperatures and/or shorter residence times. The reactive extrusion at 220 °C also showed there exists chemical changes during the process, which reduces the C-O and carbonyl index and increased hydroxyl content. The interaction between paper and plastic wastes during torrefaction can be attributed to the plastic acting as a hydrogen donor during the torrefaction of the paper, and the radicals derived from paper wastes also intensified the scission of the polymer chain, initiating the scission of the polymer chain, which increases the overall reaction rate and mass loss.

The results of flexural testing indicated that there exist synergistic effects not only between the MPW and fiber wastes, but also within the MPW. These synergistic effects can greatly help to design the process parameters to valorize mixed paper-plastic wastes.

In order to further study the dechlorination of the waste through torrefaction, a comprehensive kinetic study of thermal degradation of polyvinylchloride (PVC) was carried out since PVC was the main organic chlorine sources from the wastes. A four consecutive reactions mechanism was developed for PVC degradation at 300 °C. It was found that HCl and benzene were produced only by the first three reactions; naphthalene was produced by second and third reactions only; and anthracene was produced mostly by the second and third reaction, with some produced in the fourth reaction. The model has been validated and proved by predicting the mass loss, chlorine content, heat content and elemental composition with high precision experimental data in different reactors with/without heat transfer coupling. It is expected, however, that for higher temperatures, this model needs to be improved by adding more consecutive reactions and other products.

The study of chlorine removal through torrefaction from waste with different chlorine levels (~1,100 ppm and ~16,000 ppm) was also carried out. It was found that despite of different chlorine levels, the torrefaction behaviors of the two types of material were comparable, and their heat contents and chlorine removal efficiencies were also similarly correlated to torrefaction. The heat content of the CE material was found to increase as the mass loss increased due to the release of volatiles. It reached a peak value (~34 MJ/kg) at ~45% mass loss and gradually decreased as mass loss increased due to the formation of fixed carbon. The chlorine removal efficiency increased as mass loss increased, reaching an asymptotic value of ~80% after ~20 minutes at ~ 40% mass loss, while the remaining 20% of chlorine can be attributed to inorganic sources (mainly alkali chlorides such as KCl, NaCl). It was also observed that the chlorine content per unit heat content reduced as the mass loss increased and the lowest value was obtained at ~40% mass loss. However, if we consider reaching high chlorine removal efficiency while avoiding losing too much energy, it was found that at ~30% mass loss, the organic chlorine content per unit heat content reduced ~90%, while the heat content is ~32 MJ/kg and ~90% energy was retained.

There are still a lot of works that need further research. A specific topic that can be explored is that the potential interactions between PVC and other plastics during dechlorination. We have carried out the experiments with blend that consists of 2% PVC and 98% HDPE at various temperatures (300 °C to 500 °C) and preliminary analysis showed that there exist some interactions. Further study could be done for blends mixed with PVC and other polymers.

In addition, since MPW and MSW are also abundant and are causing more environmental problems, after studying fiber and plastic waste blends, it would greatly help if we could use MPW and MSW as feedstock to produce energy. To study the MPW and MSW, it is essential to understand their composition. However, the current material identification methods are rather time-consuming, which is not practical for industrial applications. Therefore, it would be great benefit if one can develop a technology that can identify the wastes in real-time. Further study would be done to combine the mid-infrared spectroscopy with machine learning algorithms to help identify and analyze the composition of waste feedstocks in real time.